TOPICAL REVIEW • OPEN ACCESS

A next-generation liquid xenon observatory for dark matter and neutrino physics

To cite this article: J Aalbers *et al* 2023 *J. Phys. G: Nucl. Part. Phys.* **50** 013001

OPEN ACCESS
IOP Publishing
Journal of Physics G: Nuclear and Particle Physics
J. Phys. G: Nucl. Part. Phys. **50** (2023) 013001 (115pp)
https://doi.org/10.1088/1361-6471/ac841a

Topical Review

A next-generation liquid xenon observatory for dark matter and neutrino physics

J Aalbers[1,2], S S AbdusSalam[3], K Abe[4,5], V Aerne[6], F Agostini[7], S Ahmed Maouloud[8], D S Akerib[1,2], D Y Akimov[9], J Akshat[10], A K Al Musalhi[11], F Alder[12], S K Alsum[13], L Althueser[14], C S Amarasinghe[15], F D Amaro[16], A Ames[1,2], T J Anderson[1,2], B Andrieu[8], N Angelides[17], E Angelino[18], J Angevaare[19], V C Antochi[20], D Antón Martin[21], B Antunovic[22,23], E Aprile[24], H M Araújo[17], J E Armstrong[25], F Arneodo[26], M Arthurs[15], P Asadi[27], S Baek[28], X Bai[29], D Bajpai[30], A Baker[17], J Balajthy[31], S Balashov[32], M Balzer[33], A Bandyopadhyay[34], J Bang[35], E Barberio[36], J W Bargemann[37], L Baudis[6], D Bauer[17], D Baur[38], A Baxter[39], A L Baxter[10], M Bazyk[40], K Beattie[41], J Behrens[42], N F Bell[36], L Bellagamba[7], P Beltrame[43], M Benabderrahmane[26], E P Bernard[41,44], G F Bertone[19], P Bhattacharjee[45], A Bhatti[25], A Biekert[41,44], T P Biesiadzinski[1,2], A R Binau[10], R Biondi[46], Y Biondi[6], H J Birch[15], F Bishara[47], A Bismark[6], C Blanco[20,48], G M Blockinger[49], E Bodnia[37], C Boehm[50], A I Bolozdynya[9], P D Bolton[12], S Bottaro[51,52], C Bourgeois[53], B Boxer[31], P Brás[54], A Breskin[55], P A Breur[19], C A J Brew[32], J Brod[56], E Brookes[19], A Brown[38], E Brown[57], S Bruenner[19], G Bruno[40], R Budnik[55], T K Bui[5], S Burdin[39], S Buse[6], J K Busenitz[30], D Buttazzo[52], M Buuck[1,2], A Buzulutskov[58,59], R Cabrita[54], C Cai[60], D Cai[40], C Capelli[6], J M R Cardoso[16], M C Carmona-Benitez[61], M Cascella[12], R Catena[62], S Chakraborty[63], C Chan[35], S Chang[64], A Chauvin[65], A Chawla[66], H Chen[41], V Chepel[54], N I Chott[29], D Cichon[67], A Cimental Chavez[6], B Cimmino[68], M Clark[10], R T Co[69], A P Colijn[19], J Conrad[20],

*Author to whom any correspondence should be addressed.

M V Converse[70], M Costa[51,52], A Cottle[11,71], G Cox[61], O Creaner[72], J J Cuenca Garcia[42], J P Cussonneau[40], J E Cutter[31], C E Dahl[71,73], V D'Andrea[74], A David[12], M P Decowski[19], J B Dent[75], F F Deppisch[12], L de Viveiros[61], P Di Gangi[7], A Di Giovanni[26], S Di Pede[19], J Dierle[38], S Diglio[40], J E Y Dobson[12], M Doerenkamp[65], D Douillet[53], G Drexlin[76], E Druszkiewicz[70], D Dunsky[44], K Eitel[42], A Elykov[38], T Emken[20], R Engel[42], S R Eriksen[77], M Fairbairn[78], A Fan[1,2], J J Fan[35], S J Farrell[79], S Fayer[17], N M Fearon[11], A Ferella[74], C Ferrari[46], A Fieguth[14], A Fieguth[80], S Fiorucci[41], H Fischer[38], H Flaecher[77], M Flierman[19], T Florek[10], R Foot[36], P J Fox[71], R Franceschini[81], E D Fraser[39], C S Frenk[82], S Frohlich[83], T Fruth[12], W Fulgione[46], C Fuselli[19], P Gaemers[19], R Gaior[8], R J Gaitskell[35], M Galloway[6], F Gao[60], I Garcia Garcia[84], J Genovesi[29], C Ghag[12], S Ghosh[45], E Gibson[11], W Gil[42], D Giovagnoli[40,85], F Girard[6], R Glade-Beucke[38], F Glück[42], S Gokhale[86], A de Gouvêa[73], L Gráf[67], L Grandi[21], J Grigat[38], B Grinstein[87], M G D van der Grinten[32], R Grössle[42], H Guan[10], M Guida[67], R Gumbsheimer[42], C B Gwilliam[39], C R Hall[25], L J Hall[41,44], R Hammann[67], K Han[88], V Hannen[14], S Hansmann-Menzemer[65], R Harata[89], S P Hardin[10], E Hardy[90], C A Hardy[80], K Harigaya[91,92], R Harnik[71], S J Haselschwardt[41], M Hernandez[87], S A Hertel[93], A Higuera[79], C Hils[83], S Hochrein[6], L Hoetzsch[67], M Hoferichter[94,95], N Hood[87], D Hooper[71,96], M Horn[97], J Howlett[24], D Q Huang[15], Y Huang[49], D Hunt[11], M Iacovacci[68], G Iaquaniello[53], R Ide[89], C M Ignarra[1,2], G Iloglu[10], Y Itow[89], E Jacquet[17], O Jahangir[12], J Jakob[14], R S James[12], A Jansen[42], W Ji[1,2], X Ji[25], F Joerg[67], J Johnson[31], A Joy[20], A C Kaboth[32,66], L Kalhor[3,10], A C Kamaha[49,98], K Kanezaki[99], K Kar[34], M Kara[42], N Kato[4], P Kavrigin[55], S Kazama[89], A W Keaveney[10], J Kellerer[76], D Khaitan[70], A Khazov[32], G Khundzakishvili[10], I Khurana[12], B Kilminster[6], M Kleifges[33], P Ko[100,101], M Kobayashi[89], D Kodroff[61], G Koltmann[55], A Kopec[10,87], A Kopmann[33], J Kopp[83,91], L Korley[15], V N Kornoukhov[9,102], E V Korolkova[103], H Kraus[11], L M Krauss[104], S Kravitz[41], L Kreczko[77], V A Kudryavtsev[103], F Kuger[38], J Kumar[105], B López Paredes[17], L LaCascio[76], R Laha[106], Q Laine[40], H Landsman[55], R F Lang[10,*], E A Leason[107], J Lee[108], D S Leonard[108], K T Lesko[41], L Levinson[55], C Levy[49], I Li[79], S C Li[10], T Li[109], S Liang[79], C S Liebenthal[79], J Lin[41,44], Q Lin[110], S Lindemann[38], M Lindner[67], A Lindote[54], R Linehan[1,2], W H Lippincott[37,71], X Liu[107], K Liu[60], J Liu[88],

J Loizeau[40], F Lombardi[83], J Long[21], M I Lopes[54], E Lopez Asamar[54], W Lorenzon[15], C Lu[35], S Luitz[1], Y Ma[87], P A N Machado[71], C Macolino[74], T Maeda[99], J Mahlstedt[20], P A Majewski[32], A Manalaysay[41], A Mancuso[7], L Manenti[26], A Manfredini[6], R L Mannino[13], N Marangou[17], J March-Russell[11], F Marignetti[68], T Marrodán Undagoitia[67], K Martens[5], R Martin[8], I Martinez-Soler[111], J Masbou[40], D Masson[38], E Masson[8], S Mastroianni[68], M Mastronardi[68], J A Matias-Lopes[16], M E McCarthy[70], N McFadden[6], E McGinness[44], D N McKinsey[41,44], J McLaughlin[73], K McMichael[57], P Meinhardt[38], J Menéndez[112,113], Y Meng[88], M Messina[46], R Midha[10], D Milisavljevic[10], E H Miller[1,2], B Milosevic[22], S Milutinovic[22], S A Mitra[83], K Miuchi[99], E Mizrachi[25,114], K Mizukoshi[99], A Molinario[18], A Monte[37,71], C M B Monteiro[16], M E Monzani[1,2,43], J S Moore[10], K Morå[24], J A Morad[31], J D Morales Mendoza[1,2], S Moriyama[4,5], E Morrison[29], E Morteau[40], Y Mosbacher[55], B J Mount[115], J Mueller[38], A St J Murphy[107], M Murra[24], D Naim[31], S Nakamura[116], E Nash[31], N Navaieelavasani[83], A Naylor[103], C Nedlik[93], H N Nelson[37], F Neves[54], J L Newstead[10,36], K Ni[87], J A Nikoleyczik[13], V Niro[117,118], U G Oberlack[83], M Obradovic[22], K Odgers[57], C A J O'Hare[50], P Oikonomou[26], I Olcina[41,44], K Oliver-Mallory[17], A Oranday[79], J Orpwood[103], I Ostrovskiy[30], K Ozaki[89], B Paetsch[55], S Pal[54], J Palacio[67], K J Palladino[11,13], J Palmer[66], P Panci[52,119], M Pandurovic[22], A Parlati[68], N Parveen[49], S J Patton[41], V Pěč[120], Q Pellegrini[8], B Penning[15], G Pereira[54], R Peres[6], Y Perez-Gonzalez[121], E Perry[12], T Pershing[114], R Petrossian-Byrne[122], J Pienaar[21], A Piepke[30], G Pieramico[74], M Pierre[40], M Piotter[67], V Pizzella[67], G Plante[24], T Pollmann[19], D Porzio[54], J Qi[87], Y Qie[70], J Qin[10], F Quevedo[123], N Raj[124], M Rajado Silva[38], K Ramanathan[125], D Ramírez García[38], J Ravanis[62], L Redard-Jacot[6], D Redigolo[91,126], S Reichard[6,42], J Reichenbacher[29], C A Rhyne[35], A Richards[17], Q Riffard[41,44], G R C Rischbieter[49], A Rocchetti[38], S L Rosenfeld[10], R Rosero[86], N Rupp[67], T Rushton[103], S Saha[45], P Salucci[127], L Sanchez[79], P Sanchez-Lucas[6], D Santone[66], J M F dos Santos[16], I Sarnoff[26], G Sartorelli[7], A B M R Sazzad[30], M Scheibelhut[83], R W Schnee[29], M Schrank[42], J Schreiner[67], P Schulte[14], D Schulte[14], H Schulze Eissing[14], M Schumann[38], T Schwemberger[6,64], A Schwenk[67,128,129], T Schwetz[42], L Scotto Lavina[8], P R Scovell[32], H Sekiya[4,5], M Selvi[7], E Semenov[40], F Semeria[7], P Shagin[79], S Shaw[37], S Shi[24], E Shockley[87],

T A Shutt[1,2], R Si-Ahmed[8], J J Silk[25], C Silva[54], M C Silva[16], H Simgen[67], F Šimkovic[130,131,132], G Sinev[29], R Singh[10], W Skulski[70,133], J Smirnov[20], R Smith[41,44], M Solmaz[37,76], V N Solovov[54], P Sorensen[41], J Soria[41,44], T J Sparmann[10], I Stancu[30], M Steidl[42], A Stevens[12,17], K Stifter[1,2], L E Strigari[134], D Subotic[22], B Suerfu[41,44], A M Suliga[13,44], T J Sumner[17], P Szabo[55], M Szydagis[49], A Takeda[4,5], Y Takeuchi[99], P-L Tan[20], C Taricco[18], W C Taylor[35], D J Temples[71,73], A Terliuk[65], P A Terman[134], D Thers[40], K Thieme[6], T Thümmler[42], D R Tiedt[97], M Timalsina[29], W H To[1,2], F Toennies[38], Z Tong[17], F Toschi[38], D R Tovey[103], J Tranter[103], M Trask[37], G C Trinchero[18], M Tripathi[31], D R Tronstad[29], R Trotta[17,135], Y D Tsai[136], C D Tunnell[79], W G Turner[137], R Ueno[99], P Urquijo[36], U Utku[12], A Vaitkus[35], K Valerius[42], E Vassilev[79], S Vecchi[7], V Velan[44], S Vetter[76], A C Vincent[138], L Vittorio[51,52], G Volta[6], B von Krosigk[42], M von Piechowski[14], D Vorkapic[22], C E M Wagner[21,139], A M Wang[1,2], B Wang[30], Y Wang[41,44], W Wang[13,93], J J Wang[15,30], L-T Wang[21], M Wang[140], Y Wang[70], J R Watson[41,44], Y Wei[87], C Weinheimer[14], E Weisman[10], M Weiss[55], D Wenz[83], S M West[66], T J Whitis[1,37], M Williams[15], M J Wilson[42], D Winkler[67], C Wittweg[6], J Wolf[76], T Wolf[67], F L H Wolfs[70], S Woodford[39], D Woodward[61], C J Wright[77], V H S Wu[42], P Wu[141], S Wüstling[33], M Wurm[83], Q Xia[41], X Xiang[35], Y Xing[40], J Xu[114], Z Xu[24], D Xu[60], M Yamashita[5], R Yamazaki[89], H Yan[113], L Yang[87], Y Yang[88], J Ye[87], M Yeh[86], I Young[71], H B Yu[142], T T Yu[64], L Yuan[21], G Zavattini[143], S Zerbo[24], Y Zhang[24], M Zhong[87], N Zhou[88], X Zhou[144], T Zhu[24], Y Zhu[40], Y Zhuang[134], J P Zopounidis[8], K Zuber[145] and J Zupan[56]

[1] SLAC National Accelerator Laboratory, Menlo Park, CA 94025, United States of America

[2] Kavli Institute for Particle Astrophysics and Cosmology, Stanford University, Stanford, CA 94305, United States of America

[3] Department of Physics, Shahid Beheshti University, Tehran, Islamic Republic of Iran

[4] Kamioka Observatory, Institute for Cosmic Ray Research, The University of Tokyo, Higashi-Mozumi, Kamioka, Hida, Gifu, 506-1205, Japan

[5] Kavli Institute for the Physics and Mathematics of the Universe (WPI), The University of Tokyo, Kashiwa, Chiba, 277-8582, Japan

[6] Physik-Institut, University of Zurich, 8057 Zurich, Switzerland

[7] Department of Physics and Astronomy, University of Bologna and INFN-Bologna, 40126 Bologna, Italy

[8] LPNHE, Sorbonne Université, CNRS/IN2P3, 75005 Paris, France

[9] National Research Nuclear University 'MEPhI' (Moscow Engineering Physics Institute), Moscow, 115409, Russia

[10] Department of Physics and Astronomy, Purdue University, West Lafayette, IN 47907, United States of America
[11] Department of Physics, University of Oxford, Keble Rd, Oxford OX1 3RH, United Kingdom
[12] Department of Physics and Astronomy, University College London, London WC1E 6BT, United Kingdom
[13] Department of Physics, University of Wisconsin−Madison, Madison, WI 53706, United States of America
[14] Institut für Kernphysik, Westfälische Wilhelms-Universität Münster, 48149 Münster, Germany
[15] University of Michigan, Randall Laboratory of Physics, Ann Arbor, MI 48109, United States of America
[16] LIBPhys, Department of Physics, University of Coimbra, 3004-516 Coimbra, Portugal
[17] Department of Physics, Blackett Laboratory, Imperial College London, London SW7 2BW, United Kingdom
[18] INAF-Astrophysical Observatory of Torino, Department of Physics, University of Torino and INFN-Torino, 10125 Torino, Italy
[19] Nikhef and the University of Amsterdam, Science Park, 1098XG Amsterdam, The Netherlands
[20] Oskar Klein Centre, Department of Physics, Stockholm University, AlbaNova, Stockholm SE-10691, Sweden
[21] Department of Physics & Kavli Institute for Cosmological Physics, The University of Chicago, Chicago, IL 60637, United States of America
[22] Vinca Institute of Nuclear Science, University of Belgrade, Mihajla Petrovica Alasa 12−14, Belgrade, Serbia
[23] Faculty of Architecture, Civil Engineering and Geodesy, University of Banja Luka, Bulevar vojvode Petra Bojovica 1a, 78000 Banja Luka, Bosnia and Herzegovina
[24] Physics Department, Columbia University, New York, NY 10027, United States of America
[25] Department of Physics, University of Maryland, College Park, MD 20742, United States of America
[26] Division of Science, New York University Abu Dhabi, Saadiyat Island, Abu Dhabi, United Arab Emirates
[27] Center for Theoretical Physics, Massachusetts Institute of Technology, Cambridge, MA 02139, United States of America
[28] Department of Physics, Korea University, Anam-ro 145, Sungbuk-gu, Seoul 02841, Republic of Korea
[29] South Dakota School of Mines and Technology, Rapid City, SD 57701, United States of America
[30] University of Alabama, Department of Physics & Astronomy, Tuscaloosa, AL 34587, United States of America
[31] University of California Davis, Department of Physics, One Shields Ave., Davis, CA 95616, United States of America
[32] STFC Rutherford Appleton Laboratory (RAL), Didcot, OX11 0QX, United Kingdom
[33] Institute for Data Processing and Electronics, Karlsruhe Institute of Technology, Karlsruhe, Germany
[34] Ramakrishna Mission Vivekananda Educational and Research Institute, Belur Math, Howrah 711202, India
[35] Department of Physics, Brown University, 182 Hope Street, Providence, RI 02912, United States of America

[36] ARC Centre of Excellence for Dark Matter Particle Physics, School of Physics, The University of Melbourne, VIC 3010, Australia
[37] Department of Physics, University of California, Santa Barbara, Santa Barbara, CA 93106, United States of America
[38] Physikalisches Institut, Universität Freiburg, 79104 Freiburg, Germany
[39] University of Liverpool, Department of Physics, Liverpool L69 7ZE, United Kingdom
[40] SUBATECH, IMT Atlantique, Université de Nantes, CNRS/IN2P3, Nantes 44307, France
[41] Lawrence Berkeley National Laboratory, Berkeley, CA 94720, United States of America
[42] Institute for Astroparticle Physics, Karlsruhe Institute of Technology, Karlsruhe, Germany
[43] Vatican Observatory, Castel Gandolfo, V-00120, Vatican City State
[44] Department of Physics, University of California Berkeley, Berkeley, CA 94720, United States of America
[45] Saha Institute of Nuclear Physics, HBNI, 1/AF Bidhannagar, Kolkata 700064, India
[46] INFN-Laboratori Nazionali del Gran Sasso and Gran Sasso Science Institute, 67100 L'Aquila, Italy
[47] Deutsches Elektronen-Synchrotron DESY, Notkestr. 85, 22607 Hamburg, Germany
[48] Department of Physics, Princeton University, Princeton, NJ 08544, United States of America
[49] Department of Physics, The University at Albany, The State University of New York, Albany, NY 12222, United States of America
[50] School of Physics, The University of Sydney, NSW 2006 Camperdown, Sydney, Australia
[51] Scuola Normale Superiore, Piazza dei Cavalieri 7, 56126 Pisa, Italy
[52] INFN, Sezione di Pisa, Largo Bruno Pontecorvo 3, I-56127 Pisa, Italy
[53] LAL, Université Paris-Sud, CNRS/IN2P3, Université Paris-Saclay, F-91405 Orsay, France
[54] LIP-Coimbra, Department of Physics, University of Coimbra, 3004-516 Coimbra, Portugal
[55] Department of Particle Physics and Astrophysics, Weizmann Institute of Science, Rehovot 7610001, Israel
[56] Department of Physics, University of Cincinnati, Cincinnati, OH 45221, United States of America
[57] Department of Physics, Applied Physics and Astronomy, Rensselaer Polytechnic Institute, Troy, NY 12180, United States of America
[58] Budker Institute of Nuclear Physics SB RAS, Lavrentiev Avenue 11, 630090 Novosibirsk, Russia
[59] Novosibirsk State University, Pirogov Street 2, 630090 Novosibirsk, Russia
[60] Department of Physics & Center for High Energy Physics, Tsinghua University, Beijing 100084, People's Republic of China
[61] Department of Physics, Pennsylvania State University, 104 Davey Lab, University Park, PA 16802, United States of America
[62] Chalmers University of Technology, Department of Physics, SE-412 96 Göteborg, Sweden
[63] Department of Physics, Indian Institute of Technology—Guwahati, Guwahati 781039, India
[64] Department of Physics and Institute for Fundamental Science, University of Oregon, Eugene, OR 97403, United States of America

[65] Physikalisches Institut, Ruprecht-Karls-Universität Heidelberg, Heidelberg, Germany
[66] Royal Holloway, University of London, Department of Physics, Egham, TW20 0EX, United Kingdom
[67] Max-Planck-Institut für Kernphysik, 69117 Heidelberg, Germany
[68] Department of Physics 'Ettore Pancini', University of Napoli and INFN-Napoli, 80126 Napoli, Italy
[69] William I Fine Theoretical Physics Institute, School of Physics and Astronomy, University of Minnesota, Minneapolis, MN 55455, United States of America
[70] Department of Physics and Astronomy, The University of Rochester, Rochester, NY 14627, United States of America
[71] Fermi National Accelerator Laboratory, Batavia, IL 60510, United States of America
[72] Dublin Institute for Advanced Studies, Dublin, D02 XF86, Ireland
[73] Department of Physics & Astronomy, Northwestern University, Evanston, IL 60208, United States of America
[74] Department of Physics and Chemistry, University of L'Aquila, 67100 L'Aquila, Italy
[75] Department of Physics, Sam Houston State University, Huntsville, TX 77341, United States of America
[76] Institute of Experimental Particle Physics, Karlsruhe Institute of Technology, Karlsruhe, Germany
[77] University of Bristol, H H Wills Physics Laboratory, Bristol, BS8 1TL, United Kingdom
[78] Physics, King's College London, Strand, London WC2R 2LS, United Kingdom
[79] Department of Physics and Astronomy, Rice University, Houston, TX 77005, United States of America
[80] Physics Department, Stanford University, Stanford, CA 94305, United States of America
[81] Università degli Studi and INFN Roma Tre, Via della Vasca Navale 84, I-00146, Rome, Italy
[82] Institute for Computational Cosmology, Department of Physics, University of Durham, South Road, Durham, DH1 3LE, United Kingdom
[83] Institut für Physik & Exzellenzcluster PRISMA, Johannes Gutenberg-Universität Mainz, 55099 Mainz, Germany
[84] Kavli Institute for Theoretical Physics, University of California, Santa Barbara, CA 93106, United States of America
[85] IPHC, CNRS, 67037 Strasbourg, France
[86] Brookhaven National Laboratory (BNL), Upton, NY 11973, United States of America
[87] Department of Physics, University of California San Diego, La Jolla, CA 92093, United States of America
[88] School of Physics and Astronomy, Shanghai Jiao Tong University, Shanghai, 200240, People's Republic of China
[89] Kobayashi–Maskawa Institute for the Origin of Particles and the Universe, and Institute for Space–Earth Environmental Research, Nagoya University, Aichi 464-8602, Japan
[90] University of Liverpool, Department of Mathematical Sciences, Liverpool L69 3BX, United Kingdom
[91] Theoretical Physics Department, CERN, 1211 Geneva 23, Switzerland
[92] School of Natural Sciences, Institute for Advanced Study, Princeton, NJ 08540, United States of America

[93] Department of Physics, University of Massachusetts, Amherst, MA 01003, United States of America
[94] Albert Einstein Center for Fundamental Physics, Institute for Theoretical Physics, University of Bern, Sidlerstrasse 5, 3012 Bern, Switzerland
[95] Institute for Nuclear Theory, University of Washington, Seattle, WA 98195, United States of America
[96] Department of Astronomy and Astrophysics & Kavli Institute for Cosmological Physics, The University of Chicago, Chicago, IL 60637, United States of America
[97] South Dakota Science and Technology Authority (SDSTA), Sanford Underground Research Facility, Lead, SD 57754, United States of America
[98] Physics & Astronomy Department, University of California, Los Angeles, CA 90095, United States of America
[99] Department of Physics, Kobe University, Kobe, Hyogo 657-8501, Japan
[100] School of Physics, KIAS, 85 Hoegiro, Seoul 02455, Republic of Korea
[101] Quantum Universe Center, KIAS, 85 Hoegiro, Seoul 02455, Republic of Korea
[102] Institute for Nuclear Research, Moscow, 117312, Russia
[103] University of Sheffield, Department of Physics and Astronomy, Sheffield S3 7RH, United Kingdom
[104] Origins Project Foundation, Phoenix, AZ 85020, United States of America
[105] Department of Physics and Astronomy, University of Hawai'i, Honolulu, HI 96822, United States of America
[106] Centre for High Energy Physics, Indian Institute of Science, Bangalore 560012, India
[107] SUPA, School of Physics and Astronomy, University of Edinburgh, Edinburgh, EH9 3FD, United Kingdom
[108] IBS Center for Underground Physics (CUP), Yuseong-gu, Daejeon, Republic of Korea
[109] School of Physics, Nankai University, Tianjin 300071, People's Republic of China
[110] Department of Physics, University of Science and Technology of China, Hefei, Anhui, People's Republic of China
[111] Department of Physics & Laboratory for Particle Physics and Cosmology, Harvard University, Cambridge, MA 02138, United States of America
[112] Department of Quantum Physics and Astrophysics and Institute of Cosmos Sciences, University of Barcelona, 08028 Barcelona, Spain
[113] Center for Nuclear Study, The University of Tokyo, 113-0033 Tokyo, Japan
[114] Lawrence Livermore National Laboratory, Livermore, CA 94550, United States of America
[115] Black Hills State University, School of Natural Sciences, Spearfish, SD 57799, United States of America
[116] Department of Physics, Faculty of Engineering, Yokohama National University, Yokohama, Kanagawa 240-8501, Japan
[117] Université de Paris, CNRS, Astroparticule et Cosmologie, F-75013 Paris, France
[118] Institute for Theoretical Physics, University of Heidelberg, Philosophenweg 16, D-69120 Heidelberg, Germany
[119] Dipartimento di Fisica E Fermi, Università di Pisa, Largo B Pontecorvo 3, I-56127 Pisa, Italy
[120] Institute of Physics, Czech Academy of Sciences, 182 00 Prague, Czech Republic
[121] Institute for Particle Physics Phenomenology, Durham University, South Road, Durham, United Kingdom
[122] International Centre for Theoretical Physics, Strada Costiera 11, 34151, Trieste, Italy

[123] DAMTP, University of Cambridge, Wilberforce Road, Cambridge, CB3 0WA, United Kingdom
[124] TRIUMF, 4004 Wesbrook Mall, Vancouver, BC V7A 4N4, Canada
[125] Division of Physics, Mathematics, & Astronomy, California Institute of Technology, Pasadena, CA 91125, United States of America
[126] INFN, Sezione di Firenze Via G Sansone 1, 50019 Sesto Fiorentino, Italy
[127] SISSA, Astrophysics and Cosmology Group, Via Bonomea 265, 34136 Trieste, Italy
[128] Department of Physics, Technische Universität Darmstadt, 64289 Darmstadt, Germany
[129] ExtreMe Matter Institute EMMI, GSI Helmholtzzentrum für Schwerionenforschung GmbH, 64291 Darmstadt, Germany
[130] Bogoliubov Laboratory of Theoretical Physics, Joint Institute for Nuclear Research, 141980 Dubna, Russia
[131] Department of Nuclear Physics and Biophysics, Comenius University, Mlynská dolina F1, SK-842 15 Bratislava, Slovakia
[132] Institute of Experimental and Applied Physics, Czech Technical University, 128 00 Prague, Czech Republic
[133] SkuTek Instrumentation, West Henrietta, NY 14586, United States of America
[134] Mitchell Institute for Fundamental Physics and Astronomy, Texas A & M University, College Station, TX 77843, United States of America
[135] SISSA, Theoretical and Scientific Data Science Group, Via Bonomea 265, 34136 Trieste, Italy
[136] Department of Physics and Astronomy, University of California, Irvine, CA 92697, United States of America
[137] Oliver Lodge Laboratory, University of Liverpool, Liverpool, United Kingdom
[138] Department of Physics, Engineering Physics and Astronomy, Queen's University, Kingston ON K7L 3N6, Canada
[139] High Energy Physics Theory Group, Argonne National Laboratory Argonne, IL 60439, United States of America
[140] School of Physics, Shandong University, Jinan, 250100, People's Republic of China
[141] School of Physics, Southeast University, Nanjing 211189, People's Republic of China
[142] Department of Physics and Astronomy, University of California, Riverside, CA 92521, United States of America
[143] Department of Physics and Earth Sciences, University of Ferrara and INFN-Ferrara, 44122, Italy
[144] School of Physics, Beihang University, Beijing, 100083, People's Republic of China
[145] Technische Universität Dresden, 01069 Dresden, Germany

E-mail: rafael@purdue.edu

Received 30 March 2022, revised 22 June 2022
Accepted for publication 26 July 2022
Published 22 December 2022

Abstract

The nature of dark matter and properties of neutrinos are among the most pressing issues in contemporary particle physics. The dual-phase xenon time-projection chamber is the leading technology to cover the available parameter

space for weakly interacting massive particles, while featuring extensive sensitivity to many alternative dark matter candidates. These detectors can also study neutrinos through neutrinoless double-beta decay and through a variety of astrophysical sources. A next-generation xenon-based detector will therefore be a true multi-purpose observatory to significantly advance particle physics, nuclear physics, astrophysics, solar physics, and cosmology. This review article presents the science cases for such a detector.

Keywords: dark matter, neutrinoless double-beta decay, neutrinos, supernova, direct detection, astroparticle physics, xenon

(Some figures may appear in colour only in the online journal)

Contents

1. Introduction

1.1. An observatory for rare events

Identifying the true nature of dark matter is one of the most important questions in physics today. As we show in this review, liquid xenon time projection chambers (TPCs) are the leading technology in searches for a large variety of dark matter particle candidates. Following two decades of evolution of this technology, now is the time to design the next-generation dark matter experiment in order to probe the widest possible range of dark matter candidates. A possible realization of such a detector has been proposed by the DARWIN collaboration [1] and is pursued by the XLZD consortium. This experiment will also have competitive sensitivity to search for neutrinoless double-beta decay and other rare events. Furthermore, we show in this review that such an experiment serves as a versatile astroparticle physics observatory that is sensitive to neutrinos from our Sun, the atmosphere, and Galactic supernovae. Figures 1 and 2 illustrate these topics.

1.2. Evidence for dark matter

Strong evidence on astronomical and cosmological scales suggests gravitational interaction between baryonic matter and an unknown type of non-luminous matter, called dark matter [2]. First evidence that much matter in the Universe remained unseen in telescopes started to accumulate already in the early 1900s [3, 4]. This motivated the original use of the term 'dark matter' to mean invisible matter whose existence is inferred only from its gravitational effects, possibly in the form of dark stars [5]. In 1922, James Jeans realized that 'there must be about three dark stars in the Universe to every bright star' [6]. The next decade, Jan Oort used the vertical kinematics of Milky Way stars to constrain the local dark matter content [7], while Fritz Zwicky became the first to use the virial theorem to infer the presence of dark matter within the Coma Cluster [8].

Crucial evidence for dark matter in galaxies came in the late 1970s when Vera Rubin and collaborators established that optical rotation velocities of stars in spiral galaxies consistently differ from those expected from the distribution of their baryonic matter [9, 10]. Albert Bosma soon after confirmed this finding by means of 21 cm rotation curves, well outside the edge of stellar disks [11]. Galactic rotation curves [12, 13] and dynamics [14, 15] provide evidence for the existence of a uniformly-distributed halo of dark matter around all spiral galaxies and very likely around every Galaxy [16]. The critical role of dark matter in the formation of galaxies [17] such as our own Milky Way [18] underlines its significance to our very existence.

Evidence for dark matter has now been found across all time and length scales [19], spanning from the Big Bang to today, and from the cosmos as a whole down to individual galaxies [20]. Gravitational effects of dark matter can be observed in the cosmic microwave background (CMB), e.g. with the Planck satellite [21]. Detailed measurements of the power spectrum from the CMB put the dark matter mass–energy density at five times that of baryonic matter [22] and significantly constrain any electromagnetic coupling of dark matter [23]. Our understanding of large-scale structure formation points to the existence of non-relativistic (cold) dark matter [24–26]. Gravitational lensing suggests the presence of a significant amount of non-baryonic matter with no observable electromagnetic interaction [27], both when observing strong (e.g. reference [28]) and weak lensing (e.g. reference [29]). Merging Galaxy clusters, made famous by the initial reports from the Bullet Cluster [30], have now become a laboratory for dark matter physics [31]. Taken together, cosmological and astrophysical observations are not only used to identify some of the characteristics of dark matter [32], but in particular also to constrain its coupling to ordinary matter [33].

Science Drivers

- The ultimate probe of WIMPs down to the neutrino fog, with potentially transformative implications for particle physics and our view of the Universe
- A competitive and economic search for neutrinoless double-beta decay, which is so fundamental to nuclear physics and the origin of matter
- Measurements of multiple astrophysical neutrino signals at lowest energies, with key insights into the physics of neutrinos, our Sun, and supernova explosions

Figure 1. Main science drivers for the next-generation liquid xenon observatory.

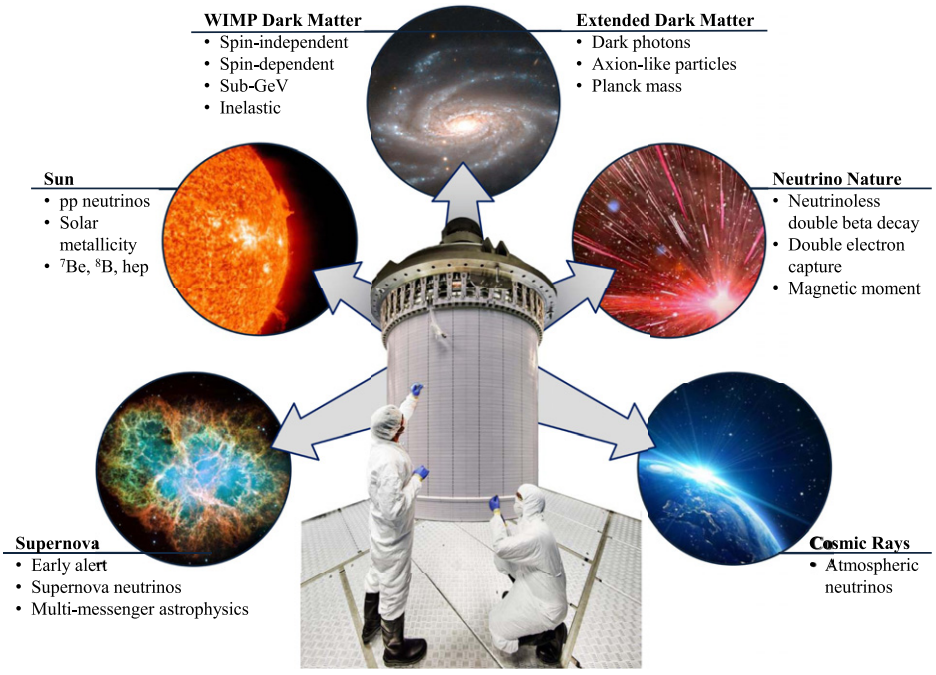

Figure 2. The science channels of a next-generation liquid xenon observatory for rare events spans many areas and is of interest to particle physics, nuclear physics, astrophysics, solar physics, and cosmology.

A precise determination of the local dark matter halo density is required for interpreting results from direct detection experiments. Observational density estimates come from a variety of studies [18, 34, 35]. Methods used to determine the local dark matter density can be broadly classified into local methods and global methods. Local methods focus on dynamics of stars in a small volume around the Solar System, while global methods determine the dark matter

halo in the whole Galaxy and obtain the local dark matter density from our position within it. Global methods based on the galactic rotation curve yield a local density $\varrho = (0.4–0.5)$ GeV cm^{-3} [36]. Using the Gaia data release 2 [37], the local density has recently been determined to be in the range $\varrho = (0.3–0.4)$ GeV cm^{-3} [38], in good agreement with the former values when one adopts the same local speed $v_\odot$. Local methods in contrast yield a wider range of $\varrho = (0.4–1.5)$ GeV cm^{-3} [39–41] with some tendency toward higher values [42]. Note though that the two methods, global and local, measure, in principle, different quantities: the properties of a sphere of 1 kpc radius around the Sun could be different with respect to the average $(D/\text{kpc})^2$ spheres located at the same galactocentric distance D which are considered by global methods. When presenting results from direct dark matter searches, it is common to assume $\varrho = 0.3$ GeV cm^{-3} [43], which ensures both historical compatibility of the derived direct detection results, as well as a conservative interpretation of such results.

While the existence of dark matter is thus well established, its physical characteristics remain elusive. The absence of electromagnetic coupling observed in the CMB, the lack of any observed thermal emission from dark matter, and the dynamics of merging Galaxy clusters, indicate that dark matter takes the form of new quanta outside the current Standard Model (SM) of particle physics [44]. The nature of this non-baryonic dark matter is still unknown: its existence is one of the strongest pieces of evidence that the current theory of fundamental particles and forces, summarized in the SM, is incomplete. A number of proposed candidates have been put forward over time, with some of the most popular candidates being probed by the experiment discussed here, as elaborated in sections 2 and 3.

1.3. Dark matter direct detection

The fact the cosmological dark and luminous matter densities are of the same order [21], as well as observed scaling relations in galaxies [45], suggest that the dark sector and the SM are coupled through additional interactions stronger than gravity. Since the 1980s, there have been large efforts to develop experiments on Earth that are able to directly search for dark matter, particularly for weakly interacting massive particles (WIMPs) [46–49], one popular dark matter candidate. Given the low expected interaction strength, the probability of multiple collisions of dark matter particles within a detector is negligible, resulting in a recoil spectrum of single scattering events.

In the effort to directly detect dark matter, many technologies have been developed to measure dark matter interactions with target nuclei. Complementary searches with different targets, discussed further in section 8, are essential to unveil the nature of dark matter. In the most common approach, experiments attempt to measure the nuclear recoil (NR) energy produced by collisions between dark matter candidates and target nuclei in the detector. The recoiling nucleus can deposit energy in the form of ionization, heat, and/or light that is subsequently detected. Different technologies have been explored so far to achieve this goal [50]. Successful targets include solid state crystals [51–59], metastable fluids [60, 61], and noble liquids [62–67].

A possible dark matter signature would be an annual modulation of the interaction count rate due to the motion of the Earth around the Sun [48, 49, 68]. The relative velocity of dark matter particles in the Milky Way halo with respect to the detector on Earth depends on the time of year; therefore, the measured count rate is expected to exhibit a sinusoidal dependence with time, where the amplitude and phase of modulation will depend on the dark matter distribution within the halo [69]. While there is general consensus on standard values to be used to calculate expectations for direct experiments [43], this scenario can be modified in a number of possible

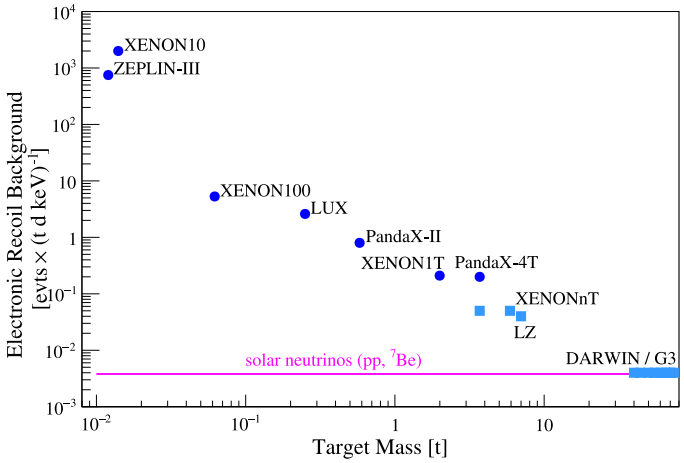

Figure 3. The background rates in liquid xenon TPCs (before ER/NR discrimination) have decreased exponentially over the years. This has been a key accomplishment that has enabled an exponential gain in sensitivity with ever-larger detectors. Solid dots are the best achieved limits, open squares the expected sensitivities. The experiment discussed here is labeled DARWIN/G3 and will at low energies be dominated by the signal from solar neutrinos. See text for references.

astrophysical scenarios such as the presence of dark matter streams [70, 71], halo substructure [72–74], a dark disk [75] or local captured populations of WIMPs resulting from interactions in the Sun [76] and Earth [77], which all have the common feature of *increasing* the local dark matter density.

1.4. An evolution of scales

Liquid xenon TPCs in particular have demonstrated their exceptional capabilities for rare event detection as a result of an intense, decade-long development. The interested reader is referred to [78–80] for detailed discussions of this technique. The two-phase (or dual-phase) emission detector that underlies liquid xenon TPCs was proposed a half-century ago [81]. Its use for the detection of dark matter particles and neutrinos was proposed in 1995 [82], with more mature conceptional designs developed around the turn of the millennium [83, 84]. Evolving out of ZEPLIN-I [85], the ZEPLIN-II [86] detector was the first two-phase xenon dark matter experiment, with both experiments setting competitive limits on WIMP interactions at that time. This technology was further advanced in ZEPLIN-III [87, 88] and with XENON10 [89] saw the first leading limits on WIMP interactions. XMASS built the first two-phase xenon dark matter detector underground [90], and with a single-phase detector provided an impressive demonstration of fiducialization in liquid xenon (section 7.2) [91]. Further evolution progressed through successively larger, cleaner, and thus more sensitive detectors: from XENON100 [92, 93], LUX [63], PandaX-I [94] and PandaX-II [95] to XENON1T [96] and the current generation PandaX-4T [97], XENONnT [98], and LZ [99] (figure 3).

In 2021, scientists from the DARWIN/XENON and LZ collaborations signed a Memorandum of Understanding, forming the XLZD consortium, to jointly work on the design, construction and eventual operation of a next-generation detector. This experiment is labeled DARWIN/G3 in figure 3 [100] and represents a natural continuation of this evolution toward larger xenon exposures, as presented in the sensitivity studies shown below. Scaling up the same mature technology (to a compact size of only $\sim$3 m in height and diameter), and exploiting the

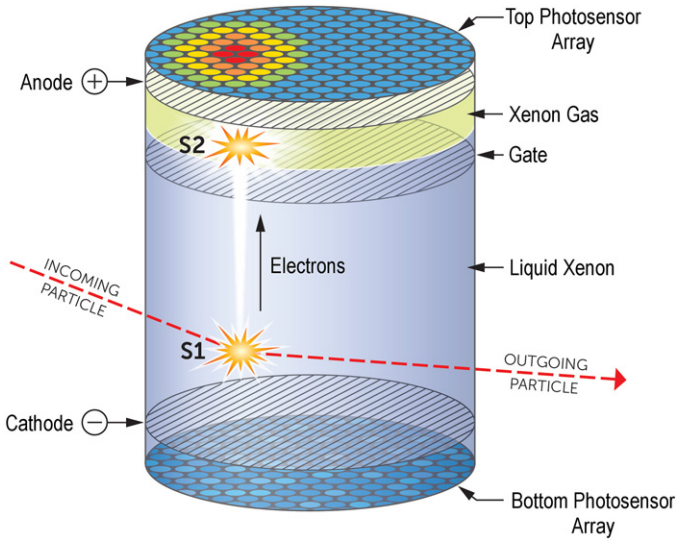

Figure 4. Principle of a dual-phase liquid xenon TPC. Energy from a particle interaction within the active liquid xenon volume produces prompt scintillation light (S1) and a delayed signal (S2) from electroluminescence (proportional scintillation) in the gaseous xenon layer. The localization of the S2 signal and the time difference between S1 and S2 allows for determination of the original vertex location.

collective experience of the participating scientists, drastically reduces risks otherwise inherent in such projects. Continued research and development is ongoing using dozens of dedicated setups at the participating institutions. At the same time, experience from the operation and analysis of the current generation of detectors provides important lessons. It is thus timely to review the science case of such a rare event observatory.

1.5. The liquid xenon time projection chamber

Conventionally, a next generation liquid xenon TPC will consist of a central liquid xenon volume surrounded by light reflectors for vacuum ultra-violet (VUV) light, allowing maximum light detection [101]. Two arrays of light sensors, such as photomultiplier tubes (PMTs) [102, 103] or silicon photomultipliers (SiPMs) [104, 105], are arranged on the top and bottom part of the TPC to detect light signals, see figure 4.

A particle incident on the liquid xenon target deposits energy and produces both prompt scintillation light and ionization electrons. The scintillation signal is immediately detected by the photosensors as the S1 signal. The *active* liquid xenon volume is defined by a cathode and a gate electrode, separated by $\sim$3 m to provide a drift field for the electrons. These drifting ionization electrons are then extracted into the gas phase above the liquid xenon, where they produce electroluminescent light [106]. Typical dual phase detectors operate at $\sim$1.5 bar, where 5 kV cm^{-1} for the extraction field is sufficient to create proportional scintillation. This electroluminescence is then detected by the same photosensors and is known as the S2 signal [101, 107, 108].

The time delay between S1 and S2 in addition to the localization of the S2 light pattern on the top photosensor array [109–111] allows precise reconstruction of the three-dimensional interaction vertex [112]. Fiducialization in event selection (section 7.2) enables an effective way to suppress external gamma and neutron background for all rare event searches and to

minimize effects from imperfections of the TPC near its surface. The ratio of S2 and S1 signals further allows for discrimination between different types of interaction in the liquid xenon TPC: NRs and electronic recoils (ER). NRs are most notably induced by WIMPs, through coherent elastic neutrino-nucleus scattering (CEνNS), and by neutrons; whereas ERs are produced by gamma rays and internal beta decays [113, 114]. NRs exhibit a lower S2/S1 ratio and can therefore be distinguished from ERs [114, 115]. Excellent energy resolution further helps to differentiate various signals from relevant background [116]. As we explain in section 3.2, the scientific reach of these TPCs can be extended toward lower energies by dropping the requirement of the presence of an S1; this results in sensitivity to single electrons.

1.6. Xenon as a detector medium

Xenon as a detection medium exhibits several desirable features [117, 118], giving it a significant advantage as a target material. Xenon has a very low work function, requiring only 11.5 eV averaged over scintillation and ionization to produce an excitation [119]. This leads to signal yields as high as $\sim$65 photons per keV for gamma rays that are of order $\sim$100 keV [120, 121], similar to other excellent scintillators such as NaI and CsI. For NRs, the yields are still $\sim$10% of that, even below $\sim$10 keV [122, 123]. Energy resolutions better than 1% (σ/E) have been achieved at MeV scales [116] and mm-level position resolution can routinely be achieved [105, 124, 125].

Liquid xenon is a well-understood and well-characterized detector medium. Based on world data, its response can be accurately modeled using the Noble Element Simulation Technique (NEST), a code package to simulate interactions in liquid xenon (and argon) and their detection in a TPC [121, 126–128]. This includes various interactions of interest, such as ERs induced by gamma and beta rays, NRs, energy deposits by alphas, and more complex decays such as that from ^{83m}Kr. These models have been demonstrated to correctly reproduce the mean yields and their widths across a wide range of detector parameters and energies even down to 300 eV, making this simulation package a mature, comprehensive tool for liquid xenon experiments. As a result of this and other efforts [129–135], the light and charge yields can now be accurately described and predicted, with good comparisons to existing calibration data sets, as a function of energy, stopping power, drift electric field, extraction electric field, particle and interaction type, and in some cases even concerning density, phase, and angle of the recoil relative to the drift field.

Liquid xenon may be naturally contaminated with radioactive isotopes that could produce a dark matter background, such as ^{37}Ar, ^{85}Kr or ^{222}Rn. However, purification to very high levels has already been demonstrated in dark matter [63, 96, 136, 137] and neutrinoless double-beta decay experiments [138]. Cosmogenically-produced ^{37}Ar decays away quickly [139], and purity levels achieved for ^{85}Kr are already sufficient for the next-generation detector discussed here. Further advantages of xenon are obtained through its high charge number Z, mass number A, and density; these allow for self-shielding of gamma-ray and neutron backgrounds, which will multiply-scatter, especially in the outer limits of the fiducial volume (FV). Xenon also contains odd-neutron isotopes for spin-dependent neutron coupling (section 2.4), and enough residual spin-dependent proton sensitivity to produce competitive results for that science channel. In addition, natural xenon possesses promising isotopes for the search for neutrinoless double-beta decay (section 4.1) and double electron capture (section 4.2). Finally, the mass of the xenon nucleus makes it kinematically ideal for WIMPs in the mass range above $\sim$10 GeV/c^2.

In the following sections, we highlight the science case for a large, next-generation liquid xenon TPC detector for astroparticle physics. In section 2, we overview various WIMP dark matter models, and the expected sensitivity when probing such models. In section 3, we discuss

other dark matter models that a next-generation liquid xenon TPC is sensitive to. In section 4, we review double-beta processes to probe physics beyond the SM. In section 5, we discuss the science channels using neutrinos for astroparticle physics and particle physics. In section 6, we collect physics channels that are not part of the above categories. Mitigation and rejection of detector backgrounds is sketched out in section 7. The relation of a next-generation liquid xenon TPC to other future experimental efforts is discussed in section 8. Finally, we review some of the already-documented support for such a detector in the particle physics community in section 9 before concluding in section 10.

2. Dark matter WIMPs

2.1. WIMP direct detection

A well-motivated candidate for particle dark matter is the WIMP [140, 141]. This is a special case of a thermal relic particle, i.e., one that in the early Universe was in thermal equilibrium with the primordial plasma, permanently annihilating and being produced. Once the annihilation rate becomes slower than the Hubble expansion rate, the particle is said to *freeze out*, its relic density becoming fixed at that point [20]. While the list of possible dark matter candidates is now quite long, the WIMP model remains a leading scenario, with large regions of well-motivated yet unprobed parameter space [142]. The hierarchy problem [143], specifically the surprisingly and unnaturally low mass of the Higgs particle, continues to strongly motivate searches for new physics and new particles at the $\sim$100 GeV scale of the electroweak force [44]. In addition, if a new stable particle existed in this mass range, and if it interacted with SM particles via some force also at the electroweak scale, then a simple thermal freeze-out process in the early Universe would result in the observed dark matter density [144]. While this link most tightly constrains the WIMP annihilation cross-section [145], crossing symmetry provides a connection to the direct scattering cross-section as well. It is this surprising connection of particle physics at the weak scale and the evolution of the macroscopic density in the early Universe that continues to motivate searches for WIMP dark matter. Few other models can point to as clear a convergence.

The assumption of a massive (electroweak scale) mediator implies a lower bound on the WIMP mass, the so-called Lee-Weinberg limit [146]. A heavy mediator will suppress the dark matter annihilation cross section. Thus, for dark matter with a mass of less than $\sim$2 GeV$/c^2$, the thermal freeze-out process of the early Universe ends too early and results in a dark matter density that is too high and inconsistent with observation.

Because WIMPs are so well-motivated, searches for particles satisfying these criteria are underway in parallel following three general and complementary strategies [147, 148] (see also section 8): (1) WIMP production at high energy colliders such as the Large Hadron Collider (LHC) [149]; (2) indirectly via WIMP annihilation in dense astrophysical environments that produce astrophysical signals in various SM particle channels [150]; and (3) directly via observation of NRs produced by dark matter scattering as proposed here [48, 151]. This latter approach is particularly powerful. In fact, the original WIMP in the sense of a weak interaction via Z-boson exchange at tree level was ruled out using direct detection already in 1987 [152]. Today, experiments such as the one discussed here probe scattering cross-sections typical of e.g. coupling via a Z boson at loop level, or some of the well-motivated models discussed in this section. The next-generation liquid xenon-based experiment discussed here is thus complementary to the next generation of astrophysical searches [153] and the high-luminosity LHC [154] and at a similar time scale.

Direct detection experiments are particularly interesting for a variety of reasons. As scattering interactions happen at energies far below the electroweak scale itself, the interaction

mechanism can be simplified and described as a contact interaction. A diverse set of high-energy models will therefore appear nearly identical at these low energies, distinguished almost exclusively by the characteristic scattering cross section. This generality of direct detection via low-energy scattering is a significant advantage to this detection approach. Also, for a large set of WIMP models and a wide range of WIMP masses, direct dark matter experiments depend only linearly on the local dark matter density, which makes results robust against astrophysical uncertainties. Further, for relics produced by the freeze-out process, such as WIMPs, the relic density is inversely related to the thermal annihilation cross section, such that a dimensional argument can be made that the expected scattering rate in a detector (which goes like density times cross section) should be roughly independent of details of the theory. Another expression of the generality of the direct detection approach is its sensitivity to a large mass range [155]. The kinematics for non-relativistic scattering remain unchanged once the WIMP mass is much larger than the target mass, rendering these experiments sensitive to dark matter masses well beyond 100 TeV (and in principle even up to the Planck mass [156], see section 3.15). Thus, a single experiment can probe many orders of magnitude of the allowed dark matter mass parameter space.

Xenon in particular is expected to couple well to WIMP dark matter for several reasons [157]. First, in the low momentum-transfer regime of direct detection, a generic spin-independent scattering (section 2.3) will interact with the nucleus as a whole as a many-nucleon object, and this coherence provides a significant boost to the corresponding scattering cross section [47, 48], scaling roughly as the square of the number of nucleons. Therefore, a heavy nucleus like xenon is significantly favored over lighter options. A second advantage is the large number of common natural xenon isotopes, resulting in a diversity of nuclear properties. This variety of isotopes gives xenon significant sensitivity to other interaction models as well, such as spin-dependent (section 2.4) or various effective couplings (section 2.5).

2.2. WIMP sensitivity projections: method

Figures 5 and 7 show sensitivity estimates for a liquid xenon TPC with only neutrino-induced backgrounds and the double beta decay of ^{136}Xe considered. We use a binned likelihood in position-corrected cS1 and cS2 (see e.g. references [158, 159]), and assume the log-likelihood ratio test statistic is asymptotically distributed [160].

Particle yields and the detector response to ER and NRs is simulated using NEST v2.1.0 [128] with the `LUXrun03` detector model, roughly corresponding to the model presented in reference [161] for the first science run of LUX. The modeled detector response is similar to the models assumed for the sensitivity projections for LZ [99] and XENONnT [98]. For S1 scintillation signals, the detector model assumes a g_1 value of 0.12 phd/photon and a two-fold photon hit threshold for S1s. For S2 ionization signals, the g_2 value depends primarily on the photon yield g_1^{gas} and field strength in the gas gap, which are 0.1 phd/photon and 6.4 kV cm^{-1}, respectively; more details can be found in [161]. This corresponds roughly to a $g_2 = 13.8$ phd/e. The S2 threshold is assumed as 165 phd. The spatially varying drift field for this simulation is between $\sim$90 V cm^{-1} and 300 V cm^{-1}, and the electron lifetime assumed is $\sim$16 times the maximum drift length. We leave a detailed parametric investigation of the sensitivity of such a next-generation detector to a future study.

The background model is made up of the intrinsic ER and NR backgrounds. The expectation value is dominated by ERs from naturally occurring ^{136}Xe and solar (mostly pp) neutrinos scattering off electrons. ER events can be distinguished from a WIMP signal using the ionization signal.

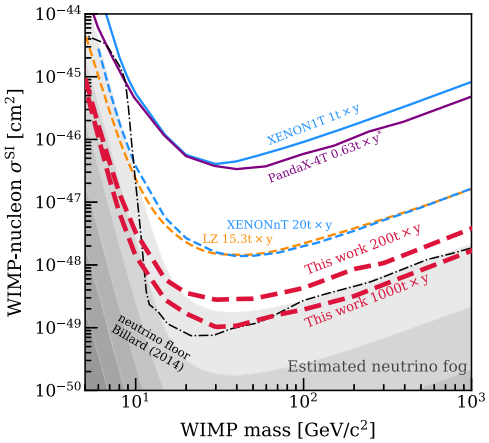

Figure 5. Projections for the next-generation experiment discussed here, together with projected and current leading 90% upper limits, on the spin-independent WIMP–nucleon cross section. Blue and purple solid lines show the current limits from XENON1T [96] and PandaX-4T [173] (non-blind*). Dashed blue and orange lines indicate sensitivity projections from LZ [99] (15.3 t × y, one-sided) and XENONnT [98] (20 t × y). Projected median upper limits for exposures of 200 t × y and 1000 t × y are plotted in dashed red. The dashed line shows one definition of the 'neutrino floor' [164], the shaded gray area indicates the 'neutrino fog', specifically where more than one, 10, 100, etc neutrino events are expected in the 50% most signal-like S1/S2 region. Calculations follow references [166, 167].

NR events from neutrons scattering in the detector volume can be separated to some degree from a WIMP signal based on the recoil energy spectrum and their tendency to scatter multiple times. Further, neutrons can be tagged surrounding the detector with an active neutron veto. We thus only include NR backgrounds from ^{8}B, HEP, diffuse supernovae and atmospheric neutrinos. These neutrino signals, while being an interesting signal in their own right (section 5), may significantly affect the sensitivity to dark matter as they are becoming the dominant background (section 2.17).

The neutrino recoil spectra, as well as flux uncertainties on the different components, are taken to be the same as in reference [98], with spectra from references [162–165]. WIMP recoil spectra are computed using the `wimprates` package [166], with spin-independent computations from reference [167], spin-dependent computations from reference [168], and WIMP–pion recoil spectra from references [169, 170]. We use the background and signal distributions to construct signal regions for each WIMP interaction and mass as the 50% most signal-like region in S1 and S2, ordered by signal-to-background ratio. We indicate the region at which neutrinos become an appreciable background as the cross section where the WIMP and neutrino expectation in the signal region are equal. Levels where the neutrino signal is equal, 10 times, 100 times etc of the WIMP signal are indicated by the shared gray regions labeled 'neutrino fog' in figures 5 and 7. Estimates of where experimental sensitivity will improve only very slowly with exposure depend crucially on the uncertainty on the neutrino signal and detector response. Attempts to quantify the 'neutrino floor', such as [171, 172] (the former is included as a dashed line in figure 5) often assume e.g. very low experimental energy thresholds in order to reflect the ultimate limit. Further discussion of the neutrino background may be found in section 2.17.

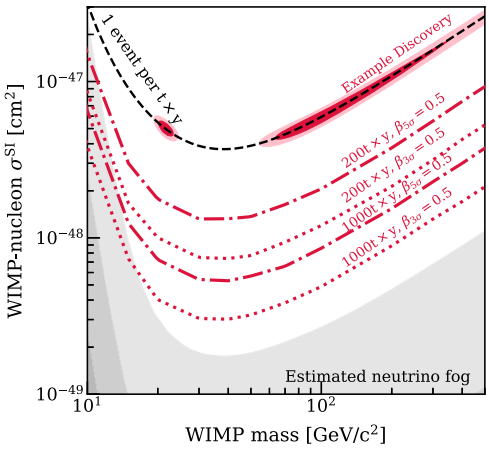

Figure 6. Illustration of discovery potential and example discovery contours for the same detector model as in figure 5. The black dashed line shows the cross-section giving 1 observed event per tonne-year, and the contours show the 1- and 2-sigma (dark and light red) confidence intervals on spin-independent WIMP signals with a 1000 t × y exposure and WIMP masses of either 20 or 100 GeV/c^2. Dash-dotted (dotted) red lines show the cross-section where the median significance equals 3-sigma (5-sigma) for 200 t × y (upper two lines) and 1000 t × y exposure. Gray bands indicating the neutrino fog as in figure 5.

2.3. Spin-independent WIMPs

Traditionally, WIMP detection has been limited primarily by the experiment's exposure (expressed in mass × time), and sensitivity has progressed proportionally to that exposure. This linear scaling will hold as long as contamination by any non-WIMP recoils remains small. This next-generation WIMP detector will be the last to benefit from this proportional scaling over much of its operating time. Any larger experiment would face a rate of CEνNS from astrophysical sources [164, 174]. While that is an interesting signal in its own right (section 5), neutrinos present an unavoidable background to WIMP sensitivity.

The energy threshold of this search is also important. A recoil threshold of ∼keV is required in order to efficiently test WIMP hypotheses down to the Lee-Weinberg limit of few GeV/c^2 mass. The goal for any WIMP dark matter detector, then, can be described as testing the entire WIMP mass range (∼2 GeV/c^2 to ∼100 TeV/c^2) at least down to cross sections limited by neutrino scattering. Such a detector also has sensitivity to many theoretically interesting and yet unexplored dark matter candidates (section 3) and probes the coupling of dark matter to the Higgs boson [175].

To indicate the WIMP mass and cross section resolution expected for a signal from WIMPs roughly one order of magnitude below current constraints (one event per tonne-year), figure 6 shows confidence intervals for spin-independent WIMP signals at 20 and 100 GeV/c^2. At high masses, spin-independent WIMP spectra are degenerate in WIMP mass (as the kinematics only depend on the reduced mass). This leads to poor mass resolution, which can be significantly improved using additional, different target materials [176]. An excess for intermediate and low masses will be well-constrained both in mass and cross section using a xenon target alone.

A simple variation of the vanilla spin-independent WIMP scenario is to allow the interaction strength to depend on the nucleon type (proton or neutron) with non-trivial coupling strengths f_p, f_n [177]. The deviation of the ratio f_p/f_n from 1 will then depend on the specific dark matter

model. If for a given nuclear isotope, $f_p/f_n = (Z-A)/Z$, then this isotope would give no constraint. Fortunately, the mixture of multiple isotopes in xenon detectors provides sensitivity to even the most difficult case of $f_p/f_n \simeq -1.4$ [178–180], providing yet another benefit of xenon as a target material.

2.4. Spin-dependent scattering

The simplest deviation from the spin-independent scattering to a more complicated coupling can be modeled by allowing the WIMP to interact solely with the nuclear spin but with different couplings a_p, a_n to protons and neutrons. This scenario is typically referred to as spin-dependent scattering [182–184]. If one simplifies this picture by assuming that one coupling vanishes, then the derivation of a differential rate of scattering events by WIMPs depends on the spins and nuclear structure (mostly of the unpaired nucleon) of the nuclei in the target. Contributions from two-nucleon currents improve the sensitivity to the spin-dependent WIMP–proton coupling in xenon, see section 2.5.2.

For xenon detectors, the two naturally occurring isotopes ^{129}Xe (spin-1/2) and ^{131}Xe (spin-3/2), with natural abundances of 26.4% and 21.2%, respectively, are most relevant for this spin-dependent coupling. Both have an unpaired neutron, making xenon also an ideal target for detecting the spin-dependent WIMP–neutron cross section. The projected sensitivity for a next-generation liquid xenon TPC is shown in figure 7, calculated using the same assumptions and method as in figure 5.

2.5. Effective field theory

The spin-independent and spin-dependent scattering discussed in the previous sections 2.3 and 2.4 are the more frequently studied interactions of the WIMP with SM fields. Their motivation dates back to dark matter candidates in supersymmetric theories [183] defining the leading responses related to the nuclear density (therefore scaling coherently with the number of nucleons A, spin-independent interactions) or to the nuclear spin (spin-dependent interactions). A more systematic picture covering more general WIMP–nucleus interactions beyond standard spin-independent and spin-dependent scattering has been worked out recently using effective field theories (EFTs). This includes both a nonrelativistic framework, see section 2.5.1, as well as chiral EFT, see section 2.5.2, which incorporates the constraints from QCD at low energies.

2.5.1. Nonrelativistic effective field theory. The nonrelativistic EFT (NREFT) [185–187] integrates out all degrees of freedom except for nucleons and the WIMP. The effective operators that describe the coupling of the WIMP to nucleons are constructed imposing Galilean invariance in terms of the momentum transfer q, the WIMP transverse relative velocity $v^\perp$, and the spins of the nucleon and the WIMP [185–187]. At lowest (zeroth) order in q and $v^\perp$, the only contributions correspond to the leading operators considered for spin-independent and spin-dependent scattering. Up to second order in q and first order in $v^\perp$, 14 operators appear at the single-nucleon level for spin-1/2 dark matter, each with different isoscalar and isovector (or, equivalently, proton and neutron) couplings [187]. The corresponding coefficients, usually considered to be independent, have been constrained from several experiments [188–191]. With few exceptions, the best constraints are given by experiments using a xenon target. For an extension of NREFT to dark matter of spin 1 or higher, see [192–194]. Even given the significant uncertainties in the WIMP halo phase space distribution, NREFT coefficients could nevertheless be constrained by a single next-generation direct detection experiment, if some dozen events would be detected [195].

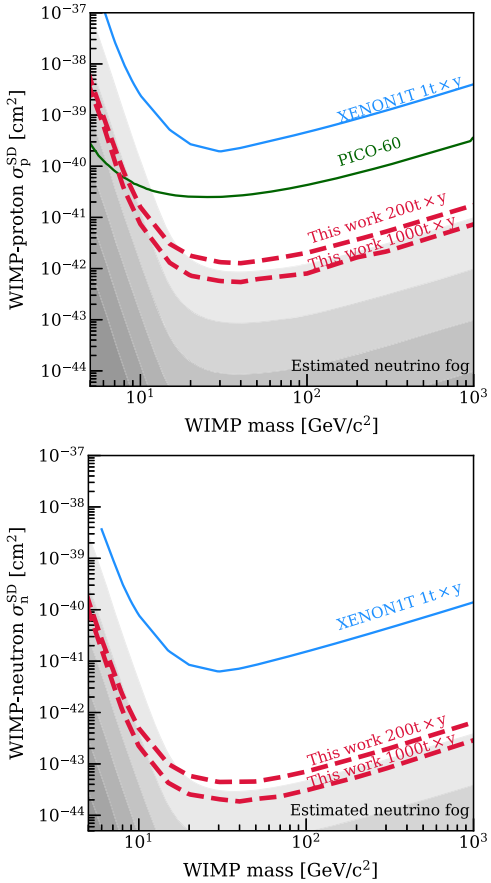

Figure 7. Projections and current leading 90% upper limits on the spin-dependent WIMP–nucleon cross section, assuming that the WIMP couples only to proton spins (top) or neutron spins (bottom). Green and blue solid lines show the current leading limits by PICO-60 [67] and XENON1T [96, 181]. Projected median upper limits for exposures of 200 t × y and 1000 t × y are plotted in red. The shaded gray areas indicate the 'neutrino fog' with the lightest area showing the WIMP cross section where more than one neutrino event is expected in the 50% most signal-like S1, S2 region. Subsequent shaded areas indicate tenfold increases of the neutrino expectation. Calculations follow references [166, 168].

Since the NREFT is limited to nucleons as degrees of freedom, additional matching steps are required to constrain particular WIMP models from experimental limits. This is because the NREFT coefficients contain information on the underlying WIMP–quark or WIMP–gluon operators, but also on hadronic matrix elements (section 2.6). In addition, there is *a priori* no hierarchy among the various NREFT operators apart from their scaling in q and $v^{\perp}$. In that sense, the NREFT can be considered minimal, as even constraints from QCD are not imposed. In addition, the NREFT formalism has also been used to represent contributions beyond the applicability of the strict EFT. For example, long-range effects due to pion exchange (as occurs in chiral EFT) or electromagnetic interactions (such as dipole operators) can be expressed in terms of q-dependent NREFT Wilson coefficients. For a complete description, however, the corresponding degrees of freedom need to be included in the EFT.

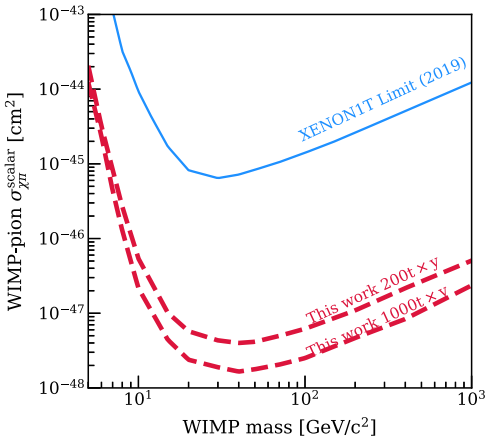

Figure 8. Projections and current leading 90% upper limits on the scalar WIMP–pion interaction cross section. Blue solid lines show the current leading limits by XENON1T [169]. Projected median upper limits for exposures of 200 t × y and 1000 t × y are plotted in red. Calculations follow references [166, 170].

2.5.2. Chiral effective field theory. Chiral EFT [196–198] classifies the possible interactions of the WIMP with nucleons according to their chiral scaling, i.e., the scaling with momenta and quark masses, with nucleons and WIMPs but also pions (and, in SU(3), kaons and η-mesons) as active degrees of freedom. In this way, the constraints from the chiral symmetry of QCD are automatically included. The chiral regime is appropriate to study WIMP–nucleus scattering because the typical momentum transfer q is of the order of the mass of the pion, the pseudo-Nambu–Goldstone boson resulting from the spontaneous breakdown of chiral symmetry. This is also the relevant scale for the typical momenta in heavier nuclei, such as xenon, used for direct detection experiments.

At the single-nucleon level, the chiral analysis can be mapped onto the NREFT operator basis [199–201]. This provides a prediction for an additional hierarchy of the NREFT operators based on their chiral scaling, which significantly simplifies the number of one-body operators relevant for WIMP–nucleus scattering. A second important advantage of the chiral EFT framework is that it predicts subleading multi-nucleon effects. For example, contributions in which the WIMP couples to a virtual pion exchanged between the nucleons inside the nucleus (section 2.5.3) appear at subleading order in the chiral expansion. Such meson-exchange currents (or two-body currents) provide subleading contributions to generalized spin-independent and spin-dependent scattering and have been studied in a number of papers [168, 170, 199, 202–210]. For a xenon target, two-nucleon currents improve the sensitivity to spin-dependent WIMP–proton scattering by more than an order of magnitude.

2.5.3. WIMP–pion coupling. A novel contribution to WIMP–nucleus scattering that emerged from the chiral EFT analysis (section 2.5.2) concerns meson-exchange currents. In the simplest case, the WIMP couples to a virtual pion exchanged between two nucleons within the nucleus. Interestingly, meson-exchange contributions, which enter at subleading order in chiral EFT, can scale coherently with the number A of nucleons. The combination of the nuclear and chiral hierarchies defines a scaling that lies between the spin-independent and spin-dependent responses, coherent but suppressed in the chiral counting. Chiral EFT also predicts the leading meson-exchange currents to dominate over all other NREFT operators except the standard spin-independent one.

As observed in reference [169], once an underlying quark-level operator is specified, the resulting limits can be expressed in terms of a WIMP–pion cross section, in close analogy to the spin-independent and spin-dependent WIMP–nucleon cross sections. The proposed next-generation liquid xenon experiment will improve this result by a similar factor as the standard spin-independent limit, shown in figure 8.

2.5.4. Three-flavor EFT and the ultraviolet. From a particle physics point of view, the most immediate parameterization of dark matter interactions at low energies, $\mu \simeq 2$ GeV, is in terms of three-flavor dark matter EFT that has been studied extensively [170, 199–201, 206, 211–219]. This model has as degrees of freedom the dark matter particle, the lightest three flavors of quarks (u, d, s), the gluon, and the photon. Dark matter interactions are organized in terms of dimensions of the operators, so that the effective Lagrangian takes the form $\mathcal{L}_{\rm DM\ EFT} = \sum_{d,a} \mathcal{C}_a^{(d)} \mathcal{Q}_a^{(d)} / \Lambda^{d-4}$, where $\mathcal{C}_a^{(d)}$ are dimensionless Wilson coefficients and Λ the typical scale of the ultraviolet (UV) theory for dark matter. The sum is over different types, a, and dimensions, d, of the operators $\mathcal{Q}_a^{(d)}$. An example of a dimension-six operator for fermionic dark matter is $(\bar{\chi}\gamma^\mu\chi)(\bar{q}\gamma_\mu q)$ for dark matter–quark vector interactions, or a dimension-seven operator $m_q(\bar{\chi}\chi)(\bar{q}q)$ for scalar interactions, both of which lead to spin-independent scattering. The full basis of up to and including dimension-seven operators in the limit $\Lambda \gg m_\chi \sim m_W$ can be found in reference [219]. The case of the heavy dark matter limit is discussed in reference [216, 217, 220, 221]). The chiral EFT of section 2.5.2 then gives the hadronization of the three-flavor dark matter EFT and the nuclear response.

The three-flavor dark matter EFT is a valid description for dark sector mediators that are heavier than a few hundred MeV. In this case, the mediators are heavier than the typical momenta exchanged in the dark matter scattering on nuclei and can be integrated out. The Wilson coefficients, $\mathcal{C}_a^{(d)}$, are constants that contain all the UV dark matter physics. In the absence of a complete UV theory of dark matter they can be freely varied when comparing the results of dark matter direct detection experiments. For Λ well above the nuclear scale, the higher dimension operators are suppressed, making the framework predictive. For instance, for $\Lambda \gg m_\chi$, a truncation at dimension seven is expected to capture most new physics models.

The connection between the three-flavor dark matter EFT at $\mu = 2$ GeV and the UV theory at $\mu \simeq \Lambda$ is achieved by going through a series of appropriate EFTs and performing the matchings at each threshold [214, 215, 222–224]. In this way the results of indirect dark matter searches and the dark matter searches at the LHC can be reliably compared with the direct detection results. From the perspective of direct detection experiments, the UV physics is encoded in the values of Wilson coefficients $\mathcal{C}_a^{(d)}$. One can then compare the constraints on $\mathcal{C}_a^{(d)}$ obtained from direct detection experiments with the constraints imposed by the LHC and indirect dark matter searches on either complete dark matter models or on simplified models by going through the above series of matchings and renormalization group evolutions.

2.6. Nuclear structure factors

The WIMP–nucleus cross section is proportional to the nuclear structure factors, which encode the relevant information of the structure of the target nuclei. The EFT operators at the WIMP–nucleon level generate, at the nuclear level, six different nuclear one-body responses analogous to semileptonic weak interactions [225–227]. In addition, chiral EFT predicts two-nucleon nuclear responses associated with meson-exchange currents. The cor-

responding nuclear structure factors are obtained from the one-body nuclear responses $\mathcal{F}^M$, $\mathcal{F}^{\Phi''}$, $\mathcal{F}^{\Sigma'}$, $\mathcal{F}^{\Sigma''}$, $\mathcal{F}^{\tilde{\Phi}'}$, and $\mathcal{F}^{\Delta}$ [183, 187], and the two-body nuclear responses $\mathcal{F}_\pi$, $\mathcal{F}_\mathrm{b}$ [170, 206]. The one-body structure factors decompose into isoscalar and isovector (or, equivalently, proton and neutron) contributions, e.g. $\mathcal{F}^M_\pm$. $\mathcal{F}^M$ and the two-body $\mathcal{F}_\pi$, $\mathcal{F}_\mathrm{b}$ can receive coherent contributions from all A nucleons in the nucleus while about one in five nucleons contributes coherently to $\mathcal{F}^{\Phi''}$. These responses dominate spin-independent ($\mathcal{F}^M$) and scalar WIMP–pion ($\mathcal{F}_\pi$) scattering. $\mathcal{F}^{\Sigma'}$ and $\mathcal{F}^{\Sigma''}$ are usually rewritten in terms of the more common S_{00}, S_{01}, S_{11} or S_p, S_n in spin-dependent analyses. They are related to the spin distribution in the nucleus and are not coherent because the nuclear pairing interaction couples nucleons in spin-zero pairs.

The nuclear structure factors allow one to factorize the nuclear response from the hadronic matrix elements and the couplings of the WIMP. Schematically, the WIMP–nucleus cross section decomposes as

$$\frac{\mathrm{d}\sigma_{\chi\mathcal{N}}}{\mathrm{d}q^2} \propto \sum_i \left|c_i \mathcal{F}_i(q^2)\right|^2 + \text{interference terms}, \tag{1}$$

where the $\mathcal{F}_i(q^2)$ denote the nuclear structure factors and the c_i involve a convolution of hadronic matrix elements and WIMP couplings. Thus, in the case of scalar operators, the role of the pion–nucleon σ term is well known in the literature [228–233]. In special cases, the WIMP–nucleus cross section can be expressed in terms of single-particle cross sections: (i) if only c^M_+ is non-vanishing it can be expressed by the spin-independent isoscalar WIMP–nucleon cross section (section 2.3); (ii) if only the coefficients of S_p or S_n are non-vanishing, by the spin-dependent WIMP–proton or WIMP–neutron cross section (section 2.4); and (iii) if only c_π is non-vanishing, by the scalar WIMP–pion cross section (section 2.5.3).

In general, reliable nuclear structure factors for any nuclear response require a good description of the nuclear target. The only exception is the leading $\mathcal{F}^M_+$ structure factor in spin-independent scattering, for which the purely phenomenological Helm form factor [167, 234] is a common and good description [235]. For heavy targets such as xenon, structure factors need to be calculated from nuclear theory. The nuclear shell model is presently the method of choice with significant progress in recent years. The shell model solves the many-body problem in a relatively small configuration space (one or two harmonic oscillator shells near the Fermi surface) with a phenomenological nuclear interaction adapted to the configuration space [236]. The description of excitation energies, charge radii, and electromagnetic properties of medium- and heavy-mass nuclei, including all stable xenon isotopes, is already very good [168, 170, 235]. State-of-the-art nuclear structure factors are easily available in dedicated notebooks documented in references [170, 187]. Figure 9 shows nuclear structure factors for a general coherent WIMP scattering off ^{132}Xe (26.9% natural abundance) with the hierarchy given by chiral EFT.

More advanced nuclear structure *ab initio* calculations treat explicitly all nucleons in the nucleus (see e.g. references [237–242]). They can use nuclear interactions based on chiral EFT, thus consistently providing the nuclear states and WIMP–nucleon operators that enter the calculation of the structure factors. This will allow one to estimate theoretical uncertainties. While nuclear structure factors obtained with *ab initio* many-body techniques have historically been limited to light nuclei with $A \leqslant 6$ [207, 209, 243], recent progress has been significant and *ab initio* spin-dependent structure factors have been calculated very recently [210] with the valence-space in-medium similarity renormalization group method.

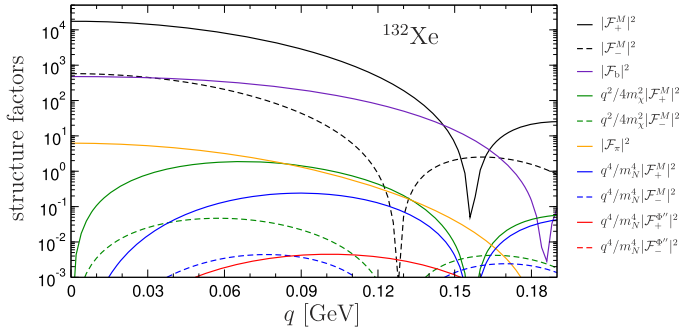

Figure 9. Structure factors for ^{132}Xe from one- and two-body contributions (without interference terms). Solid lines show isoscalar and two-body contributions while dashed lines indicate isovector couplings. Reproduced from [170]. CC BY 4.0.

2.7. Inelastic scattering

The recoil energy spectrum resulting from spin-dependent interactions is similar to the one expected from spin-independent interactions. Using different target materials with other experiments can help to break that degeneracy, as would be a different mixture of isotopes of xenon in a target. In addition, liquid xenon TPCs can even differentiate between these two interaction channels with one and the same exposure, as WIMPs might alternatively scatter inelastically off nuclei that possess low-lying excited states up to ∼100 keV [244], including ^{129}Xe and ^{131}Xe [245–247]. This inelastic scattering in the nuclear sector is not to be confused with dark matter models in which the WIMP can be excited, as is discussed in the context of the inelastic dark matter (iDM) model in section 2.13.

Inelastic scattering is always non-coherent, because of the different initial and final nuclear states. This would allow one to narrow the nature of the underlying WIMP–nucleon interaction, testing the spin-dependent case upon detection in the simplest scenario. In addition to the NR, a prompt ER is caused by the de-excitation of the up-scattered xenon nucleus. Such interactions thus suffer from the larger background of ERs. However, since they would only be expected for non-coherent spin-dependent interactions, given sufficient statistics, a single xenon detector would be able to extract information about dark matter that is inaccessible to the elastic channel alone.

Observation of such inelastic scattering would provide a range of further insights to the nature of dark matter: each unique nuclear excitation is sensitive to a distinct portion of the WIMP halo, so that multiple contributions from the inelastic channel could be combined with that of the elastic channel to constrain the WIMP velocity distribution [245]. In addition, the range of observed recoil energies as well as the energy at which the inelastic channel begins to overtake the elastic one would indicate the mass of the incident WIMP. Finally, in contrast to the elastic channel, the inelastic event rate may be enhanced or suppressed with the enrichment or depletion of ^{129}Xe and ^{131}Xe. This flexibility would allow one to optimize data acquisition in a xenon detector. The most stringent limit on inelastic WIMP–nucleon scattering currently comes from the XMASS detector [248]. Prospects for a future detection of dark matter detection with inelastic xenon transitions are further discussed in reference [249].

2.8. Discriminating between WIMP–nucleus responses

Given the number of different nuclear responses (section 2.6), a key question is how they could, in the event of a detection, be distinguished in order to extract information on the nature

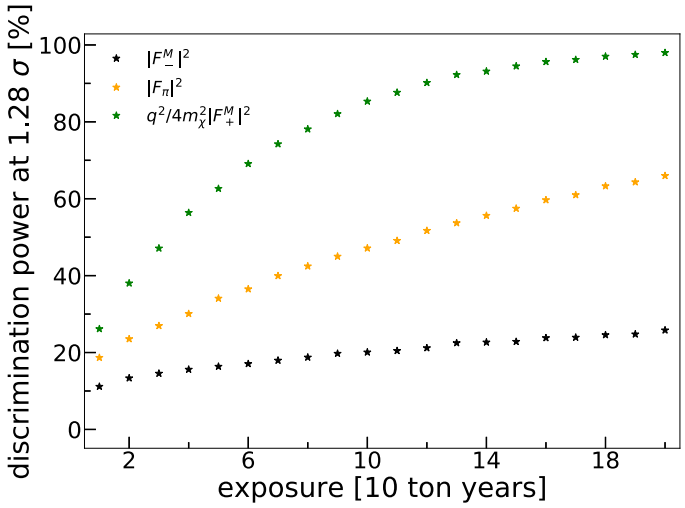

Figure 10. Discrimination power against $|\mathcal{F}_+^M|^2$ vs exposure for three selected structure factors, $|\mathcal{F}_-^M|^2$ (black), $|\mathcal{F}_\pi|^2$ (orange), and $q^2/4m_\chi^2|\mathcal{F}_-^M|^2$ (green). The detector setting is like the one discussed here, for a WIMP mass of $m_\chi = 100$ GeV$/c^2$ and interaction strength $\sigma_0 = 10^{-47}$ cm^2. Reproduced from [250]. CC BY 4.0.

of the WIMP [195]. One possible strategy concerns the study of inelastic scattering into low-lying excited states of the xenon target, discussed in the previous section 2.7. The detection of the inelastic channel, in addition to the elastic scattering would primarily point to the non-coherent character of the WIMP–nucleus interaction, suggesting a spin-dependent interaction as the prime choice.

A second handle to discriminate the nuclear responses exploits their different dependence on the momentum transfer, see figure 9. The feasibility of this approach has been explored for several WIMP–nucleon interactions [250, 251]. In particular, reference [250] considered realistic detector settings, including projections for a next-generation experiment like the one proposed here, see figure 10. As with inelastic scattering, for most responses a discrimination becomes possible with sufficient statistics. However, due to the similarities in the q-dependence, a separation of isoscalar and isovector responses will be difficult.

Finally, the nature of the WIMP–nuclear response and in particular its spin-dependent character can be tested by varying the enrichment or depletion on the isotopes with odd A ^{129}Xe and ^{131}Xe that is possible with a liquid xenon target. In this case it will be most powerful to combine the results of the proposed experiment with searches using spinless nuclear targets, such as argon, to further test the spin-dependent hypothesis. Likewise, to discriminate between isoscalar and isovector responses the most promising strategy takes advantage of the different proton to neutron ratios in different target nuclei. In this sense, xenon isotopes exhibit the smallest proton to neutron ratios, in contrast to the largest ones which are found e.g. in fluorine or argon.

2.9. Scattering at high momentum transfer

Traditional momentum- and velocity-independent dark matter models used to drive experimental developments already starting in the 1990s. Those lead to the well-known low-energy

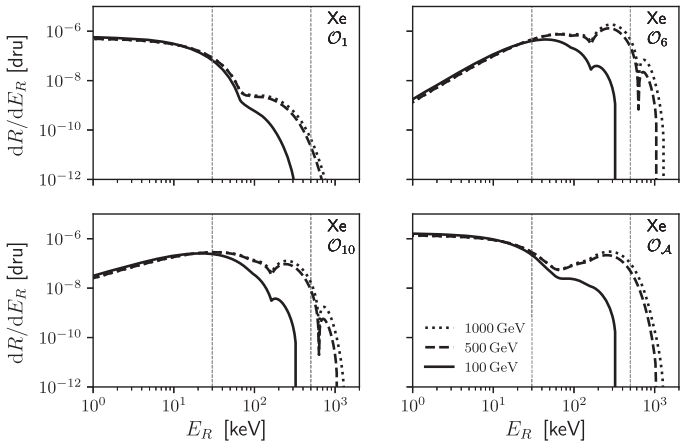

Figure 11. The expected recoil spectrum for EFT operators, $O(1)$ (top left panel), $O(6)$ (top right panel), $O(10)$ (bottom left panel), and for anapole interactions (bottom right panel) in a xenon experiment. The dark matter particle mass is chosen to be $m_\chi = 100\ \mathrm{GeV}/c^2$ (solid), $500\ \mathrm{GeV}/c^2$ (dashed), and $1000\ \mathrm{GeV}/c^2$ (dotted). The vertical dashed lines represent $E_{\mathrm{max}} = 30$ keV and 500 keV. Units are per (keV kg d) and the coupling for each operator has been fixed to produce 100 events in the energy range [3, 30] keV. Reproduced from [259].

recoil spectra, resembling simple distributions exponentially falling with energy [167]. Consequently, significant experimental effort went into lowering the energy threshold, the calibration for NRs in this energy regime, and improved understanding of relevant background sources.

However, many models, such as momentum-dependent effective models or non-trivial mixtures of interactions, result in a more complex NR signature with characteristic peaks in the higher nuclear energy regime. This includes many of the models discussed in the following, such as inelastic, composite, exothermic, and magnetic dark matter [188, 252–256] but also the well-known EFT operators for elastic scattering [189, 257, 258]. These effects manifest themselves often outside the traditionally analyzed energy ranges. The fact that most particles in the SM adhere to such more complex interactions provides strong motivation to explore this important higher-energy parameter space. Figure 11 show possible recoil spectra for selected interactions, taken from reference [259]. Further motivation to also probe higher recoil energies stems from the presence of Galactic streams that may result in higher recoil energies than from the customarily assumed isothermal halo [71, 72, 260–264].

In case of discovery, features in the higher NR tails of recoil energy spectra might be used to determine the property of the dark matter–matter interaction. Further, the high-energy NR tails of the recoil spectrum are especially sensitive to astrophysical parameters that describe the dark matter velocity distribution, such as the maximum velocity, Galactic escape speed [42, 265], or the presence of tidal streams [74, 266, 267]. By employing multiple experiments with different target materials, it is possible to significantly reduce astrophysical uncertainties. For example, the complementarity between argon and xenon-based targets aids to determine the properties of the dark matter particle [157, 176, 268–271].

2.10. Simplified models

Despite the fact that dark matter–nucleus scattering is characterized by low-energy processes (for which EFTs could provide swift analyses and some general conclusions), further explo-

ration of the internal structures in the interactions between dark matter and SM particles would involve high-energy processes such as those probed at colliders and in the early Universe. At sufficiently high energies, the EFT treatment will break down, as the internal mediators generating the effective dark matter–SM couplings become on-shell.

Simplified models of dark matter can provide a predictable framework to remedy the aforementioned problem, while keeping the number of free parameters manageable, see e.g. references [272–276] and references therein for review and [277–282] for some specific studies. In the simplest scenario, only the dark matter mass, mediator mass and a few couplings (depending on the specific models) connecting the dark sector to ours are assumed. This can readily build the interplay among dark matter signals in direct detection, high-energy colliders and astrophysical/cosmological evolution. In light of these complementary approaches, it should be noted that a next-generation xenon experiment is particularly well-suited to probe most of the remaining parameter space in some broad classes of simplified models, e.g. Z' mediated WIMP models [283]. In some realizations of simplified models, the tree-level dark matter–nucleon scattering cross section could exhibit either velocity-suppressed or spin-dependent features to pass the current strong constraints from the existing liquid xenon limits. Examples are a pseudoscalar or axial-vector current in the interactions of the mediator with the SM quarks and/or the dark sector [284]. It is also worth mentioning that the tree-level interactions between the dark matter and the SM in simplified models can generate loop processes which may still induce detectable signals. These can play important roles in future of direct detection experiments such as the one proposed here [285–303].

2.11. Electroweak multiplet dark matter

One particularly simple case among WIMP candidates is the dark matter particle as the lightest member of an electroweak multiplet. This is in essence the original WIMP model, sometimes also called the 'minimal dark matter' scenario [304–306]. Where 'WIMP' refers to particles interacting through the weak force, this WIMP is the same an as electroweak multiplet, by definition. The interaction between the dark matter and the SM particles are therefore mediated by the SM gauge bosons and the Higgs boson, without the need to introduce additional mediators. Since the interactions are governed by the SM gauge invariance, this is a very predictive scenario and serves as an example of a simple and elegant WIMP dark matter model that is still largely unexplored by experimental searches.

In this model, the fermionic multiplets only have gauge interactions at the renormalizable level. One of the simplest models is a singlet with an additional neutral scalar stabilised by a Z_2 symmetry [307]. In general, we could consider multiplets $(1, n, Y)$ under the SM gauge group $\mathrm{SU}(3)_C \times \mathrm{SU}(2)_L \times \mathrm{U}(1)_Y$. The mass scale of the electroweak multiplet is set by a vector-like mass parameter. After electroweak symmetry breaking, the mass spectrum of the multiplet is not exactly degenerate. Minimally, the degeneracy will be lifted by electroweak loop corrections [304, 305, 308–311]. For a large multiplet $n > 7$, the Landau pole will be about one order of magnitude above the mass of electroweak multiplet [312], which makes the model contrived; conversely, new physics below the scale of the Landau pole may lead to an asymptotically safe scenario [313]. Ultimately, perturbative unitarity of the annihilation cross section provides a limit of $n < 14$ [311, 314].

Sommerfeld enhancement [315–320] and bound state effects [321–325] need to be included in accurate calculations of predictions. Target masses of the electroweak multiplet dark matter are in the range of 1–30 TeV [306, 324, 326] for $n < 7$, but can approach the unitarity bound for larger multiplets, which saturates at $n = 13$ [311, 314]. These masses are beyond the reach of the LHC [327–330] and would require one of the proposed future high energy colliders

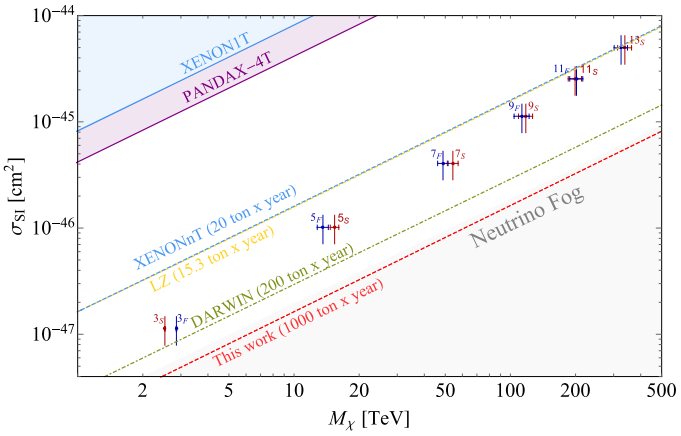

Figure 12. Expected spin-independent scattering cross-section for Majorana multiplets (red) and for real scalar multiplets (blue), assuming the Higgs portal coupling $\lambda_H = 0$). Vertical errors correspond to LQCD uncertainties on the elastic cross-section, horizontal errors indicate uncertainties from the determination of the WIMP freeze out mass. The next-generation experiment discussed here will fully probe these classes of highly motivated WIMP dark matter models. Reproduced from [311]. CC BY 4.0.

[311, 331–333]. In contrast, the direct detection of the electroweak multiplet dark matter is through one-loop processes involving the SM W, Z, and Higgs bosons. The spin-independent cross sections have been computed to be around 10^{-47} cm^2 for the Majorana triplet (wino) [334] and 10^{-48} cm^2 for the Dirac doublet (Higgsino) [335]. The other cases are expected to be within the same order [314]. As shown in figure 12, this level of spin-independent cross section is well within the reach of the next-generation liquid xenon detector discussed here [311, 336, 337]. To avoid confusion, note that the LZ line in reference [311] corresponds to the sensitivity from the LZ design reports [108, 338] instead of the goals shown reference [99]. For an explicit phenomenological framework which captures most minimal supersymmetric Standard Model (MSSM) parameters [339], the significant boost of the next-generation xenon experiment to probe the possibility that the lightest supersymmetric particle is the dark matter, see e.g. figure 3(a) in reference [340].

2.12. Implications for supersymmetry

One classic WIMP dark matter model is the lightest supersymmetric partner (LSP). Supersymmetric models, such as the MSSM, with an exact *R*-parity, predicts that a stable electrically neutral LSP could be a cold dark matter candidate [140]. There are three possibilities for a stable neutral LSP: sneutrino, gravitino and neutralino. Among them, the most attractive scenario for direct detection is neutralino dark matter. For a general review on supersymmetry (SUSY) and its low-energy phenomenology, see [341].

In the MSSM, two neutral higgsinos and two neutral gauginos could mix with each other after electroweak symmetry breaking to form four mass eigenstates called neutralinos. Current direct detection is sensitive to the scattering of WIMPs off nuclei through tree-level Higgs exchange. Thus, existing data has ruled out a significant part of the parameter space of the 'well-tempered' neutralino scenario [342], in which the LSP is a mixed neutralino (e.g. mixed bino and higgsino) with the right thermal relic abundance and couplings to the nucleus through the Higgs boson.

Yet, there are large regions of parameter space unprobed by current experiments. In the MSSM, the reason is that for an LSP that is predominantly a bino, there is a general reduction of the spin-independent direct detection cross section for negative values of the higgsino mass parameter μ. This reduction is induced by a decrease of the coupling of the bino to the Higgs boson [343], as well as by a destructive interference between the contributions of the standard Higgs with the ones of non-standard Higgs bosons [344, 345]. The same happens in other minimal supersymmetric extensions, like the NMSSM, but for a singlino dark matter candidate, the reduction occurs for positive values of μ [346]. Moreover, there are regions of parameter space, called blind spots, in which the scattering amplitude is drastically reduced [343, 344, 346, 347]. The precise parameter space associated with these blind spots is slightly modified by loop corrections [348]. Quite generally, for the appropriate signs of μ, the spin-independent scattering cross section can easily be below 10^{-47} cm^2 [346, 349–351]. This range of cross sections are out of the reach of current experimental searches but can be probed by next generation direct detection experiments like the one discussed here.

In addition to the well-tempered neutralino at the blind spot, nearly pure wino or higgsino dark matter can scatter off nuclei elastically at one-loop level with a small cross section [220, 352]. The pure wino scenario has been strongly constrained by indirect detection of gamma rays from the Galactic center [353, 354] and local spheroidal satellite galaxies [355, 356], although the former is subject to large uncertainty from the dark matter profile. The spin-independent pure wino-nucleon cross section is around 2×10^{-47} cm^2 [334], which can be probed by next-generation direct detection experiments. The elastic scattering cross section of the higgsino is found to be below 10^{-48} cm^2 with a large theoretical uncertainty [335]. Depending on the mass splitting between neutral higgsinos, the inelastic scattering of higgsino dark matter could be potentially probed with such a future experiment [256].

It is also possible that dark matter could have multiple components, such as a combination of very light QCD axions and neutralinos in a supersymmetric theory that solves the strong CP problem [357]. In this scenario, direct detection experiments probe the dark matter fraction of the WIMP times its scattering cross section, and the next-generation experiment is motivated as its improved sensitivity now corresponds to a sensitivity to smaller fractions of dark matter [358–363]. In a most optimistic scenario, this same detector might then even detect multiple different components of dark matter, see section 3.

2.13. Inelastic dark matter

iDM was originally proposed [252] to resolve the tension between results published by the DAMA/LIBRA collaboration [364–366] and other direct and indirect observations [367–369]. Multiple particle candidates have since been proposed as iDM [319, 370], mostly motivated by the measured DAMA/LIBRA spectrum and the constraints for other experiments. Although ultimately this model failed given later exclusions from XENON100 [371], iDM has sparked significant theory development and has remained as an interesting and well-studied family of dark matter models. A common feature is a dark matter particle that scatters off SM particles through an excited state of the dark matter particle itself. The mass difference of the excited state δ imposes a threshold on the energy transfer of the interaction, below which interactions are suppressed. This threshold on the energy transfer $E_{\rm nr}$ limits the population of dark matter that can interact with a given target to those with a minimum velocity $\beta_{\rm min}$ expressed by

$$\beta_{\rm min} = \sqrt{\frac{1}{2M_N E_{\rm nr}}}\left(\frac{M_N E_{\rm nr}}{\mu} + \delta\right), \tag{2}$$

where M_N is the nucleus mass and μ is the reduced mass of the dark matter and target particles. Enforcing this constraint alters the spectrum of the expected interaction and can result

in peaked recoil spectra [71, 252], strong dependencies on the particular target material [372], or halo distributions with differing high velocity behavior [373]. Note that number-changing interactions that involve multiple dark matter and one standard model particle (Co-SIMPs) lead to similar effects, since rest mass is converted to kinetic energy [374]. Calculating this spectrum for a given detector can be done in a model-independent way; software packages have been developed [375] to perform these calculations in a consistent manner. Dedicated searches for iDM are thus required and have been carried out in XENON100 [189], PandaX-II [376], and LUX [377].

2.14. Self-interacting dark matter

Self-interacting dark matter (SIDM) [379, 380] is a leading candidate that can resolve both long-standing and more recent tensions between small-scale structure observations and prevailing cold dark matter predictions, see [381] for a review. SIDM phenomenology is also expected if the dark matter is composite (section 3.10) or arises from a mirror world scenario (section 3.12). Dark matter self-interactions, analogous to the nuclear interactions, can thermalize the inner Galactic halo in the presence of the stellar component and tie dark matter and baryon distributions in accord with observations [382–385]. In many particle physics realizations of SIDM, there exists a light force carrier that mediates dark matter self-interactions [386–397]. When the mediator couples to SM particles, it may generate dark matter signals in direct detection experiments [398]. For a typical SIDM model, the mediator mass is comparable to or less than the momentum transfer in NRs. Compared to WIMPs with a contact interaction, the SIDM signal spectrum is then more peaked toward low recoil energies [378, 399], see figure 13. Thus the detection of such a spectrum can be an indication of the self-scattering nature of dark matter. Even a null result can put a stringent constraint on the coupling constant between the two sectors. Recently, the PandaX-II collaboration analyzed their data based on an SIDM model with a dark photon mediator and derived an upper bound of $\sim 10^{-10}$ [400, 401] on the kinematic mixing parameter between the dark and visible photons. Limits from liquid xenon experiments set the strongest constraints also on light SIDM models [402]. The next-generation liquid xenon experiment discussed in this review will further test SIDM models, and dark matter models with a light mediator in general.

2.15. Leptophilic interactions

While past efforts in direct dark matter detection have mostly focused on WIMP couplings to nucleons, it is also possible that dark matter would couple preferentially to leptons. Such 'leptophilic' dark matter candidates have been discussed extensively in the context of the cosmic ray positron excess observed by PAMELA [403] and AMS-02 [404], as well as the bright 511 keV x-ray signal from the Galactic Center [405], and the high-energy cosmic ray electron data from DAMPE [406]. Leptophilic dark matter is easily realized in concrete models. This is the case, for instance, if dark matter interactions with the SM particles are mediated by a new gauge boson that couples predominantly to leptons [407–409]. Another example are dark matter interactions mediated by new scalar particles carrying lepton number, such as the sleptons in supersymmetric models [410–414].

Even if the tree-level interactions of dark matter are leptophilic, couplings to nucleons can be induced at loop level. In that case the WIMP–nucleon scattering is the more promising detection channel, despite loop-suppression, as long as the WIMP is much heavier than the electron [409, 413, 415–421]. The reason for this is the more favorable kinematics: the scattering of a heavy WIMP ($\gg$MeV) on an electron leads to a very small momentum transfer, mostly invisible to a typical direct detection experiment.

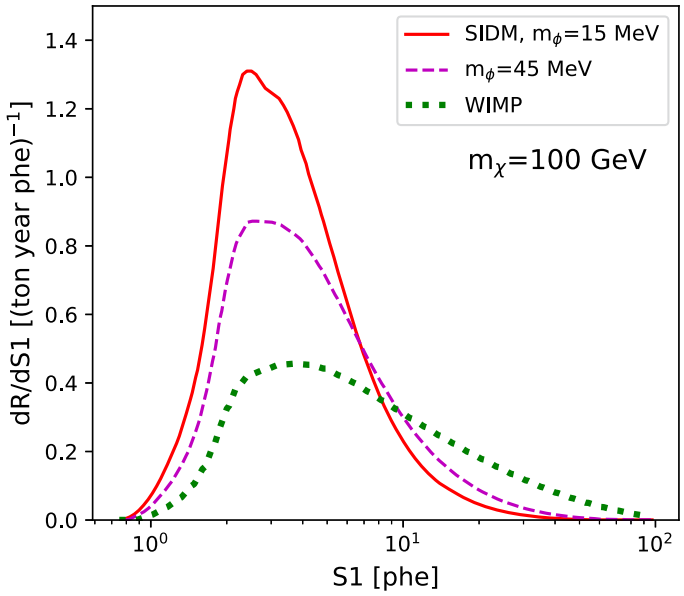

Figure 13. Predicted event rates at a xenon-based experiment for a SIDM model with a light mediator (solid red), a model with three times the mediator mass (dashed magenta), and the vanilla WIMP model with contact interaction (dotted green). The spectra are normalized to have the same number of total events within the signal range. See [378] for details.

However, there are scenarios in which WIMP couplings to nucleons are absent even at the loop level. This can happen for instance if WIMP–lepton interactions are mediated by a new axial vector boson. In this case, the dominant direct detection signal is dark matter scattering on electrons [415, 420, 422], and searches for this process have been carried out by many experiments, including XENON100 [423–425] and LUX [426]. Scattering on electrons is particularly efficient for sub-GeV dark matter [427], making it the primary detection channel in that mass range.

Scattering on electrons is also the most efficient channel for dark matter capture in the Sun [415, 428, 429]. Therefore, if dark matter annihilates into a final state including high-energy neutrinos, searches for these neutrinos from the Sun leads to highly competitive and complementary limits. On the collider side, strong limits on leptophilic dark matter are obtained from LEP data [430]. Future lepton collider would lead to further improvements [431–433]. Progress with these experiments will be complementary to advances from the experiment proposed here.

2.16. Modulation searches

As the Earth revolves around the Sun, a sinusoidal annual modulation should be observable in the dark matter flux hitting direct detection experiments underground [49, 434], with details depending on the phase space distribution of the halo [435, 436]. The DAMA/LIBRA collaboration upholds a long-standing claimed observation of an annually modulating event rate [366] with a statistical significance in excess of 9σ. However, most interpretations of this signal in terms of WIMPs have been ruled out by numerous other experiments. A substantial level of particle model fine-tuning is now required to reconcile the DAMA/LIBRA observation with other null results [69, 437]. Moreover, experiments such as ANAIS [438, 439], COSINE-100

[440, 441] and SABRE [442] attempt to replicate DAMA/LIBRA with an identical sodium iodide target but have not found any evidence of modulation.

A next-generation liquid xenon experiment will be robustly constructed using long-term infrastructure that is made to last multiple years or even decades. Combined with the extremely low background and large target mass, a next-generation experiment may be the ideal experiment to perform an annual modulation search. An annual modulation analysis thus is an integral part of the primary dark matter data analysis, with a sensitivity enhanced by the long data taking time spanning many annual cycles.

A diurnal modulation is guaranteed for most dark matter candidates due to the varying speed of the Earth relative to the dark matter wind as the Earth rotates, though this will be around two orders of magnitude smaller than the annual modulation. However, if dark matter interacts more strongly inside the Earth, then there may be a much larger diurnal modulation effect as the Earth's 'shadow' eclipses the dark matter wind from the perspective of an experiment [443–446]. Such shadowing effect also provides additional sensitivity to cosmic-ray boosted dark matter (CRDM) with mass lower than around 1 GeV [447]. Many models within the scope of a future xenon experiment will exhibit such a modulation (section 3).

Experimentally, the challenge for detecting diurnal modulations remains to understand sub-1% variations in detector parameters on a daily basis rather than from weekly or monthly calibrations. In a massive next-generation detector, spatial variation of quantities such as light collection efficiencies may be inherently greater, but there is no reason to assume that temporal variation will be worse than in contemporary detectors. These experiments can teach us how to better control variation, through existing logging of temperature and pressure data as function of time, and excellent handles for temporal systematic uncertainties [64, 108], especially when coupled to frequent calibrations using fast-decaying radioisotopes such as ^{83m}Kr [448, 449].

2.17. Confronting the neutrino fog

As the size and sensitivity of direct detection experiments improves, the detectable signal of dark matter will become so small that it will reach a level similar to the strength of the CEνNS signal of astrophysical neutrinos [164, 174, 450]. While there is a substantial science case for the detection of astrophysical neutrinos in their own right (section 5), for dark matter searches they are a critical background.

When searching for a signal that is mimicked by a background, discovery is only possible when an excess in events is larger than the expected statistical fluctuations and systematic uncertainties of that background. For the neutrino background, the systematic uncertainties on the flux normalizations dominate, which range from 1%–50%. Many of the particle models discussed here will eventually be limited in some way by the neutrino background, in both the ER [451, 452] and NR channels [164, 453–456]. This background is often referred to as the 'neutrino floor', or more accurately, the 'neutrino fog', as it represents a gradual worsening of sensitivity and a dependence on the systematics of the neutrino flux. Various definitions of this neutrino fog have been put forward [457]. Just like any generic limit on dark matter, the shape of a neutrino fog is dependent on nuclear [458], astrophysical [172] and particle model [258, 454, 455] inputs for the dark matter signal. Given non-standard neutrino-nucleus interactions, these could be further modified [459, 460] and even raised by several orders of magnitude [461].

Unlike many other backgrounds, neutrinos cannot be shielded, so they must be dealt with statistically, or by searching for some discriminating features. Techniques that have been discussed in the past include exploiting the differing annual modulation signatures [462], or the complementarity between different target nuclei [463]. However, only direction-dependence

provides enough of a discriminant to fully subtract the background [464–468], but measuring this in any large-scale experiment is extremely challenging.

Fortunately for the next-generation xenon experiment, extending the dark matter physics reach below the neutrino fog will be facilitated by complementary measurements made by neutrino experiments. Taking the example of standard WIMP–nucleon cross sections, the most important backgrounds will be ^{8}B solar neutrinos for WIMP masses below $\sim$10 GeV/c^2, and atmospheric neutrinos above that. The ^{8}B flux is measured at the 2% level from Solar neutrino data [469]. The atmospheric flux on the other hand, is difficult to measure and to theoretically predict at the relevant sub-100 MeV energies, so it still has a $\sim$20% uncertainty (section 5.3 and [165]). Any reduction in these uncertainties will, in effect, 'lower' the neutrino fog. Indeed, gradual improvements in neutrino flux measurements are expected independent of the experiment under discussion here. For example, experiments like SNO+ [470], JUNO [471] and DUNE [472, 473] will be either operating or under construction over a similar timescale to the next-generation xenon experiment.

In figure 14 we show how the minimum discoverable spin-independent cross section for a 100 GeV WIMP evolves with increasing exposure in a xenon experiment. The brief plateau in the discovery limit is the impact of the atmospheric neutrino background. However, in the limit of high statistics, the number of observed background events will eventually be large enough to account for the finite uncertainty. At this point, the discovery limit breaks past the neutrino fog and smaller cross sections can be accessed. Comparing the different lines, we see clearly the importance of the systematic uncertainty. A future improvement down to $\sim$4% would be enough to extend the reach of a 1000 tonne-year xenon experiment almost an order of magnitude into the neutrino fog at high masses [474]. This is where much of the remaining supersymmetric WIMP candidates [352, 475–477], as well as many alternative WIMP models [289, 478, 479] lie.

3. Broadening the dark matter reach

Liquid xenon experiments have already demonstrated that they are versatile detectors with significant sensitivity to a variety of non-WIMP dark matter models. Traditionally, WIMPs are searched-for using analyses that exploit the ER/NR discrimination capability of liquid xenon and achieve the lowest NR background of any dark matter direct detection technology. To broaden this reach, a number of different analyses and technologies are available as presented in this section. This in turn enables liquid xenon experiments to achieve competitive sensitivity to a number of dark matter models that are also described here. In particular, subsections 3.1–3.5 describe dedicated analyses and technologies to lower the energy threshold of liquid xenon TPCs. Subsections 3.6–3.9 describe models that especially profit from such lower thresholds, and subsections 3.8–3.13 models where the signal can be in the ER band. Subsections 3.14 and 3.15 describe two models that require dedicated analyses to increase the reach of liquid xenon TPCs to complex interactions and up to Planck mass dark matter, respectively.

With the WIMP model being probed extensively by experiment, the community is in parallel starting to work on detector concepts that can probe dark matter over a much wider mass range [480], in particular covering thermal relic particles in the MeV/c^2 to GeV/c^2 mass range [427, 480–484]. Searches in this lower mass range were pioneered with liquid xenon detectors [485]. While many experiments optimized for very low-energy recoils now exist [486–490], liquid argon [491, 492] and xenon [181, 493, 494] TPCs still remain the leading technologies even for sub-GeV masses. There is thus significant interest in achieving the lowest-possible energy threshold in a next-generation liquid xenon detector.

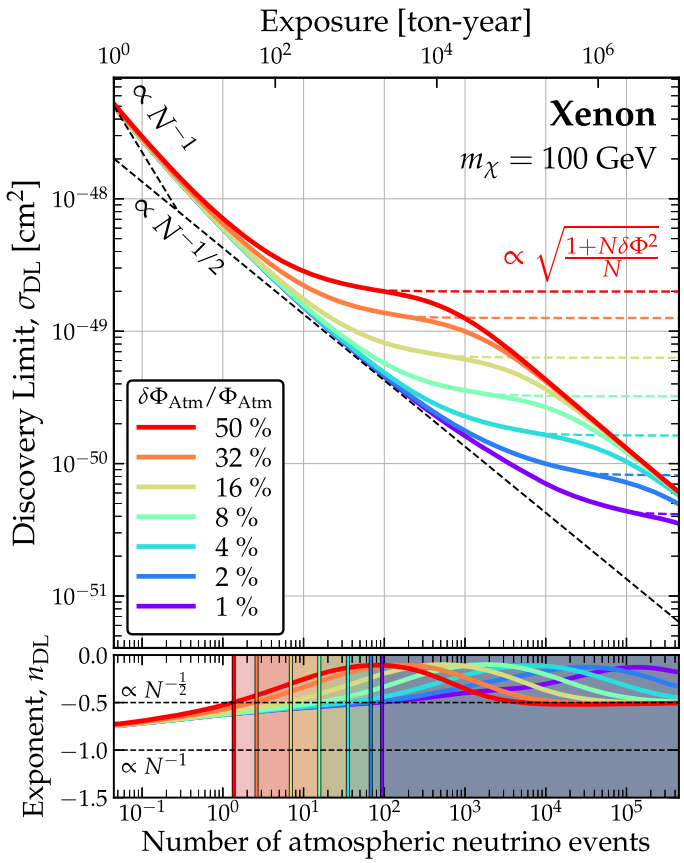

Figure 14. Spin-independent discovery limits at $m_\chi = 100$ GeV as a function of the expected number of atmospheric CEνNS events N, and the fractional uncertainty on the atmospheric neutrino flux, $\delta\Phi_{\rm Atm}/\Phi_{\rm Atm}$. Reprinted (figure) with permission from [474], Copyright (2020) by the American Physical Society. Three scaling regimes as a function of N are shown with dashed lines: (1) 'background-free' $\sigma \sim N^{-1}$, (2) Poissonian $\sigma \sim N^{-1/2}$, and (3) saturation $\sigma \sim \sqrt{(1+\delta\Phi^2 N)/N}$. The bottom panels in each case show the logarithmic scaling exponent defined as: $n_{\rm DL} \equiv {\rm dln}\,\sigma_{\rm DL}/{\rm dln}\,N$. This figure shows the importance of the neutrino flux systematic uncertainty in extending the dark matter physics reach below the neutrino fog.

Figure 15 visualizes the relevant dark matter scattering kinematics. For a maximum-velocity dark matter particle ($v = v_{\rm esc} + v_{\rm Earth}$) and a head-on dark matter–nucleus collision, it shows the maximum recoil energy for either elastic scatters resulting in a nuclear xenon recoil, or inelastic scatters resulting in ERs. For a given energy threshold, this translate into a minimum mass for the dark matter particle to be able to leave a signal in the xenon target. As can be seen, lowering the threshold increases the dark matter mass range that the detector is sensitive to. Further, inelastic scatters as discussed below can be used to probe drastically lighter dark matter candidates (see e.g. reference [497]).

3.1. Double photoelectron emission

In the traditional analysis where both primary scintillation (S1) and ionization (S2) signals are read out, the energy threshold of two-phase liquid xenon TPCs is set by the smallest scintillation

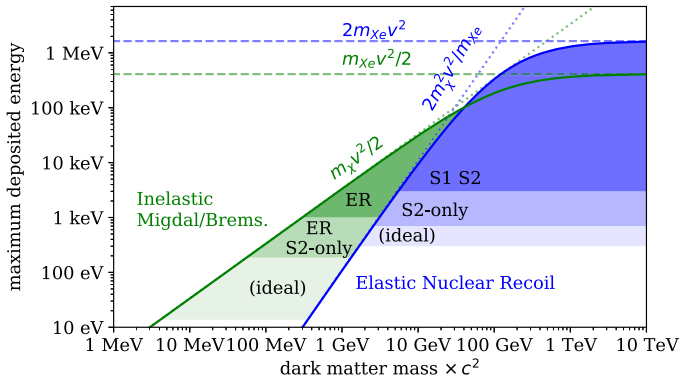

Figure 15. Maximum recoil energy transferred in elastic dark matter interactions to a xenon nucleus (blue) or in iDM interactions to an electron (green). Currently-achieved energy thresholds are indicated for both the traditional S1 + S2 analysis [96, 495] as well as a S2-only analysis [181]. The ultimate thresholds for an ideal detector are also shown (13.7 eV for inelastic scatters [119] and 0.3 keV for elastic NRs [496]).

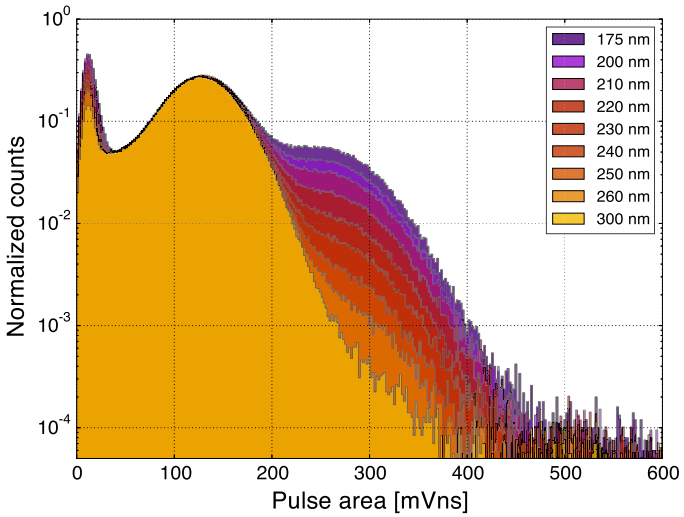

Figure 16. Superposition of single photon pulse area spectra of a R11410 PMT for different wavelengths. Each spectrum is normalized by the integral in the region between 50–120 mV ns in order to show the effect more clearly. Reproduced from [500].

signal that can be confidently discriminated from background sources. Typically, dark matter experiments require an n-fold coincidence of PMTs within a short time window for a pulse to be classified as an S1. The optimal value of n (typically in the range 2–4) is a compromise between signal efficiency and the rejection of fake S1 pulses, caused by random coincidences of PMT dark counts [498].

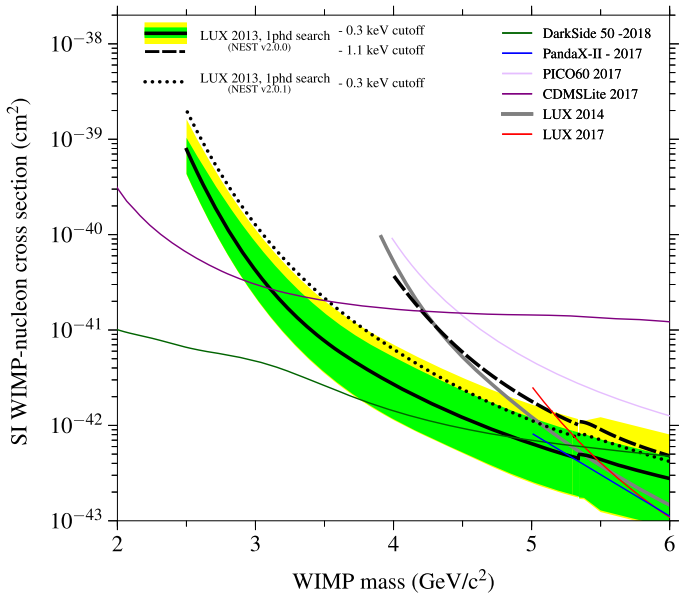

Figure 17. 90% CL upper limits on the spin-independent WIMP–nucleon cross section obtained using the single-photon population producing DPE in the LUX 2013 WIMP search. The observed limit with a 0.3 keV NR energy cut-off is shown in solid black, with 1σ and 2σ sensitivity bands shown in green and yellow. The dashed black line is derived from the same analysis but with a model cut-off at 1.1 keV. Both of these results correspond to the NEST v.2.0.0 model. The upper limit using a 0.3 keV NR energy cut-off with the newer NEST v.2.0.1 model is shown using a dotted black line. Also shown are other results current at the time, namely from the LUX 2013 search [504] (gray), the LUX complete exposure [63] (red), DarkSide-50 [491] (green), PandaX-II [65] (blue), PICO60 [67] (lilac) and CDMSLite [486] (purple). Reprinted (figure) with permission from [503], Copyright (2020) by the American Physical Society.

This methodology makes no attempt to otherwise discriminate dark count background pulses from actual photon-induced pulses. However, it is known that, for some PMT photocathodes, the energy of the liquid xenon scintillation photons (175 nm or 7 eV [499]) is enough to produce two photoelectrons on the PMT photocathode a fraction of the time, resulting in pulses that are on average twice as large as a single photoelectron pulse.

This so-called double photoelectron emission (DPE) effect can therefore be exploited to increase the signal efficiency beyond the standard n-fold optimisation, provided that the DPE fraction and efficiency gain can be properly calibrated. This requires the precise determination of the PMT DPE probability, which depends strongly on the wavelength of the impinging light, as well as on the composition and thickness of the photocathode. For the widely-used Hamamatsu R11410 PMT model, a wavelength scan was performed with single photons down to the VUV range on one unit [500] (see figure 16). The inter-PMT variability due to the photocathode manufacturing process has also been measured at low temperature with a batch of 35 R11410-22 PMTs [501]. Measuring the DPE probability is also crucial for pulse area calibration. A pulse area in 'photoelectrons' does not represent the number of photon hits detected, but can be understood and calibrated if the DPE probability is known. Experiments have reported average values of their PMT DPE probability of around $\sim$10%–20% given liquid xenon scintillation light [502, 503].

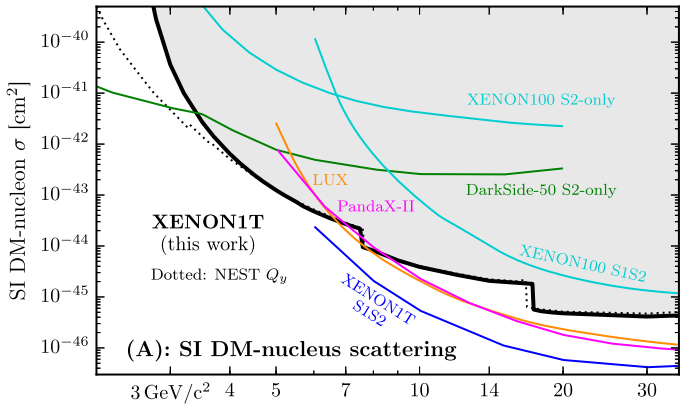

Figure 18. Shown are 90% confidence level upper limits (black lines with gray shading above) on spin-independent dark matter–nucleus scattering with the dark matter mass, m_χ, on the horizontal axis. The thick black line is the result from the XENON1T charge-only analysis. Other results are shown from XENON1T in blue [96], LUX in orange [63], PandaX-II in magenta [400], DarkSide-50 in green [491], XENON100 in turquoise [137, 506]. Dotted lines show the XENON1T limit when assuming the Q_y from NEST v2.0.1 [516] cut off below 0.3 keV. Reproduced from [181].

The LUX experiment exploited this DPE to lower the coincidence condition from two PMTs to just a single PMT with an S1 pulse consistent with DPE [503] (figure 17). In general, an experiment may lower its n-fold condition by requiring that a subset of PMT hits are consistent with DPE. A PMT with a low dark count rate and high DPE probability might enhance the low-energy reach of a next-generation dark matter experiment with a straightforward extension of the analysis [505].

3.2. Charge-only analysis

Interactions from WIMP candidates below $\sim$ GeV/c^2 would produce scintillation (S1) signals close to or below the typical low-energy threshold of liquid xenon TPCs. This loss of efficiency can be bypassed by removing the requirement that the S1 signal be detected at all, and leveraging the inherent gain in the S2 signal [181, 491, 505–508]. Relaxing the requirement of an observed S1 allows events which resulted in even a single extracted electron to be analyzed. This increased sensitivity to low-mass dark matter candidates comes at the expense of recoiling particle discrimination (usually from the S2/S1 ratio) and accurate determination of the z-coordinate (usually from the delay between the S1 and S2 signals). While sometimes these analyses still make use of S1 pulses to reject background events, when they do not require an S1 to be present, they are commonly referred to as 'charge-only' or 'S2-only' analyses.

Thus far, charge-only analyses have been background-limited due to large single- and few-electron backgrounds, which have yet to be reliably quantified and mitigated [507–515]. The extended drift volume of a next-generation detector may be subject to stronger electron lifetime effects, but will also provide improved identification of S2s originating from the bottom of the detector because of increased electron diffusion (resulting in wider S2 pulses). Additionally, xenon contamination from out-gassing or surface detachment of impurities will benefit from the relative scaling of volume and surface area. Despite being background limited, charge-only analyses have been used to set leading limits on dark matter interaction rates, see figure 18. The sensitivity of liquid xenon TPCs to signals at the level of single electrons results in leading sensitivity to sub-GeV WIMPs as well as other particle models. Specifically, charge-only analyses are especially good for detecting ER signals, as their S1 is much smaller than for a NR

of the same S2 size. A charge-only analysis in a next-generation detector will further improve this sensitivity over the current generation of xenon TPCs (see also figure 15).

3.3. General dark matter-induced atomic responses

A dark matter particle with mass in the MeV–GeV range can deposit enough energy in the collision with an electron in a xenon atom to ionise the target and produce a detectable S2 signal in a TPC detector [415, 427]. This charge-only analysis has mainly been performed with models where the interaction between dark matter and electrons is mediated by a new hypothetical force carrier such as the dark photon [181, 492, 507]. To avoid confusion, here the dark photon acts as force carrier, as opposed to the analysis described in section 3.8.1, where the dark photon itself is the dark matter candidate. In this framework, the total ionisation rate for a given xenon orbital can be expressed in terms of a single target-dependent ionisation form factor, which is a function of the initial and final state electron wave functions [415, 427].

Xenon detectors can also probe more complex models, such as those where the amplitude for dark matter scattering by a free electron, $\mathcal{M}$, depends on the initial electron momentum [517]. These include models where dark matter couples to electrons via magnetic dipole or anapole interactions. By expanding $\mathcal{M}$ using effective theory methods similar to the ones previously discussed in the context of dark matter–nucleon interactions (see section 2.5.1), reference [517] found that the most general form for the total ionisation rate of a given xenon orbital is a linear combination of four target-dependent atomic responses, which are defined in terms of initial and final state electron wave function overlap integrals. Assuming that dark matter is made of fermions with mass in the MeV–GeV range and interactions dominated by electromagnetic moments of higher order, such as the electric and magnetic dipoles or the anapole moment, reference [518] showed that liquid xenon TPCs can shed light on whether dark matter is a Dirac or Majorana particle. By using Monte Carlo simulations and a non-trivial extension of the likelihood ratio test to the case where one of the hypotheses lies on the boundary of the parameter space, only about 45–610 signal events are required to reject Majorana dark matter in favour of Dirac dark matter at 3 sigma confidence level.

3.4. Migdal effect and bremsstrahlung

The progressive loss of the scintillation (S1) response with decreasing NR energy impedes the ability of liquid xenon TPCs to reach sensitivity for sub-GeV dark matter masses. However, the standard dark matter–nucleus interaction can also induce an inelastic atomic scattering signal. The Migdal effect [521] predicts the ionization of the atom with some (small) probability due to the sudden nuclear acceleration caused by the dark matter collision, resulting in excitation and ionization processes from the electrons [522]. Since ERs produce a more detectable signal than NRs, this channel enables liquid xenon detectors to reach dark matter masses of order $\sim$100 MeV/c^2 [494, 519, 523, 524], see figure 19. The sensitivity of liquid xenon detectors to sub-GeV dark matter achieved using the Migdal effect is competitive with other detectors that are dedicated to searches of light dark matter [56, 58, 490]. Figure 20 shows a conservative projected Migdal sensitivity for a next-generation detector assuming LZ detector parameters with an extended exposure of 300 tonne-years, equivalent to e.g. a 56 tonne fiducial mass and 5.4 live-years. However, the Migdal effect has not yet been observed directly in dark matter targets. A dedicated calibration could be performed using a low-energy neutron beam [525]. This could provide a direct test of the theoretical predictions of the Migdal effect.

Similar to the Migdal effect, nuclear bremsstrahlung searches leverage the fact that in liquid xenon at low energies, ERs produce a stronger signal than NRs [497]. Bremsstrahlung searches consider the emission of a photon from the recoiling atomic nucleus. In the atomic picture this

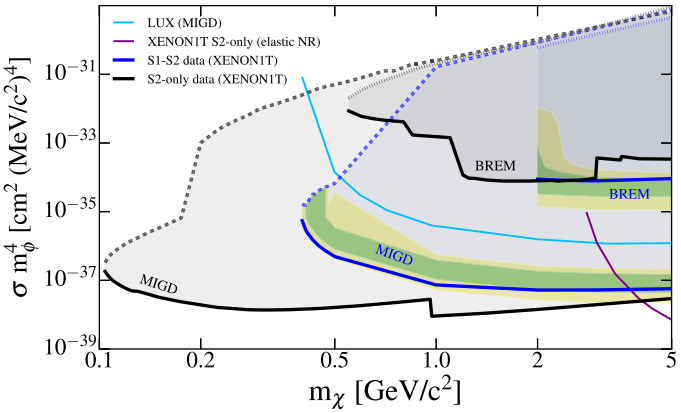

Figure 19. Limits on the spin-independent light mediator dark matter–nucleon interaction cross section at 90% confidence level using signal models from the Migdal effect and bremsstrahlung in the XENON1T experiment with the S1–S2 data (blue contours and lines) and charge-only data (black contours and lines). The solid and dashed (dotted) lines represent the lower boundaries (also referred to as upper limits) and Midgal (bremsstrahlung) upper boundaries of the excluded parameter regions. Green and yellow shaded regions give the 1 and 2σ sensitivity contours for upper limits derived using the S1–S2 data, respectively. The upper limits on the spin-independent dark matter–nucleon interaction cross sections from LUX [494] and XENON1T charge-only (elastic NR results) [181] are also shown. Reproduced from [519]. CC BY 4.0.

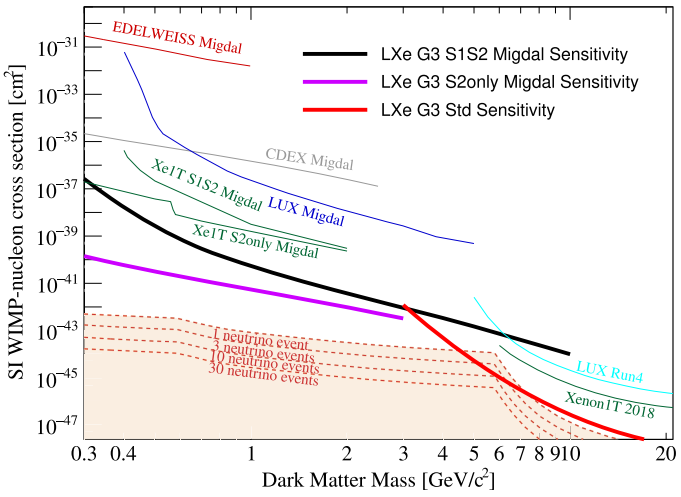

Figure 20. Spin-independent sensitivity for the ER-inducing Migdal effect for the case of a heavy scalar mediator. The S1–S2 sensitivity (black, solid) and the charge-only sensitivity (violet, solid) are shown. The charge-only analysis improves the sensitivity by more than two orders of magnitude with respect to the standard S1–S2 analysis (red, solid). Experimental limits from similar analyses in LUX (blue, solid) [494], XENON1T (green, solid) [181] and CDEX (gray, solid) [520] are also shown.

can be viewed as the dipole emission of a photon from a xenon atom that has been polarized in the dark matter–nucleus scattering. In xenon, the emission of the bremsstrahlung photon is more heavily suppressed compared to the Migdal effect and hence results in a weaker signal for all interaction types [526]. The theoretical motivation and event rates for bremsstrahlung have been derived in reference [497] and searches using liquid xenon detectors have been published in reference [66, 494, 527].

3.5. Hydrogen doping

Kinematically, the large xenon nucleus (average mass 122 GeV/c^2) is not well suited for an efficient transfer of energy from Galactic dark matter with mass $\lesssim$1 GeV/c^2. As a result, nearly all of the resulting xenon NRs fall below the energy threshold for detection. A possible solution for enhancing the sub-GeV sensitivity of liquid xenon TPCs is to dissolve a lighter species in the liquid xenon bulk [528]. In this configuration, the lighter nucleus becomes the dark matter target, and the xenon becomes the sensing medium.

This strategy exploits two of the primary advantages of the liquid xenon medium. First, the high atomic number and density of liquid xenon provides excellent self-shielding of external backgrounds from the central volume of the detector. Such a suppression would not be possible in a similarly-sized detector comprised of the light species alone. Second, the high yield of detectable quanta (electrons and photons) resulting from low-energy particle interactions makes xenon an ideal sensor for the recoiling light nuclei.

Having the lightest nucleus of any element, hydrogen is kinematically the best candidate species for detecting interactions from sub-GeV dark matter and astrophysical neutrinos [529]. The lone proton comprising hydrogen's nucleus additionally provides unique sensitivity to the spin-dependent dark matter coupling to protons. Likewise, doping the xenon target with deuterium would provide similar sensitivity to the neutron-only couplings. There are still significant open questions concerning the actual feasibility of adding H_2 to a liquid xenon TPC. Drifting electrons in the detector's gas space will be cooled down by the hydrogen and therefore the electric field strength needed to extract quasi-free electrons out of the liquid and into the gas space will be increased [530]. Furthermore, the light yield of xenon electroluminescence will be suppressed. Molecular species within the liquid space are also known to quench the S1 light production. S1 as well as ionization signals for H_2 mole fractions up to 5.7% have been observed in a 26 atm gaseous xenon TPC from ^{241}Am 5.5 MeV alpha particles [531], although there is a reported loss of about half of the S1 and electron signals for an H_2 mole fraction of 1.1%. Helium is also a viable option as the light mass target species, as it would not have the signal quenching properties of H_2, but its spin-dependent sensitivity would be comparatively poor. Introduction of helium into the detector might not be suitable if PMTs are used as a photosensor due to its ability to diffuse into and degrade the PMT vacuum [532], but could be considered if SiPMs are used instead of PMTs.

3.6. Upscattered dark matter

The sensitivity reach of liquid xenon detectors for sub-GeV dark matter is significantly enhanced if some dark matter particles receive a kinematic boost from up-scattering with cosmic rays [456, 533–538]. This process, often denoted CRDM, will create a small population of fast or even relativistic dark matter particles. This in turn provides sensitivity to liquid xenon experiments to dark matter with masses several orders of magnitude below 1 GeV. Cosmic ray up-scattered dark matter is only a fraction of the Galactic dark matter population, with an abundance and flux that depends on the dark matter–cosmic ray scattering cross section, the local dark matter density, and the local interstellar spectrum of cosmic rays. Relatively large cross

section values of e.g. $\sigma_{\chi N} \gtrsim 10^{-31}$ cm^2 for $m_\chi = 1$ GeV are required to have a notable impact on the sensitivity of a typical liquid xenon detector. For spin-independent interactions, liquid xenon experiments are competitive with and complementary to existing neutrino experiments [447, 533, 535], which have sensitivity in a similar region of parameter space. Additionally, cosmic-ray upscattering extends the sensitivity of liquid xenon detectors to iDM models with mass splittings up to ∼100 MeV [539].

Another upscattering mechanism extending the sensitivity of liquid xenon detectors to dark matter masses down to keV scales is a process called 'solar reflection' [540–545]. This is based on the observation that scatterings on thermal electrons and nuclei within the Sun can accelerate light dark matter particles. This could give rise to an observable flux of highly energetic particles in a liquid xenon TPC detector.

3.7. Dark matter annihilation products

In several models of so-called 'neutrino portal' dark matter, Galactic dark matter self-annihilates into neutrinos [546–550]. These in turn may be detected at direct detection experiments with high rates via CEνNS (see section 5.1.1). A next-generation liquid xenon detector would be sensitive to the flux of these neutrinos for dark matter mass (respective neutrino energy) of [0.01–1] GeV$/c^2$ [551]. The sensitivity to this neutrino flux would complement neutrino detectors such as Super-Kamiokande.

Similarly, dark matter may annihilate into another component of dark matter, which, if relatively light, may receive a Lorentz boost [552, 553]. Thanks to its higher kinetic energy, such a light annihilation product might in turn be discovered in a direct detection experiment. A next-generation liquid xenon TPC will be sensitive to the effective baryonic coupling of thermal boosted dark matter that is as low as the weak interaction [551].

Alternatively, dark matter may annihilate or decay within the target volume of future liquid xenon detectors [554]. Considering deposited energies up to a few MeV, the relevant final states include annihilation into $\gamma\gamma$ and e^-e^+, and decays into $\gamma\gamma$, $\gamma\nu$ and e^-e^+. Although the sensitivity obtained is not as high as the current limits from cosmological considerations [555] and x-ray measurements [556], this is a complementary approach in a well-understood background environment and free of the large uncertainties typically present in indirect detection experiments.

3.8. FIMPs and super-WIMPs

Broad classes of non-WIMP dark matter candidates are feebly interacting massive particles (FIMPs), which are produced by the thermal freeze-in mechanism [557, 558], as well as super weakly interacting massive particles (super-WIMPs), which are produced by the decay of a freeze out-produced state to a lighter state which is secluded from the SM [559]. Both classes share the feature that they couple to SM particles with cross sections far smaller than the weak scale. These include fermions such as sterile neutrinos [560] and gravitinos, both of which only couple to the SM gravitationally and thus are impossible to observe in a typical direct detection experiment. However, both multi-GeV bosonic and fermionic FIMPs and keV-scale bosonic FIMPs or super-WIMPs can couple to light SM particles in such way to be observed with low-background experiments [561–563]. We note here that dark sectors with non-trivial dynamics, for instance an early Universe thermal phase transition, allow freeze-in production of dark matter in the mass range 10 keV$/c^2 \lesssim m \lesssim 100$ MeV$/c^2$ with relatively large scattering cross section with nucleons and/or electrons, which blurrs the distinction between FIMPs and WIMPs [564]. In the following, we give two examples of possible keV-scale candidates, namely dark photons and axion-like particles (ALPs), and discuss related signals.

3.8.1. Dark photons. Dark photons, more properly dark Z' vector bosons, are a possible FIMP or super-WIMP candidate if they are stable over cosmological time scales [561], and even if unstable, they can act as the mediator of dark matter–SM interactions [481]. Like axions, they are well motivated in many UV constructions, and have the advantage over some other candidates of having a mass which is naturally protected from large corrections. In addition to production related to the usual thermal freeze-in or freeze-out, there is also an attractive universal inflationary fluctuation mechanism that gives the observed relic density depending only on the vector-boson mass and inflationary scale [565]. Furthermore, dark photons can be produced in a non-thermal way through the misalignment mechanism [566] if they have a non-minimal coupling to gravity [567, 568]. As is known from the related case of axions, the relic density then has contributions from inflationary perturbations or the vacuum condensate, and thus can produce a cold dark matter candidate despite the low mass of the relevant particle.

A well-studied interaction of dark photons with the SM is via kinetic mixing [569] with hypercharge, and thus with both the SM photon and the Z-boson [570, 571]. As a consequence, dark photons can be absorbed in a detector with a cross section proportional to the photoelectric cross section. The expected signal is therefore a mono-energetic ER peak at the dark photon mass.

Direct detection experiments have set competitive constraints on kinetic mixing parameter κ of dark photons, in a mass range from several to hundreds of keV [181, 495, 568]. A next-generation detector such as the one discussed here will have improved sensitivity to this mixing parameter κ. Further, dedicated low-energy calibrations, for example using ^{37}Ar diluted in the liquid xenon, will help to improve the search in the keV mass range and reduce the relevant detector-specific systematics to negligible levels for a discovery experiment. Using a low-energy charge-only analysis (section 3.2), the sensitive mass range can be extended to the sub-keV level, see e.g. reference [572]. In addition, XENON1T data already results in the current-best limits on the solar emission of dark photons for some masses [573]. These channels offer significant room for improvement with a next-generation detector.

3.8.2. Axions and axion-like particles. The QCD axion is a pseudoscalar Nambu–Goldstone boson originally proposed as a solution to the strong CP problem of QCD [574–576]. The QCD axion is also an excellent dark matter candidate [577–581]: as they acquire their mass via non-perturbative QCD effects, they are stable on cosmological timescales. Further, QCD axions offer a variety of well-motivated production mechanisms [582]. They couple to the SM very weakly, with couplings suppressed by a high energy scale f_a. In terms of this unknown (but constrained) scale, QCD axions are predicted to have a mass $m_a \simeq 5.7\ \mu\text{eV}(10^{12}\ \text{GeV}/f_a)$ [583]. The strict lower bound $f_a \gtrsim$ few $\times\ 10^7$ GeV (see [584]) arising from astrophysical constraints [585–589] and the solar axion helioscope CAST [590] implies that QCD axion dark matter is beyond the reach of detectors like the one discussed here, and requires dedicated experiments. However, axions produced in the Sun would have thermal spectra with keV energies, and could be detected with a xenon TPC as discussed in section 6.1.

ALPs are a generalization of the QCD axion in that they share many of the same properties, except that the strict relationship between the mass and the scale f_a is relaxed and that the various possible couplings of ALPs to the SM vary over greater ranges than the QCD axion. In particular ALPs can be both much lighter than the QCD axion or much heavier. These particles do not solve the strong CP problem, but nevertheless are good dark matter candidates and can show up abundantly in theories for physics beyond the SM, in particular string theory [591–595]. In a similar way to dark photons, ALPs can be detected via an analogous process

to the photoelectric effect [596]. For dark matter ALPs, the resulting signal is again a mono-energetic spectrum of ERs at the ALP mass, with an event rate proportional to the square of the dimensionless axion–electron coupling g_{ae}.

Due to their ultra-low ER background levels, liquid xenon TPCs have placed the strongest constraints to date on keV ALP dark matter [181, 495, 507, 572, 597–602]. Next-generation detectors including the one discussed here will continue to set world-leading constraints [1].

3.8.3. Solar axions, dark matter, and baryon asymmetry. As discussed in section 6.1, a liquid xenon TPC can detect the QCD axion and ALPs from the Sun for sufficiently large couplings of the axion with electrons or photons. Such relatively large couplings correspond to a small decay constant, f_a, of the axion. In this case, the cosmological abundance of axions produced by conventional mechanisms [577–579, 603] is too small for the axion to explain the observed dark matter. However, the axion abundance can be large enough to be dark matter in the various scenarios proposed in references [604–610], with couplings that are sufficiently large to be detected in the proposed detector.

In one such cosmological scenario for example [609], a non-zero field velocity delays the onset of field oscillations, enhancing the axion abundance relative to the conventional misalignment mechanism. For ALPs, this field velocity can simultaneously explain the baryon asymmetry of the Universe [611]. Fitting the ratio of dark matter to baryon abundances predicts the axion coupling in terms of its mass m_a

$$g_{a\gamma} \simeq 2 \times 10^{-11} c_\gamma \ \mathrm{GeV}^{-1} \left(\frac{m_a}{\mathrm{meV}}\right)^{1/2}, \tag{3}$$

where c_γ is a model-dependent constant of order unity. For any axion mass, this is much larger than the photon coupling of the QCD axion. A next-generation liquid xenon TPC with a 1000 ton-year exposure can probe this coupling down to $g_{a\gamma} \sim 3 \times 10^{-11}$ GeV^{-1} [612], corresponding to $m_a \sim$ meV.

3.9. Asymmetric dark matter

Asymmetric dark matter is one of the most motivated non-WIMP dark matter candidate. Similar to the physics that sets the SM cosmic baryon abundance, asymmetric dark matter posits that the dark matter relic density is determined by a dark-sector particle–antiparticle asymmetry associated to a new conserved quantity [613–624]. Then, similarly to protons and baryon number, the lightest symmetry-carrying state in the dark sector is cosmologically stable. If η_{B} and η_{dm} are, respectively, the baryon and dark matter asymmetries, and if like for baryons and anti-baryons the process of particle–antiparticle annihilation is efficient in the dark sector, then the ratio of the dark matter to the baryon densities is given by

$$\frac{\Omega_{\mathrm{dm}}}{\Omega_{\mathrm{B}}} = \left|\frac{\eta_{\mathrm{dm}}}{\eta_{\mathrm{B}}}\right| \frac{m_{\mathrm{dm}}}{m_{\mathrm{B}}}. \tag{4}$$

Here, m_{dm} is the mass of the lightest asymmetry-carrying dark matter particle.

In many beyond the SM theories, the asymmetries are naturally equal and opposite, up to a computable coefficient which is of order $\sim$1. Thus, in this case we have an explanation of why the observed baryon and dark matter densities are so close, $\Omega_{\mathrm{dm}} \simeq 5\Omega_{\mathrm{B}}$, if $m_{\mathrm{dm}} \sim$ few GeV$/c^2$. This strongly motivates searches for dark matter particles in the $\sim$1–10 GeV$/c^2$ mass range. Independently-motivated theories, such as those based on 'neutral naturalness' Twin Higgs [625] or composite Higgs explanations of the LHC-data driven little hierarchy problem for the weak scale also predict dark-sector states in this mass range [395, 626–628].

In theories such as Twin Higgs, the leading interactions of the individual asymmetric dark matter particles with the SM are due to Higgs-portal and/or kinetic mixing with hypercharge, so often the direct-detection phenomenology is similar to the case of WIMPs with these interactions. In other cases the leading higher-dimensional interaction of the individual asymmetric dark matter particles arises from the 'connector' interaction that determines the relation between $\eta_{\rm dm}$ and $\eta_{\rm B}$ [389, 629–632], or can sometimes be related to a freeze-out process involving heavier states [633]. In effect, since the freeze-out mechanism is no longer setting the dark matter density, the scattering cross section of asymmetric dark matter with the SM can be smaller (or larger) than that for WIMPs.

3.10. Composite dark matter

Similar to the rich set of cosmologically stable composite states that exist in the SM sector, all or part of the dark matter density might be in the form of bound states of individual dark matter particles. This is a natural possibility if the dark matter is part of a dark sector (as is in turn often so in explicit constructions of physics beyond the SM), or if the dark matter is self-interacting. These composites may be strongly-bound 'dark (hidden) pions' or 'dark (hidden) baryons' in dark (hidden) QCD [634–638]; 'dark nuclei' or 'dark nuggets' [255, 639–644] of possibly extremely large dark nucleon number; 'dark atoms' [395, 645, 646] made of dissimilar stable dark matter particles; or they could be weakly bound two-body 'dark-onium' states of identical or conjugate particles [321, 647–650]. Further, topological solitons such as 't Hooft–Polyakov monopoles [651, 652] might exist in the dark sector and provide a form of composite dark matter with a rich phenomenology [392]. Q-balls [653] can also be thought of as a form of nontopological composite states, carrying a conserved quantum number, the Q-ball description sometimes applying to bound states of bosonic dark matter particles.

Such composite states typically give rise to a variety of new or modified signatures in direct detection experiments. One of the most studied case is that of large dark nuclei in which case the recoil spectrum is modified by a characteristic quasi-universal dark sector form factor [255, 654–656]. Since there is often an N^2 ($N \gg 1$) dark nucleon number coherent enhancement in the direct detection scattering cross-section, which is not present in the collider production of (pairs of) individual dark matter particles, the usual collider bounds on direct detection cross sections can be significantly weakened [255]. In addition, many of these composite states have low-lying excitations, leading to a rich set of possible inelastic signatures (section 2.13). It is also possible to have an enhanced diurnal modulation signal as a consequence of the dissipative dynamics that is naturally associated with such composite dark matter states [657].

3.11. Absorption dark matter

If a dark matter particle is absorbed in a direct detection experiment, its mass energy may be transferred to the nucleus, leading to a recently-proposed, distinct dark matter direct detection signal [658, 659]. Such a process can be realized from a UV-complete theory where the dark matter has a mass-mixing with the SM neutrino and the incoming dark matter is converted into a neutrino after scattering through a neutral current (NC), $\chi + N \to \nu + N$. Since the mass of the dark matter dominates this process, the resulting NR energy has a sharp peak at $E_r \sim m_\chi^2/(2m_N)$. The first search for such a mono-energetic recoil signature was performed in PandaX-4T [660], with a resulting constraint on the absorption dark matter–nucleon scattering cross section at the level of 10^{-50} cm^2.

Another possible absorption process is the induced beta-decay through a charged current (CC) $\chi + {}^{A}_{Z}\mathrm{N} \to e^- + {}^{A}_{Z-1}N$. The corresponding signature has multiple correlated signals: the ejected energetic electron, the recoil of the daughter nucleus, a gamma from the de-excitation

of the daughter nucleus, and possibly another beta-decay of the final nucleus if that is unstable. It is also possible that such an absorption happens when dark matter interacts with electrons [661–663]. The signature in a direct detection experiment is a mono-energetic ER. Currently the strongest constraints on this channel are also provided by PandaX-4T [664].

3.12. Mirror dark matter

Closely related to both asymmetric and composite dark matter is the idea of mirror dark matter [665–668]. This is the intriguing idea that an exact copy of the SM in the dark sector is invoked with an unbroken symmetry between the two. Like some other asymmetric and composite dark matter models, mirror dark matter can generate signatures both in NRs similar to those expected from $\sim$7 GeV$/c^2$ WIMPs with a cross section around 10^{-44} cm^2, as well as in ERs [669–671]. The strongest direct detection constraint on the kinetic mixing currently comes from LUX [672], with a factor of $\sim$2 better projected sensitivity for the current-generation detectors [572]. Mirror dark matter as a hypothesis is potentially entirely falsifiable by the next-generation liquid xenon experiment discussed here [673].

3.13. Luminous dark matter

It is possible to construct models where the dominant signal of the dark matter originates from photons. These photons could be observed in direct detection experiments as a monoenergetic line produced by dark matter decay from an excited state [674, 675]. The excited state could be populated through upscattering in or near the detector (and have short lifetimes $\sim$1 μs) or in the Earth (lifetimes $\sim$ (1–10) s). For this scenario to work, the elastic cross section needs to be small relative to the inelastic cross section. A simple way to achieve this is with a magnetic dipole operator which couples two distinct Majorana fermions that have a keV-order mass splitting. Such 'luminous dark matter' was first proposed as a potential explanation of the DAMA/LIBRA modulation [674] and has since been used to explain the recent XENON1T excess [676]. While the former scenario is now strongly constrained, the latter scenario will be confirmed or ruled out by a next-generation liquid xenon experiment.

3.14. Magnetic inelastic dark matter

A natural scenario where dark matter dominantly scatters off nuclei through an inelastic transition in the dark sector (section 2.13) is the case of a magnetic dipole interaction [677]. This model relies on the fact that fermionic dipole operators vanish for Majorana fermions. Thus, if a dark matter Dirac fermion state is split into two nearly degenerate Majorana fermions, an elastic dipole transition is forbidden, leaving the leading dark matter interaction to be an inelastic magnetic dipole transition [678–681].

For magnetic iDM, the sensitivity of a direct detection experiment is modified by both the kinematic constraints of inelastic transitions and by the dependence on the charge and magnetic dipole moment of the target nuclei [677]. Depending on the dark matter mass splitting and the size of the dipole moment, the excited dark matter state can also decay in the detector, thus yielding both a NR from the initial scatter and an ER from the decay shortly thereafter. Searching for the photons produced by this decay can be an additional handle on uncovering such a scenario [675, 682]. A dedicated search has been performed by XENON100 [683], with the proposed experiment providing significantly improved sensitivity not only due to the lower background and longer exposure, but also due to the larger size of the detector, which translates into a sensitivity to longer decay times.

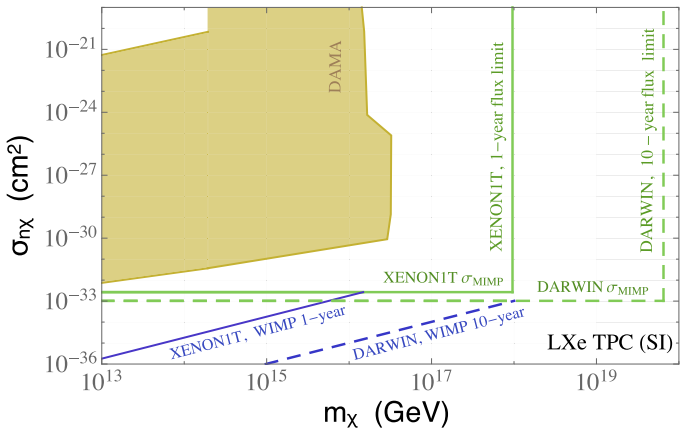

Figure 21. Per-nucleon spin-independent scattering cross sections and dark matter masses that can be probed by liquid xenon dark matter detectors via dedicated searches for multi-scatter signals. For cross sections above σ_{MIMP} (horizontal green lines) one expects dark matter to scatter multiple times in the detector while transiting. The maximum mass reachable (vertical green lines) is limited by the total integrated flux of dark matter in the detector over the run-time of the experiment. Masses up to and beyond the Planck mass $\simeq 10^{19}$ GeV$/c^2$ may be probed with a next-generation detector. Only smaller cross-sections and smaller masses are probed by the standard single-scatter analyses (blue lines). Reproduced from [156]. CC BY 4.0.

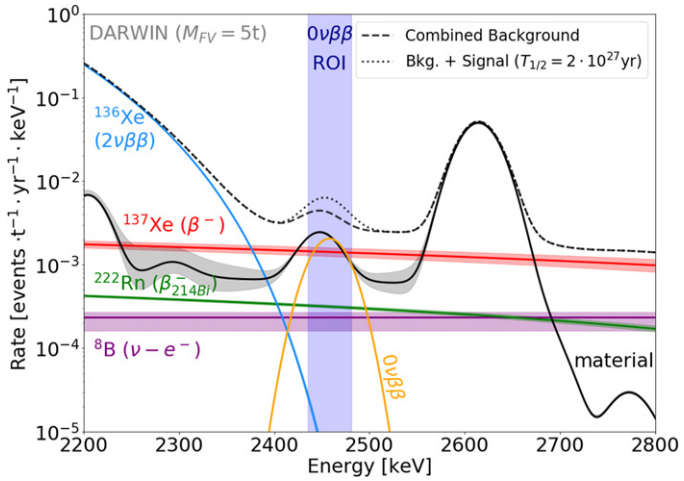

Figure 22. Predicted background spectrum around the $0\nu\beta\beta$ energy region of interest (ROI) for a proposed next-generation dark matter experiment. Rates are averaged over a FV containing 5000 kg of liquid xenon with natural isotopic abundance. Bands indicate $\pm 1\sigma$ uncertainties. The orange line represents a hypothetical signal corresponding to $T_{1/2} = 2 \times 10^{27}$ years. Reproduced from [710]. CC BY 4.0.

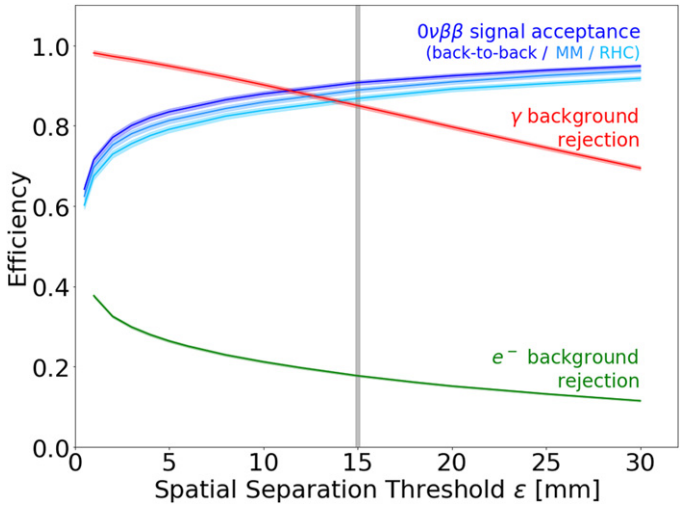

Figure 23. Efficiency of $0\nu\beta\beta$ signal acceptance and background rejection as a function of the minimum distance for individual reconstruction of energy depositions. The three signal lines (blue) compare different energy and angular distributions for the $0\nu\beta\beta$ signal based on a back-to-back electron emission, a mass mixing mechanism and a right-handed current model. The background rejection efficiency is shown for γs (red) and electrons (green) with $E = Q_{\beta\beta} = 2457.8$ keV. The vertical line (gray) corresponds to the value assumed here. Bands indicate $\pm 2\sigma$ uncertainties. Reproduced from [710]. CC BY 4.0.

3.15. Dark matter around the Planck mass

The observed local dark matter mass density could be made up of few but very massive dark matter particles with masses around the Planck mass $\simeq 10^{19}$ GeV$/c^2$, as opposed to numerous lighter particles. Super-massive species are motivated by supersymmetric and grand unified theories (GUTs) [684], or production by Hawking evaporation of early Universe primordial black holes [685, 686]. In extensions of the WIMP scenario, with two thermal relics, one of which has a finite lifetime, super-massive dark matter particles with stronger interactions than typical electroweak WIMPs are naturally expected [687], and provide excellent targets. The detection of any such particles could help determine parameters of the early Universe such as inflation [688], or an epoch of early matter domination [687, 689] leading to efficient primordial black hole production. Their existence could also imply new light mediators beyond the SM [690].

Due to the small number density, the flux of these particles through a given detector would be very low, and thus any detection would both imply and require a very high scattering cross section, such that almost all particles impinging on the detector prompt a signal. When the cross section becomes high enough that these particles would interact more than once in the detector, discovery requires a dedicated analysis looking for multiple-scatter events. Such events are typically discarded in WIMP-like dark matter analyses, leaving many orders of magnitude of unexplored parameter space, see figure 21. In this multiple scattering regime, a next-generation liquid xenon experiment would be capable of probing dark matter masses up to and beyond the Planck mass $\simeq 10^{19}$ GeV [156], in a complementary way to the range that could be probed using dedicated neutrino experiments [691–693]. A dedicated search using the DEAP-3600 liquid argon detector has already been published [694]. Clusters of dark matter formed through self-attraction [640, 654, 695], such as 'dark blobs' or 'dark nuggets' [255, 640, 655, 656] could exist at these high masses and create tracks if they have sufficiently large cross-sections.

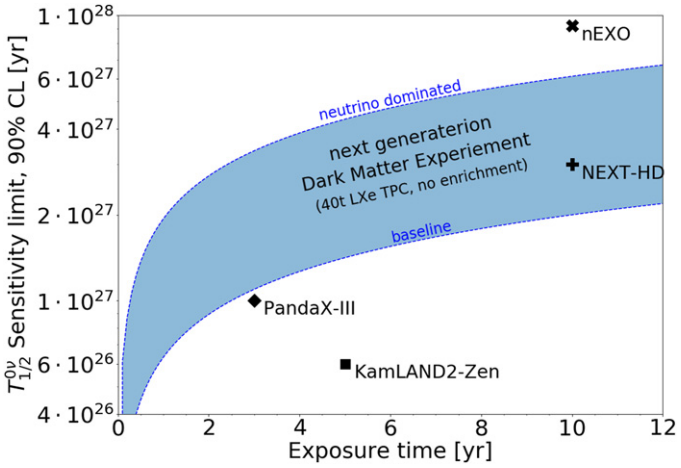

Figure 24. Predicted median $T^{0\nu}_{1/2}$ sensitivity at 90% CL as a function of the exposure time for a next generation TPC detector containing 40 t of liquid xenon with natural isotopic abundance. The band indicates the sensitivity range between a baseline radio purity scenario at a depth of 3500 m water equivalent to a scenario with neutrino dominated background. Sensitivity projections for future ^{136}Xe $0\nu\beta\beta$ experiments [710–714] are shown for comparison. Reproduced from [710]. CC BY 4.0.

4. Double beta processes

4.1. Neutrinoless double beta decay of ^{136}Xe

Among the main intellectual challenges facing the nuclear and particle physics communities today are the neutrino-mass generation mechanism, the absolute neutrino-mass scale, and the neutrino-mass spectrum. One of the best ways to address these fundamental questions is to search for neutrinoless double beta decay ($0\nu\beta\beta$) [696–699]. The observation of this rare nuclear decay process, forbidden in the SM, would imply that the lepton number is violated by two units and confirm the Majorana nature of the neutrinos. It would also provide invaluable information about the dominance of matter over antimatter in the Universe, because two matter particles—electrons—are emitted in the decay without the balance of the corresponding antiparticles. Double beta decay can occur in the two xenon isotopes ^{134}Xe [700] and ^{136}Xe, with the latter offering a larger sensitivity to the $0\nu\beta\beta$ half-life ($T^{0\nu}_{1/2}$). The best experimental constraint on the ^{136}Xe $0\nu\beta\beta$ half-life, $T^{0\nu}_{1/2} > 1.07 \times 10^{26}$ years (90% CL), is set by the KamLAND-Zen collaboration using ^{136}Xe dissolved in a liquid scintillator [701]. Among double-beta experiments, only ^{76}Ge, ^{82}Se, ^{100}Mo and ^{130}Te offer $0\nu\beta\beta$ half-life limits comparable to ^{136}Xe [702–707]. The EXO-200 collaboration demonstrated that better energy resolution and background rejection can be achieved with a liquid xenon TPC [708], and the PandaX-II collaboration conducted a first search using a dual-phase natural xenon detector [709]. XENON1T recently demonstrated that energy resolutions below $\sigma/\mu = 1\%$ at $Q_{\beta\beta}$ can be achieved in liquid xenon TPCs used for dark matter searches [116].

A next-generation liquid xenon detector will contain multiple tonnes of the ^{136}Xe isotope, either at the natural abundance of 8.9%, or, as a possible upgrade, using enriched xenon. Given a TPC design optimized for WIMP searches, a detector instrumenting ∼40 000 kg of non-enriched xenon can already improve the sensitivity to $0\nu\beta\beta$ decay by more than one order of magnitude over current limits, without any interference with its primary dark matter

science goal. Taking advantage of the excellent self-shielding of liquid xenon, the material-induced gamma ray background can be suppressed below the total intrinsic background rate (section 7.2). Figure 22 shows the relevant sources of background with a hypothetical $0\nu\beta\beta$ signal for the innermost 5000 kg of natural xenon in the TPC of a proposed next-generation detector [710]. The background from material-induced gamma rays will be further reduced in more massive detectors than the one simulated in figure 22.

Selecting ultra-low background materials for construction can further reduce the material contribution as well as the background rate from ^{222}Rn, which emanates from material surfaces into the target volume. A sufficiently deep laboratory suppresses cosmogenic background sources, such as the *in situ* activation of ^{136}Xe by muon-induced neutrons (producing ^{137}Xe) [715, 716], down to the limit set by electron scattering of solar ^{8}B neutrinos. Optimizing the detector design for an improved spatial resolution would allow to further exploit background rejection, based on the different topology of background and signal events caused by bremsstrahlung radiation, as shown in figure 23. Combining these measures, the experimental sensitivity can be further enhanced to make a next-generation dark matter detector competitive to dedicated next-generation, tonne-scale $0\nu\beta\beta$ experiments, as shown in figure 24. Naturally, a larger target mass would allow further gains in self-shielding and even more competitive sensitivity to rival the next generation of dedicated experiments. Isotopic enrichment in ^{136}Xe would further improve this sensitivity, as it linearly increases the signal, although this also increases the background rate from the two-neutrino double beta decay ($2\nu\beta\beta$) of ^{136}Xe and β-decay of ^{137}Xe.

In addition, there exist mechanisms of $0\nu\beta\beta$ decay where the lepton-number violation necessary for the decay is due to a lepton-number violating mechanism other than the standard scenario of exchange of light neutrinos. A large fraction of these models can be tested using an EFT approach [717–726] which in the case of chiral EFT also provides a hierarchy for the relevant nuclear matrix elements [727–736], along similar lines as described in section 2.5 for dark matter. These theoretical models can thus be used as a low-energy test of new physics phenomena that complements high-energy searches at accelerators.

Besides the search for $0\nu\beta\beta$ decay, precision measurements of the $2\nu\beta\beta$ decay can reduce the experimental uncertainty on the $2\nu\beta\beta$ nuclear matrix element [737] and constrain the underlying nuclear theories [699, 738, 739]. *In situ* measurement of this decay can be performed directly in the detector, even with a natural xenon target [740]. This is especially relevant regarding $0\nu\beta\beta$ decay, because predictions of nuclear matrix elements disagree by a factor three or more, severely limiting the interpretation of current limits and the physics reach of future searches, for instance in terms of neutrino masses [699, 739]. The nuclear many-body methods used to calculate $0\nu\beta\beta$ nuclear matrix elements are generally the same that are also used to obtain the nuclear structure factors in section 2.6. The nuclear shell model among other more phenomenological approaches yields most predictions [725, 741–749], complemented by recent *ab initio* studies [736, 750–752]. A precise $2\nu\beta\beta$ spectrum shape measurement can provide insights toward reliable $0\nu\beta\beta$ nuclear matrix element calculations [753]. In addition, precision measurements of $2\nu\beta\beta$ decay can also be used to probe new physics. For example, right-handed lepton currents affect the angular and energy distributions of the decay [754], MeV-scale sterile neutrinos can be searched for through kinks in the $2\nu\beta\beta$ spectrum [755, 756], and neutrino self-interactions can leave an imprint on the spectrum as well [757]. Because lepton number is not necessarily violated in $2\nu\beta\beta$ decay, this is independent of the neutrino nature and can be used to constrain or pinpoint properties of both Majorana and Dirac neutrinos.

4.2. Double electron capture on ^{124}Xe

Similar to double beta decay, double electron capture is a second order weak interaction process [758, 759] with extremely long half-lives. Two electrons are captured from the atomic shell and two protons are converted into neutrons. In the SM decay, two neutrinos carrying virtually the total Q-value are emitted and leave the active volume undetected (2νECEC). The measurable signal is constituted by the atomic de-excitation cascade of x-rays and Auger electrons that occurs when the vacancies of the captured electrons are refilled. In a liquid xenon detector, this cascade is measured as a single resolvable signal at 64.3 keV for the double K-capture [760] as the most likely case [761]. The half-life of this decay is of great interest with regard to nuclear matrix element calculations, as it provides a benchmark point from the proton-rich side of the nuclide chart [762–764]. A precise measurement would help to narrow down uncertainties, which in turn have implications on the neutrino mass scale derived from $0\nu\beta\beta$ as discussed in section 4.1.

Following hints in XMASS [765], the half-life of the ^{124}Xe double K-capture has recently been measured by XENON1T [766]. At $T^{2\nu\mathrm{KK}}_{1/2} = (1.8 \pm 0.5_{\mathrm{stat}} \pm 0.1_{\mathrm{sys}}) \times 10^{22}$ years, it agrees with recent theoretical predictions [762–764]. For comparison, this is about one order of magnitude slower than the $2\nu\beta\beta$ decay of ^{136}Xe due to the small overlap of the K-electron with the nucleus. Assuming a natural isotopic abundance similar to XENON1T, a next-generation experiment would record on the order of 10 000 events in its full exposure. This will allow a precision measurement of the double K-capture half-life to the percent level. Additionally, an observation of the KL-capture and LL-capture would be within reach [761]. Their measurement would help to decouple the nuclear matrix element from phase-space factors.

Beyond the SM, the double electron capture on ^{124}Xe without neutrino emission (0νECEC) can complement $0\nu\beta\beta$ in addressing fundamental questions about the mass and nature of the neutrino [767, 768]. To conserve energy and momentum, 0νECEC is possible if the ^{124}Xe decay populates an excited state of the ^{124}Te daughter nucleus, so that the final energy matches the initial one. This scenario would allow a resonant enhancement of this channel, which would be needed to provide accessible half-lives [769]. A suitable daughter state exists, but current measurements of the Q-value indicate only an approximate match of the ^{124}Te level, two-hole energy, and Q-value that would only provide a minor enhancement [760]. If this decay is realized, the experimental signature contains multiple γ-rays emitted in a cascade, so coincidence techniques could increase experimental sensitivity [770].

4.3. Other double-beta processes

The ^{124}Xe Q-value of 2857 keV also allows second-order decays involving positrons [771]. Examples are the as-yet unobserved SM $2\nu\mathrm{EC}\beta^+$ and $2\nu\beta^+\beta^+$ decays, as well as the hypothetical $0\nu\mathrm{EC}\beta^+$ and $0\nu\beta^+\beta^+$ decays. The decay $2\nu\mathrm{EC}\beta^+$ is predicted to have a half-live one order of magnitude above that of 2νECEC [772]. Exploiting the coincidence signature of the positron annihilation and the atomic de-excitation cascade, this decay could already be within reach of LZ and XENONnT [770, 773] and be a sure signal in the next-generation detector. The $2\nu\beta^+\beta^+$ decay is expected to be several orders of magnitude slower [772]. It exhibits a unique signature with five point-like ionization clusters, located in the same plane with the central vertex [774].

On the neutrinoless side, $0\nu\mathrm{EC}\beta^+$ would be favoured in the absence of resonance enhancement for 0νECEC, even though the decay rate is expected to be suppressed by about three orders of magnitude with respect to the $0\nu\beta\beta$ decay of ^{136}Xe [772, 775–777]. Here, the current lower limits on the half-lives are on the order of 10^{21} years [778–780]. These would be accessible to a large extent in a next-generation liquid xenon experiment when exploiting

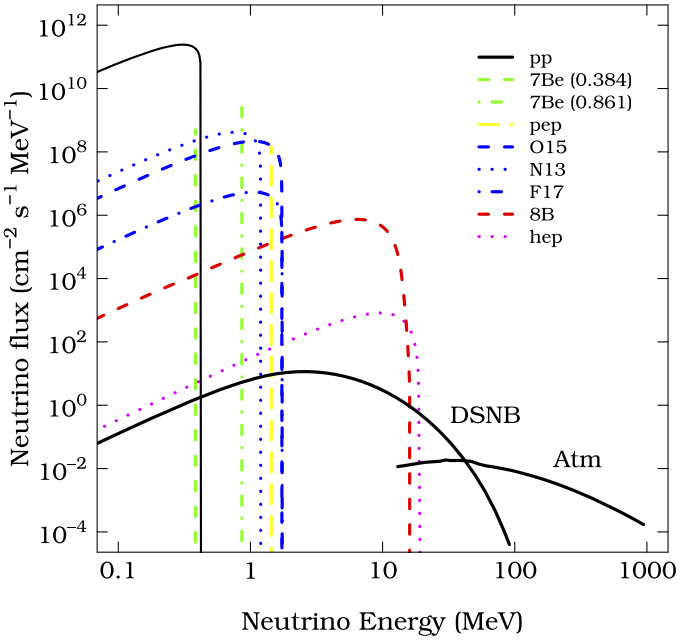

Figure 25. Astrophysical neutrino fluxes span many orders of magnitude in flux and energy. This explains the different exposures and energy thresholds required to measure them. Reproduced with permission from [786].

the coincidence signature of the atomic relaxation, the mono-energetic positron, and the two subsequent back-to-back γ-rays. Moreover, limits on half-lives of neutrinoless second-order weak decays in ^{124}Xe could complement $0\nu\beta\beta$ searches in ^{136}Xe and other nuclei and help to identify the decay mechanism [770, 781–783]. These channels provide an exciting avenue for the next-generation detector discussed here to complement ongoing searches for double-weak processes.

5. Neutrinos for astrophysics

Many sources of astrophysical neutrinos exist [784, 785], and those in the relevant energy range for xenon experiments are shown in figure 25 [786]. Overall, the flux is dominated by pp solar neutrinos, which will be the leading source of low-energy ERs. Atmospheric neutrinos have the highest energy and can induce sizable NRs of tens of keV through CEνNS; their measurement is a goal of the next-generation liquid xenon experiment. A prominent source is ^{8}B solar neutrinos as they lie in a sweet spot: their energy is high enough that NRs are visible in dedicated xenon TPCs, while their flux is so large that a first measurement can be achieved already with the currently-running generation of liquid xenon experiments.

A next-generation detector will make important advances in neutrino astrophysics, covering low-energy realms that are out of the reach of experiments such as Hyper-K [787] or DUNE [788]. This section outlines the scientific scope of the next-generation detector, including solar, atmospheric, and supernova neutrinos, and discusses the unique interaction channels that this detector will be sensitive to.

5.1. Neutrino interactions

Neutrinos can interact with liquid xenon through CC and/or NC interactions to produce detectable ER and NRs. The neutrino-induced rate is

$$\frac{\mathrm{d}R}{\mathrm{d}T_{\mathrm{R}}} = \mathcal{N} \times \int_{E_\nu^{\min}} \phi(E_\nu) \times \frac{\mathrm{d}\sigma(E_\nu, T_{\mathrm{R}})}{\mathrm{d}T_{\mathrm{R}}}\,\mathrm{d}E_\nu \tag{5}$$

where $\mathcal{N}$ is the number of target nuclei or electrons per unit of mass of detector material (for nuclear and ERs, respectively), $\phi(E_\nu)$ is the neutrino flux as a function of the neutrino energy as shown in figure 25 [786], and $E_\nu^{\min}$ is the minimum neutrino energy required to generate a recoil at an energy T_{R}. For a NR, in the limit where $m_N \gg E_\nu$, the minimum energy is given by

$$E_\nu^{\min} = \sqrt{\frac{m_N T_{\mathrm{R}}}{2}}, \tag{6}$$

whereas in the case of an ER, it is given by

$$E_\nu^{\min} = \frac{1}{2}\left(T_{\mathrm{R}} + \sqrt{T_{\mathrm{R}}(T_{\mathrm{R}} + 2m_e)}\right). \tag{7}$$

The differential cross section depends on the nature of the interaction. In the next two sections, we discuss CEνNS and the electroweak interaction, which constitute the major contributions to the potential detectable signal for liquid xenon detectors.

5.1.1. Coherent elastic neutrino-nucleus scattering. In the SM, elastic neutrino-nucleon scattering proceeds only through NC interaction with the exchange of a Z-boson. The resulting differential neutrino-nucleus cross section as a function of the NR energy T_{R} and the incoming neutrino energy E_ν is

$$\frac{\mathrm{d}\sigma(E_\nu, T_{\mathrm{R}})}{\mathrm{d}T_{\mathrm{R}}} = \frac{G_{\mathrm{f}}^2}{\pi} m_N \left(Z g_v^p + N g_v^n\right)^2 \left(1 - \frac{m_N T_{\mathrm{R}}}{2E_\nu^2}\right) F^2(T_{\mathrm{R}}), \tag{8}$$

where m_N is the target nucleus mass, G_{f} is the Fermi coupling constant, N the number of neutrons, Z the number of protons, $g_v^n = -1/2$, and $g_v^p = 1/2 - 2\sin^2\theta_w$, where θ_w the weak mixing angle. Because $\sin^2\theta_w \simeq 0.23$, the cross section scales roughly with the number of neutrons squared. The nuclear form factor $F(T_{\mathrm{R}})$ describes the loss of coherence due to the internal structure of the nucleus. For momentum transfers less than the inverse of the size of the nucleus, the coherence condition is largely satisfied and $F(T_{\mathrm{R}}) \to 1$. In lieu of experimental data on the neutron distribution in the nucleus, a typical parameterization is the Helm form factor [234] that is also commonly used for WIMP direct detection [167, 789]. Note that equation (8) gives the leading form of the cross section, keeping only the coherently enhanced part of the vector interaction; reference [790] has the complete expressions.

In effect, this CEνNS [791] increases the cross section for heavy nuclei such as xenon, while pushing the recoil energy spectrum to small energies of keV or less. Given the excellent performance of liquid xenon detectors at such low energies, this channel thus opens the possibility to detect neutrinos from astrophysical sources with a target mass that is modest in comparison to other neutrino detectors, see figure 26. In addition to providing the possibility to measure some astrophysical neutrino sources for the first time, the fact that this interaction is flavor-independent provides complementary information for sources that have been measured by other neutrino detectors [792, 793].

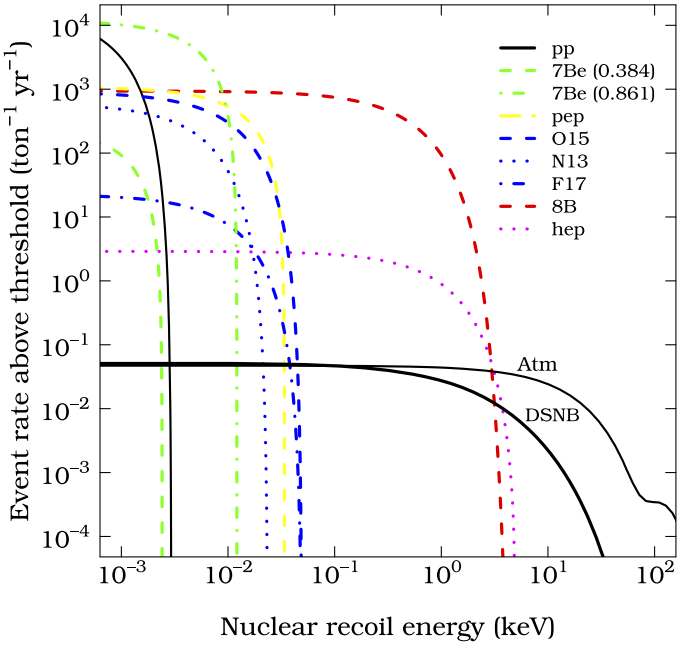

Figure 26. NR event rates from astrophysical neutrinos via CEνNS. ^{8}B solar neutrinos are expected to be measured first in the currently-running generation of experiments. The detector proposed here targets a precision measurement of that flux, and a first measurement of the atmospheric neutrino flux. Reproduced with permission from [786].

5.1.2. Electroweak interaction. The neutrino-electron electroweak interaction proceeds through both CC (W-boson exchange) and NC (Z-boson exchange) interactions. In the free electron approximation, the resulting differential neutrino-electron cross section as a function of the ER energy $T_{\rm R}$ and the incoming neutrino energy E_ν is

$$\frac{{\rm d}\sigma(E_\nu, T_{\rm R})}{{\rm d}T_{\rm R}} = \frac{G_{\rm f}^2 m_e}{2\pi}\left[(g_v + g_a)^2 + \left(g_a^2 - g_\nu^2\right)\frac{m_e T_{\rm R}}{E_\nu^2} + (g_v - g_a)^2\left(1 - \frac{T_{\rm R}}{E_\nu}\right)^2\right], \tag{9}$$

where $m_{\rm e}$ is the electron mass, $G_{\rm f}$ is the Fermi coupling constant, $g_v = 2\sin^2\theta_{\rm w} - 1/2$ and $g_a = 1/2$ are respectively the vectorial and axial coupling, and $\theta_{\rm w}$ is the weak mixing angle. In the context of $\nu_e + e \to \nu_e + e$ scattering, the interference coming from the addition of the charge current leads to a shift in axial and vectorial couplings such as: $g_v \to g_v + 1$ and $g_a \to g_a + 1$. This is then contributing to enhance the $\nu_e + e \to \nu_e + e$ scattering cross section with respect to the $\nu_{\tau,\mu} + e \to \nu_{\tau,\mu} + e$ cross section by about one order of magnitude. Further, neutrino oscillations also are an important factor that needs to be taken into account to properly calculate neutrino-induced event rates.

Low-energy ER starts to deviate from the simple free electron approximation below a few tens of keV. Therefore, it is important to include corrections for the stepping of atomic shells and atomic binding. This has been included into the calculation by using the relativistic random phase approximation (RRPA) as presented in reference [163]. The inclusion of these atomic effects result in a reduction of the neutrino-induced ER event rate below ∼5 keV. Importantly, this reduces the neutrino background in the [2–10] keV energy range by ∼22%. Figure 27

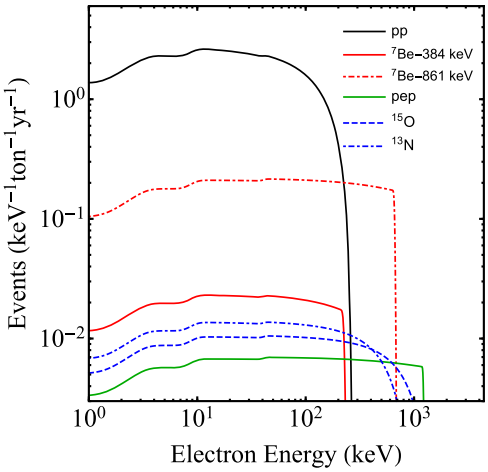

Figure 27. ER scattering rates from solar neutrinos. The step-wise decrease in event rate toward low energies is due to the stepping approximation, where each step corresponds to the energy levels of electrons in the xenon atom. Reprinted (figure) with permission from [802], Copyright (2019) by the American Physical Society.

shows the ER event rate for different neutrino flux contributions. The wavy features in the energy spectra are due to the stepping of atomic shells, smoothed by detector resolution effects.

5.2. Solar neutrinos

Experimental studies of solar neutrinos date back to over half of a century ago [794]. The primary goal of these experiments is to measure the different components of the solar neutrino flux, in order to provide an understanding of the physics of the solar interior. Many different types of solar neutrino experiments were operated, and they have evolved in their size and scientific scope since the original experiments [795]. The combination of all solar neutrino data with terrestrial experiments that study neutrinos in the same energy range has led to the LMA-MSW solution to neutrino flavor transformation from the Sun to the Earth [796]. With this solution, at low energies $\lesssim 5$ MeV, vacuum oscillations describe the neutrino flavor transformation, and the electron neutrino survival probability is $\gtrsim 50\%$. At energies $\gtrsim 5$ MeV, matter-induced transformations describe the flavor transformation, with a corresponding survival probability of $\gtrsim 1/3$.

However, in spite of all the theoretical and experimental progress in the field of solar neutrino physics over the past several decades, there are still outstanding questions that surround some of the data. For example, three experiments (Super-Kamiokande [797], SNO [798], and Borexino [799]) that are sensitive to ERs from neutrino-electron elastic scattering find that, at ER energies of a few MeV, the data are $\sim 2\sigma$ discrepant relative to the prediction of the best-fitting LMA-MSA solution. In addition, the recent measurement of the solar mass-squared difference from solar neutrino data, in particular from the day–night Super-Kamiokande data [797], is discrepant at the $\sim 2\sigma$ level relative to that measured by KamLAND [800]. Non-standard interactions (NSIs) provide a possible solution to this discrepancy [801].

Another outstanding question relates to the measured neutrino flux, and how it is able to inform the physics of the solar interior. There is a long-standing problem with standard solar models (SSMs) and predictions of the abundances of heavy elements, or metals, in the Sun.

Older abundance calculations [803] relied on many simplifying assumptions, but nevertheless fit solar observables well, in particular helioseismology data. More recent calculations however [804], while more sophisticated in construction, were ultimately worse fits to the data [804–807]. These calculations are referred to as high-Z and low-Z models respectively, according to their relative predicted metallicities. Their disagreement is known as the solar abundance problem [808], and has not yet been resolved. A global analysis of all solar neutrino fluxes remains inconclusive [469]. A step toward resolving this problem will be to accurately measure the flux of solar neutrinos from the carbon, nitrogen, oxygen (CNO) nuclear fusion cycle, first achieved by Borexino [809], which is possible with the experiment discussed here (section 5.2.4).

5.2.1. Boron-8 solar neutrinos (NR). Combined with the neutrino-electron scattering data from SNO, Super-Kamiokande and Borexino, precision measurements of ^{8}B neutrino induced CEνNS in a next-generation liquid xenon detector will constrain the ν_e survival probability in the 5–15 MeV range. A significant deficit from the theoretical prediction can be interpreted as evidence of active-to-sterile neutrino oscillation [171]. A next-generation liquid xenon detector will provide an independent measurement of the NC component of the solar ^{8}B neutrino flux, with an expected event rate of $\sim$90 events per tonne-year [1], measured to be right in between that predicted by the low and high metallicity SSM [498, 799, 810].

5.2.2. Hep solar neutrinos (NR). A future next-generation detector may detect neutrinos from the minor branch of the pp chain that generates the most energetic neutrinos via the reaction $^3\mathrm{He} + p \rightarrow {}^4\mathrm{He} + e^- + \nu_e$. Along with ^{8}B neutrinos, neutrinos from this hep reaction also undergo adiabatic conversion in the solar interior. Neutrinos from the hep reaction have not been directly identified in solar neutrino experiments; the best upper bound from the SNO experiment is $\sim$4 times greater than the SSM prediction [811].

5.2.3. pp solar neutrinos (ER). The possibility to use liquid xenon as a low-energy solar neutrino detector by means of $\nu + e$ scattering was suggested in reference [812] but only now is becoming a realistic measurement. A next-generation liquid xenon detector will provide a new, high-precision observation of the ER energy spectrum induced by elastic scattering of pp neutrinos, see figure 27. This, in turn, will improve measurements of the Sun's (neutrino) luminosity. The pp neutrino flux was first indirectly identified as a component of the Gallium data, and Borexino was the first experiment to make a measurement of the spectral energy distribution of ER events induced by pp neutrinos [813]. The Borexino measurement uncertainty on this component is now down to $\lesssim$10% [799]. Further improving upon the measurement of this component will better constrain the 'neutrino luminosity' of the Sun because pp neutrinos account for 86% of all solar neutrino emission [814]. Projections for a next-generation xenon experiment indicate that the pp neutrino flux can be measured to 0.15% uncertainty with 300 tonne-years of exposure. Combined with a 1% measurement of the next-largest component, ^{7}Be, such a detector could ultimately achieve 0.2% uncertainty in the neutrino-inferred solar luminosity [815]. This will also have the important consequence of constraining alternative sources of energy production in the solar interior [802].

5.2.4. CNO neutrinos (ER). The flux of CNO neutrinos from the Sun makes up less than 1% of the Sun's total neutrino luminosity but is sensitively dependent on the solar metallicity, with higher metallicity models predicting a higher CNO component. A precise measurement of the CNO flux would provide the necessary information to discriminate between the low and high-Z calculations, thereby resolving the solar abundance problem directly. The very

first measurement of CNO neutrinos was achieved recently by Borexino [809], though with insufficient statistics to yet conclusively resolve the abundance problem.

Due to the small CNO luminosity fraction, measuring the CNO flux in a xenon TPC will require large experimental exposures and well controlled backgrounds. A next-generation liquid xenon detector would be capable of measuring the ^{13}N and ^{15}O fluxes individually (20%–25%) even in the presence of the $2\nu\beta\beta$ decay background from ^{136}Xe [815]. Significant improvements to the precision of these measurements can be achieved through depletion of the natural xenon target from the ^{136}Xe isotope [802], while negating the possibility of a $0\nu\beta\beta$ search (section 4.1). Hence, both a natural xenon target and a ^{136}Xe-depleted target provide exciting physics opportunities for a next-generation liquid xenon detector.

5.2.5. Neutrino capture on xenon-131 and xenon-136. Solar neutrinos may also be observed through the neutrino capture process on xenon: $\nu_e + {}^{A}_{54}\mathrm{Xe} \rightarrow {}^{A}_{55}\mathrm{Cs}^{(*)} + e^-$ [816]. The isotopes ^{131}Xe and ^{136}Xe have sufficiently low reaction thresholds of $Q = 355$ keV and $Q = 90.3$ keV for capture of all solar neutrino species. The prompt electron gives an ER with an energy that is offset from that of the captured neutrino as $E_e = E_\nu - Q - E_{\mathrm{ex}}$, where E_{ex} is the excitation energy of the resulting Cs nucleus.

The possibility of tagging neutrino capture events which populate excited states in the product Cs nuclei has been explored in reference [817]. The emission of γ-rays and/or conversion electrons during relaxation of the excited nuclear state in conjunction with the primary fast electron provides opportunities for background rejection.

An especially high suppression of background can be achieved if a delayed coincidence signature in the Cs de-excitation could be exploited. The product isotopes ^{131}Cs and ^{136}Cs are unstable with half-lives 9.7 days and 13.0 days, respectively. Detection of the corresponding electron-capture and β-decay signatures which occur long after the initial capture event may also be possible. With abundances of 21.2% and 8.9%, one expects 0.6 and 0.7 neutrino capture events per tonne of natural Xe per year on ^{131}Xe and ^{136}Xe, respectively [817].

5.3. Atmospheric neutrinos (NR)

The collisions of cosmic rays in the atmosphere produce neutrinos over a wide range of energies. A precise determination of this atmospheric neutrino flux depends on several factors, including the cosmic-ray flux at the top of the Earth's atmosphere, the propagation of cosmic rays through the atmosphere, and the decay of the mesons and muons as they propagate though the atmosphere to Earth's surface. Since the flavors of neutrinos that are produced in the decays are known, theoretical models accurately predict the ratio of the flavor components of neutrinos across all energies. However, the normalizations of the fluxes differ depending upon the theoretical input.

While the atmospheric neutrino flux for energies $\gtrsim$1 GeV has been well studied by the aforementioned experiments, the low-energy flux of atmospheric neutrinos, $\lesssim$ 100 MeV, is difficult to both model and measure [818]. The resulting energy spectrum of neutrinos corresponds to that from muon and pion decay at rest, but the absolute normalization of the flux is less well constrained, due to uncertainties that arise from several uncertain physical processes. A next-generation dark matter detector will measure this neutrino flux at so-far unexplored low energy, see figure 28. The flux at these energies is impacted by the geomagnetic field and modulated by the solar cycle, but the corresponding effects, namely a larger modulation at higher latitudes but an overall smaller flux at lower latitudes [819] will be challenging to discern, given the low interaction rates. In fact, measuring atmospheric neutrinos will require an exposure of order 700 tonne-years [165], thus providing a benchmark target exposure for a next-generation liquid xenon observatory.

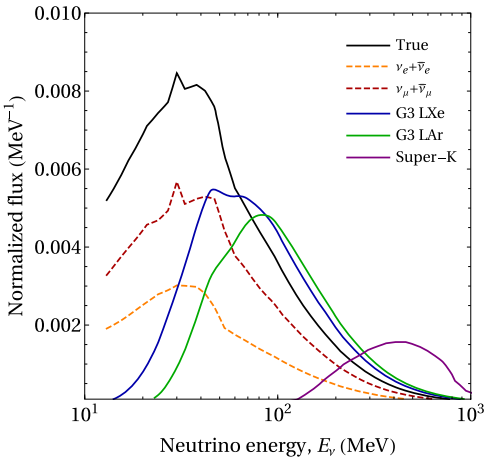

Figure 28. The differential fluxes of atmospheric neutrinos that are accessible by various experiments, normalized such that the area under the curves is equal to unity. The flux accessible to a next-generation xenon experiment (labeled G3 LXe) is shown in blue, and reaches much lower in energy than Super-Kamiokande currently does (shown as solid violet). Reprinted (figure) with permission from [165], Copyright (2021) by the American Physical Society.

5.4. Supernova neutrinos (NR)

The next supernova event in the Milky Way or in nearby galaxies will provide unprecedented information on the physics of neutrino propagation from the supernova core [820, 821]. For example, large water Cherenkov detectors such as Super-Kamiokande will measure thousands of events, mostly through the charged-current inverse beta decay channel, and hundreds of events through various other elastic and inelastic channels [822–824]. Dark matter detectors can play an important role in supernova neutrino astrophysics through their sensitivity to supernova neutrinos via coherent elastic scattering, yielding complementary information for example on the nature of stellar collapse and the explosion energy of the supernova [825, 826].

5.4.1. Galactic supernova neutrinos. Current and future liquid xenon dark matter detectors are uniquely sensitive to neutrinos of all flavors through CEνNS [827, 828], whether from core-collapse (type II) [829, 830] or thermonuclear runaway fusion (type Ia) [831]. This provides a calorimetric measurement of the explosion energy going into neutrinos, independent of oscillation effects [830]. The physics available with the statistics collected by a next-generation liquid xenon detector would complement that of larger, dedicated neutrino observatories: in a next-generation detector, there are of order 100 expected events from a core-collapse supernova within 10 kpc of Earth [830].

CEνNS is the primary detection interaction from galactic neutrinos in liquid xenon detectors, but charge current reactions are also possible. A supernova within 10 kpc could produce a handful of charge current interactions in a next-generation detector, particularly interacting with the ^{136}Xe isotope [832, 833]. Even the large water Cherenkov veto volumes that typically surround these detectors may record notable supernova neutrino event rates [834].

Also possible are inelastic CC interactions of the supernova electron neutrinos with the xenon nuclei. Such interactions, while creating an electron in the final state, leave the post-interaction target nucleus in an excited state. Its subsequent de-excitation produces, among other particles, gamma rays and neutrons [835, 836]. The electron and the de-excitation gamma rays give rise to ERs. On the other hand, neutrino-induced neutrons (νIn) from the de-excitation of the final state nucleus can create, through their multiple scattering on the xenon nuclei, additional xenon NR events. The rate of νIn NR events is generally low compared to CEνNS NRs. However, it may still be possible to identify these νIn NR events using the capability of large liquid xenon detectors to tag neutrons which undergo multiple scatterings, both within the TPC and using the external neutron veto detector. Detection and identification of both ER and NRs from supernova ν_e CC interactions, together with the NR events from NC CEνNS, may thus provide an additional probe of the distribution of the total supernova explosion energy going into different neutrino flavors.

Observations of astrophysical neutrinos are complementary to terrestrial experiments which are sensitive to MeV-scale neutrinos [822]. The recent detection of CEνNS has provided novel bounds on new physics, for example in the form of kinetic mixing, hidden sector models, flavor models, and sterile neutrinos [791]. Future measurements of supernova neutrinos at dark matter detection experiments can improve on this sensitivity [837], providing further information on new physics models (see also section 6).

5.4.2. Pre-supernova neutrinos. In the event of a near-Earth ($d <$ kpc) core-collapse supernova, future liquid xenon detectors will also be sensitive to neutrinos of all flavors that are emitted by a massive star in its silicon-burning stage, a few hours *prior to* core collapse [839, 840]. Due to lower stellar temperatures before collapse, these 'pre-supernova' neutrinos are $\mathcal{O}(10)$ softer than supernova neutrinos, and therefore require low thresholds for detection [841]. Figure 29 indicates that a next-generation liquid xenon experiment operating at 0.1 keV energy threshold would detect, in a 12 h window prior to collapse, $\mathcal{O}(100)$ pre-supernova neutrinos from a massive star 200 pc away, e.g. Betelgeuse [838]. Such a detection would constitute the first measurement of the final stages of stellar evolution, and provide a valuable warning before the explosion. Pre-supernova neutrinos can also help constrain dark photon, axion, and ALPs parameters [842–844].

5.4.3. Supernova early warning system. In order to be optimally prepared for the next supernova, the supernova early warning system (SNEWS) was developed [845]. SNEWS is an inter-experiment network to prepare and provide an early warning for Galactic supernovae: in contrast to the optical signal, neutrinos basically free-stream from the collapsing star and thus reach Earth minutes, hours or even days before the optical counterpart becomes visible. Therefore, by detecting supernova neutrinos, an early alert can be sent to astronomers to facilitate early observations of the Supernova [846]. SNEWS is in the process of being revamped and amplified to SNEWS2.0 which will have a larger physics reach [847, 848]. The next-generation detector discussed here will be able to contribute to this network.

5.4.4. Diffuse supernova neutrinos. In addition to the yield from a Galactic supernova event, an exciting prospect is the detection of the diffuse supernova neutrino background (DSNB) [849–851], i.e., the neutrinos emitted from past supernovae occurring across the Universe. Modern predictions put this flux at approximately 6 $\mathrm{cm}^{-2}\,\mathrm{s}^{-1}$ [852] for neutrino energies above 17.3 MeV, including contributions from all neutrino flavors. In addition to being a probe on supernova physics, the DSNB is an independent probe of the local core-collapse supernova and cosmic star formation rate [849, 853]. Although this signal has not yet been directly detected, there are strong upper bounds on the $\bar{\nu}_e$ component of the flux from Super-Kamiokande [854].

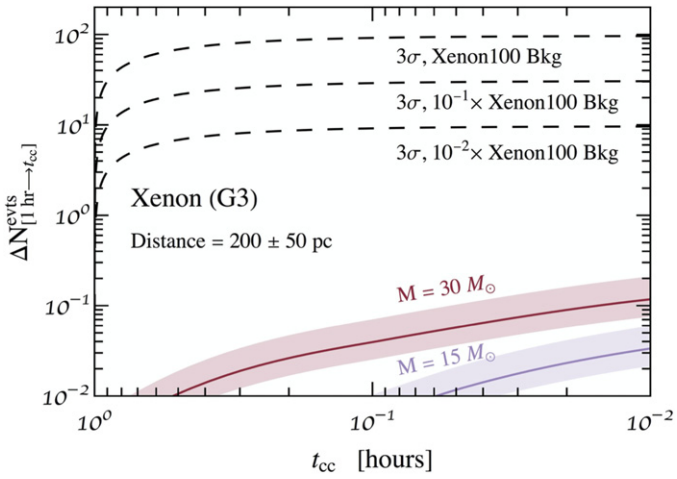

Figure 29. For a next-generation liquid xenon dark matter experiment with an assumed target mass of 50 tonnes, the expected number of pre-supernova neutrinos above the detection threshold is shown as function of time until the core collapse, for two different stellar masses at a distance of 200 pc. Reproduced from [838]. CC BY 4.0.

The best predictions for the flux of all flavors, with an expected event rate of ∼0.05 events per tonne-year, implies that liquid xenon dark matter detectors with exposures ∼1000 tonne-year may have discovery potential to this signal above known backgrounds [450, 855]. Besides, these detectors might be the only ones capable of probing the non-electron component of the DSNB, thanks to their excellent sensitivity.

5.5. Terrestrial antineutrinos (ER)

The Earth is a rich source of antineutrinos with energies in the MeV range, due to radioactive decays in Earth's crust and interior [849]. A signal from these geoneutrinos has been measured at Kamland [856] and Borexino [857]. Coherent neutrino interactions with xenon will produce recoil energies that are likely below experimental thresholds. However, depending on exposure time, mass, and other backgrounds, several neutrino-electron scattering events may be detectable in a next-generation xenon detector.

5.6. Other neutrino physics

5.6.1. Measuring the Weinberg angle. The solar pp flux is very strongly determined by the luminosity constraint on the total neutrino flux, to a precision of ∼0.4% [469]. The dependence of the neutrino-electron cross section on the Weinberg (weak) angle $\sin^2\theta_w$ thus allows for an independent measurement of this quantity, at energies far below the reach of colliders. Precision determinations of $\sin^2\theta_w$ must be made by running LEP measurements (at ∼100 GeV) down to lower energies. At present, the lowest-energy determination of $\sin^2\theta_w$ remains above the MeV scale [858]. ERs from pp neutrinos yield an exchanged momentum on the order of ∼keV, so a detection of the pp flux via ERs in next-generation xenon experiments will cover new and uncharted territory. The next-generation xenon detector discussed here would be able to constrain $\sin^2\theta_w$ with (4–5)% precision [815] even without any additional constraints from other experiments. Alternatively, using the solar luminosity condition, a liquid xenon experiment with a 200 tonne-year exposure can already yield a measurement

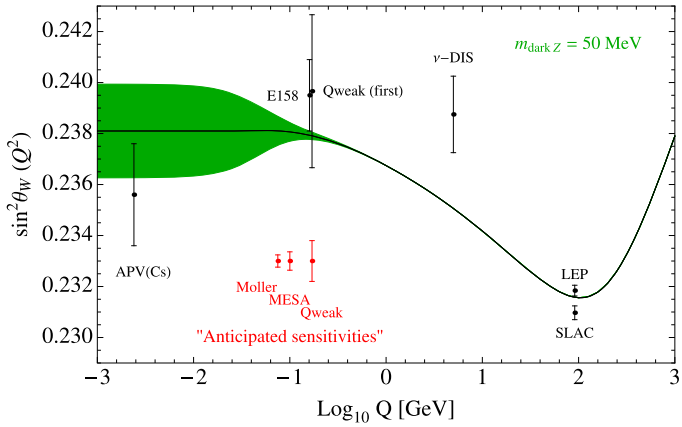

Figure 30. Running of the Weinberg angle $\sin^2\theta_{\text{w}}$ as a function of momentum scale Q^2, along with measured values. A deviation from SM predictions (black line) could indicate the presence of new physics effects. The green band indicates the effect of a new Z' with $m_{Z'} = 50$ MeV, where the width of the band is determined by the strength of the kinetic mixing parameter with $U(1)_Y$. An $\mathcal{O}$(tonne-year) xenon dark matter observatory can extend the reach of these measurements down to the keV scale, significantly to the left of this plot, via the measurement of the pp solar neutrino flux. Reprinted (figure) with permission from [861], Copyright (2014) by the American Physical Society.

of $\sin^2\theta_{\text{w}}$ with a precision of 1.5% at the keV scale [859]. This is complementary to measurements using CEνNS of pion-decay neutrinos as achieved by the COHERENT collaboration [860]. Applying the RRPA correction (see section 5.1.2 and [163]), the expected ER rate from solar pp neutrinos is ∼90 counts per 1000 tonne-day in the (0–15) keV energy range (or 780 counts per 1000 tonne-day in the full energy range). Hence, a 150 tonne-year exposure can reduce the statistical uncertainty in the measurement of $\sin^2\theta_{\text{w}}$ down to 1.4% for the energy transfer in the range of (0–15) keV.

A deviation of $\sin^2\theta_{\text{w}}$ from the computed value at low energies would be an indication of new physics. For example, a new light gauge boson could lead to a different value at low momentum Q^2. Figure 30 shows an example of the variation that could be produced by a 50 MeV Z'-mediator, with a coupling in the range required to simultaneously explain the muon $(g-2)_\mu$ anomaly [861–863].

5.6.2. Electron-type neutrino survival probability. The total electron-neutrino scattering rate receives neutral-current contributions from all three flavors, but charge-current contributions only from the electron-type neutrino. Consequently, a high-statistics observation of solar pp neutrinos enables a liquid xenon experiment to directly measure the oscillation probability of the electron-type neutrinos emitted from the Sun in an energy range that is not accessible to any other experiment. Figure 31 shows that with an exposure of 300 tonnes-years, a liquid xenon detector would measure the low-energy survival probability to 3%–4% [815]. Such a measurement would serve as a test of the Mikheyev–Smirnov–Wolfenstein large mixing angle (MSW-LMA) solution of neutrino oscillation and a probe of exotic neutrino properties and NSIs. This can also be used to perform a solar-neutrino-only measurement of the magnitude of the U_{e3} entry of the neutrino mixing matrix, to search for very light sterile neutrinos in currently unexplored regions of parameter space, and one can extend the sensitivity to the hypothesis that neutrinos are pseudo-Dirac fermions by an order of magnitude [864].

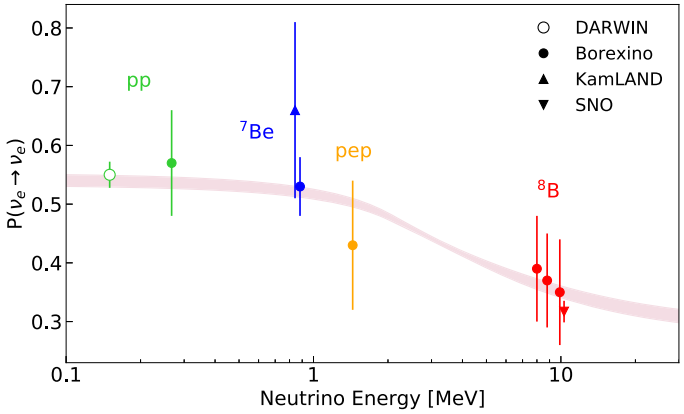

Figure 31. The ν_e survival probability versus neutrino energy, assuming the high-Z SSM. Dots represent the solar measurements of pp (green), ^{7}Be (blue), pep (orange), and ^{8}B (red) from Borexino. The upward (downward) triangle shows a measurement of ^{7}Be (^{8}B) from KamLAND (SNO). The open point indicates that a next-generation liquid xenon experiment could enhance the precision of the ν_e survival probability to 0.02 below 200 keV, using solar pp neutrino events. The pink band represents the 1σ prediction of the MSW-LMA solution. Reproduced from [815]. CC BY 4.0.

5.6.3. Searching for new physics of neutrinos. A next-generation liquid xenon detector will also be a powerful tool to search for new physics of neutrinos via elastic neutrino-electron scattering. An extensively-studied scenario of new physics of neutrinos is the so-called NSI [865], which might play a potentially important role in future long-baseline experiments such as DUNE [866]. In addition, there has also been rising interest in new interactions mediated by light mediators [867–870]. A next-generation liquid xenon detector can significantly improve the sensitivity to sterile neutrino mixing parameters, particularly if solar neutrino detection via elastic neutrino-electron scattering (pp component) and the CEνNS channel (^{8}B component) is combined with reactor neutrino data from JUNO [871]. Notably, the correlation of the mixing angles $\sin^2\theta_{12}$ and $\sin^2\theta_{14}$ can be broken by a combined analysis of these complementary data sets.

It has been shown that when combined with a radioactive source, a multi-tonne-scale liquid xenon detector can significantly improve current bounds on leptonic NSIs [872] and light mediators, thanks to the high electron density in liquid xenon. In addition, xenon nuclei lie in a range where radiative corrections are particularly sensitive to new weak isospin conserving processes from new physics and are insensitive to isospin violating processes [873]. Considering solar neutrinos as the source, since the Borexino experiment has demonstrated excellent sensitivities to such new interactions [874, 875], especially to ν_τ interactions, it is expected that a next-generation liquid xenon detector will be superior in searching for new physics of neutrinos [876].

6. Additional physics channels

At the time of writing, an excess of ER events below 7 keV has been reported by XENON1T [495]. With a statistical significance of about 3σ, this excess has received enormous interest from the community [374, 573, 602, 612, 661, 676, 868, 869, 877–1004]. We refrain here from

discussing whether one or the other explanation is more likely and instead mention the various explanations in the respective sections of this review.

6.1. Solar axions

Originally postulated to resolve the strong CP problem in QCD [574–576], axions have emerged as a suitable non-baryonic dark matter candidate [577–579, 1005, 1006]. As such, there has been a growing interest in the last few decades to search for axion particles in general, and for axion dark matter in particular [594, 1007–1012]. They may be sought in the dark matter galactic halo within which they would cluster [1013] as a cold dark matter axion.

Independently of being dark matter, if an axion or ALP exists in nature, then it should be produced copiously in the hot solar plasma [1014, 1015]. Due to the ∼keV temperature of the Sun, solar axions are produced with roughly thermal fluxes in the 1–10 keV energy range, and are thus well-suited for detection in xenon experiments. Via their coupling to the photon, $g_{a\gamma}$, the most widely considered process of axion production is Primakoff conversion in which photons convert into axions inside the electromagnetic fields of the electrons and ions of the solar plasma. This flux is dominant in hadronic QCD axion models like the 'KSVZ' axion [1016, 1017]. Another widely considered QCD axion model labeled the 'DFSZ' axion [1018, 1019] possesses a tree-level coupling to electrons, g_{ae}, which brings sizable fluxes from the so-called 'ABC' processes: atomic recombination and deexcitation, bremsstrahlung, and Compton scattering [1020].

The primary way for xenon experiments to measure the axion is through the axioelectric effect [596], which allows constraints to be set on g_{ae}. Xenon experiments may also constrain $g_{a\gamma}$: both by measuring the Primakoff component [1021] of the solar flux (which is dependent only on $g_{a\gamma}$), as well as by exploiting inverse Primakoff conversion inside the detector [612, 945]: $aZ \rightarrow \gamma Z$. In the latter case, the sensitivity to solar axions is boosted, even if the value of $g_{a\gamma}$ is small. A final component of the solar axion flux beyond 'ABC' and Primakoff components is the ^{57}Fe axion–nucleon interaction, which depends on g_{an} [1022]. A next-generation xenon experiment with a ∼1000 tonne-year exposure may even be able to out-perform devoted solar axion telescopes [612] such as the planned International Axion Observatory (IAXO) [1023].

The ER background level of the detector is the main limiting factor for its sensitivity to solar axions. Liquid xenon TPCs are well known for their very low ER background levels and are therefore ideal for this search. Among underground detectors, liquid xenon TPCs place the strongest constraints to-date on g_{ae} with solar axions [495, 597, 599, 600, 1024, 1025].

The excess of ER events seen in XENON1T [495] has a spectrum that matches the expected solar axion flux. However, the amplitude of the excess would require large couplings that would place the excess in conflict with more stringent astrophysical bounds [589, 890, 926, 976]. The proposed next-generation liquid xenon TPC will enable this excess to be robustly tested, should it persist, perhaps leading to the discovery of solar axions.

6.2. Neutrino dipole moments and light mediators

Dark matter searches start to probe various novel neutrino-induced signals, see e.g. references [164, 872]. Therefore, the interpretation of potential discoveries as coming from new neutrino physics becomes increasingly plausible. As a result, next-generation dark matter detectors will be capable of placing interesting limits on models of new physics in the neutrino sector, often complementary with other experiments [876].

This is apparent in limits from ERs. In figure 32 we show the observed ER spectrum observed by several dark matter as well as neutrino experiments, adopted from references

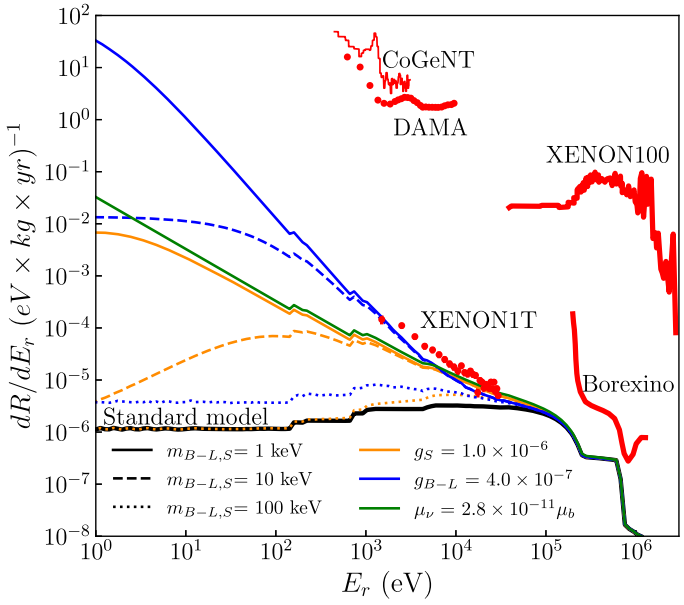

Figure 32. Neutrinos may show up in dark matter experiments well above the neutrino fog. Shown in red are the electron recoil spectra in several experiments taken from references [1026, 1027], with the background level in XENON1T indicated [64, 495]. The spectrum expected from SM solar neutrinos is in solid black. The colored curves are the solar neutrino spectra for several new physics models discussed in the text, with linestyles corresponding to various mediator masses. The jagged steps below ∼5 keV are an effect of the electron binding energy as discussed in reference [1028].

[1026, 1027] with the most recent XENON1T measurements [64] included. They represent about two orders of magnitude improvement over the XENON100 background rate.

The next generation of experiments will have further sensitivity [892, 962]. In figure 32 we show several spectra from new physics models which lead to an enhanced scattering rate at low energies. The green curve shows the recoil spectrum in the case that the neutrino possesses a magnetic dipole moment around that which is allowed by current solar neutrino data from Borexino [1029]. In this case the differential cross section is

$$\frac{\mathrm{d}\sigma}{\mathrm{d}E_r} = \mu_\nu^2 \alpha \left(\frac{1}{E_r} - \frac{1}{E_\nu} \right), \tag{10}$$

where μ_ν is the neutrino dipole moment and E_r is the recoil energy of the electron. At high recoil energies, the dipole-induced scattering is lower than the SM rate and in agreement with the Borexino rate. However, due to the E_r^{-1} falloff, the rate is higher at low recoil energies. Already an analysis of XENON1T [495] improves the limit in dipole moments to $<3 \times 10^{-11}$ times a Bohr magneton. The next-generation experiment will precisely measure the pp solar neutrino spectrum at low energies and thus further improve this sensitivity. In addition to the neutrino magnetic moment, a new interaction mediated by a scalar propagator will also fall as E_r^{-1} as described in reference [1027]. An example of such a scalar-mediated interaction is plotted in orange in figure 32.

One can also consider models with a faster falling spectrum. For example, blue curves of figure 32 are the spectra in a model with a new very light B–L gauge boson which is mediating a new interaction between neutrinos and electrons. The cross section is

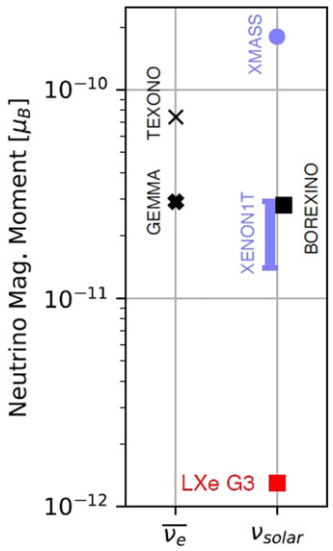

Figure 33. Projected neutrino magnetic moment sensitivity (red) along with current limits from reactor-based experiments (left markers) and experiments exposed to a solar flavor mixture (right markers). All the upper limits are reported at 90% CL, except the XENON1T result, which shows the 10%–90% confidence interval [495, 1029, 1032].

$$\frac{\mathrm{d}\sigma}{\mathrm{d}E_r} = \frac{g_{\mathrm{B-L}}^4 m_e}{4\pi(2m_e^2E_r^2 + m_{\mathrm{B-L}}^2)^2}, \tag{11}$$

where $m_{\mathrm{B-L}}$ and $g_{\mathrm{B-L}}$ are the mass and coupling. Here, we have dropped subleading terms in E_r/E_ν as well as interference with the SM process which is unimportant at most recoil energies. If the mass of the gauge boson is small, the cross section falls as E_r^{-2}. This behavior is due to the $1/(q^2 - m_{\mathrm{B-L}}^2)$ propagator in the amplitude, with $q^2 = 2m_eE_r$. Again it can be seen that a next-generation experiment will have significant sensitivity, well beyond that achieved by the Borexino experiment [1030], the GEMMA reactor experiment [1031], or the XMASS experiment [1032]. In fact, the discussion around the possible excess observed by XENON1T [495] can already be used to place a constraint on $g_{\mathrm{B-L}} < 3.6 \times 10^{-7}$ for mediators with mass $m_{\mathrm{B-L}} < 10$ keV. This is already comparable with the constraint from GEMMA [901]. A next-generation liquid xenon experiment will be able to strengthen this bound.

It is interesting to consider a scenario in which the next generation of xenon experiments uncovers an excess above the solar neutrino fog. In this case we will immediately entertain both the possibility of dark matter and that of new neutrino physics, as evidenced by the list of papers discussing the excess observed by XENON1T. Fortunately, this degeneracy can be disentangled with reactor neutrino experiments. To those that stand within 100 m of the core, nuclear reactors are a brighter source of neutrinos than the Sun. A low-threshold detector near a reactor, such as GEMMA [1031], can thus place strong limits or distinguish whether an excess is coming from dark matter or neutrinos. Figure 33 shows the current limits on the neutrino magnetic moment from both large underground detectors and reactor experiments, as well as the projected sensitivity for a next-generation liquid xenon detector with a 750 tonne-year exposure, complementary to dedicated experiments such as CONNIE [1033].

In addition to the physics discussed in section 6.5, a mono-energetic neutrino source in combination with a large xenon detector could set very competitive sensitivities to neutrino magnetic dipole moments and sterile neutrino oscillation [1034]. A 50 days run with a 3 MCi ^{51}Cr source produces 82 ν–e elastic scattering events in the XENON1T detector, which corresponds to 9.8 times better signal-to-noise ratio compared to using solar neutrinos [925]. The next-generation experiment discussed here could set much more stringent bounds on the neutrino magnetic moment, if combined with an electron capture source.

6.3. Fractionally charged particles

The quantization of the electric charge has been one of the long-standing mysteries stemming from empirical observation. In principle, the SM $U(1)$ allows arbitrarily small real-number charge, but so far, experiments indicate that there is a fundamental unit of electric charge of $1/3e$. This has sparked theoretical explanations including Dirac quantization [1035] and provides one of the major motivations for a GUT [1036, 1037]. The search for such fractionally charged or millicharged particles is a test of the paradigm of charge quantization [1038–1052]. If such a particle was found, its small charge may or may not be the new electric charge unit, but in either case it will inevitably change our understanding of the current charge quantization built on quark charges, and contradict the predictions of certain GUTs.

One can consider the kinetic mixing between the SM $U(1)_Y$ and an additional gauge group $U(1)_D$, with additional matter particles ξ charged under a dark $U(1)_D$. In the limit when the dark $U(1)_D$ vector boson (often called a dark photon, see section 3.8.1) is massless, the would-be dark sector particles which are charged under $U(1)_D$ become electromagnetically 'fractionally charged' or 'millicharged'. The level of kinetic mixing is often $\sim 10^{-3}$ or smaller, from loop effects in either QFT or string theory [569, 1053, 1054], which naturally gives small electric charges. For masses of such new particles below $\sim \mathrm{MeV}/c^2$, the limits on the kinetic mixing parameter (and thus the fractional charges) are stringent $< 10^{-15}$ [1040]. For heavier states, the limits are weaker [1055]. Direct detection experiments can possibly observe bound state formation between $q < 0$ millicharged particles and nuclei [1056]. One can also look for millicharged particles without massless gauge bosons in regimes where the dark photon is constrained [1051]. A search for such a particle can be a test of GUTs and certain string compactification scenarios [1057]. Further, liquid xenon detectors are sensitive to the possible millicharge of solar neutrinos [1032].

6.4. Nucleon decay

In the SM, the conservation of baryon number B is an empirically observed symmetry. If B were an exactly conserved quantum number, then protons, being the lightest baryons, would be stable. However, baryon number could be an approximate symmetry of Nature, and violated by small amounts, as predicted for example by many GUTs. This could explain the observed matter–antimatter asymmetry of the Universe [1058].

Several liquid xenon detectors, such as DAMA-LXe [1059, 1060] and EXO-200 [1061], explored the possibility to investigate nucleon decay through so-called invisible decay modes, where the final states (neutrinos, or more exotic particles such as dark fermions) are not detected. One example for an invisible mode is $n \to \nu\nu\nu$, as proposed in reference [1062]. Following such a decay, the daughter nuclei would be left in an excited state, and would emit a detectable signal, such as a γ-ray, once they de-excite. Table 1 illustrates the various signatures for two xenon isotopes, ^{129}Xe and ^{136}Xe. These decays can be searched-for with a next-generation liquid xenon detector with unprecedented sensitivity.

Table 1. The daughter isotopes and their decay modes that follow the invisible mono- and di-nucleon decays of ^{129}Xe and ^{136}Xe as well as the tri-nucleon decays of ^{136}Xe. This table is adapted after [1059, 1060]. The Q-values are reported in MeV.

Isotope	Invisible decay mode	Daughter	Subsequent decays
^{129}Xe	n	^{128}Xe	Stable
	p	^{128}I	$^{128}\mathrm{I} \rightarrow [Q = 2.217]\beta^{-}{}^{128}\mathrm{Xe}$ Or $^{128}\mathrm{I} \rightarrow [Q = 1.258]\mathrm{EC} + \beta^{+}{}^{128}\mathrm{Te}$
	nn	^{127}Xe	$^{127}\mathrm{Xe} \rightarrow [Q = 0.664]\mathrm{EC}{}^{127}\mathrm{I}$
	pn	^{127}I	Stable
	pp	^{127}Te	$^{127}\mathrm{Te} \rightarrow [Q = 0.694]\beta^{-}{}^{127}\mathrm{I}$
^{136}Xe	n	^{135}Xe	$^{135}\mathrm{Xe} \rightarrow [Q = 1.151]\beta^{-}{}^{135}\mathrm{Cs}$
	p	^{135}I	$^{135}\mathrm{I} \rightarrow [Q = 2.648]\beta^{-}{}^{135}\mathrm{Xe}$ $\rightarrow [Q = 1.151]\beta^{-}{}^{135}\mathrm{Cs}$
	nn	^{134}Xe	Stable
	np	^{134}I	$^{134}\mathrm{I} \rightarrow [Q = 4.175]\beta^{-}{}^{134}\mathrm{Xe}$
	pp	^{134}Te	$^{134}\mathrm{Te} \rightarrow [Q = 1.550]\beta^{-}{}^{134}\mathrm{I}$ $\rightarrow [Q = 4.175]\beta^{-}{}^{134}\mathrm{Xe}$
	nnn	^{133}Xe	$^{133}\mathrm{Xe} \rightarrow [Q = 0.4274]\beta^{-}{}^{133}\mathrm{Cs}$
	nnp	^{133}I	$^{133}\mathrm{I} \rightarrow [Q = 1.770]\beta^{-}{}^{133}\mathrm{Xe}$ $\rightarrow [Q = 0.4274]\beta^{-}{}^{133}\mathrm{Cs}$
	npp	^{133}Te	$^{133}\mathrm{Te} \rightarrow [Q = 2.920]\beta^{-}{}^{133}\mathrm{I}$ $\rightarrow [Q = 1.770]\beta^{-}{}^{133}\mathrm{Xe}$ $\rightarrow [Q = 0.4274]\beta^{-}{}^{133}\mathrm{Cs}$
	ppp	^{133}Sb	$^{133}\mathrm{Sb} \rightarrow [Q = 4.003]\beta^{-}{}^{133}\mathrm{Te}$ $\rightarrow [Q = 2.920]\beta^{-}{}^{133}\mathrm{I}$ $\rightarrow [Q = 1.770]\beta^{-}{}^{133}\mathrm{Xe}$ $\rightarrow [Q = 0.4274]\beta^{-}{}^{133}\mathrm{Cs}$

6.5. Short-baseline oscillations

Persistent anomalies in short baseline experiments, including LSND and MiniBooNE, are suggestive of an additional undiscovered neutrino mass eigenstate at the $\sim$1 eV mass scale [1063]. However, there is significant tension between different experiments that has yet to be explained [1064]. Given the energy of ^{51}Cr neutrinos, the oscillation pattern is expected to be within a meter-scale detector. This would make a next-generation liquid xenon TPCs well-suited to conclusively test the existence of sterile neutrinos [1034]. In addition, such an experiment would be able to rule out portions of currently allowed parameter space, potentially resolving the existing tension if sterile neutrinos do not exist [1034].

7. Background considerations

As discussed in this present paper, the proposed next-generation liquid xenon experiment is a versatile observatory for a number of relevant science channels, spanning low-energy NRs in particular for dark matter, ERs for a number of measurements, and reaching up to high energy events expected from neutrinoless double-beta decay. In order to support this broad physics reach, multiple background sources must be considered. In addition to improved xenon purification, further scrutiny of materials in assays and exploration of discrimination techniques will be necessary to minimize backgrounds for rare event searches. The choice of host facility

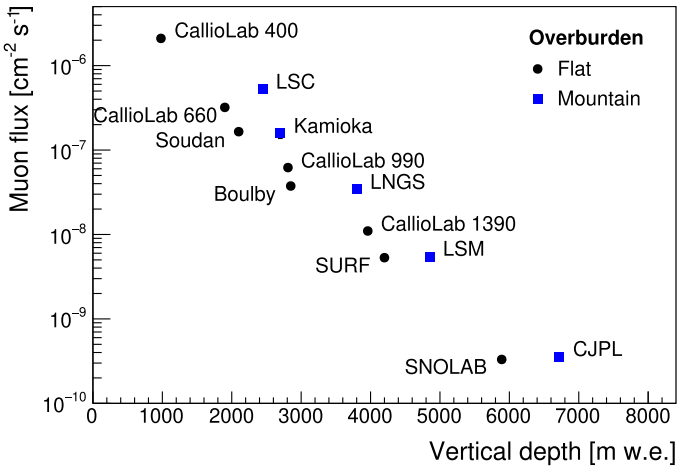

Figure 34. Depth-dependent muon flux at various underground laboratories (measured in 'meters water equivalent' (m.w.e.). While the depth increases from 620 m.w.e. to 6720 m.w.e., the muon flux decreases by more than four orders of magnitude. The data points represent the following measurements: CallioLab (Pyhäsalmi, Finland) at various depths [1071], LSC (Canfranc, Spain) [1072] (with depth taken from [1073]), Soudan (Minnesota, USA) [1074], Kamioka (Japan) [1075] (conversion from muon rate to flux based on simulations from [1076]), Boulby (UK) at 1100 m level (2850 m.w.e.) [1077], LNGS (Gran Sasso, Italy) [1078], SURF (South Dakota, USA) [1079] (depth taken from [1080]), LSM (Modane, France) [1081], SNOLAB (Sudbury, Canada) [1082], and Jingping (China) [1083].

and detector design are also important considerations that will impact which and how backgrounds manifest. Modeling of detector performance and simulations of background events will be critical in informing the design of the experiment, deriving sensitivities, and ultimately in achieving final science results [151].

7.1. Underground laboratories

Muons traversing detectors or surrounding materials will induce primary backgrounds as well as secondary neutrons and cosmogenic backgrounds from activation of materials [1065, 1066]. Dark matter detectors are thus deployed in deep underground laboratories, where cosmic-ray muon backgrounds are greatly reduced by the rock overburden [1067]. Nevertheless, for high-sensitivity experiments, active muon shielding is still required in order to tag remaining muon-related background events and reduce the muon-induced background to a negligible level compared to other sources. Muon fluxes at the typical underground laboratories range from 1 muon m^{-2} h^{-1} at the Laboratori Nationali del Gran Sasso (LNGS, 3100 m water equivalent deep) [1065, 1068] to about 5 muons m^{-2} month^{-1} at China's Jinping underground laboratory (CJPL, 6720 m water equivalent deep) [1069, 1070] (figure 34).

There are a host of underground laboratories that can be considered as location for the next-generation observatory discussed here. This includes the laboratories hosting the current generation of liquid xenon detectors: LNGS [1084] (location of XENONnT), CJPL [1085] (location of PandaX-4T) and SURF [1086] (location of LZ). The Boulby Underground Laboratory has a similar muon flux to LNGS with notably low radon levels [1087]. The Modane Underground Laboratory [1088] includes a facility for radon-free air, and the entire scientific

campus of SNOLAB [1089] is equipped as a cleanroom with some of the lowest available muon flux. Several of these laboratories entertain feasibility studies for creating additional underground space for scientific use. All in all, there is a favorable outlook that suitable underground space can be made available for the next-generation liquid xenon observatory. While radioactive and muon-induced backgrounds are dominated by the rock composition and overburden, respectively, the varying geomagnetic field at different latitudes has a (modest) impact on the science that can be done with atmospheric neutrinos [819]. To select an adequate underground location for the next-generation detector, in addition to such background considerations, relevant questions are related to e.g. the availability of underground space, constraints in accessing it, operational considerations, the local support infrastructure, and funding.

7.2. Fiducialization

The dominant background component in liquid xenon detectors at a given energy range has evolved with increasing detector size. In earlier detectors (e.g. XENON100 [1090], LUX and PandaX-I/II), the gamma radiation from radioactive contaminants of detector construction materials contributed significantly to the ER background for dark matter searches in the keV energy range. A FV selection is typically applied to reduce these backgrounds, which predominantly appear toward the boundaries of the bulk xenon: with larger detector masses and hence smaller surface-to-volume ratios, fiducialization can preserve a higher proportion of the active volume for a physics search. Gamma-induced ERs will remain a significant background for rare event searches at the MeV scale such as the $0\nu\beta\beta$-decay of ^{136}Xe (section 4.1, figure 22).

Radioactive contaminants of detector materials are also the source of radiogenic neutrons through spontaneous fission or (α, n) reactions. Fiducialization of the liquid xenon target is not quite as effective for neutrons compared to gamma radiation. Therefore, current and future liquid xenon detectors are equipped with dedicated neutron veto systems for efficient mitigation of NR background events.

Design studies for a next-generation detector will need to optimize the use of veto systems to achieve the largest possible FV. From the inside to the outside, this required research concerns the xenon skin region as used in XENON100 [92] and LZ [1091]; a neutron veto for which LZ uses boxed gadolinium-loaded liquid scintillator [1091] whereas XENONnT implements a gadolinium-loaded water Cherenkov design [98]; and the size of a muon veto, which may be constrained by or put constrains on the respective underground laboratory. Further studies to optimize the FV concern the electric field configuration inside the TPC, in order to reduce the loss of signal from regions near the surface where charge collection is reduced or signal yields are non-optimal [1092].

7.3. Material selection

The selection of materials featuring the lowest contamination with radioactive impurities is the most important strategy for background mitigation in current and future liquid xenon experiments [1093, 1094]. Trace amounts of uranium and thorium can be detected by means of highly sensitive gamma-spectrometers, inductively-coupled plasma mass spectrometry measurements or neutron activation analysis. Radon emanation rates are determined in dedicated setups where the radon which is emanating from the sample accumulates in an ambient carrier gas, before the radon activity in this sample gas is measured, typically using proportional counters or electrostatic radon monitors [1094, 1095].

Various material samples are measured in intensive screening campaigns in order to preselect and built radiopure detector components which fit the requirements for a next-generation liquid xenon experiment [103]. Once the materials are selected, the screening measurements

are used for background modeling by means of simulation. Precise knowledge of emanation sources can further be used to optimize the online purification systems. Following multiple iterations of low-background xenon experiments, much of this process is now well-established. However, its application to a next-generation detector can be challenging, as substantial dedicated screening infrastructure is needed with sufficient measurement time to achieve the required sensitivity. This in turn necessitates an early start, years ahead of the construction of the next-generation detector.

7.4. Intrinsic background mitigation

Sources of so-called intrinsic backgrounds are typically radioactive noble gases which are homogeneously mixed within the liquid xenon target. Thus, any type of shielding remains ineffective. Trace amounts of ^{85}Kr that stay in the xenon during its distillation from air will cause, if not removed, a low-energy ER background from its beta decay. Due to the absence of krypton sources within the detector, the ^{85}Kr contamination is constant over time and scales with the liquid xenon mass. ^{85}Kr thus needs to be removed through cryogenic separation of the xenon target, as pioneered by the XMASS collaboration [136]. The purification of xenon from trace amounts of ^{85}Kr has been successfully demonstrated using both cryogenic distillation [136, 1096, 1097] and adsorption [1098, 1099] as separation techniques. Cryogenic distillation in particular is appropriate to process large amount of xenon gas before being filled into the experiment, but also an online krypton purification at a running detector has been demonstrated. Starting with a Kr-nat contamination of several ppm in commercial xenon, a purification to (360 ± 60) ppq was achieved in XENON1T using the online krypton purification [1100]. The lowest concentration to-date was measured in the outlet of the XENON1T distillation system to be below 26 ppq (90% CL) [1097], using an enhanced rare gas mass spectrometer with a sensitivity of 8 ppq [1101]. This level is well below even the requirements of a next-generation liquid xenon experiment.

^{222}Rn is not immanent in the xenon gas, but continuously emanates from surfaces of detector materials. Due to its subsequent beta decays, radon is the dominant background source in current liquid xenon detectors. A smaller surface-to-volume ratio will naturally decrease the radon concentration in next-generation liquid xenon detectors. However, further mitigation strategies are needed to achieve a level of about 0.1 μBq kg^{-1} that is required in order to render radon-induced backgrounds sub-dominant versus the irreducible contributions from neutrino signals. Once a new detector has been built, its emanation rate of ^{222}Rn is set and expected to be constant over the lifetime of the experiment. A further suppression of the radon induced background can be achieved through continuous purification of the xenon target. The key for an efficient radon removal is a good separation technique and a high purification flow which revolves the entire xenon target fast with respect to the 3.8 days half-life of radon. Radon removal based on cryogenic distillation has been successfully tested in large scale liquid xenon experiments [1102] and is used also in XENONnT [1103]. Radon purification systems designed for small purification flows can also significantly reduce the radon concentration in xenon. Since the dominating radon emanation sources in an experiment are known from screening, dedicated purge flows toward the radon removal system can prevent radon to enter the liquid xenon target [1094]. For the next-generation detector discussed here, a strict radon mitigation protocol will need to be developed and implemented, including extensive screening for radon emanation; strategies to limit radon emanation (e.g. reference [1104]); radon removal from xenon both within the TPC and outside the shielding; optimized xenon flow; etc.

Another intrinsic background source is the decay of ^{137}Xe, with particular relevance for the search for neutrinoless double-beta decay [710, 716]. It is naturally created inside the

xenon target through activation by muon-induced neutrons. Thus, the ^{137}Xe induced background strongly depends on the muon rate at the experimental site. Short-lived cosmogenic isotopes such as ^{37}Ar are of little concern for the anticipated experiment [139].

7.5. Isolated light and charge signals and accidental coincidences

Due to the large electroluminescence gain that is exploited in dual-phase liquid xenon TPCs, even a single extracted electron can produce a detectable S2 of tens of photoelectrons in size [509, 1105–1110]. A standalone search with S2s (i.e. without requiring an accompanying S1 signal, see section 3.2) can thus lower the energy threshold, improving the reach to low-mass WIMPs, solar axions and solar neutrinos, and other physics that have associated low-energy recoil signatures [181]. However, this sensitivity to any process that can release even single electrons from their shell brings in additional instrumental backgrounds. Several sources of S2-only, single and few-electron backgrounds are known [507, 509–515, 1111]; significant research is needed to further understand and eventually mitigate those backgrounds. Photoionization backgrounds caused by large S2s die away within a maximum drift time after the S2 [509]. Emission from metal surfaces would be evident in specific locations that could be avoided with positional cuts. The most impactful background appears to be S2s up to five electrons in size that continue for times up to seconds after a large S2. The rates of these correlated small S2s, which appear in the same location as a previous large S2, decrease according to a power law with time after the large S2 [507, 513, 514]. This background can be mitigated with positional and temporal cuts after large S2s.

S1-only backgrounds also exist due to interactions in areas insensitive to the charge channel. One such origin of lone S1 events is from outside of the main drift field region of the TPC, notably below the cathode. Another origin is from volumes where charges are depleted, or where electrons cannot reach the extraction region. Most notably this can be as a result of the field configuration toward the edges of the detector [63]. Unrelated, isolated S1-only and S2-only signals can be close enough in time to be mis-identified as a single event. Such accidental coincidences of instrumental backgrounds can thus mimic a physics interaction for a conventional search in S1–S2 phase space. As both lone S1s and S2s are more likely to manifest at smaller signal values, these accidental coincidence backgrounds are particularly problematic for the WIMP search ROI. The absolute incidence of such accidental events could increase in a next-generation detector, as the corresponding surfaces and volumes from which lone S1s and S2s can arise become larger. However, their impact on the WIMP search will decrease with increasing detector size, due to the favorable surface-to-volume ratio. In the XENON1T experiment, this background was tackled in a data-driven approach (reference [1112] and figure 35): lone S1 and lone S2 events where characterized with high statistics in the available parameter spaces. The expected distribution of accidental coincidences was then simulated by randomly drawing an S1 and an S2 event from these distributions. This allowed for a detailed characterization of this background and thus modest impact on sensitivity. Combined with detailed detector simulations, and the lower rate per exposure unit, such an approach is expected to be sufficient to control this background for a next-generation experiment.

7.6. Monte-Carlo simulation of backgrounds

7.6.1. Background model. To construct a model of expected backgrounds, the activities and normalizations found from material assays and physics estimates must be paired with the corresponding detection efficiencies of the associated events. These efficiencies are determined through Monte Carlo simulations of event primaries, such as daughters from radioactive decay,

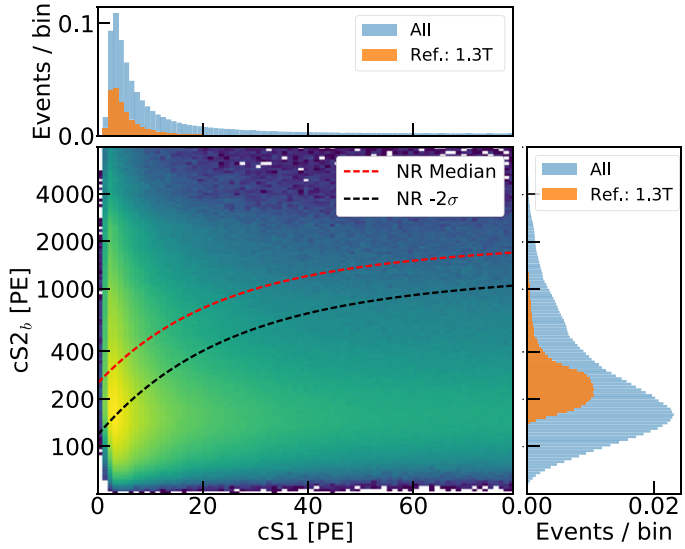

Figure 35. Illustration of the accidental coincidence background distribution from XENON1T in cS1 and $\log_{10}$(cS2b), with projections on each axis showing the expected distribution within the entire analysis space (blue), and in the reference region for 1.3 tonne FV. The reference region lies between the NR median and -2σ quantile lines, marked by red and black lines, respectively. Reprinted (figure) with permission from [1112], Copyright (2019) by the American Physical Society.

within a realistic representation of the experiment. Simulations are used to determine the energy depositions from backgrounds within the detector, and in translating them into observed signals.

A framework based on the GEANT4 toolkit [1113] allows for the tracking of particles within a rendering of the detector geometry. Custom additions can enhance the modeling of various physics processes and phenomena beyond the standard physics lists available, as in the case of modeling neutron captures on Gd using ANNRI [1114, 1115] or DICEBOX [1116] derived outcomes for an improved veto assessment. Bespoke event generators enable the simulation and study of more involved scenarios that are not well-captured in default GEANT4, such as (α, n) reactions accompanied by a varying multiplicity of gammas, or events from atmospheric muons which penetrate the laboratory rock overburden [1117].

Analysis cuts can be applied to remove events with coincident scatters in veto detectors, and restrict to an energy ROI and/or a FV. Persistent background counts can then be compared to those anticipated from potential signals. This approach has been used in predicting the background burden of many present-generation experiments, forming the basis of WIMP sensitivity estimates for XENONnT [98], LZ [99] and PandaX-4T [97].

7.6.2. Generation of S1 and S2 signals. Generally, energy depositions are converted to observable S1s and S2s to construct PDFs for background components and signal for likelihood-based analysis [1126]. The microphysics behind the interactions of particles with the active xenon is captured by the NEST [121, 126–128, 1127]. NEST offers a comprehensive and mature framework to simulate the atomic and nuclear physics of energy deposition and the resulting detector response. Using world data from previous experiments including LUX, XENON, PIXeY [515, 1128], neriX [1129, 1130], ZEPLIN-III [502], and Xurich

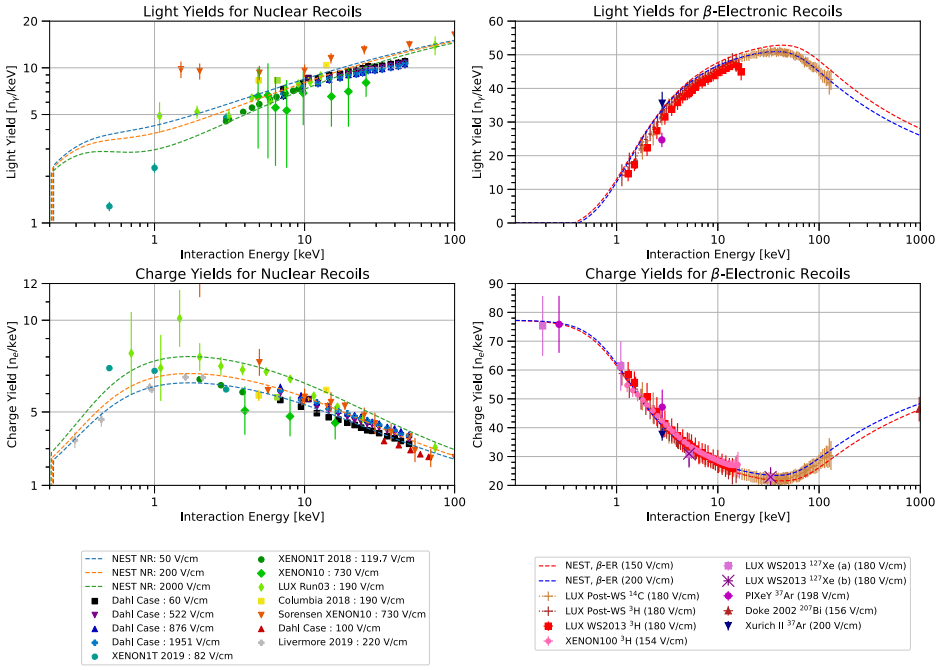

Figure 36. The light and charge yields for nuclear and ERs, as measured by various experiments and as modeled by the NEST v2.3.5 [128]. The light (charge) yield is defined as the number of photons (electrons) leaving the recoil site after electron–ion recombination, per unit energy. For ERs, NEST has two models for β-induced and γ-induced recoils, respectively, and we show the β model. Correspondingly, we only show experimental measurements from β calibrations or low-energy line sources, which are observed to fit the β model better than the γ model. The NR data points are from Dahl's thesis [130], XENON1T [1112], XENON10 [129, 132, 1107, 1118], LUX Run 3 (WS2013) [1119], and dedicated xenon TPCs at Columbia University [122], Case Western Reserve University [115], and Lawrence Livermore National Lab [496]. The ER data points are from LUX [1120–1123], XENON100 [1124], PIXeY [1125], Xurich II [105], and a paper by Doke *et al* [117].

[105, 1131], the NEST collaboration has developed models for the light and charge yields of various interactions. These models are semi-empirical and reproduce calibration data from alphas, betas, gammas, NRs, and exotic interactions like the two-step internal conversion of ^{83m}Kr. The excellent agreement between the NEST models and data can be seen in figure 36. Further research will be needed to further improve this understanding in particular at even lower recoil energies. Physicists on a next-generation liquid xenon experiment are thus able to take advantage of NEST to accurately simulate the signals induced by both signals and backgrounds, including their S1, S2, position, and pulse timing.

7.7. Electronic/nuclear recoil discrimination

The results of simulating events from a type of source, be it ER or NRs, are a list of S1 and S2 values for each event. Binning these events into a 2D histogram will show how a given type of interaction looks like in terms of the signals received. An example shown in figure 37 is the histogram of a 50 GeV spin-independent WIMP, which is lower in S2 than that of ER events. This difference allows for distinction between these two types of interactions and can

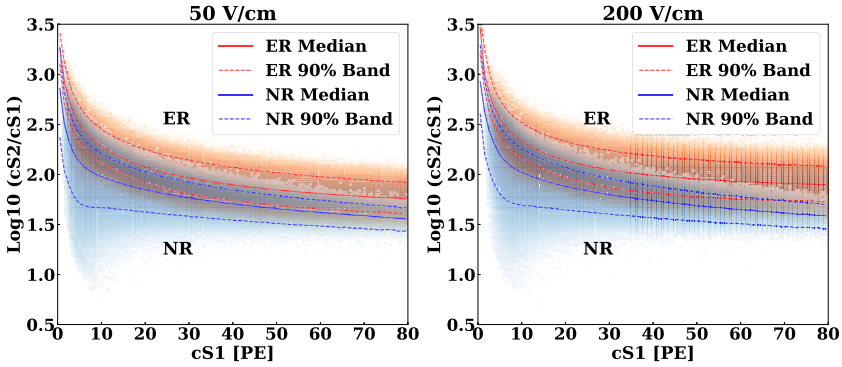

Figure 37. Histograms for a flat ER spectrum and a NR spectrum as from a 50 GeV spin-independent WIMP, simulated for different electric fields (using NEST 2.3.5). The top band for each plot is the ER band, the bottom is the NR band. Red lines refer to the median for either band, and the white dotted lines delimit the one-sigma region. Already-demonstrated ER/NR discrimination is expected to be sufficient for a next-generation detector.

be measured quantitatively in a few ways. Leakage is the proportion of ER events per bin that lie below the NR median line; rejection is the percentage of background events that are not in the ROI given by (1 − leakage). Various instrumental parameters affect the discrimination capability. For example, the drift field affects the gap between the nuclear and ER spectra, as does the g_1 parameter which measures the S1 light yield in the detector. As can be seen from figure 37, even moderate drift fields provide satisfactory ER/NR discrimination. Discrimination is also affected by the atomic structure of xenon, leading to increased leakage from neutrino and Compton scatters on L-shell electrons due to the accompanying atomic de-excitation via Auger electron cascades. This effect is still under study, but available measurements indicate a reduction in rejection by a factor of 6× near the L-shell binding energy (5.2 keV) compared to predictions from valence ERs and β-decays [1132, 1133]. Including this effect for the solar neutrino-induced ER background results in an 8% relative increase in leakage from 5.2–8 keV, for 50% NR acceptance.

Importantly, already with the performance of running detectors, discrimination between ER and NRs in liquid xenon is sufficient to achieve the various science goals presented in this review, whether they pertain to WIMPs, neutrino-induced signals in both the ER and NR band, or the search for neutrinoless double-beta decay. The accuracy of these simulation results is confirmed *in situ* using dedicated calibration sources, such as dissolved gamma line sources ^{83m}Kr [448], dissolved beta-spectrum sources ^{220}Rn [1134, 1135], TH_3C [1121], as well as various neutron sources [1119, 1136, 1137].

8. Complementarity with other experimental efforts

8.1. Crossing symmetry for freeze-out relic particles

Production, decay and scattering of dark matter particles are often governed by the same or similar interaction. Relic particles such as WIMPs are a textbook example of this situation, where the production through freeze-out from the thermal equilibrium in the early Universe creates the observed relic density [32, 1138, 1139]. The three principal approaches to discover

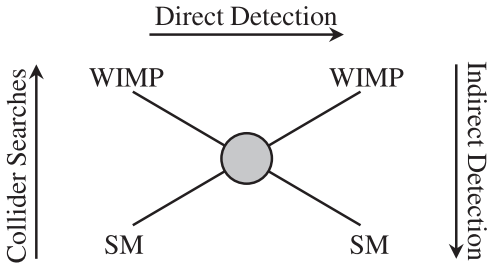

Figure 38. Based on the general idea of thermal relic particles (such as WIMPs) interacting with the SM, three detection techniques are possible: production at colliders, scattering from a target material (direct detection) and annihilation resulting in cosmic rays (indirect detection).

thermal freeze-out relic particles correspond to the *s*- or *t*-channel processes of dark matter production or scattering, and the time-reversed process to production, which might lead to annihilation of dark matter. This results in the following detection channels, related through crossing symmetry [1140] (see also figure 38):

(a) *Direct detection*: direct detection of particle dark matter in the Galactic halo in underground experiments as described here;
(b) *Collider production*: production of dark matter in the laboratory, usually using high energy particle collisions;
(c) *Indirect detection*: detection of products of dark matter annihilating or decaying in our local Universe.

8.2. Dark matter at colliders

The electroweak energy scale is powerfully probed by the LHC at CERN [1141]. The freeze-out mechanism requires significant couplings between the dark matter and the SM, which further motivates searches at a particle collider. Moreover, many 'beyond the SM' theories in high energy physics require new particles at the electroweak scale, which are either viable dark matter candidates or might couple to particle dark matter. The most prominent example of such a theory that connects naturally astrophysical and theoretical motivation is SUSY, which not only remedies many known problems of the SM, such as the hierarchy problem, but also provides an excellent dark matter candidate [140, 341, 1142, 1143].

Another motivation for collider searches is the potential to study dark matter in the laboratory. Collider production implies production of the mediator, i.e., the force carrier that connects the dark sector with the visible sector of the SM. Hence, collider dark matter searches are in essence searches for the mediator rather than dark matter. Most collider dark matter searches assume maximal decay of the mediator into dark matter [212, 213]. This is in particular true for 'mono-X' searches, where the main signature is missing momentum in the transverse plane due to the dark matter particle escaping the detector undetected. Constraints placed on the mediator masses are typically about twice as strong as the constraints on the dark matter mass itself. Other analyses attempt to place constraints on the nature of dark matter by looking for deviations in the properties of known particles, for example the Higgs boson, or to search for the mediator directly, such as in dijet searches [1144]. Further complementarity stems from searches at colliders for ALPs and dark photons, see e.g. references [1145, 1146].

8.3. Indirect dark matter searches

Dark matter annihilation and decay into SM particles lead to potential signatures in the CMB [555, 1147, 1148] and astrophysical observables such as x-rays [1149–1151], gamma rays [367, 1152–1178], antiprotons [1179–1184], positrons [358, 1185–1189], neutrinos [1190–1201], or other particles [1202–1212]. Thermal relic dark matter candidates are generically expected to have a thermally averaged annihilation cross section $\langle\sigma v\rangle \simeq 2.2 \times 10^{-26}$ cm^3 s^{-1} [20, 145], though other production mechanisms or annihilation channels are known to predict much smaller or larger annihilation cross sections, e.g. Sommerfeld enhancement [319, 1213], non-thermal/out-of-equilibrium production [1214–1217], asymmetric dark matter [624, 1218–1220], co-annihilation [1221–1223], velocity-dependent annihilation, or non-standard cosmologies [1214, 1215, 1224–1230]. The thermal relic cross section, however, provides an important benchmark for indirect detection efforts. While this leads to a characteristic signature of dark matter in the corresponding cosmic ray spectrum [150, 1152, 1155], the topology, spectral shape and strength of such a signal is rather model dependent and affected by astrophysical foregrounds.

Since the annihilation rate of dark matter is proportional to the square of the dark matter density at the location of annihilation, the brightest signals are expected to come from dense structures. Present searches for annihilation signatures aim at a variety of targets, with the Galactic center and local spheroidal satellite galaxies (dSphs) of the Milky Way being among the most prominent ones. The former is expected to be the brightest source in the sky because of the large dark matter overdensity, but it also has the brightest foregrounds and complex dynamics. The latter are the most extreme dark matter-dominated galaxies known to us, but have a much lower J-factor [1231, 1232] compared to the Galactic center (around 10^{17} to 10^{19} GeV^2 cm^{-5} for dSphs and about 10^{22} GeV^2 cm^{-5} for the Galactic center, leading to a fainter potential signal.

In contrast, the flux of particles from decaying dark matter is only proportional to a single power of density, so it is predicted to give rise to less clumpy signals compared to those from annihilating dark matter. Constraints on decaying dark matter come for example from isotropic gamma-ray and neutrino observations [1175, 1197].

There is more than just phenomenological support for the hypothesis that dark matter self-annihilates. N-body simulations suggest that dark matter halos, in the absence of baryonic effects, follow a density profile which behaves like $\varrho \propto r^{-1}$ irrespective of initial conditions. This is referred to as a Navarro–Frenk–White profile [1233, 1234]. Measured profiles of disk and spheroidal galaxies appear to follow a shallower density profile: $\varrho \propto r^0$ [1235–1239]. This disagreement is referred to as the 'core-cusp-problem' and could possibly be resolved by co-annihilating or SIDM [379] (section 2.14).

8.4. Measurements of standard model parameters

In some models of dark matter, the dark matter mass and nucleon–dark matter scattering cross section are predicted or bounded as functions of SM parameters such as the top quark mass and the strong coupling constant. In such scenarios, dark matter searches constrain the SM parameters, which can be precisely measured by future colliders [1240–1244] and lattice QCD computations [1245].

For example, in a model that solves the strong CP problem by a space–time parity symmetry [1246], the dark matter mass is proportional to the energy scale at which the SM Higgs quartic coupling vanishes (10^9 to 10^{12} GeV), which is sensitive to the SM parameters. Dark matter couples to a massless dark photon and the dark matter–nucleon scattering arises from unavoidable quantum corrections leading to photon-dark photon mixing.

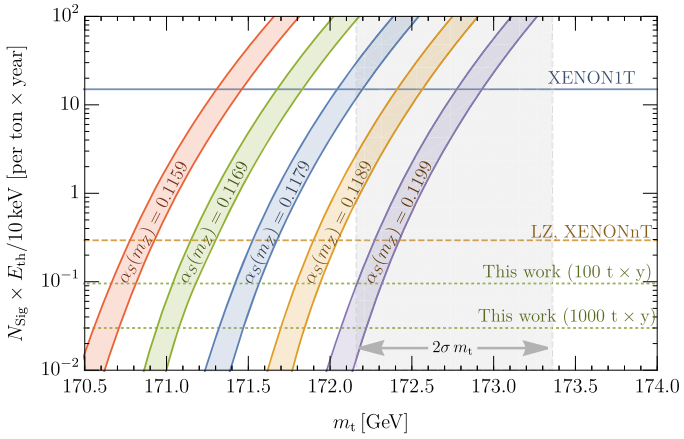

Figure 39. The expected number of signals per tonne-year exposure as a function of the top quark mass, m_t, and the strong coupling constant evaluated at the Z-boson mass scale, $\alpha_s(m_Z)$, in the model described in reference [1246]. The signal count is inversely proportional to the threshold energy $E_{\rm th}$. The thickness of each colored band corresponds to 2σ uncertainty in the Higgs mass.

The resultant correlation between the dark matter signal rate and the SM parameters that determine the scale where the Higgs quartic coupling vanishes is shown in figure 39. Here, to estimate the projections for next-generation experiments, we scale the limit from XENON1T according to the projections in the high mass region shown in figure 5. Another example is sneutrino or higgsino dark matter in supersymmetric theories, where the dark matter mass is predicted to be smaller than the scale at which the SM Higgs quartic coupling vanishes [1247]. Dark matter scatters with nuclei via tree-level Z-boson exchange, generating signals detectable in a 1000 tonne-year exposure even for a dark matter mass as large as 10^{12} GeV. Detection of or constraints on nucleon–dark matter scattering signals will give an upper bound on the top quark mass and a lower bound on the strong coupling constant.

8.5. Other direct dark matter searches

In the search for dark matter directly interacting with a laboratory target, a host of synergistic detectors are required to overcome signal degeneracies, particularly as experiments begin probing the neutrino fog. With different technologies and targets, complimentary experiments can confirm potential dark matter signatures and disentangle them from both neutrino-induced (CEνNS) signals and instrumental backgrounds. Additionally, a large variety of detectors can probe a wider dark matter mass range, as shown in figure 40. Target materials range from solid state crystals to dense liquids [44, 151]. Even within the context of liquid xenon TPCs, larger detectors are required for dark matter nuclear scattering searches, but smaller detectors optimized for single-electron signals might achieve better sensitivity to lower masses and dark matter scattering with electrons [1248].

8.5.1. Solid state detectors. Germanium detectors (HPGe detectors) are a well-understood target for dark matter searches and have been used particularly by CoGeNT [51] and EDELWEISS [54]. DAMIC [55] and SENSEI [57] are using silicon CCDs to look for dark matter interactions, in particular through the ER channel. SuperCDMS [52] measures both phonons and ionization in silicon and germanium crystals cooled to millikelvin temperatures. CRESST

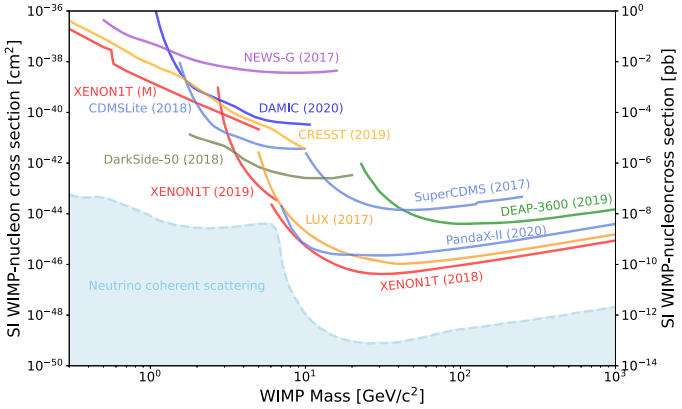

Figure 40. Spin-independent dark matter–nuclear scattering limits set by leading direct detection experiments. Complementary experiments with different targets are essential for breaking degeneracies between signals from CEνNS and WIMP dark matter. Additionally, a variety of targets covers a wider range of potential dark matter masses. Reproduced from [584]. Image stated to be in the public domain.

[56] uses calcium tungstate crystals at millikelvin temperatures to read both phonons and scintillation. Sodium iodide is used by ANAIS [439], SABRE [54] as well as DAMA/LIBRA [1060]. Depending on the target and readout, crystals have different sensitivities to different dark matter interaction energies, but largely overlap across dark matter masses in the GeV and sub-GeV range.

8.5.2. Liquid target detectors. The PICO experiment [67] uses octafluoropropane in a bubble chamber to search for dark matter-induced signals with a particularly strong sensitivity for spin-dependent interactions. Piezo-electric sensors detect bubble formation in the superheated target during an interaction, and cameras record the bubble nucleation. Perhaps the most complementary experiments to liquid xenon TPCs are liquid argon TPCs, such as darkside [62]. The operating principle is identical to the detector described here, but the smaller atomic mass of argon and its effect on collision kinematics makes argon invaluable for breaking the energy degeneracy of dark matter scatters and coherent elastic neutrino-nucleus scatters, once observed in liquid xenon TPCs. While self-shielding of external backgrounds is better in xenon, the ability to discriminate ER from NRs is better in argon. Taken together, the two target elements provide a complementary approach to probing dark matter down to the signal from atmospheric neutrinos.

8.6. Neutrinoless double beta decay experiments

Experimental searches for $0\nu\beta\beta$ decay [1249] span a variety of isotopes, including ^{76}Ge, ^{82}Se, ^{100}Mo, ^{130}Te, ^{136}Xe, and ^{150}Nd. The choice of isotope is driven by the Q-value of the $2\nu\beta\beta$ mode, the ability to obtain high isotopic abundance, and compatibility with a suitable detection technique. Detection techniques include semiconductor crystals, cryogenic bolometers, TPCs, and organic and inorganic scintillators. The choice of detection technique is a balance of the detector energy resolution at the Q-value, the scalability of the technology to large masses, and ability to achieve ultra low backgrounds. The leading experimental efforts to date include MAJORANA [705], GERDA [1250], CUORE [1251], EXO-200 [706], and KamLAND-Zen [701, 1252]. The next generation of $0\nu\beta\beta$ searches includes LEGEND [1253], nEXO [713],

NEXT [1254], CUPID [1255], KamLAND2-Zen [1256], and SNO+ [1257]. Compared to the experiments using semiconductors and bolometers, a next-generation liquid xenon detector will have significantly larger isotopic mass, even with a natural abundance of ^{136}Xe, but it will have poorer energy resolution compared to other technologies. The ability to fiducialize the detector means that the backgrounds from radiogenic sources are significantly reduced. A next-generation liquid xenon dark matter detector can have a $0\nu\beta\beta$ sensitivity comparable to those of the next generation of dedicated $0\nu\beta\beta$ experiments (section 4.1).

8.7. CEνNS experiments

The identification of neutrinos in dark matter experiments, in particular through the CEνNS channel, will be complementary to terrestrial neutrino experiments which operate in a similar energy regime. The COHERENT experiment [1258] uses a stopped-pion source of neutrinos, generated by the Spallation Neutron Source (SNS) at the Oak Ridge National Laboratory. Muon neutrinos with energy 30 MeV are produced from charged pion decays, and $\bar{\nu}_\mu$ and ν_e are produced with a Michel energy spectrum from the subsequent decay of muons at rest. $\bar{\nu}_\mu$ and ν_e from muon decays are delayed relative to the 30 MeV ν_μ neutrinos produced from the prompt pion decay. With characteristic energies of tens of MeV, a large sample of the neutrino-nucleus interactions are coherent, which together with the timing structure, permits a measurement of the CEνNS process.

Using 14.6 kg CsI[Na] scintillator detectors, the COHERENT collaboration announced the first detection of CEνNS in 2017 [791], with a best-fit count of 134 ± 22 CEνNS events, which is 77 ± 16 percent of the SM prediction. From this initial detection, COHERENT was able to constrain NSIs in a regime of parameter space that had not been possible to probe. In particular, the COHERENT data is sensitive to u- and d-type NSIs for flavor-diagonal muon components, $\epsilon_{\mu\mu}$. The COHERENT detection also set new constraints on exotic solutions to solar neutrino mixing, places novel constraints on new physics that manifests through the neutrino sector (e.g. reference [1259]), constrains the neutron form factor for CsI [1260], sterile neutrinos [1261, 1262], and the $g-2$ anomaly [862, 863, 1263]. The collaboration has since also measured CEνNS on argon [1264].

Nuclear reactors have been purposed as a copious source of electron anti-neutrinos. The characteristic neutrino energy is $\lesssim 1$ MeV; as such, the coherence condition for the recoil is largely preserved over the entire reactor energy regime. The primary difficulty in detecting CEνNS using reactors is that detectors have not been able to achieve the low threshold required to identify the CEνNS NR signal. With further improvements in detector technology, several experiments are poised to identify CEνNS at reactors [1033, 1265–1271]. The two-phase noble gas detection technique is very promising for this purpose [1271, 1272], and currently the RED-100 detector (with $\sim$160 kg of active liquid xenon) is being tested at the Kalinin NPP site. This is the first CEνNS experiment using a two-phase emission technique, and other experiments, such as NUXE with liquid xenon and CHILLAX with xenon-doped liquid argon, are currently being developed.

8.8. Solar neutrino experiments

Direct real-time measurements of solar neutrinos have been observed for the first time by the Borexino experiment [799, 809, 1273]. A next-generation liquid xenon experiments can offer complementary measurements when detecting solar neutrinos through elastic neutrino-electron scattering (section 5.2). Neutrinos that contribute to the signal are generated from the *pp*-reaction chain, produced from the electron-capture decay of beryllium-7, and emitted in the CNO fusion cycle. The measurement of CNO neutrinos in liquid xenon-based detectors is

limited by the presence of the two-electron spectrum arising from the $2\nu\beta\beta$-decay of ^{136}Xe. Depletion of ^{136}Xe by at least a factor of 100 relative to its natural abundance would be necessary to detect the CNO solar neutrino component in the next-generation xenon-based detector [802].

8.9. Gravitational wave searches

Liquid xenon-based detectors can be utilized to look for neutrinos and gamma-rays released in association with gravitational waves emitted during cataclysmic cosmic events. Such 'simultaneous' observation is related then to supernova detection and multi-messenger astrophysics, as discussed in section 5.4.

8.10. Xenon in medical physics

The great advantages of using liquid xenon for medical imaging have been noticed already back in the 1970s [1274, 1275]. Its fast primary scintillation and sufficiently large ionization yield make it especially attractive for positron emission tomography (PET). The two-phase emission detector with condensed xenon as working medium has been tested in the 1980s as a high-quality gamma-camera for nuclear medicine [1276]. The 1990s saw compressed xenon gas being proposed for very effective, collimator-less SPECT systems [1277–1279]. The first liquid xenon detector prototypes for PET scans were built and tested around the same time [1280–1282]. Further developments of liquid xenon detectors for PET came recently [1283–1286]. In a PET scan, patients are injected with small amounts of chemicals, such as sugar, where molecules have had common stable carbon atoms replaced with positron-emitting isotopes. Position–electron annihilation in the electron shells of atoms in the body leads to back-to-back 511 keV γ-rays. Cancerous tumors will preferentially absorb more sugar than other parts of the body due to higher rates of metabolic activity [1287]. Liquid xenon is being explored due to its advantageous spatial, temporal, and energy resolutions. Already, PETALO is a full-body PET scanner using the S1 signals in liquid xenon to achieve a high resolution image with reduced patient radioactivity exposure [1288]. Many of the developments in liquid xenon detector technology for particle physics thus directly benefit other scientific disciplines, such as medicine, as evidenced here.

Xenon in its gaseous form has also come into use as an alternate anesthetic with minimal dangerous side-effects [1289]. Xenon anesthesia results in a more stable blood pressure, a lower heart rate, and faster emergence from anesthesia than other conventional methods, despite a higher risk of nausea [1290]. Most oddly and uniquely, there are some studies that suggest it is useful for treating traumatic brain injuries and post-traumatic stress disorder [1291, 1292]. While in the United States these claims have not been evaluated by the Food and Drug Administration (FDA), in Russia, the inhalation of xenon is used for selective 'deletion' of traumatic memories, associated with negative emotions [1292]. All this serves to illustrate the extreme versatility of the element. The study of xenon for particle physics may thus have side-effects spilling over into numerous other fields that seem entirely unrelated.

8.11. Liquid xenon TPCs for nuclear security

The neutron is the gold-standard calibration particle of choice for any WIMP detector, since it is supposed to emulate the NR generated by dark matter WIMPs. This implies that a WIMP dark matter detector is also an outstanding neutron detector. Liquid xenon TPCs stationed at seaports and airports can allow for non-intrusive inspection of fissionable materials in cargo, by detecting gamma rays and fast neutrons emitted spontaneously or by stimulation from nuclear

materials [1293]. The ability of discriminating between nuclear and ERs allows to better discriminate against activation from other backgrounds. This holds true even through shielding, given the low ∼keV energy thresholds achieved recently for dark matter searches.

Another homeland security application is monitoring of nuclear reactors at power plants for fuel rod theft, which could change the outgoing neutrino (and not just neutron) flux, or rod type replacement, which could change the balance of uranium and plutonium amounts. This concept has been explored by the Nucifer Experiment [1294] with a scintillating liquid. Liquid xenon could be ideal for detecting the resulting change in the rate of CEνNS, already discussed in detail above. Liquid xenon is being considered for detecting CEνNS by the RED [1271] and NUXE [1272] collaborations.

8.12. Data-intensive and computational sciences

All of the aforementioned scientific deliverables require the development of cyber-infrastructure such as algorithms, methods, and tools, for the wider benefit of data-intensive sciences. Years of substantial improvements in dark matter detectors means that the field launched into the realm of petabyte data science. The computational science pursued in this field includes, but is not limited to: how ultra-low-energy simulations are performed, including relevant microphysics (section 1.6); how event reconstruction can be performed with the aid of e.g. machine learning [1295]; and how high-throughput/high-level triggers can be deployed on such non-collider experiments.

This effort requires computational science developments, which can benefit other scientific efforts at both small and large scales. For small scales, there has been an explosion in the number of experiments in recent years. Examples of advancements in this field that are broadly impactful to those having to harness their data are integrating smaller efforts into existing infrastructure using frameworks such as GAUDI [1296]; data management systems such as OSG [1297]; and demonstrating the effectiveness of columnar compilers in tackling data-intensive applications in high-level descriptive languages. For large scales, overcoming computational science hurdles with novel technologies means serving as a test bed for technologies for big science projects such as the HEP software project [1298]. Therefore, achieving our physical science goals requires novel computational science and cyber-infrastructure development.

9. Research community priority

The need for a next-generation liquid xenon TPC is strongly acknowledged throughout the international particle physics community. Studies toward a large-scale liquid xenon dark matter detector started already in 2009 within the EU-ASPERA program, which eventually led to the DARWIN project. The support for DARWIN was strongly recommended in the 2011 update of the ASPERA roadmap [1299]. During the 'snowmass' process to plan research priorities in 2013, US particle physicists concluded that the discovery goal of liquid xenon dark matter detectors must be to 'search for WIMPs over a wide mass range (1 GeV to 100 TeV)…until we encounter the coherent neutrino scattering signal that will arise from solar, atmospheric and supernova neutrinos. [1300]. In 2017, the Astro Particle Physics European Consortium (APPEC) devised a European Strategy, which aimed to converge 'with its global partners' on the realization of at least one 'ultimate dark matter detector based on xenon' [1301].

The Division of Particles and Fields of the American Physical Society defined the next step for the detection of WIMPs to be 'to partner with Europe and Asia on one large international generation-3 detector' [1302] and they note that detector R & D looks promising for

'the scaling up of liquid noble…detectors to cover the WIMP mass range to the coherent neutrino floor' [1303]. The Chinese community also endorses a next generation deep underground xenon observatory as one of the top priorities in particle astrophysics [1304]. The APPEC dark matter report states that underground dark matter programs with the sensitivity to reach down to the 'neutrino floor at the shortest possible timescale' should receive enhanced support [1305]. Clearly, the main goal is to search for dark matter, but it is understood that this detector will have important implications for astrophysics and the quest for the nature of neutrinos. This present paper is a response to the global support for a next-generation liquid xenon TPC, as evidenced here. Progress is also made in assembling a strong global liquid xenon detector community, evidenced for example by the signing in 2021 of a joint Memorandum of Understanding between the members of the LZ and XENON collaborations forming the XLZD consortium.

9.1. Dark matter

In the past two decades, the goal of liquid xenon TPCs has been to detect theorized elastic scatters of WIMP dark matter off xenon nuclei. In addition to WIMPs, these detectors have sensitivity to a large host of well-motivated dark matter candidates, as outlined in this work. About 10 different xenon-based dark matter detectors were built over the years, increasing the xenon target mass by almost three orders of magnitude, reducing the ER background by about four orders of magnitude and improving the sensitivity to WIMP dark matter by more than a factor 1000. After the pioneering work by ZEPLIN-II/III and XENON10, XENON100, LUX and PandaX managed to build a suite of detectors with world-leading sensitivity. XENON1T was the first TPC with a target above the tonne-scale. The current generation of detectors, XENONnT [98], LUX-ZEPLIN (LZ) [99], and PandaX-4T [97], feature multi-tonne liquid xenon targets. Despite a lack of definitive signal so far, these detectors are clear leaders in sensitivity to WIMPs and other physics channels, and scale reliably in mass [96]. It is for these reasons that a next-generation liquid xenon TPC is of such high interest to the international physics community.

The Update of the European Strategy for Particle Physics (ESPP) from 2020 points out that the search for dark matter is a crucial part of the search for new physics and that experiments that offer 'potential high-impact' should be supported [1306]. The APPEC report on the direct detection of dark matter (2021) states that 'the search for dark matter with the aim of detecting a direct signal of dark matter particle interactions with a detector should be given top priority in astroparticle physics, and in all particle physics' [1305]. Already in 2014, the US Particle Physics Project Prioritization Panel (P5) highlighted the identification of the new physics of dark matter as one of the five science drivers for all of particle physics and recommended that US funding agencies 'support one or more third-generation (G3) direct detection experiments…(with) a globally complementary program and increased international partnership in G3 experiments' [1307]. Consolidation of the world-wide xenon community already took place when the members of the ZEPLIN collaboration joined LUX, and XMASS teamed up with XENON. Another important step toward the realization of this next-generation detector happened in 2021, when the scientists from the XENON/DARWIN and LUX-ZEPLIN collaborations agreed to join forces in the XLZD consortium toward the realization of this observatory.

The German [1308], Swiss [1309] and Dutch [1310] particle physics communities likewise identified the multi-tonne liquid xenon observatory DARWIN of particular interest for their national strategy roadmaps and support R & D toward this goal via national funding programs. Other countries are strong members of the XENON experiment and it is expected that

its follow-up project (e.g. DARWIN) will also be supported. The UK's Particle Astrophysics roadmap also stresses the importance of a xenon-based next-generation ('G3') observatory, explicitly recommending R & D toward this detector as the highest priority in dark matter. Relevant R & D is also supported through multiple European Research Council (ERC) grants.

9.2. Neutrinoless double beta decay

Understanding the physics of neutrino mass is another important science driver for particle physics identified by the US P5 and APPEC, which noted the importance of neutrinoless double beta decay searches in that context [1301, 1307]. Such experiments are also a top priority in the 2015 US Long Range Plan for Nuclear Science [1311], with one of the four main recommendations being the construction of a massive detector. The European APPEC double beta report (2019) states that 'the search for neutrinoless double beta decay is a top priority in particle and astroparticle physics' and acknowledges that the $0\nu\beta\beta$ sensitivity of a next generation *dark matter* detector opens up an exciting scenario [1312]. Similar statements of support for neutrinoless double beta decay detection, especially in dark matter detectors, can be found in UK [1313], Russian [1314], CERN/European [1315], and Chinese [1316] particle and nuclear physics priority planning documents. The APPEC dark matter report states on this topic that 'the potential of dark matter detectors to search for rare nuclear decays has been demonstrated spectacularly when XENON1T observed for the first time double electron capture on ^{124}Xe [766]' [1305].

9.3. Neutrinos

Recently, the observed phenomenon of CEνNS [791] has made large dark matter detectors, such as the one discussed here, particularly desirable for studying neutrinos. Such a detector would be invaluable to the field of astrophysics for measuring Galactic supernovae neutrinos of all flavors. A next-generation liquid xenon detector would be able to probe multiple solar, atmospheric and supernova neutrino signals, which are invaluable measurements in their own right. The US Nuclear Physics community, in the 2015 Long Range Plan for Nuclear Science (LRP) [1311], notes that measuring the CNO cycle and addressing the 'metallicity problem' in the Sun—both accessible to this detector technology—are the next big challenges in solar neutrino research.

Taken together, the experiment discussed here addresses a number of high-priority science issues. Spanning across (astro-)particle physics, astrophysics, and nuclear physics, such a detector will significantly advance fundamental science on a variety of fronts.

10. Summary

The compelling and versatile science case for a next-generation liquid xenon experiment, combined with its mature technology and minimal technological risk, renders such a detector a paramount facility for the next decade of particle physics, nuclear physics, and astrophysics. This detector will be sensitive to many types of dark matter interactions. Probing the remaining, well-motivated parameter space for spin-independent WIMP scattering down to the neutrino fog will be a milestone in the quest to unravel the nature of dark matter. With its xenon target, this detector will have unprecedented sensitivity to a variety of dark matter models, including spin-dependent couplings, ALPs, dark photons, and sterile neutrinos. With the help of optimized analyses, it covers dark matter masses ranging from kilo-electronvolts all the way up to the Planck mass. This next-generation experiment will therefore have significant and lasting impact on dark matter physics.

Simultaneously, such a next-generation liquid xenon experiment will be a competitive experiment in the search for neutrinoless double-beta decay, using a very cost-effective natural xenon target. It will therefore directly address one of the most pressing problems of nuclear physics. Isotopic separation of the natural xenon target can be used to further this sensitivity, or to enable a direct measurement of solar CNO neutrinos.

Furthermore, this next-generation experiment will be a true observatory for a number of relevant physics. Examples include a precision measurement of the Solar pp neutrino flux, a measurement of the Solar metallicity through boron-8 neutrinos, as well as a first measurement of atmospheric neutrinos in the mega-electronvolt energy range. This detector also has the chance to observe neutrinos from a Galactic supernova in a complementary, flavor-independent channel, if such an event were to occur in the lifetime of the experiment.

Finally, this detector provides the opportunity to search for a host of signatures from physics beyond the SM of particle physics. No other technology is capable of probing this many different signals, spanning areas from cosmology to nuclear physics, particle physics, and solar astrophysics.

Acknowledgments

This work has been supported by the US National Science Foundation (NSF, Grants PHYS-1719271, PHYS-2112796, PHYS-2112801, PHYS-2112802, PHYS-2112803, PHYS-2112851, PHYS-2137911); by the Department of Energy (DOE), Office of Science (Grants DE-AC02-05CH11231, DE-AC02-07CH11359, DE-AC02-76SF00515, DE-AC52-07NA27344, DE-FG02-00ER41132, DE-FG02-10ER46709, DE-NA0003180, DE-SC0006605, DE-SC0008475, DE-SC0009999, DE-SC0010010, DE-SC0010072, DE-SC0010813, DE-SC0011640, DE-SC0011702, DE-SC0012161, DOE-SC0012447, DE-SC0012704, DE-SC0013542, DE-SC0014223, DE-SC0015535, DE-SC0015708, DE-SC0018982, DE-SC0019066, DE-SC0020216, UW PRJ82AJ); by the UK Science & Technology Facilities Council (Grants ST/M003655/1, ST/M003981/1, ST/M003744/1, ST/M003639/1, ST/M003604/1, ST/R003181/1, ST/M003469/1); by the German Research Foundation (DFG) [Grants KO 4820/4-1, EXC-2118, 279384907 (SFB 1245)]; by the Max Planck Gesellschaft; by the Dutch Research Council (NWO); by the Swiss National Science Foundation (Grants PCEFP2_181117, 200020-188716); by the European Research Council (ERC) under the European Union's Horizon 2020 research and innovation program (Grants 742789, 101020842); by the Portuguese Foundation for Science and Technology (FCT) (Grants PTDC/FIS-PAR/28567/2017); by the Institute for Basic Science, Korea (Grant IBS-R016-D1); by the Australian Research Council through the ARC Center of Excellence for Dark Matter Particle Physics, CE200100008; and by the Marie Skodowska-Curie Grant Agreement No. 860881. BvK acknowledges support from Emmy Noether Grant No. 420484612; AM *et al* acknowledge additional support from the STFC Boulby Underground Laboratory in the UK, the GridPP [1317, 1318] and IRIS Collaborations, in particular at Imperial College London and additional support by the University College London (UCL) Cosmoparticle Initiative. This research used resources of the National Energy Research Scientific Computing Center, a DOE Office of Science User Facility supported by the Office of Science of the U.S. Department of Energy under Contract No. DE-AC02-05CH11231. The University of Edinburgh is a charitable body, registered in Scotland, with the registration number SC005336. PK and SB from the National Research Foundation of Korea (NRF) Grants NRF-2018R1A2A3075605 and NRF-2019R1A2C3005009 and by KIAS Individual Grant No. PG021403; RC from an individual research grant from the Swedish Research

Council (Dnr 2018-05029); RC and TE from the Knut and Alice Wallenberg project Light Dark Matter (Dnr KAW 2019.0080 and 2019.0080); PB and SS from the Dr Raja Ramanna Fellowship program of the Department of Atomic Energy (DAE), Government of India. RB acknowledges ISF and the Pazy foundation. Finally, RFL acknowledges support from the Purdue University Department of Physics and Astronomy and from the Purdue Research Foundation without which this paper could not have been realized.

Data availability statement

No new data were created or analysed in this study.

References

[1] Aalbers J *et al* (DARWIN) 2016 *J. Cosmol. Astropart. Phys.* JCAP11(2016)017
[2] Bertone G and Hooper D 2018 *Rev. Mod. Phys.* **90** 045002
[3] Kelvin L W T 1904 *Baltimore Lectures on Molecular Dynamics and the Wave Theory of Light* (London: C.J. Clay and Sons) https://books.google.com/books?id=qgA1AQAAMAAJ & printsec=frontcover & source=gbs_ge_summary_r & cad=0#v=onepage & q & f=false
[4] Poincaré H 1906 *Pop. Astron.* **14** 475
[5] Kapteyn J C 1922 *Astrophys. J.* **55** 302
[6] Jeans J H 1922 *Mon. Not. R. Astron. Soc.* **82** 122
[7] Oort J H 1932 *Bull. Astron. Inst. Neth.* **6** 249
[8] Zwicky F 1933 *Helv. Phys. Acta* **6** 110
Zwicky F 2009 *Gen. Relativ. Gravit.* **41** 207
[9] Rubin V C and Ford W K J Jr 1970 *Astrophys. J.* **159** 379
[10] Rubin V C, Thonnard N and Ford W K J Jr 1980 *Astrophys. J.* **238** 471
[11] Bosma A 1981 *Astron. J.* **86** 1825
[12] Persic M, Salucci P and Stel F 1996 *Mon. Not. R. Astron. Soc.* **281** 27
[13] Richards E E *et al* 2015 *Mon. Not. R. Astron. Soc.* **449** 3981
[14] Sofue Y and Rubin V 2001 *Annu. Rev. Astron. Astrophys.* **39** 137
[15] Foster T and Cooper B 2011 *ASP Conf. Ser.* **438** 16 arXiv:1009.3220
[16] Salucci P 2019 *Astron. Astrophys. Rev.* **27** 2
[17] Silk J and Mamon G A 2012 *Res. Astron. Astrophys.* **12** 917
[18] Read J I 2014 *J. Phys. G: Nucl. Part. Phys.* **41** 063101
[19] Lisanti M 2016 Theoretical advanced study institute in elementary particle physics: new Frontiers in fields and strings (arXiv:1603.03797)
[20] Kolb E W and Turner M S (ed) 1990 *The Early Universe* vol 69 (Boca Raton, FL: CRC Press)
[21] Akrami Y *et al* (Planck) 2020 *Astron. Astrophys.* **641** A1
[22] Aghanim N *et al* (Planck) 2020 *Astron. Astrophys.* **641** A6
[23] Kumar S, Nunes R C and Yadav S K 2018 *Phys. Rev.* D **98** 043521
[24] Springel V, Frenk C S and White S D M 2006 *Nature* **440** 1137
[25] Knobel C 2012 arXiv:1208.5931
[26] Coil A L 2012 arXiv:1202.6633
[27] Bartelmann M and Schneider P 2001 *Phys. Rep.* **340** 291
[28] Gilman D, Birrer S, Nierenberg A, Treu T, Du X and Benson A 2020 *Mon. Not. R. Astron. Soc.* **491** 6077
[29] Montes M and Trujillo I 2019 *Mon. Not. R. Astron. Soc.* **482** 2838
[30] Clowe D, Bradač M, Gonzalez A H, Markevitch M, Randall S W, Jones C and Zaritsky D 2006 *Astrophys. J. Lett.* **648** L109
[31] Wittman D, Golovich N and Dawson W A 2018 *Astrophys. J.* **869** 104
[32] Bertone G, Hooper D and Silk J 2005 *Phys. Rep.* **405** 279
[33] Buen-Abad M A, Essig R, McKeen D and Zhong Y-M 2022 *Phys. Rep.* **961** 1
[34] de Salas P F 2020 *J. Phys.: Conf. Ser.* **1468** 012020
[35] de Salas P F and Widmark A 2021 *Rep. Prog. Phys.* **84** 104901
[36] Nesti F and Salucci P 2013 *J. Cosmol. Astropart. Phys.* JCAP07(2013)016

[37] Brown A *et al* (Gaia) 2018 *Astron. Astrophys.* **616** A1
[38] de Salas P F, Malhan K, Freese K, Hattori K and Valluri M 2019 *J. Cosmol. Astropart. Phys.* JCAP10(2019)037
[39] Hagen J H J and Helmi A 2018 *Astron. Astrophys.* **615** A99
[40] Buch J, Leung S C J and Fan J 2019 *J. Cosmol. Astropart. Phys.* JCAP04(2019)026
[41] Widmark A 2019 *Astron. Astrophys.* **623** A30
[42] Wu Y, Freese K, Kelso C, Stengel P and Valluri M 2019 *J. Cosmol. Astropart. Phys.* JCAP10(2019)034
[43] Baxter D *et al* 2021 *Eur. Phys. J.* C **81** 907
[44] Tanabashi M *et al* (Particle Data Group) 2018 *Phys. Rev.* D **98** 030001
[45] Salucci P, Turini N and Di Paolo C 2020 *Universe* **6** 118
[46] Drukier A and Stodolsky L 1984 *Phys. Rev.* D **30** 2295
[47] Smith P F and Lewin J D 1983 *Phys. Lett.* B **127** 185
[48] Goodman M W and Witten E 1985 *Phys. Rev.* D **31** 3059
[49] Drukier A K, Freese K and Spergel D N 1986 *Phys. Rev.* D **33** 3495
[50] Schumann M 2019 *J. Phys. G: Nucl. Part. Phys.* **46** 103003
[51] Aalseth C E *et al* (CoGeNT) 2014 arXiv:1401.3295
[52] Agnese R *et al* (SuperCDMS) 2014 *Phys. Rev. Lett.* **112** 241302
[53] Armengaud E *et al* (EDELWEISS) 2016 *J. Cosmol. Astropart. Phys.* JCAP05(2016)019
[54] Shields E, Xu J and Calaprice F 2015 *Phys. Proc.* **61** 169
[55] Aguilar-Arevalo A *et al* (DAMIC) 2016 *Phys. Rev.* D **94** 082006
[56] Abdelhameed A H *et al* (CRESST) 2019 *Phys. Rev.* D **100** 102002
[57] Crisler M, Essig R, Estrada J, Fernandez G, Tiffenberg J, Sofo haro M, Volansky T and Yu T-T (SENSEI) 2018 *Phys. Rev. Lett.* **121** 061803
[58] Amaral D W *et al* (SuperCDMS) 2020 *Phys. Rev.* D **102** 091101
[59] Alkhatib I *et al* (SuperCDMS) 2021 *Phys. Rev. Lett.* **127** 061801
[60] Behnke E *et al* 2017 *Astropart. Phys.* **90** 85
[61] Szydagis M, Levy C, Huang Y, Kamaha A C, Knight C C, Rischbieter G R C and Wilson P W 2018 arXiv:1807.09253
[62] Aalseth C E *et al* 2018 *Eur. Phys. J. Plus* **133** 131
[63] Akerib D S *et al* (LUX) 2017 *Phys. Rev. Lett.* **118** 021303
[64] Aprile E *et al* (XENON) 2017 *Eur. Phys. J.* C **77** 881
[65] Cui X *et al* (PandaX-II) 2017 *Phys. Rev. Lett.* **119** 181302
[66] Kobayashi M *et al* (XMASS) 2019 *Phys. Lett.* B **795** 308
[67] Amole C *et al* (PICO) 2017 *Phys. Rev. Lett.* **118** 251301
[68] Freese K, Lisanti M and Savage C 2013 *Rev. Mod. Phys.* **85** 1561
[69] Copi C J and Krauss L M 2003 *Phys. Rev.* D **67** 103507
[70] Savage C, Freese K and Gondolo P 2006 *Phys. Rev.* D **74** 043531
[71] Lang R F and Weiner N 2010 *J. Cosmol. Astropart. Phys.* JCAP06(2010)032
[72] Kuhlen M, Weiner N, Diemand J, Madau P, Moore B, Potter D, Stadel J and Zemp M 2010 *J. Cosmol. Astropart. Phys.* JCAP02(2010)030
[73] Schneider A, Krauss L and Moore B 2010 *Phys. Rev.* D **82** 063525
[74] O'Hare C A J, Evans N W, McCabe C, Myeong G and Belokurov V 2020 *Phys. Rev.* D **101** 023006
[75] Ling F-S, Nezri E, Athanassoula E and Teyssier R 2010 *J. Cosmol. Astropart. Phys.* JCAP02(2010)012
[76] Damour T and Krauss L M 1999 *Phys. Rev.* D **59** 063509
[77] Krauss L M and Romanelli P 1989 *Phys. Rev.* D **39** 1225
[78] Bolozdynya A I 2010 *Emission Detectors* (Singapore: World Scientific)
[79] Suzuki S and Hitachi A 2010 *Charged Particle and Photon Interactions with Matter* ed Y Hatano, Y Katsumura and A Mozumder (Boca Raton, FL: CRC Press)
[80] Akimov D Y, Bolozdynya A I, Buzulutskov A F and Chepel V 2021 *Two-Phase Emission Detectors* (Singapore: World Scientific)
[81] Dolgoshein B A, Lebedenko V N and Rodionov B U 1970 *JETP Lett.* **11** 351 http://jetpletters.ru/ps/1724/article_26181.shtml
[82] Bolozdynya A, Egorov V, Rodionov B and Miroshnichenko V 1995 *IEEE Trans. Nucl. Sci.* **42** 565
[83] Cline D *et al* 2000 *Astropart. Phys.* **12** 373

[84] Aprile E *et al* 2002 Technique and Application of Xenon Detectors *Proc., Int. Workshop* (Kashiwa, Japan 3–4 December 2001) pp pp 165–78
[85] Alner G J *et al* (UK Dark Matter) 2005 *Astropart. Phys.* **23** 444
[86] Alner G J *et al* 2007 *Astropart. Phys.* **28** 287
[87] Lebedenko V N *et al* 2009 *Phys. Rev.* D **80** 052010
[88] Araujo H M *et al* 2012 *Astropart. Phys.* **35** 495
[89] Angle J *et al* (XENON) 2008 *Phys. Rev. Lett.* **100** 021303
[90] Yamashita M *et al* 2002 *Technique and Application of Xenon Detectors* (Singapore: World Scientific)
[91] Abe K *et al* (XMASS) 2019 *Phys. Lett.* B **789** 45
[92] Aprile E *et al* (XENON100) 2012 *Astropart. Phys.* **35** 573
[93] Aprile E *et al* (XENON100) 2012 *Phys. Rev. Lett.* **109** 181301
[94] Xiao M *et al* (PandaX) 2014 *Sci. China Phys. Mech. Astron.* **57** 2024
[95] Wang Q *et al* (PandaX-II) 2020 *Chin. Phys.* C **44** 125001
[96] Aprile E *et al* (XENON) 2018 *Phys. Rev. Lett.* **121** 111302
[97] Zhang H *et al* (PandaX) 2019 *Sci. China Phys. Mech. Astron.* **62** 31011
[98] Aprile E *et al* (XENON) 2020 *J. Cosmol. Astropart. Phys.* JCAP11(2020)031
[99] Akerib D S *et al* (LUX-ZEPLIN) 2020 *Phys. Rev.* D **101** 052002
[100] Schumann M, Baudis L, Bütikofer L, Kish A and Selvi M 2015 *J. Cosmol. Astropart. Phys.* JCAP10(2015)016
[101] Aprile E *et al* 2005 *Nucl. Phys. Proc. Suppl.* **138** 156
[102] Akerib D S *et al* 2013 *Nucl. Instrum. Methods Phys. Res.* A **703** 1
[103] Aprile E *et al* (XENON) 2015 *Eur. Phys. J.* C **75** 546
[104] Aprile E, Cushman P, Ni K and Shagin P 2006 *Nucl. Instrum. Methods Phys. Res.* A **556** 215
[105] Baudis L, Biondi Y, Galloway M, Girard F, Hochrein S, Reichard S, Sanchez-Lucas P, Thieme K and Wulf J 2020 *Eur. Phys. J.* C **80** 477
[106] Lansiart A, Seigneur A, Moretti J-L and Morucci J-P 1976 *Nucl. Instrum. Methods* **135** 47
[107] Yamashita M, Doke T, Kikuchi J and Suzuki S 2003 *Astropart. Phys.* **20** 79
[108] Mount B J *et al* 2017 arXiv:1703.09144
[109] Zhang D *et al* (PandaX) 2021 *J. Inst.* **16** P11040
[110] Liang S, Higuera A, Peters C, Roy V, Bajwa W U, Shatkay H and Tunnell C D 2021 arXiv:2112.07995
[111] Akerib D S *et al* (LUX) 2018 *J. Inst.* **13** P02001
[112] Angle J *et al* (XENON) 2007 *Nucl. Phys. Proc. Suppl.* **173** 117
Angle J *et al* (XENON) 2008 *Nucl. Phys. Proc. Suppl.* **175** E3 (erratum)
[113] Aprile E (XENON) 2005 arXiv:astro-ph/0502279
[114] Akerib D S *et al* (LUX) 2020 *Phys. Rev.* D **102** 112002
[115] Aprile E *et al* 2006 *Phys. Rev. Lett.* **97** 081302
[116] Aprile E *et al* (XENON) 2020 *Eur. Phys. J.* C **80** 785
[117] Doke T, Hitachi A, Kikuchi J, Masuda K, Okada H and Shibamura E 2002 *Japan. J. Appl. Phys.* **41** 1538
[118] Aprile E, Bolotnikov A E, Bolozdynya A L and Doke T 2008 *Noble Gas Detectors* (New York: Wiley)
[119] Baudis L, Sanchez-Lucas P and Thieme K 2021 *Eur. Phys. J.* C **81** 1060
[120] Chepel V and Araújo H 2013 *J. Inst.* **8** R04001
[121] Lenardo B, Kazkaz K, Manalaysay A, Mock J, Szydagis M and Tripathi M 2015 *IEEE Trans. Nucl. Sci.* **62** 3387
[122] Aprile E *et al* 2018 *Phys. Rev.* D **98** 112003
[123] Yan B *et al* (PandaX-II) 2021 *Chin. Phys.* C **45** 075001
[124] Solovov V N *et al* 2012 *IEEE Trans. Nucl. Sci.* **59** 3286
[125] Aprile E *et al* (XENON100) 2014 *Astropart. Phys.* **54** 11
[126] Szydagis M *et al* 2011 *J. Inst.* **6** P10002
[127] Szydagis M, Fyhrie A, Thorngren D and Tripathi M 2013 *J. Inst.* **8** C10003
[128] Szydagis M *et al* (NEST Collaboration) 2022 Noble element simulation technique v2.3.5 zenodo:6028483 https://zenodo.org/record/6028483
[129] Sorensen P *et al* (XENON10) 2009 *Nucl. Instrum. Methods Phys. Res.* A **601** 339
[130] Dahl C E 2009 *PhD Thesis* Princeton University https://princeton.edu/physics/graduate-program/theses/theses-from-2009/E.Dahlthesis.pdf

[131] Bezrukov F, Kahlhoefer F, Lindner M, Kahlhoefer F and Lindner M 2011 *Astropart. Phys.* **35** 119
[132] Sorensen P 2010 *J. Cosmol. Astropart. Phys.* JCAP09(2010)033
[133] Mu W, Xiong X and Ji X 2015 *Astropart. Phys.* **61** 56
Mu W, Xiong X and Ji X 2016 *Astropart. Phys.* **72** 109 (corrigendum)
[134] Mu W and Ji X 2015 *Astropart. Phys.* **62** 108
[135] Wang L and Mei D-M 2017 *J. Phys. G: Nucl. Part. Phys.* **44** 055001
[136] Abe K *et al* (XMASS) 2009 *Astropart. Phys.* **31** 290
[137] Aprile E *et al* (XENON100) 2016 *Phys. Rev.* D **94** 122001
[138] Albert J B *et al* (EXO-200) 2014 *Nature* **510** 229
[139] Aalbers J *et al* (LUX-ZEPLIN) 2022 *Phys. Rev.* D **105** 082004
[140] Jungman G, Kamionkowski M and Griest K 1996 *Phys. Rep.* **267** 195
[141] Gelmini G and Gondolo P 2010 arXiv:1009.3690
[142] Arcadi G, Dutra M, Ghosh P, Lindner M, Mambrini Y, Pierre M, Profumo S and Queiroz F S 2018 *Eur. Phys. J.* C **78** 203
[143] Witten E 1981 *Nucl. Phys.* B **188** 513
[144] Bertone G (ed) 2010 *Particle Dark Matter: Observations, Models and Searches* (Cambridge: Cambridge University Press)
[145] Steigman G, Dasgupta B and Beacom J F 2012 *Phys. Rev.* D **86** 023506
[146] Kolb E W and Olive K A 1986 *Phys. Rev.* D **33** 1202
Kolb E W and Olive K A 1986 *Phys. Rev.* D **34** 2531 (erratum)
[147] Balázs C, Li T and Newstead J L 2014 *J. High Energy Phys.* JHEP08(2014)061
[148] Roszkowski L, Sessolo E M and Trojanowski S 2018 *Rep. Prog. Phys.* **81** 066201
[149] Kahlhoefer F 2017 *Int. J. Mod. Phys.* A **32** 1730006
[150] Gaskins J M 2016 *Contemp. Phys.* **57** 496
[151] Undagoitia T M and Rauch L 2016 *J. Phys. G: Nucl. Part. Phys.* **43** 013001
[152] Ahlen S P, Avignone F T, Brodzinski R L, Drukier A K, Gelmini G and Spergel D N 1987 *Phys. Lett.* B **195** 603
[153] Ong R A (CTA) 2018 *Proc. Sci.* **301** 1071
[154] Arduini G *et al* 2016 *J. Inst.* **11** C12081
[155] Smith P F and Lewin J D 1985 *Acta Phys. Pol.* B **16** 837
[156] Bramante J, Broerman B, Lang R F and Raj N 2018 *Phys. Rev.* D **98** 083516
[157] Newstead J L, Jacques T D, Krauss L M, Dent J B and Ferrer F 2013 *Phys. Rev.* D **88** 076011
[158] Akerib D S *et al* (LUX) 2018 *Phys. Rev.* D **97** 102008
[159] Aprile E *et al* (XENON) 2019 *Phys. Rev.* D **100** 052014
[160] Wilks S S 1938 *Ann. Math. Stat.* **9** 60
[161] Akerib D S *et al* (LUX) 2020 *J. Inst.* **15** T02007
[162] Kotila J and Iachello F 2012 *Phys. Rev.* C **85** 034316 https://nuclear theory.yale.edu/double-beta-decay-phase-space-factors
[163] Chen J-W, Chi H-C, Liu C-P and Wu C-P 2017 *Phys. Lett.* B **774** 656
[164] Billard J, Strigari L and Figueroa-Feliciano E 2014 *Phys. Rev.* D **89** 023524
[165] Newstead J L, Lang R F and Strigari L E 2021 *Phys. Rev.* D **104** 115022
[166] Aalbers J, Pelssers B and Morå K D 2019 wimprates: v0.3.0 https://doi.org/10.5281/zenodo.3345959
[167] Lewin J D and Smith P F 1996 *Astropart. Phys.* **6** 87
[168] Klos P, Menéndez J, Gazit D and Schwenk A 2013 *Phys. Rev.* D **88** 083516
Klos P, Menéndez J, Gazit D and Schwenk A 2014 *Phys. Rev.* D **89** 029901 (erratum)
[169] Aprile E *et al* (XENON) 2019 *Phys. Rev. Lett.* **122** 071301
[170] Hoferichter M, Klos P, Menéndez J and Schwenk A 2019 *Phys. Rev.* D **99** 055031
[171] Billard J, Strigari L E and Figueroa-Feliciano E 2015 *Phys. Rev.* D **91** 095023
[172] O'Hare C A J 2016 *Phys. Rev.* D **94** 063527
[173] Meng Y *et al* (PandaX-4T) 2021 *Phys. Rev. Lett.* **127** 261802
[174] Monroe J and Fisher P 2007 *Phys. Rev.* D **76** 033007
[175] Feng L, Profumo S and Ubaldi L 2015 *J. High Energy Phys.* JHEP03(2015)045
[176] Pato M, Baudis L, Bertone G, Ruiz de Austri R, Strigari L E and Trotta R 2011 *Phys. Rev.* D **83** 083505
[177] Kamionkowski M, Krauss L M and Ressell M T 1994 arXiv:hep-ph/9402353

[178] Chang S, Liu J, Pierce A, Weiner N and Yavin I 2010 *J. Cosmol. Astropart. Phys.* JCAP08(2010)018
[179] Feng J L, Kumar J, Marfatia D and Sanford D 2011 *Phys. Lett.* B **703** 124
[180] Frandsen M T, Kahlhoefer F, March-Russell J, McCabe C, McCullough M and Schmidt-Hoberg K 2011 *Phys. Rev.* D **84** 041301
[181] Aprile E *et al* (XENON) 2019 *Phys. Rev. Lett.* **123** 251801
[182] Iachello F, Krauss L M and Maino G 1991 *Phys. Lett.* B **254** 220
[183] Engel J, Pittel S and Vogel P 1992 *Int. J. Mod. Phys.* E **1** 1
[184] Tovey D R, Gaitskell R J, Gondolo P, Ramachers Y and Roszkowski L 2000 *Phys. Lett.* B **488** 17
[185] Fan J, Reece M and Wang L-T 2010 *J. Cosmol. Astropart. Phys.* JCAP11(2010)042
[186] Fitzpatrick A L, Haxton W, Katz E, Lubbers N and Xu Y 2013 *J. Cosmol. Astropart. Phys.* JCAP02(2013)004
[187] Anand N, Fitzpatrick A L and Haxton W C 2014 *Phys. Rev.* C **89** 065501
[188] Schneck K *et al* (SuperCDMS) 2015 *Phys. Rev.* D **91** 092004
[189] Aprile E *et al* (XENON) 2017 *Phys. Rev.* D **96** 042004
[190] Xia J *et al* (PandaX-II) 2019 *Phys. Lett.* B **792** 193
[191] Angloher G *et al* (CRESST) 2019 *Eur. Phys. J.* C **79** 43
[192] Dent J B, Krauss L M, Newstead J L and Sabharwal S 2015 *Phys. Rev.* D **92** 063515
[193] Catena R, Fridell K and Krauss M B 2019 *J. High Energy Phys.* JHEP08(2019)030
[194] Gondolo P, Kang S, Scopel S and Tomar G 2021 *Phys. Rev.* D **104** 063017
[195] Krauss L M and Newstead J L 2018 arXiv:1801.08523
[196] Epelbaum E, Hammer H-W and Meißner U-G 2009 *Rev. Mod. Phys.* **81** 1773
[197] Machleidt R and Entem D R 2011 *Phys. Rep.* **503** 1
[198] Hammer H-W, Nogga A and Schwenk A 2013 *Rev. Mod. Phys.* **85** 197
[199] Hoferichter M, Klos P and Schwenk A 2015 *Phys. Lett.* B **746** 410
[200] Bishara F, Brod J, Grinstein B and Zupan J 2017 *J. Cosmol. Astropart. Phys.* JCAP02(2017)009
[201] Bishara F, Brod J, Grinstein B and Zupan J 2017 *J. High Energy Phys.* JHEP11(2017)059
[202] Prézeau G, Kurylov A, Kamionkowski M and Vogel P 2003 *Phys. Rev. Lett.* **91** 231301
[203] Cirigliano V, Graesser M L and Ovanesyan G 2012 *J. High Energy Phys.* JHEP10(2012)025
[204] Menéndez J, Gazit D and Schwenk A 2012 *Phys. Rev.* D **86** 103511
[205] Cirigliano V, Graesser M L, Ovanesyan G and Shoemaker I M 2014 *Phys. Lett.* B **739** 293
[206] Hoferichter M, Klos P, Menéndez J and Schwenk A 2016 *Phys. Rev.* D **94** 063505
[207] Körber C, Nogga A and de Vries J 2017 *Phys. Rev.* C **96** 035805
[208] Hoferichter M, Klos P, Menéndez J and Schwenk A 2017 *Phys. Rev. Lett.* **119** 181803
[209] Andreoli L, Cirigliano V, Gandolfi S and Pederiva F 2019 *Phys. Rev.* C **99** 025501
[210] Hu B S, Padua-Argüelles J, Leutheusser S, Miyagi T, Stroberg S R and Holt J D 2022 *Phys. Rev. Lett.* **128** 072502
[211] Goodman J, Ibe M, Rajaraman A, Shepherd W, Tait T M P and Yu H-B 2011 *Phys. Lett.* B **695** 185
[212] Goodman J, Ibe M, Rajaraman A, Shepherd W, Tait T M P and Yu H-B 2010 *Phys. Rev.* D **82** 116010
[213] Fox P J, Harnik R, Kopp J and Tsai Y 2012 *Phys. Rev.* D **85** 056011
[214] Crivellin A, D'Eramo F and Procura M 2014 *Phys. Rev. Lett.* **112** 191304
[215] D'Eramo F and Procura M 2015 *J. High Energy Phys.* JHEP04(2015)054
[216] Hill R J and Solon M P 2015 *Phys. Rev.* D **91** 043505
[217] Hill R J and Solon M P 2015 *Phys. Rev.* D **91** 043504
[218] Bishara F, Brod J, Grinstein B and Zupan J 2017 arXiv:1708.02678
[219] Brod J, Gootjes-Dreesbach A, Tammaro M and Zupan J 2018 *J. High Energy Phys.* JHEP10(2018)065
[220] Hill R J and Solon M P 2012 *Phys. Lett.* B **707** 539
[221] Chen Q and Hill R J 2020 *Phys. Lett.* B **804** 135364
[222] Brod J, Grinstein B, Stamou E and Zupan J 2018 *J. High Energy Phys.* JHEP02(2018)174
[223] Bishara F, Brod J, Grinstein B and Zupan J 2020 *J. High Energy Phys.* JHEP03(2020)089
[224] Crivellin A and Haisch U 2014 *Phys. Rev.* D **90** 115011
[225] Serot B D 1978 *Nucl. Phys.* A **308** 457
[226] Donnelly T W and Haxton W C 1979 *At. Data Nucl. Data Tables* **23** 103
[227] Serot B D 1979 *Nucl. Phys.* A **322** 408

[228] Bottino A, Donato F, Fornengo N and Scopel S 2000 *Astropart. Phys.* **13** 215
[229] Bottino A, Donato F, Fornengo N and Scopel S 2002 *Astropart. Phys.* **18** 205
[230] Ellis J R, Olive K A and Savage C 2008 *Phys. Rev.* D **77** 065026
[231] Crivellin A, Hoferichter M and Procura M 2014 *Phys. Rev.* D **89** 054021
[232] Hoferichter M, Ruiz de Elvira J, Kubis B and Meißner U-G 2015 *Phys. Rev. Lett.* **115** 092301
[233] Gupta R, Park S, Hoferichter M, Mereghetti E, Yoon B and Bhattacharya T 2021 *Phys. Rev. Lett.* **127** 242002
[234] Helm R H 1956 *Phys. Rev.* **104** 1466
[235] Vietze L, Klos P, Menéndez J, Haxton W C and Schwenk A 2015 *Phys. Rev.* D **91** 043520
[236] Caurier E, Martínez-Pinedo G, Nowacki F, Poves A and Zuker A P 2005 *Rev. Mod. Phys.* **77** 427
[237] Kamada H *et al* 2001 *Phys. Rev.* C **64** 044001
[238] Carlson J, Gandolfi S, Pederiva F, Pieper S C, Schiavilla R, Schmidt K E and Wiringa R B 2015 *Rev. Mod. Phys.* **87** 1067
[239] Navrátil P, Quaglioni S, Hupin G, Romero-Redondo C and Calci A 2016 *Phys. Scr.* **91** 053002
[240] Hagen G, Papenbrock T, Hjorth-Jensen M and Dean D J 2014 *Rep. Prog. Phys.* **77** 096302
[241] Hergert H, Bogner S K, Morris T D, Schwenk A and Tsukiyama K 2016 *Phys. Rep.* **621** 165
[242] Stroberg S R, Hergert H, Bogner S K and Holt J D 2019 *Annu. Rev. Nucl. Part. Sci.* **69** 307
[243] Gazda D, Catena R and Forssén C 2017 *Phys. Rev.* D **95** 103011
[244] Ellis J, Flores R A and Lewin J D 1988 *Phys. Lett.* B **212** 375
[245] Baudis L, Kessler G, Klos P, Lang R F, Menéndez J, Reichard S and Schwenk A 2013 *Phys. Rev.* D **88** 115014
[246] Aprile E *et al* (XENON) 2017 *Phys. Rev.* D **96** 022008
[247] Aprile E *et al* (XENON) 2021 *Phys. Rev.* D **103** 063028
[248] Suzuki T *et al* (XMASS) 2019 *Astropart. Phys.* **110** 1
[249] McCabe C 2016 *J. Cosmol. Astropart. Phys.* JCAP05(2016)033
[250] Fieguth A, Hoferichter M, Klos P, Menéndez J, Schwenk A and Weinheimer C 2018 *Phys. Rev.* D **97** 103532
[251] Rogers H, Cerdeño D G, Cushman P, Livet F and Mandic V 2017 *Phys. Rev.* D **95** 082003
[252] Tucker-Smith D and Weiner N 2001 *Phys. Rev.* D **64** 043502
[253] Graham P W, Harnik R, Rajendran S and Saraswat P 2010 *Phys. Rev.* D **82** 063512
[254] Dienes K R, Kumar J, Thomas B and Yaylali D 2015 *Phys. Rev. Lett.* **114** 051301
[255] Hardy E, Lasenby R, March-Russell J and West S M 2015 *J. High Energy Phys.* JHEP07(2015)133
[256] Bramante J, Fox P J, Kribs G D and Martin A 2016 *Phys. Rev.* D **94** 115026
[257] Gluscevic V, Gresham M I, McDermott S D, Peter A H G and Zurek K M 2015 *J. Cosmol. Astropart. Phys.* JCAP12(2015)057
[258] Gelmini G B, Takhistov V and Witte S J 2018 *J. Cosmol. Astropart. Phys.* JCAP07(2018)009
[259] Bozorgnia N, Cerdeño D G, Cheek A and Penning B 2018 *J. Cosmol. Astropart. Phys.* JCAP12(2018)013
[260] Freese K, Gondolo P and Newberg H J 2005 *Phys. Rev.* D **71** 043516
[261] Helmi A 2004 *Astrophys. J. Lett.* **610** L97
[262] Vogelsberger M, White S D M, Helmi A and Springel V 2008 *Mon. Not. R. Astron. Soc.* **385** 236
[263] Purcell C W, Zentner A R and Wang M-Y 2012 *J. Cosmol. Astropart. Phys.* JCAP08(2012)027
[264] Buckley M R, Mohlabeng G and Murphy C W 2019 *Phys. Rev.* D **100** 055039
[265] McCabe C 2010 *Phys. Rev.* D **82** 023530
[266] O'Hare C A J, McCabe C, Evans N W, Myeong G and Belokurov V 2018 *Phys. Rev.* D **98** 103006
[267] Adhikari P *et al* (DEAP) 2020 *Phys. Rev.* D **102** 082001
[268] Bertone G, Cerdeño D G, Collar J I and Odom B 2007 *Phys. Rev. Lett.* **99** 151301
[269] Cerdeño D G *et al* 2013 *J. Cosmol. Astropart. Phys.* JCAP07(2013)028
Cerdeño D G *et al* 2013 *J. Cosmol. Astropart. Phys.* JCAP09(2013)E01 (erratum)
[270] Peter A H G, Gluscevic V, Green A M, Kavanagh B J and Lee S K 2014 *Phys. Dark Universe* **5–6** 45
[271] Edwards T D P, Kavanagh B J and Weniger C 2018 *Phys. Rev. Lett.* **121** 181101
[272] Hisano J, Nagai R and Nagata N 2015 *J. High Energy Phys.* JHEP05(2015)037
[273] De Simone A and Jacques T 2016 *Eur. Phys. J.* C **76** 367
[274] Abdallah J *et al* 2015 *Phys. Dark Universe* **9–10** 8
[275] DiFranzo A, Nagao K I, Rajaraman A and Tait T M 2013 *J. High Energy Phys.* JHEP11(2013)014

DiFranzo A, Nagao K I, Rajaraman A and Tait T M P 2014 *J. High Energy Phys.* JHEP01(2014)162 (erratum)
[276] Abercrombie D *et al* 2020 *Phys. Dark Universe* **27** 100371
[277] Arina C, Del Nobile E and Panci P 2015 *Phys. Rev. Lett.* **114** 011301
[278] Hisano J, Nagai R and Nagata N 2018 *J. High Energy Phys.* JHEP12(2018)059
[279] Balázs C, Conrad J, Farmer B, Jacques T, Li T, Meyer M, Queiroz F S and Sánchez-Conde M A 2017 *Phys. Rev.* D **96** 083002
[280] Jacques T, Katz A, Morgante E, Racco D, Rameez M and Riotto A 2016 *J. High Energy Phys.* JHEP10(2016)071
Jacques T, Katz A, Morgante E, Racco D, Rameez M and Riotto A 2019 *J. High Energy Phys.* JHEP01(2019)127 (erratum)
[281] Buckley M R, Feld D and Goncalves D 2015 *Phys. Rev.* D **91** 015017
[282] Berlin A, Hooper D and McDermott S D 2014 *Phys. Rev.* D **89** 115022
[283] Blanco C, Escudero M, Hooper D and Witte S J 2019 *J. Cosmol. Astropart. Phys.* JCAP11(2019)024
[284] Baek S, Ko P and Li J 2017 *Phys. Rev.* D **95** 075011
[285] Drees M and Nojiri M M 1993 *Phys. Rev.* D **48** 3483
[286] Hisano J, Ishiwata K and Nagata N 2010 *Phys. Rev.* D **82** 115007
[287] Baek S, Ko P and Wu P 2016 *J. High Energy Phys.* JHEP10(2016)117
[288] Baek S, Ko P and Wu P 2018 *J. Cosmol. Astropart. Phys.* JCAP07(2018)008
[289] Arcadi G, Lindner M, Queiroz F S, Rodejohann W and Vogl S 2018 *J. Cosmol. Astropart. Phys.* JCAP03(2018)042
[290] Li T 2018 *Phys. Lett.* B **782** 497
[291] Abe T, Fujiwara M and Hisano J 2019 *J. High Energy Phys.* JHEP02(2019)028
[292] Li T and Wu P 2019 *Chin. Phys.* C **43** 113102
[293] Mohan K A, Sengupta D, Tait T M P, Yan B and Yuan C-P 2019 *J. High Energy Phys.* JHEP05(2019)115
[294] Ertas F and Kahlhoefer F 2019 *J. High Energy Phys.* JHEP06(2019)052
[295] Giacchino F, Ibarra A, Honorez L L, Tytgat M H G and Wild S 2016 *J. Cosmol. Astropart. Phys.* JCAP02(2016)002
[296] Giacchino F, Lopez-Honorez L and Tytgat M H G 2014 *J. Cosmol. Astropart. Phys.* JCAP08(2014)046
[297] Ibarra A, Toma T, Totzauer M and Wild S 2014 *Phys. Rev.* D **90** 043526
[298] Ko P, Natale A, Park M and Yokoya H 2017 *J. High Energy Phys.* JHEP01(2017)086
[299] Colucci S, Fuks B, Giacchino F, Lopez Honorez L, Tytgat M H and Vandecasteele J 2018 *Phys. Rev.* D **98** 035002
[300] Colucci S, Giacchino F, Tytgat M H G and Vandecasteele J 2018 *Phys. Rev.* D **98** 115029
[301] Chao W 2019 *J. High Energy Phys.* JHEP11(2019)013
[302] LaFontaine C *et al* 2021 *Universe* **7** 270
[303] Belyaev A, Cacciapaglia G, Locke D and Pukhov A 2022 arXiv:2203.03660
[304] Cirelli M, Fornengo N and Strumia A 2006 *Nucl. Phys.* B **753** 178
[305] Cirelli M and Strumia A 2009 *New J. Phys.* **11** 105005
[306] Di Luzio L, Gröber R and Panico G 2019 *J. High Energy Phys.* JHEP01(2019)011
[307] Abdussalam S, Kazemi M J and Kalhor L 2021 *Int. J. Mod. Phys.* A **36** 2150024
[308] Thomas S and Wells J D 1998 *Phys. Rev. Lett.* **81** 34
[309] Buckley M R, Randall L and Shuve B 2011 *J. High Energy Phys.* JHEP05(2011)097
[310] Ibe M, Matsumoto S and Sato R 2013 *Phys. Lett.* B **721** 252
[311] Bottaro S, Buttazzo D, Costa M, Franceschini R, Panci P, Redigolo D and Vittorio L 2022 *Eur. Phys. J.* C **82** 31
[312] Di Luzio L, Gröber R, Kamenik J F and Nardecchia M 2015 *J. High Energy Phys.* JHEP07(2015)074
[313] Pelaggi G M, Plascencia A D, Salvio A, Sannino F, Smirnov J and Strumia A 2018 *Phys. Rev.* D **97** 095013
[314] Smirnov J and Beacom J F 2019 *Phys. Rev.* D **100** 043029
[315] Belotsky K M, Khlopov M, Legonkov S and Shibaev K 2005 *Grav. Cosmol.* **11** 27 arXiv:astro-ph/0504621
[316] Hisano J, Matsumot S, Nagai M, Saito O and Senami M 2007 *Phys. Lett.* B **646** 34
[317] Cirelli M, Strumia A and Tamburini M 2007 *Nucl. Phys.* B **787** 152

[318] March-Russell J, West S M, Cumberbatch D and Hooper D 2008 *J. High Energy Phys.* JHEP07(2008)058
[319] Arkani-Hamed N, Finkbeiner D P, Slatyer T R and Weiner N 2009 *Phys. Rev.* D **79** 015014
[320] Cassel S 2010 *J. Phys. G: Nucl. Part. Phys.* **37** 105009
[321] March-Russell J and West S M 2009 *Phys. Lett.* B **676** 133
[322] von Harling B and Petraki K 2014 *J. Cosmol. Astropart. Phys.* JCAP12(2014)033
[323] An H, Wise M B and Zhang Y 2016 *Phys. Rev.* D **93** 115020
[324] Mitridate A, Redi M, Smirnov J and Strumia A 2017 *J. Cosmol. Astropart. Phys.* JCAP05(2017)006
[325] Binder T, Filimonova A, Petraki K and White G 2021 arXiv:2112.00042
[326] Nobile E D, Nardecchia M and Panci P 2016 *J. Cosmol. Astropart. Phys.* JCAP04(2016)048
[327] Low M and Wang L-T 2014 *J. High Energy Phys.* JHEP08(2014)161
[328] Cirelli M, Sala F and Taoso M 2014 *J. High Energy Phys.* JHEP10(2014)033
Cirelli M, Sala F and Taoso M 2015 *J. High Energy Phys.* JHEP01(2015)041 (erratum)
[329] Han T, Mukhopadhyay S and Wang X 2018 *Phys. Rev.* D **98** 035026
[330] Cid Vidal X *et al* 2019 *CERN Yellow Rep. Monogr.* **7** 585 arXiv:1812.07831
[331] Ellis R K *et al* 2019 arXiv:1910.11775
[332] Han T, Liu Z, Wang L-T and Wang X 2021 *Phys. Rev.* D **103** 075004
[333] Capdevilla R, Meloni F, Simoniello R and Zurita J 2021 *J. High Energy Phys.* JHEP06(2021)133
[334] Hisano J, Ishiwata K and Nagata N 2015 *J. High Energy Phys.* JHEP06(2015)097
[335] Hill R J and Solon M P 2014 *Phys. Rev. Lett.* **112** 211602
[336] He X-G and Tandean J 2016 *J. High Energy Phys.* JHEP12(2016)074
[337] Thornberry R, Throm M, Frohaug G, Killough J, Blend D, Erickson M, Sun B, Bays B and Allen R E 2021 *Europhys. Lett.* **134** 49001
[338] Akerib D S *et al* (LZ) 2015 arXiv:1509.02910
[339] AbdusSalam S S, Burgess C P and Quevedo F 2015 *J. High Energy Phys.* JHEP02(2015)073
[340] Abdussalam S, Barzani S S and Noormandipour M 2021 *Int. J. Mod. Phys.* A **36** 2150188
[341] Martin S P 1998 *Adv. Ser. Direct. High Energy Phys.* **18** 1
[342] Arkani-Hamed N, Delgado A and Giudice G F 2006 *Nucl. Phys.* B **741** 108
[343] Cheung C, Hall L J, Pinner D and Ruderman J T 2013 *J. High Energy Phys.* JHEP05(2013)100
[344] Huang P and Wagner C E M 2014 *Phys. Rev.* D **90** 015018
[345] Huang P, Roglans R A, Spiegel D D, Sun Y and Wagner C E M 2017 *Phys. Rev.* D **95** 095021
[346] Baum S, Carena M, Shah N R and Wagner C E M 2018 *J. High Energy Phys.* JHEP04(2018)069
[347] Cabrera M E, Casas J A, Delgado A and Robles S 2020 *J. High Energy Phys.* JHEP02(2020)166
[348] Han T, Liu H, Mukhopadhyay S and Wang X 2019 *J. High Energy Phys.* JHEP03(2019)080
[349] Carena M, Osborne J, Shah N R and Wagner C E M 2018 *Phys. Rev.* D **98** 115010
[350] Cao J, Meng L, Yue Y, Zhou H and Zhu P 2020 *Phys. Rev.* D **101** 075003
[351] Wang K, Zhu J and Jie Q 2021 *Chin. Phys.* C **45** 041003
[352] Hisano J, Ishiwata K, Nagata N and Takesako T 2011 *J. High Energy Phys.* JHEP07(2011)005
[353] Cohen T, Lisanti M, Pierce A and Slatyer T R 2013 *J. Cosmol. Astropart. Phys.* JCAP10(2013)061
[354] Fan J and Reece M 2013 *J. High Energy Phys.* JHEP10(2013)124
[355] Ackermann M *et al* (Fermi-LAT) 2014 *Phys. Rev.* D **89** 042001
[356] Bhattacherjee B, Ibe M, Ichikawa K, Matsumoto S and Nishiyama K 2014 *J. High Energy Phys.* JHEP07(2014)080
[357] Baer H, Lessa A, Rajagopalan S and Sreethawong W 2011 *J. Cosmol. Astropart. Phys.* JCAP06(2011)031
[358] Zurek K M 2009 *Phys. Rev.* D **79** 115002
[359] Profumo S, Sigurdson K and Ubaldi L 2009 *J. Cosmol. Astropart. Phys.* JCAP12(2009)016
[360] Kajiyama Y, Okada H and Toma T 2013 *Phys. Rev.* D **88** 015029
[361] Herrero-Garcia J, Scaffidi A, White M and Williams A G 2017 *J. Cosmol. Astropart. Phys.* JCAP11(2017)021
[362] Herrero-Garcia J, Scaffidi A, White M and Williams A G 2019 *J. Cosmol. Astropart. Phys.* JCAP01(2019)008
[363] Scaffidi A 2020 *EPJ Web Conf.* **245** 06036
[364] Bernabei R *et al* (DAMA) 2008 *Nucl. Instrum. Methods Phys. Res.* A **592** 297
[365] Bernabei R *et al* (DAMA, LIBRA) 2010 *Eur. Phys. J.* C **67** 39
[366] Bernabei R *et al* 2018 *Nucl. Phys. At. Energy* **19** 307

[367] Ullio P, Kamionkowski M and Vogel P 2001 *J. High Energy Phys.* JHEP07(2001)044
[368] Tucker-Smith D and Weiner N 2005 *Phys. Rev.* D **72** 063509
[369] Chang S, Kribs G D, Tucker-Smith D and Weiner N 2009 *Phys. Rev.* D **79** 043513
[370] Cui Y, Morrissey D E, Poland D and Randall L 2009 *J. High Energy Phys.* JHEP05(2009)076
[371] Aprile E *et al* (XENON100) 2011 *Phys. Rev.* D **84** 061101
[372] Chang S, Lang R F and Weiner N 2011 *Phys. Rev. Lett.* **106** 011301
[373] March-Russell J, McCabe C and McCullough M 2009 *J. High Energy Phys.* JHEP05(2009)071
[374] Smirnov J and Beacom J F 2020 *Phys. Rev. Lett.* **125** 131301
[375] Barello G, Chang S and Newby C A 2014 *Phys. Rev.* D **90** 094027
[376] Chen X *et al* (PandaX-II) 2017 *Phys. Rev.* D **96** 102007
[377] Akerib D S *et al* (LUX) 2021 *Phys. Rev.* D **104** 062005
[378] Nobile E D, Kaplinghat M and Yu H-B 2015 *J. Cosmol. Astropart. Phys.* JCAP10(2015)055
[379] Spergel D N and Steinhardt P J 2000 *Phys. Rev. Lett.* **84** 3760
[380] Kaplinghat M, Tulin S and Yu H-B 2016 *Phys. Rev. Lett.* **116** 041302
[381] Tulin S and Yu H-B 2018 *Phys. Rep.* **730** 1
[382] Kaplinghat M, Keeley R E, Linden T and Yu H-B 2014 *Phys. Rev. Lett.* **113** 021302
[383] Kamada A, Kaplinghat M, Pace A B and Yu H-B 2017 *Phys. Rev. Lett.* **119** 111102
[384] Creasey P, Sameie O, Sales L V, Yu H-B, Vogelsberger M and Zavala J 2017 *Mon. Not. R. Astron. Soc.* **468** 2283
[385] Ren T, Kwa A, Kaplinghat M and Yu H-B 2019 *Phys. Rev.* X **9** 031020
[386] Feng J L, Kaplinghat M and Yu H-B 2010 *Phys. Rev. Lett.* **104** 151301
[387] Buckley M R and Fox P J 2010 *Phys. Rev.* D **81** 083522
[388] Loeb A and Weiner N 2011 *Phys. Rev. Lett.* **106** 171302
[389] March-Russell J and McCullough M 2012 *J. Cosmol. Astropart. Phys.* JCAP03(2012)019
[390] van den Aarssen L G, Bringmann T and Pfrommer C 2012 *Phys. Rev. Lett.* **109** 231301
[391] Tulin S, Yu H-B and Zurek K M 2013 *Phys. Rev.* D **87** 115007
[392] Baek S, Ko P and Park W-I 2014 *J. Cosmol. Astropart. Phys.* JCAP10(2014)067
[393] Ko P and Tang Y 2014 *J. Cosmol. Astropart. Phys.* JCAP05(2014)047
[394] Ko P and Tang Y 2014 *Phys. Lett.* B **739** 62
[395] García García I, Lasenby R and March-Russell J 2015 *Phys. Rev. Lett.* **115** 121801
[396] Kahlhoefer F, Schmidt-Hoberg K and Wild S 2017 *J. Cosmol. Astropart. Phys.* JCAP08(2017)003
[397] Chu X, Garcia-Cely C and Murayama H 2020 *Phys. Rev. Lett.* **124** 041101
[398] Kaplinghat M, Tulin S and Yu H-B 2014 *Phys. Rev.* D **89** 035009
[399] Kahlhoefer F, Kulkarni S and Wild S 2017 *J. Cosmol. Astropart. Phys.* JCAP11(2017)016
[400] Ren X *et al* (PandaX-II) 2018 *Phys. Rev. Lett.* **121** 021304
[401] Yang J *et al* (PandaX-II) 2021 *Sci. China Phys. Mech. Astron.* **64** 111062
[402] Tsai Y-D, McGehee R and Murayama H 2020 arXiv:2008.08608
[403] Adriani O *et al* (PAMELA) 2013 *Phys. Rev. Lett.* **111** 081102
[404] Aguilar M *et al* (AMS) 2019 *Phys. Rev. Lett.* **122** 041102
[405] Knödlseder J *et al* 2005 *Astron. Astrophys.* **441** 513
[406] Ambrosi G *et al* (DAMPE) 2017 *Nature* **552** 63
[407] Fox P J and Poppitz E 2009 *Phys. Rev.* D **79** 083528
[408] Baek S and Ko P 2009 *J. Cosmol. Astropart. Phys.* JCAP10(2009)011
[409] Bell N F, Cai Y, Leane R K and Medina A D 2014 *Phys. Rev.* D **90** 035027
[410] Chun E J, Park J-C and Scopel S 2010 *J. Cosmol. Astropart. Phys.* JCAP02(2010)015
[411] Bringmann T, Huang X, Ibarra A, Vogl S and Weniger C 2012 *J. Cosmol. Astropart. Phys.* JCAP07(2012)054
[412] Agrawal P, Chacko Z and Verhaaren C B 2014 *J. High Energy Phys.* JHEP08(2014)147
[413] Kopp J, Michaels L and Smirnov J 2014 *J. Cosmol. Astropart. Phys.* JCAP04(2014)022
[414] Fukushima K, Kelso C, Kumar J, Sandick P and Yamamoto T 2014 *Phys. Rev.* D **90** 095007
[415] Kopp J, Niro V, Schwetz T and Zupan J 2009 *Phys. Rev.* D **80** 083502
[416] Schmidt D, Schwetz T and Toma T 2012 *Phys. Rev.* D **85** 073009
[417] Chang S, Edezhath R, Hutchinson J and Luty M 2014 *Phys. Rev.* D **90** 015011
[418] Bai Y and Berger J 2014 *J. High Energy Phys.* JHEP08(2014)153
[419] Kile J, Kobach A and Soni A 2015 *Phys. Lett.* B **744** 330
[420] Roberts B M, Dzuba V A, Flambaum V V, Pospelov M and Stadnik Y V 2016 *Phys. Rev.* D **93** 115037
[421] D'Eramo F, Kavanagh B J and Panci P 2017 *Phys. Lett.* B **771** 339

[422] Roberts B M, Flambaum V V and Gribakin G F 2016 *Phys. Rev. Lett.* **116** 023201
[423] Aprile E *et al* (XENON100) 2015 *Science* **349** 851
[424] Aprile E *et al* (XENON100) 2015 *Phys. Rev. Lett.* **115** 091302
[425] Aprile E *et al* (XENON) 2017 *Phys. Rev. Lett.* **118** 101101
[426] Akerib D S *et al* (LUX) 2018 *Phys. Rev.* D **98** 062005
[427] Essig R, Mardon J and Volansky T 2012 *Phys. Rev.* D **85** 076007
[428] Garani R and Palomares-Ruiz S 2017 *J. Cosmol. Astropart. Phys.* JCAP05(2017)007
[429] Liang Z-L, Tang Y-L and Yang Z-Q 2018 *J. Cosmol. Astropart. Phys.* JCAP10(2018)035
[430] Fox P J, Harnik R, Kopp J and Tsai Y 2011 *Phys. Rev.* D **84** 014028
[431] Dreiner H, Huck M, Krämer M, Schmeier D and Tattersall J 2013 *Phys. Rev.* D **87** 075015
[432] Freitas A and Westhoff S 2014 *J. High Energy Phys.* JHEP10(2014)116
[433] Dutta S, Rawat B and Sachdeva D 2017 *Eur. Phys. J.* C **77** 639
[434] Freese K, Frieman J and Gould A 1988 *Phys. Rev.* D **37** 3388
[435] Copi C J, Heo J and Krauss L M 1999 *Phys. Lett.* B **461** 43
[436] Copi C J and Krauss L M 2001 *Phys. Rev.* D **63** 043507
[437] Baum S, Freese K and Kelso C 2019 *Phys. Lett.* B **789** 262
[438] Amaré J *et al* 2019 *Phys. Rev. Lett.* **123** 031301
[439] Amaré J *et al* 2021 *Phys. Rev.* D **103** 102005
[440] Adhikari G *et al* (COSINE-100) 2019 *Phys. Rev. Lett.* **123** 031302
[441] Adhikari G *et al* (COSINE-100) 2021 *Sci. Adv.* **7** eabk2699
[442] Antonello M *et al* (SABRE) 2019 *Eur. Phys. J.* C **79** 363
[443] Collar J I and Avignone F T 1993 *Phys. Rev.* D **47** 5238
[444] Hasenbalg F, Abriola D, Collar J I, Di Gregorio D E, Gattone A O, Huck H, Tomasi D, Urteaga I and Urteaga I 1997 *Phys. Rev.* D **55** 7350
[445] Kavanagh B J, Catena R and Kouvaris C 2017 *J. Cosmol. Astropart. Phys.* JCAP01(2017)012
[446] Emken T and Kouvaris C 2017 *J. Cosmol. Astropart. Phys.* JCAP10(2017)031
[447] Andriamirado M *et al* (PROSPECT Collaboration) 2021 *Phys. Rev.* D **104** 012009
[448] Kastens L, Cahn S, Manzur A and McKinsey D 2009 *Phys. Rev.* C **80** 045809
[449] Manalaysay A *et al* 2010 *Rev. Sci. Instrum.* **81** 073303
[450] Strigari L E 2009 *New J. Phys.* **11** 105011
[451] Wyenberg J and Shoemaker I M 2018 *Phys. Rev.* D **97** 115026
[452] Essig R, Sholapurkar M and Yu T-T 2018 *Phys. Rev.* D **97** 095029
[453] Baudis L, Ferella A, Kish A, Manalaysay A, Undagoitia T M and Schumann M 2014 *J. Cosmol. Astropart. Phys.* JCAP01(2014)044
[454] Dent J B, Dutta B, Newstead J L and Strigari L E 2016 *Phys. Rev.* D **93** 075018
[455] Dent J B, Dutta B, Newstead J L and Strigari L E 2017 *Phys. Rev.* D **95** 051701
[456] Dent J B, Dutta B, Newstead J L and Shoemaker I M 2020 *Phys. Rev.* D **101** 116007
[457] O'Hare C A J 2021 arXiv:2109.03116
[458] Papoulias D K, Sahu R, Kosmas T S, Kota V K B and Nayak B 2018 *Adv. High Energy Phys.* **2018** 6031362
[459] Sierra D A, Rojas N and Tytgat M H G 2018 *J. High Energy Phys.* JHEP03(2018)197
[460] Gonzalez-Garcia M C, Maltoni M, Perez-Gonzalez Y F and Zukanovich Funchal R 2018 *J. High Energy Phys.* JHEP07(2018)019
[461] Bœhm C, Cerdeño D G, Machado P A N, Olivares-Del Campo A, Perdomo E and Reid E 2019 *J. Cosmol. Astropart. Phys.* JCAP01(2019)043
[462] Davis J H 2015 *J. Cosmol. Astropart. Phys.* JCAP03(2015)012
[463] Ruppin F, Billard J, Figueroa-Feliciano E and Strigari L 2014 *Phys. Rev.* D **90** 083510
[464] Grothaus P, Fairbairn M and Monroe J 2014 *Phys. Rev.* D **90** 055018
[465] O'Hare C A J, Green A M, Billard J, Figueroa-Feliciano E and Strigari L E 2015 *Phys. Rev.* D **92** 063518
[466] Mayet F *et al* 2016 *Phys. Rep.* **627** 1
[467] Franarin T and Fairbairn M 2016 *Phys. Rev.* D **94** 053004
[468] O'Hare C A J, Kavanagh B J and Green A M 2017 *Phys. Rev.* D **96** 083011
[469] Bergström J, Gonzalez-Garcia M C, Maltoni M, Peña-Garay C, Serenelli A M and Song N 2016 *J. High Energy Phys.* JHEP03(2016)132
[470] Caden E (SNO+) 2020 *J. Phys.: Conf. Ser.* **1342** 012022
[471] Beacom J F *et al* (Jinping) 2017 *Chin. Phys.* C **41** 023002
[472] Abi B *et al* (DUNE) 2018 arXiv:1807.10334

[473] Kelly K J, Machado P A, Martinez Soler I, Parke S J and Perez Gonzalez Y F 2019 *Phys. Rev. Lett.* **123** 081801
[474] O'Hare C A J 2020 *Phys. Rev.* D **102** 063024
[475] Roszkowski L, Sessolo E M and Williams A J 2015 *J. High Energy Phys.* JHEP02(2015)014
[476] Athron P *et al* (GAMBIT) 2017 *Eur. Phys. J.* C **77** 824
[477] Kobakhidze A and Talia M 2019 *J. High Energy Phys.* JHEP08(2019)105
[478] Baker M J, Kopp J and Long A J 2020 *Phys. Rev. Lett.* **125** 151102
[479] Arina C, Beniwal A, Degrande C, Heisig J and Scaffidi A 2020 *J. High Energy Phys.* JHEP04(2020)015
[480] Battaglieri M *et al* 2017 arXiv:1707.04591
[481] Essig R *et al* 2013 *Community Summer Study 2013: Snowmass on the Mississippi (CSS2013)* (Minneapolis, MN, USA 29 July–6 August 2013) http://inspirehep.net/record/1263039/files/arXiv:1311.0029.pdf
[482] Hochberg Y, Kuflik E, Volansky T and Wacker J G 2014 *Phys. Rev. Lett.* **113** 171301
[483] Hochberg Y, Kuflik E, Murayama H, Volansky T and Wacker J G 2015 *Phys. Rev. Lett.* **115** 021301
[484] Alexander J *et al* 2016 *Dark Sectors 2016 Workshop: Community Report*
[485] Essig R, Manalaysay A, Mardon J, Sorensen P and Volansky T 2012 *Phys. Rev. Lett.* **109** 021301
[486] Agnese R *et al* (SuperCDMS) 2016 *Phys. Rev. Lett.* **116** 071301
[487] Angloher G *et al* (CRESST) 2016 *Eur. Phys. J.* C **76** 25
[488] Petricca F *et al* (CRESST) 2017 *15th Int. Conf. on Topics in Astroparticle and Underground Physics (TAUP 2017)* (Sudbury, Ontario, Canada 24–28 July 2017)
[489] Angloher G *et al* (CRESST) 2017 *Eur. Phys. J.* C **77** 637
[490] Arnaud Q *et al* (NEWS-G) 2018 *Astropart. Phys.* **97** 54
[491] Agnes P *et al* (DarkSide) 2018 *Phys. Rev. Lett.* **121** 081307
[492] Agnes P *et al* (DarkSide) 2018 *Phys. Rev. Lett.* **121** 111303
[493] Essig R, Volansky T and Yu T-T 2017 *Phys. Rev.* D **96** 043017
[494] Akerib D S *et al* (LUX) 2019 *Phys. Rev. Lett.* **122** 131301
[495] Aprile E *et al* (XENON) 2020 *Phys. Rev.* D **102** 072004
[496] Lenardo B *et al* 2019 arXiv:1908.00518
[497] Kouvaris C and Pradler J 2017 *Phys. Rev. Lett.* **118** 031803
[498] Aprile E *et al* (XENON) 2021 *Phys. Rev. Lett.* **126** 091301
[499] Fujii K *et al* 2015 *Nucl. Instrum. Methods Phys. Res.* A **795** 293
[500] Faham C H, Gehman V M, Currie A, Dobi A, Sorensen P and Gaitskell R J 2015 *J. Inst.* **10** P09010
[501] López Paredes B, Araújo H M, Froborg F, Marangou N, Olcina I, Sumner T J, Taylor R, Tomás A and Vacheret A 2018 *Astropart. Phys.* **102** 56
[502] Araújo H 2020 arXiv:2007.01683
[503] Akerib D S *et al* (LUX) 2020 *Phys. Rev.* D **101** 042001
[504] Akerib D S *et al* (LUX) 2016 *Phys. Rev. Lett.* **116** 161301
[505] Akerib D S *et al* 2021 arXiv:2101.08753
[506] Aprile E *et al* (XENON) 2016 *Phys. Rev.* D **94** 092001
Aprile E *et al* (XENON) 2017 *Phys. Rev.* D **95** 059901 (erratum)
[507] Aprile E *et al* (XENON) 2021 arXiv:2112.12116
[508] Cheng C *et al* (PandaX-II) 2021 *Phys. Rev. Lett.* **126** 211803
[509] Aprile E *et al* (XENON100) 2014 *J. Phys. G: Nucl. Part. Phys.* **41** 035201
[510] Akimov D Y *et al* 2016 *J. Inst.* **11** C03007
[511] Sorensen P and Kamdin K 2018 *J. Inst.* **13** P02032
[512] Sorensen P 2017 arXiv:1702.04805
[513] Akerib D S *et al* (LUX) 2020 *Phys. Rev.* D **102** 092004
[514] Kopec A, Baxter A L, Clark M, Lang R F, Li S, Qin J and Singh R 2021 *J. Inst.* **16** P07014
[515] Bodnia E *et al* 2021 *J. Inst.* **16** P12015
[516] Szydagis M *et al* 2019 Nestcollaboration/nest: new, flexible lxe nr yields and resolution model + g4 improvements + linear noise + much more https://doi.org/10.5281/zenodo.3357973
[517] Catena R, Emken T, Spaldin N A and Tarantino W 2020 *Phys. Rev. Res.* **2** 033195
[518] Catena R, Emken T and Ravanis J 2020 *J. Cosmol. Astropart. Phys.* JCAP06(2020)056
[519] Aprile E *et al* (XENON) 2019 *Phys. Rev. Lett.* **123** 241803
[520] Liu Z Z *et al* (CDEX) 2019 *Phys. Rev. Lett.* **123** 161301

[521] Migdal A 1941 *J. Phys. USSR* **4** 449
[522] Ibe M, Nakano W, Shoji Y and Suzuki K 2018 *J. High Energy Phys.* JHEP03(2018)194
[523] Dolan M J, Kahlhoefer F and McCabe C 2018 *Phys. Rev. Lett.* **121** 101801
[524] Wang W, Wu K-Y, Wu L and Zhu B 2021 arXiv:2112.06492
[525] Bell N F, Dent J B, Lang R F, Newstead J L and Ritter A C 2021 arXiv:2112.08514
[526] Bell N F, Dent J B, Newstead J L, Sabharwal S and Weiler T J 2020 *Phys. Rev.* D **101** 015012
[527] McCabe C 2017 *Phys. Rev.* D **96** 043010
[528] Akerib D S *et al* 2020 HydroX—using hydrogen doped in liquid xenon to search for dark matter https://snowmass21.org/docs/files/summaries/CF/SNOWMASS21-CF1_CF0_Hugh_Lippincott-106.pdf
[529] Beacom J F, Farr W M and Vogel P 2002 *Phys. Rev.* D **66** 033001
[530] Bolozdynya A I 1991 *Proc. of the 3rd Int. Conf. on Properties and Applications of Dielectric Materials* (Tokyo, Japan 8–12 July 1991) vol 2 pp pp 841–4
[531] Tezuka C *et al* 2004 *Proc., 2004 IEEE Nuclear Science Symp. and Medical Imaging Conf. (NSS/MIC 2004)* (Rome, Italy 16–22 October 2004) vol 2 pp pp 1157–9
[532] Incandela J R *et al* 1988 *Nucl. Instrum. Methods Phys. Res.* A **269** 237
[533] Bringmann T and Pospelov M 2019 *Phys. Rev. Lett.* **122** 171801
[534] Alvey J, Campos M D, Fairbairn M and You T 2019 *Phys. Rev. Lett.* **123** 261802
[535] Cappiello C V and Beacom J F 2019 *Phys. Rev.* D **100** 103011
[536] Bondarenko K, Boyarsky A, Bringmann T, Hufnagel M, Schmidt-Hoberg K and Sokolenko A 2020 *J. High Energy Phys.* JHEP03(2020)118
[537] Wang W, Wu L, Yang J M, Zhou H and Zhu B 2020 *J. High Energy Phys.* JHEP12(2020)072
Wang W, Wu L, Yang J M, Zhou H and Zhu B 2021 *J. High Energy Phys.* JHEP02(2021)052 (erratum)
[538] Dent J B, Dutta B, Newstead J L, Shoemaker I M and Arellano N T 2021 *Phys. Rev.* D **103** 095015
[539] Bell N F, Dent J B, Dutta B, Ghosh S, Kumar J, Newstead J L and Shoemaker I M 2021 *Phys. Rev.* D **104** 076020
[540] An H, Pospelov M, Pradler J and Ritz A 2018 *Phys. Rev. Lett.* **120** 141801
An H, Pospelov M, Pradler J and Ritz A 2018 *Phys. Rev. Lett.* **121** 259903 (erratum)
[541] Emken T, Kouvaris C and Nielsen N G 2018 *Phys. Rev.* D **97** 063007
[542] Liang Z-L, Mo C and Zhang P 2021 *Phys. Rev.* D **104** 096001
[543] An H, Nie H, Pospelov M, Pradler J and Ritz A 2021 *Phys. Rev.* D **104** 103026
[544] Emken T 2021 arXiv:2102.12483
[545] Chatterjee S and Laha R 2022 arXiv:2202.13339
[546] Cherry J F, Friedland A and Shoemaker I M 2014 arXiv:1411.1071
[547] González Macías V, Wudka J and Illana J I 2015 *Acta Phys. Pol.* B **46** 2173
[548] Becker M 2019 *Eur. Phys. J.* C **79** 611
[549] Lamprea J M, Peinado E, Smolenski S and Wudka J 2021 *Phys. Rev.* D **103** 015017
[550] Patel H H, Profumo S and Shakya B 2020 *Phys. Rev.* D **101** 095001
[551] McKeen D and Raj N 2019 *Phys. Rev.* D **99** 103003
[552] Agashe K, Cui Y, Necib L and Thaler J 2014 *J. Cosmol. Astropart. Phys.* JCAP10(2014)062
[553] Cherry J F, Frandsen M T and Shoemaker I M 2015 *Phys. Rev. Lett.* **114** 231303
[554] Marrodán Undagoitia T, Rodejohann W, Wolf T and Yaguna C E 2021 arXiv:2107.05685
[555] Slatyer T R 2016 *Phys. Rev.* D **93** 023527
[556] Ng K C, Roach B M, Perez K, Beacom J F, Horiuchi S, Krivonos R and Wik D R 2019 *Phys. Rev.* D **99** 083005
[557] McDonald J 2002 *Phys. Rev. Lett.* **88** 091304
[558] Hall L J, Jedamzik K, March-Russell J and West S M 2010 *J. High Energy Phys.* JHEP03(2010)080
[559] Feng J L, Rajaraman A and Takayama F 2003 *Phys. Rev. Lett.* **91** 011302
[560] Dodelson S and Widrow L M 1994 *Phys. Rev. Lett.* **72** 17
[561] Pospelov M, Ritz A and Voloshin M 2008 *Phys. Rev.* D **78** 115012
[562] Hambye T, Tytgat M H G, Vandecasteele J and Vanderheyden L 2018 *Phys. Rev.* D **98** 075017
[563] Bélanger G, Delaunay C, Pukhov A and Zaldivar B 2020 *Phys. Rev.* D **102** 035017
[564] Elor G, McGehee R and Pierce A 2021 arXiv:2112.03920
[565] Graham P W, Mardon J and Rajendran S 2016 *Phys. Rev.* D **93** 103520
[566] Nelson A E and Scholtz J 2011 *Phys. Rev.* D **84** 103501

[567] Arias P, Cadamuro D, Goodsell M, Jaeckel J, Redondo J and Ringwald A 2012 *J. Cosmol. Astropart. Phys.* JCAP06(2012)013
[568] An H, Pospelov M, Pradler J and Ritz A 2015 *Phys. Lett.* B **747** 331
[569] Holdom B 1986 *Phys. Lett.* B **166** 196
[570] Babu K S, Kolda C and March-Russell J 1996 *Phys. Rev.* D **54** 4635
[571] Babu K S, Kolda C and March-Russell J 1998 *Phys. Rev.* D **57** 6788
[572] Akerib D S *et al* (LZ) 2021 *Phys. Rev.* D **104** 092009
[573] An H, Pospelov M, Pradler J and Ritz A 2020 *Phys. Rev.* D **102** 115022
[574] Peccei R D and Quinn H R 1977 *Phys. Rev. Lett.* **38** 1440
[575] Weinberg S 1978 *Phys. Rev. Lett.* **40** 223
[576] Wilczek F 1978 *Phys. Rev. Lett.* **40** 279
[577] Preskill J, Wise M B and Wilczek F 1983 *Phys. Lett.* B **120** 127
[578] Abbott L F and Sikivie P 1983 *Phys. Lett.* B **120** 133
[579] Dine M and Fischler W 1983 *Phys. Lett.* B **120** 137
[580] Krauss L M 1985 *Theoretical Advanced Study Institute in Elementary Particle Physics*
[581] Irastorza I G 2021 Les Houches Summer School on Dark Matter (arXiv:2109.07376)
[582] Choi K, Im S H and Shin C S 2021 *Annu. Rev. Nucl. Part. Sci.* **71** 225
[583] Grilli di Cortona G, Hardy E, Pardo Vega J and Villadoro G 2016 *J. High Energy Phys.* JHEP01(2016)034
[584] Zyla P A *et al* (Particle Data Group) 2020 *Prog. Theor. Exp. Phys.* **2020** 083C01
[585] Raffelt G G 2008 *Lect. Notes Phys.* **741** 51
[586] Sikivie P 2008 *Lect. Notes Phys.* **741** 19
[587] Ayala A, Domínguez I, Giannotti M, Mirizzi A and Straniero O 2014 *Phys. Rev. Lett.* **113** 191302
[588] Chang J H, Essig R and McDermott S D 2018 *J. High Energy Phys.* JHEP09(2018)051
[589] Capozzi F and Raffelt G 2020 *Phys. Rev.* D **102** 083007
[590] Anastassopoulos V *et al* (CAST) 2017 *Nat. Phys.* **13** 584
[591] Witten E 1984 *Commun. Math. Phys.* **92** 455
[592] Svrcek P and Witten E 2006 *J. High Energy Phys.* JHEP06(2006)051
[593] Conlon J P 2006 *J. High Energy Phys.* JHEP05(2006)078
[594] Arvanitaki A, Dimopoulos S, Dubovsky S, Kaloper N and March-Russell J 2010 *Phys. Rev.* D **81** 123530
[595] Cicoli M, Goodsell M D and Ringwald A 2012 *J. High Energy Phys.* JHEP10(2012)146
[596] Derevianko A, Dzuba V A, Flambaum V V and Pospelov M 2010 *Phys. Rev.* D **82** 065006
[597] Aprile E *et al* (XENON100) 2014 *Phys. Rev.* D **90** 062009
Aprile E *et al* (XENON100) 2017 *Phys. Rev.* D **95** 029904 (erratum)
[598] Abe K *et al* (XMASS) 2014 *Phys. Rev. Lett.* **113** 121301
[599] Akerib D S *et al* (LUX) 2017 *Phys. Rev. Lett.* **118** 261301
[600] Fu C *et al* (PandaX) 2017 *Phys. Rev. Lett.* **119** 181806
[601] Abe K *et al* (XMASS) 2018 *Phys. Lett.* B **787** 153
[602] Zhou X *et al* (PandaX-II) 2020 arXiv:2008.06485
[603] Davis R L 1986 *Phys. Lett.* B **180** 225
[604] Sikivie P 1982 *Phys. Rev. Lett.* **48** 1156
[605] Visinelli L and Gondolo P 2010 *Phys. Rev.* D **81** 063508
[606] Hiramatsu T, Kawasaki M and Saikawa K 2011 *J. Cosmol. Astropart. Phys.* JCAP08(2011)030
[607] Co R T, Hall L J and Harigaya K 2018 *Phys. Rev. Lett.* **120** 211602
[608] Co R T, Gonzalez E and Harigaya K 2019 *J. High Energy Phys.* JHEP05(2019)163
[609] Co R T, Hall L J and Harigaya K 2020 *Phys. Rev. Lett.* **124** 251802
[610] Hook A, Marques-Tavares G and Tsai Y 2020 *Phys. Rev. Lett.* **124** 211801
[611] Co R T, Hall L J and Harigaya K 2021 *J. High Energy Phys.* JHEP01(2021)172
[612] Dent J B, Dutta B, Newstead J L and Thompson A 2020 *Phys. Rev. Lett.* **125** 131805
[613] Nussinov S 1985 *Phys. Lett.* B **165** 55
[614] Gelmini G B, Hall L J and Lin M J 1987 *Nucl. Phys.* B **281** 726
[615] Kaplan D B 1992 *Phys. Rev. Lett.* **68** 741
[616] Hooper D, March-Russell J and West S M 2005 *Phys. Lett.* B **605** 228
[617] Kitano R and Low I 2005 *Phys. Rev.* D **71** 023510
[618] Cosme N, Lopez Honorez L and Tytgat M H G 2005 *Phys. Rev.* D **72** 043505
[619] Kaplan D E, Luty M A and Zurek K M 2009 *Phys. Rev.* D **79** 115016
[620] March-Russell J, McCabe C and McCullough M 2010 *J. High Energy Phys.* JHEP03(2010)108

[621] Frandsen M T and Sarkar S 2010 *Phys. Rev. Lett.* **105** 011301
[622] Frandsen M T, Sarkar S and Schmidt-Hoberg K 2011 *Phys. Rev.* D **84** 051703
[623] Petraki K and Volkas R R 2013 *Int. J. Mod. Phys.* A **28** 1330028
[624] Zurek K M 2014 *Phys. Rep.* **537** 91
[625] Chacko Z, Goh H-S and Harnik R 2006 *Phys. Rev. Lett.* **96** 231802
[626] Garcia Garcia I, Lasenby R and March-Russell J 2015 *Phys. Rev.* D **92** 055034
[627] Craig N and Katz A 2015 *J. Cosmol. Astropart. Phys.* JCAP10(2015)054
[628] Cacciapaglia G, Frandsen M T, Huang W-C, Rosenlyst M and Sørensen P 2021 arXiv:2111.09319
[629] Hall L J, March-Russell J and West S M 2010 arXiv:1010.0245
[630] Buckley M R and Randall L 2011 *J. High Energy Phys.* JHEP09(2011)009
[631] Buckley M R 2011 *Phys. Rev.* D **84** 043510
[632] March-Russell J, Unwin J and West S M 2012 *J. High Energy Phys.* JHEP08(2012)029
[633] Cui Y and Shamma M 2020 *J. High Energy Phys.* JHEP12(2020)046
[634] Hur T, Jung D-W, Ko P and Lee J Y 2011 *Phys. Lett.* B **696** 262
[635] Bai Y and Hill R J 2010 *Phys. Rev.* D **82** 111701
[636] Hur T and Ko P 2011 *Phys. Rev. Lett.* **106** 141802
[637] Bai Y and Schwaller P 2014 *Phys. Rev.* D **89** 063522
[638] Antipin O, Redi M, Strumia A and Vigiani E 2015 *J. High Energy Phys.* JHEP07(2015)039
[639] Detmold W, McCullough M and Pochinsky A 2014 *Phys. Rev.* D **90** 115013
[640] Hardy E, Lasenby R, March-Russell J and West S M 2015 *J. High Energy Phys.* JHEP06(2015)011
[641] Detmold W, McCullough M and Pochinsky A 2014 *Phys. Rev.* D **90** 114506
[642] Wise M B and Zhang Y 2015 *J. High Energy Phys.* JHEP02(2015)023
Wise M B and Zhang Y 2015 *J. High Energy Phys.* JHEP10(2015)165 (erratum)
[643] Gresham M I, Lou H K and Zurek K M 2017 *Phys. Rev.* D **96** 096012
[644] Bai Y, Long A J and Lu S 2019 *Phys. Rev.* D **99** 055047
[645] Kaplan D E, Krnjaic G Z, Rehermann K R and Wells C M 2011 *J. Cosmol. Astropart. Phys.* JCAP10(2011)011
[646] Petraki K, Pearce L and Kusenko A 2014 *J. Cosmol. Astropart. Phys.* JCAP07(2014)039
[647] Wise M B and Zhang Y 2014 *Phys. Rev.* D **90** 055030
Wise M B and Zhang Y 2015 *Phys. Rev.* D **91** 039907 (erratum)
[648] Petraki K, Postma M and Wiechers M 2015 *J. High Energy Phys.* JHEP06(2015)128
[649] Laha R 2015 *Phys. Rev.* D **92** 083509
[650] Laha R and Braaten E 2014 *Phys. Rev.* D **89** 103510
[651] 't Hooft G 1974 *Nucl. Phys.* B **79** 276
[652] Polyakov A M 1974 *JETP Lett.* **20** 194
[653] Coleman S 1985 *Nucl. Phys.* B **262** 263
Coleman S R 1986 *Nucl. Phys.* B **269** 744 (addendum)
[654] Butcher A, Kirk R, Monroe J and West S M 2017 *J. Cosmol. Astropart. Phys.* JCAP10(2017)035
[655] Grabowska D M, Melia T and Rajendran S 2018 *Phys. Rev.* D **98** 115020
[656] Coskuner A, Grabowska D M, Knapen S and Zurek K M 2019 *Phys. Rev.* D **100** 035025
[657] Foot R and Vagnozzi S 2015 *Phys. Lett.* B **748** 61
[658] Dror J A, Elor G and Mcgehee R 2020 *Phys. Rev. Lett.* **124** 181301
[659] Dror J A, Elor G and Mcgehee R 2020 *J. High Energy Phys.* JHEP02(2020)134
[660] Gu L *et al* (PandaX) 2022 arXiv:2205.15771
[661] Dror J A, Elor G, McGehee R and Yu T-T 2021 *Phys. Rev.* D **103** 035001
Dror J A, Elor G, McGehee R and Yu T-T 2022 *Phys. Rev.* D **105** 119903 (erratum)
[662] Ge S-F, He X-G, Ma X-D and Sheng J 2022 *J. High Energy Phys.* JHEP05(2022)191
[663] Li T, Liao J and Zhang R-J 2022 *J. High Energy Phys.* JHEP05(2022)071
[664] Zhang D *et al* 2022 arXiv:2206.02339
[665] Hodges H M 1993 *Phys. Rev.* D **47** 456
[666] Berezhiani Z 2004 *Int. J. Mod. Phys.* A **19** 3775
[667] Okun' L B 2007 *Phys.-Usp.* **50** 380
[668] Foot R 2007 *Int. J. Mod. Phys.* A **22** 4951
[669] Foot R 2010 *Phys. Rev.* D **82** 095001
[670] Foot R 2014 *Int. J. Mod. Phys.* A **29** 1430013
[671] Foot R 2019 *Phys. Lett.* B **789** 592
[672] Akerib D S *et al* (LUX) 2020 *Phys. Rev.* D **101** 012003

[673] Clarke J D and Foot R 2017 *Phys. Lett.* B **766** 29
[674] Feldstein B, Graham P W and Rajendran S 2010 *Phys. Rev.* D **82** 075019
[675] Pospelov M, Weiner N and Yavin I 2014 *Phys. Rev.* D **89** 055008
[676] Bell N F, Dent J B, Dutta B, Ghosh S, Kumar J and Newstead J L 2020 *Phys. Rev. Lett.* **125** 161803
[677] Chang S, Weiner N and Yavin I 2010 *Phys. Rev.* D **82** 125011
[678] Kumar K, Menon A and Tait T M P 2012 *J. High Energy Phys.* JHEP02(2012)131
[679] Patra S and Rao S 2011 arXiv:1112.3454
[680] Weiner N and Yavin I 2013 *Phys. Rev.* D **87** 023523
[681] Pierce A and Zhang Z 2014 *Phys. Rev.* D **90** 015026
[682] Lin T and Finkbeiner D P 2011 *Phys. Rev.* D **83** 083510
[683] Aprile E *et al* (XENON) 2017 *J. Cosmol. Astropart. Phys.* JCAP10(2017)039
[684] Kolb E W and Long A J 2017 *Phys. Rev.* D **96** 103540
[685] Fujita T, Harigaya K, Kawasaki M and Matsuda R 2014 *Phys. Rev.* D **89** 103501
[686] Lennon O, March-Russell J, Petrossian-Byrne R and Tillim H 2018 *J. Cosmol. Astropart. Phys.* JCAP04(2018)009
[687] Asadi P, Slatyer T R and Smirnov J 2021 arXiv:2111.11444
[688] Chung D J H, Kolb E W and Riotto A 1999 *Phys. Rev.* D **59** 023501
[689] Hamdan S and Unwin J 2018 *Mod. Phys. Lett.* A **33** 1850181
[690] Davoudiasl H and Mohlabeng G 2018 *Phys. Rev.* D **98** 115035
[691] Bramante J, Broerman B, Kumar J, Lang R F, Pospelov M and Raj N 2019 *Phys. Rev.* D **99** 083010
[692] Bramante J, Kumar J and Raj N 2019 *Phys. Rev.* D **100** 123016
[693] Clark M, Depoian A, Elshimy B, Kopec A, Lang R F and Qin J 2020 *Phys. Rev.* D **102** 123026
[694] Adhikari P *et al* (DEAP Collaboration) 2022 *Phys. Rev. Lett.* **128** 011801
[695] Acevedo J F, Bramante J and Goodman A 2022 *Phys. Rev.* D **105** 023012
[696] Doi M and Kotani T 1993 *Prog. Theor. Phys.* **89** 139
[697] Avignone F T, Elliott S R, Engel J and Engel J 2008 *Rev. Mod. Phys.* **80** 481
[698] Dolinski M J, Poon A W P and Rodejohann W 2019 *Annu. Rev. Nucl. Part. Sci.* **69** 219
[699] Agostini M, Benato G, Detwiler J A, Menéndez J and Vissani F 2022 arXiv:2202.01787
[700] Akerib D S *et al* (LUX-ZEPLIN, LZ) 2021 *Phys. Rev.* C **104** 065501
[701] Gando A *et al* (KamLAND-Zen) 2016 *Phys. Rev. Lett.* **117** 082503
Gando A *et al* (KamLAND-Zen) 2016 *Phys. Rev. Lett.* **117** 109903 (addendum)
[702] Adams D Q *et al* (CUORE) 2021 arXiv:2104.06906
[703] Agostini M *et al* (GERDA) 2020 *Phys. Rev. Lett.* **125** 252502
[704] Armengaud E *et al* (CUPID) 2021 *Phys. Rev. Lett.* **126** 181802
[705] Alvis S I *et al* (Majorana) 2019 *Phys. Rev.* C **100** 025501
[706] Anton G *et al* (EXO-200) 2019 *Phys. Rev. Lett.* **123** 161802
[707] Azzolini O *et al* (CUPID) 2019 *Phys. Rev. Lett.* **123** 032501
[708] Albert J B *et al* (EXO) 2018 *Phys. Rev. Lett.* **120** 072701
[709] Ni K *et al* (PandaX-II) 2019 *Chin. Phys.* C **43** 113001
[710] Agostini F *et al* (DARWIN) 2020 *Eur. Phys. J.* C **80** 808
[711] Gomez-Cadenas J J 2019 arXiv:1906.01743
[712] Chen X *et al* 2017 *Sci. China Phys. Mech. Astron.* **60** 061011
[713] Albert J B *et al* (nEXO) 2018 *Phys. Rev.* C **97** 065503
[714] Barabash A S 2015 *Nucl. Phys.* A **935** 52
[715] Cebrián S 2020 *Universe* **6** 162
[716] Rogers L *et al* (NEXT) 2020 *J. Phys. G: Nucl. Part. Phys.* **47** 075001
[717] Päs H, Hirsch M, Klapdor-Kleingrothaus H V and Kovalenko S G 1999 *Phys. Lett.* B **453** 194
[718] Päs H, Hirsch M, Klapdor-Kleingrothaus H V and Kovalenko S G 2001 *Phys. Lett.* B **498** 35
[719] Prézeau G, Ramsey-Musolf M and Vogel P 2003 *Phys. Rev.* D **68** 034016
[720] de Gouvea A and Jenkins J 2008 *Phys. Rev.* D **77** 013008
[721] Cirigliano V, Dekens W, de Vries J, Graesser M and Mereghetti E 2017 *J. High Energy Phys.* JHEP12(2017)082
[722] Graf L, Deppisch F F, Iachello F and Kotila J 2018 *Phys. Rev.* D **98** 095023
[723] Cirigliano V, Dekens W, de Vries J, Graesser M and Mereghetti E 2018 *J. High Energy Phys.* JHEP12(2018)097

[724] Dekens W, de Vries J, Fuyuto K, Mereghetti E and Zhou G 2020 *J. High Energy Phys.* JHEP06(2020)097
[725] Deppisch F F, Graf L, Iachello F and Kotila J 2020 *Phys. Rev.* D **102** 095016
[726] Kotila J, Ferretti J and Iachello F 2021 arXiv:2110.09141
[727] Menéndez J, Gazit D and Schwenk A 2011 *Phys. Rev. Lett.* **107** 062501
[728] Wang L-J, Engel J and Yao J M 2018 *Phys. Rev.* C **98** 031301
[729] Cirigliano V, Dekens W, Mereghetti E and Walker-Loud A 2018 *Phys. Rev.* C **97** 065501
Cirigliano V, Dekens W, Mereghetti E and Walker-Loud A 2019 *Phys. Rev.* C **100** 019903 (erratum)
[730] Pastore S, Carlson J, Cirigliano V, Dekens W, Mereghetti E and Wiringa R 2018 *Phys. Rev.* C **97** 014606
[731] Cirigliano V, Dekens W, de Vries J, Graesser M L, Mereghetti E, Pastore S and Van Kolck U 2018 *Phys. Rev. Lett.* **120** 202001
[732] Cirigliano V, Dekens W, de Vries J, Graesser M, Mereghetti E, Pastore S, Piarulli M, Van Kolck U and Wiringa R 2019 *Phys. Rev.* C **100** 055504
[733] Cirigliano V, Dekens W, de Vries J, Hoferichter M and Mereghetti E 2021 *Phys. Rev. Lett.* **126** 172002
[734] Cirigliano V, Dekens W, de Vries J, Hoferichter M and Mereghetti E 2021 *J. High Energy Phys.* JHEP05(2021)289
[735] Jokiniemi L, Soriano P and Menéndez J 2021 *Phys. Lett.* B **823** 136720
[736] Wirth R, Yao J M and Hergert H 2021 *Phys. Rev. Lett.* **127** 242502
[737] Barabash A 2020 *Universe* **6** 159
[738] Saakyan R 2013 *Annu. Rev. Nucl. Part. Sci.* **63** 503
[739] Engel J and Menéndez J 2017 *Rep. Prog. Phys.* **80** 046301
[740] Si L *et al* 2022 arXiv:2205.12809
[741] Rodriguez T R and Martinez-Pinedo G 2010 *Phys. Rev. Lett.* **105** 252503
[742] Mustonen M T and Engel J 2013 *Phys. Rev.* C **87** 064302
[743] Hyvärinen J and Suhonen J 2015 *Phys. Rev.* C **91** 024613
[744] Horoi M and Neacsu A 2016 *Phys. Rev.* C **93** 024308
[745] Menéndez J 2018 *J. Phys. G: Nucl. Part. Phys.* **45** 014003
[746] Song L S, Yao J M, Ring P and Meng J 2017 *Phys. Rev.* C **95** 024305
[747] Šimkovic F, Smetana A and Vogel P 2018 *Phys. Rev.* C **98** 064325
[748] Fang D-L, Faessler A and Simkovic F 2018 *Phys. Rev.* C **97** 045503
[749] Coraggio L, Gargano A, Itaco N, Mancino R and Nowacki F 2020 *Phys. Rev.* C **101** 044315
[750] Yao J M, Bally B, Engel J, Wirth R, Rodríguez T R and Hergert H 2020 *Phys. Rev. Lett.* **124** 232501
[751] Novario S, Gysbers P, Engel J, Hagen G, Jansen G R, Morris T D, Navrátil P, Papenbrock T and Quaglioni S 2021 *Phys. Rev. Lett.* **126** 182502
[752] Belley A, Payne C G, Stroberg S R, Miyagi T and Holt J D 2021 *Phys. Rev. Lett.* **126** 042502
[753] Gando A *et al* (KamLAND-Zen) 2019 *Phys. Rev. Lett.* **122** 192501
[754] Deppisch F F, Graf L and Šimkovic F 2020 *Phys. Rev. Lett.* **125** 171801
[755] Bolton P D, Deppisch F F, Gráf L and Šimkovic F 2021 *Phys. Rev.* D **103** 055019
[756] Agostini M, Bossio E, Ibarra A and Marcano X 2021 *Phys. Lett.* B **815** 136127
[757] Deppisch F F, Graf L, Rodejohann W and Xu X-J 2020 *Phys. Rev.* D **102** 051701
[758] Winter R G 1955 *Phys. Rev.* **100** 142
[759] Blaum K, Eliseev S, Danevich F A, Tretyak V I, Kovalenko S, Krivoruchenko M I, Novikov Y N and Suhonen J 2020 *Rev. Mod. Phys.* **92** 045007
[760] Nesterenko D *et al* 2012 *Phys. Rev.* C **86** 044313
[761] Doi M and Kotani T 1992 *Prog. Theor. Phys.* **87** 1207
[762] Suhonen J 2013 *J. Phys. G: Nucl. Part. Phys.* **40** 075102
[763] Pirinen P and Suhonen J 2015 *Phys. Rev.* C **91** 054309
[764] Coello Pérez E A, Menéndez J and Schwenk A 2019 *Phys. Lett.* B **797** 134885
[765] Abe K *et al* (XMASS) 2018 *Prog. Theor. Exp. Phys.* **2018** 053D03
[766] Aprile E *et al* (XENON) 2019 *Nature* **568** 532
[767] Bernabeu J, De Rujula A and Jarlskog C 1983 *Nucl. Phys.* B **223** 15
[768] Sujkowski Z and Wycech S 2004 *Phys. Rev.* C **70** 052501
[769] Kotila J, Barea J and Iachello F 2014 *Phys. Rev.* C **89** 064319
[770] Wittweg C, Lenardo B, Fieguth A and Weinheimer C 2020 *Eur. Phys. J.* C **80** 1161

[771] Kim C W and Kubodera K 1983 *Phys. Rev.* D **27** 2765
[772] Kotila J and Iachello F 2013 *Phys. Rev.* C **87** 024313
[773] Barros N, Thurn J and Zuber K 2014 *J. Phys. G: Nucl. Part. Phys.* **41** 115105
[774] Bolozdynya A, Egorov V, Koutchenkov A, Safronov G, Smirnov G, Meddved S and Morgunov V 1997 *IEEE Trans. Nucl. Sci.* **44** 1046
[775] Rath P K, Chandra R, Chaturvedi K, Raina P and Hirsch J 2009 *Phys. Rev.* C **80** 044303
[776] Barea J, Kotila J and Iachello F 2013 *Phys. Rev.* C **87** 057301
[777] Kotila J and Iachello F 2012 *Phys. Rev.* C **85** 034316
[778] Angloher G *et al* 2016 *J. Phys. G: Nucl. Part. Phys.* **43** 095202
[779] Lehnert B, Degering D, Frotscher A, Michel T and Zuber K 2016 *J. Phys. G: Nucl. Part. Phys.* **43** 065201
[780] Alduino C *et al* (CUORE) 2018 *Phys. Rev.* C **97** 055502
[781] Hirsch M, Muto K, Oda T and Klapdor-Kleingrothaus H V 1994 *Z. Phys.* A **347** 151
[782] Deppisch F and Päs H 2007 *Phys. Rev. Lett.* **98** 232501
[783] Gehman V M and Elliott S R 2007 *J. Phys. G: Nucl. Part. Phys.* **34** 667
Gehman V M and Elliott S R 2008 Multiple-isotope comparison for determining $0\nu\beta\beta$ mechanisms *J. Phys. G: Nucl. Part. Phys.* **35** 029701
[784] Vitagliano E, Tamborra I and Raffelt G 2020 *Rev. Mod. Phys.* **92** 45006
[785] Orebi Gann G D, Zuber K, Bemmerer D and Serenelli A 2021 *Annu. Rev. Nucl. Part. Sci.* **71** 491
[786] Dutta B and Strigari L E 2019 *Annu. Rev. Nucl. Part. Sci.* **69** 137
[787] Abe K *et al* (Hyper-Kamiokande) 2018 arXiv:1805.04163
[788] Acciarri R *et al* (DUNE) 2016 arXiv:1601.05471
[789] Engel J 1991 *Phys. Lett.* B **264** 114
[790] Hoferichter M, Menéndez J and Schwenk A 2020 *Phys. Rev.* D **102** 074018
[791] Akimov D *et al* (COHERENT) 2017 *Science* **357** 1123
[792] Cabrera B, Krauss L M and Wilczek F 1985 *Phys. Rev. Lett.* **55** 25
[793] Krauss L and Wilczek F 1985 *Phys. Rev. Lett.* **55** 122
[794] Bahcall J N and Davis R 1976 *Science* **191** 264
[795] Haxton W C, Hamish Robertson R G and Serenelli A M 2013 *Annu. Rev. Astron. Astrophys.* **51** 21
[796] de Holanda P C and Smirnov A Y 2003 *J. Cosmol. Astropart. Phys.* JCAP02(2003)001
[797] Abe K *et al* (Super-Kamiokande) 2016 *Phys. Rev.* D **94** 052010
[798] Aharmim B *et al* (SNO) 2013 *Phys. Rev.* C **88** 025501
[799] Agostini M *et al* (BOREXINO) 2018 *Nature* **562** 505
[800] Gando A *et al* (KamLAND) 2011 *Phys. Rev.* D **83** 052002
[801] Liao J, Marfatia D and Whisnant K 2017 *Phys. Lett.* B **771** 247
[802] Newstead J L, Strigari L E and Lang R F 2019 *Phys. Rev.* D **99** 043006
[803] Grevesse N and Sauval A J 1998 *Space Sci. Rev.* **85** 161
[804] Asplund M, Grevesse N, Sauval A J and Scott P 2009 *Annu. Rev. Astron. Astrophys.* **47** 481pp –522
[805] Scott P, Grevesse N, Asplund M, Jacques Sauval A, Lind K, Takeda Y, Collet R, Trampedach R and Hayek W 2015 *Astron. Astrophys.* **573** A25
[806] Scott P, Asplund M, Grevesse N, Bergemann M and Jacques Sauval A 2015 *Astron. Astrophys.* **573** A26
[807] Grevesse N, Scott P, Asplund M and Jacques Sauval A 2015 *Astron. Astrophys.* **573** A27
[808] Serenelli A M, Basu S, Ferguson J W and Asplund M 2009 *Astrophys. J. Lett.* **705** L123
[809] Agostini M *et al* (BOREXINO) 2020 *Nature* **587** 577
[810] Agostini M *et al* (Borexino) 2020 *Phys. Rev.* D **101** 062001
[811] Aharmim B *et al* (SNO) 2006 *Astrophys. J.* **653** 1545
[812] Suzuki Y (XMASS) 2000 *Workshop on Solar Neutrinos below 1-MeV: NuLow*
[813] Smirnov O *et al* (Borexino) 2016 *Phys. Part. Nucl.* **47** 995
[814] Bahcall J N 2002 *Phys. Rev.* C **65** 025801
[815] Aalbers J *et al* (DARWIN) 2020 *Eur. Phys. J.* C **80** 1133
[816] Georgadze A S, Klapdor-Kleingrothaus H V, Päs H and Zdesenko Y G 1997 *Astropart. Phys.* **7** 173
[817] Haselschwardt S, Lenardo B, Pirinen P and Suhonen J 2020 *Phys. Rev.* D **102** 072009
[818] Battistoni G, Ferrari A, Montaruli T and Sala P R 2005 *Astropart. Phys.* **23** 526
[819] Zhuang Y, Strigari L E and Lang R F 2022 *Phys. Rev.* D **105** 043001

[820] Janka H, Langanke K, Marek A, Martinezpinedo G and Muller B 2007 *Phys. Rep.* **442** 38
[821] Janka H-T 2012 *Annu. Rev. Nucl. Part. Sci.* **62** 407
[822] Krauss L M, Romanelli P, Schramm D and Lehrer R 1992 *Nucl. Phys.* B **380** 507
[823] Scholberg K 2012 *Annu. Rev. Nucl. Part. Sci.* **62** 81
[824] Baxter A L *et al* (SNEWS) 2021 *J. Open Source Softw.* **6** 67
[825] Freedman D Z, Schramm D N and Tubbs D L 1977 *Annu. Rev. Nucl. Sci.* **27** 167
[826] Muñoz V, Takhistov V, Witte S J and Fuller G M 2021 *J. Cosmol. Astropart. Phys.* JCAP11(2021)020
[827] Horowitz C J, Coakley K J and McKinsey D N 2003 *Phys. Rev.* D **68** 023005
[828] Abe K *et al* (XMASS) 2017 *Astropart. Phys.* **89** 51
[829] Chakraborty S, Bhattacharjee P and Kar K 2014 *Phys. Rev.* D **89** 013011
[830] Lang R F, McCabe C, Reichard S, Selvi M and Tamborra I 2016 *Phys. Rev.* D **94** 103009
[831] Raj N 2020 *Phys. Rev. Lett.* **124** 141802
[832] Pirinen P, Suhonen J and Ydrefors E 2018 *Adv. High Energy Phys.* **2018** 9163586
[833] Ydrefors E and Suhonen J 2015 *2015 Neutrinos and Dark Matter Conf.* (Jyväskylä, Finland) https://indico.cern.ch/event/394248/contributions/1831651/attachments/789193/1081737/ndm15_e_ydrefors.pdf
[834] Litvinovich E A, Machulin I N, Pugachev D A and Skorokhvatov M D 2017 *J. Phys.: Conf. Ser.* **798** 012117
[835] Bhattacharjee P and Kar K 2021 *Eur. Phys. J. ST* **230** 505
[836] Bhattacharjee P, Bandyopadhyay A, Chakraborty S, Ghosh S, Kar K and Saha S 2020 arXiv:2012.13986
[837] Suliga A M and Tamborra I 2021 *Phys. Rev.* D **103** 083002
[838] Raj N, Takhistov V and Witte S J 2020 *Phys. Rev.* D **101** 043008
[839] Odrzywolek A, Misiaszek M and Kutschera M 2004 *Astropart. Phys.* **21** 303
[840] Odrzywolek A, Misiaszek M and Kutschera M 2004 *Acta Phys. Pol.* B **35** 1981 arXiv:astro-ph/0405006
[841] Kato C, Ishidoshiro K and Yoshida T 2020 *Annu. Rev. Nucl. Part. Sci.* **70** 121
[842] Sieverding A, Rrapaj E, Guo G and Qian Y-Z 2021 *Astrophys. J.* **912** 13
[843] Mori K, Takiwaki T and Kotake K 2021 arXiv:2107.12661
[844] Ge S-F, Hamaguchi K, Ichimura K, Ishidoshiro K, Kanazawa Y, Kishimoto Y, Nagata N and Zheng J 2020 *J. Cosmol. Astropart. Phys.* JCAP11(2020)059
[845] The SNEWS Collaboration 2022 Homepage, SuperNova Early Warning System (http://snews.bnl.gov/)
[846] Antonioli P *et al* 2004 *New J. Phys.* **6** 114
[847] Al Kharusi S *et al* (SNEWS) 2021 *New J. Phys.* **23** 031201
[848] Baxter A L *et al* (Agile Scrum Development in an ad hoc Software Collaboration) 2021 arXiv:2101.07779
[849] Krauss L M, Glashow S L and Schramm D N 1984 *Nature* **310** 191
[850] Lunardini C 2016 *Astropart. Phys.* **79** 49
[851] Beacom J F 2010 *Annu. Rev. Nucl. Part. Sci.* **60** 439
[852] Horiuchi S, Beacom J F and Dwek E 2009 *Phys. Rev.* D **79** 083013
[853] Hopkins A M and Beacom J F 2006 *Astrophys. J.* **651** 142
[854] Bays K *et al* (Super-Kamiokande) 2012 *Phys. Rev.* D **85** 052007
[855] Suliga A M, Beacom J F and Tamborra I 2022 *Phys. Rev.* D **105** 043008
[856] Araki T *et al* 2005 *Nature* **436** 499
[857] Bellini G *et al* (Borexino) 2010 *Phys. Lett.* B **687** 299
[858] Bouchiat C and Piketty C A 1983 *Phys. Lett.* B **128** 73
[859] Cerdeño D G, Fairbairn M, Jubb T, Machado P A N, Vincent A C and Bœhm C 2016 *J. High Energy Phys.* JHEP05(2016)118
Cerdeño D G, Fairbairn M, Jubb T, Machado P A N, Vincent A C and Bœ hm C 2016 *J. High Energy Phys.* JHEP09(2016)048 (erratum)
[860] Cadeddu M, Dordei F, Giunti C, Li Y F and Zhang Y Y 2020 *Phys. Rev.* D **101** 033004
[861] Davoudiasl H, Lee H-S and Marciano W J 2014 *Phys. Rev.* D **89** 095006
[862] Aoyama T *et al* 2020 *Phys. Rep.* **887** 1
[863] Abi B *et al* (Muon g-2) 2021 *Phys. Rev. Lett.* **126** 141801
[864] de Gouvêa A, McGinness E, Martinez-Soler I and Perez-Gonzalez Y F 2021 arXiv:2111.02421
[865] Bhupal Dev P S *et al* 2019 Neutrino non-standard interactions: a status report *Phys. Proc.* **2** 001

[866] de Gouvêa A and Kelly K J 2016 *Nucl. Phys.* B **908** 318
[867] Datta A, Kumar J, Liao J and Marfatia D 2018 *Phys. Rev.* D **97** 115038
[868] Aristizabal Sierra D, De Romeri V, Flores L J and Papoulias D K 2020 *Phys. Lett.* B **809** 135681
[869] Khan A N 2020 *Phys. Lett.* B **809** 135782
[870] Fernandez-Moroni G, Harnik R, Machado P A N, Martinez-Soler I, Perez-Gonzalez Y F, Rodrigues D and Rosauro-Alcaraz S 2021 arXiv:2108.07310
[871] Goldhagen K, Maltoni M, Reichard S and Schwetz T 2021 arXiv:2109.14898
[872] Link J M and Xu X-J 2019 *J. High Energy Phys.* JHEP08(2019)004
[873] Krauss L M 1991 *Phys. Lett.* B **269** 407
[874] Khan A N, Rodejohann W and Xu X-J 2020 *Phys. Rev.* D **101** 055047
[875] Kamada A and Yu H-B 2015 *Phys. Rev.* D **92** 113004
[876] Dutta B, Lang R F, Liao S, Sinha S, Strigari L and Thompson A 2020 *J. High Energy Phys.* JHEP09(2020)106
[877] Abe T, Hamaguchi K and Nagata N 2021 *Phys. Lett.* B **815** 136174
[878] Abellan G F, Murgia R, Poulin V and Lavalle J 2020 arXiv:2008.09615
[879] Aboubrahim A, Klasen M and Nath P 2021 *J. High Energy Phys.* JHEP02(2021)229
[880] Alhazmi H, Kim D, Kong K, Mohlabeng G, Park J-C and Shin S 2021 *J. High Energy Phys.* JHEP05(2021)055
[881] Alonso-Álvarez G, Ertas F, Jaeckel J, Kahlhoefer F and Thormaehlen L J 2020 *J. Cosmol. Astropart. Phys.* JCAP11(2020)029
[882] Amaral D W P, Cerdeno D G, Foldenauer P and Reid E 2020 *J. High Energy Phys.* JHEP12(2020)155
[883] An H and Yang D 2021 *Phys. Lett.* B **818** 136408
[884] Anchordoqui L A, Antoniadis I, Benakli K and Lust D 2020 *Phys. Lett.* B **810** 135838
[885] Arcadi G, Bally A, Goertz F, Tame-Narvaez K, Tenorth V and Vogl S 2021 *Phys. Rev.* D **103** 023024
[886] Argüelles Delgado C A, Kelly K J and Muñoz Albornoz V 2021 *J. High Energy Phys.* JHEP11(2021)099
[887] Arias-Aragón F, D'Eramo F, Ferreira R Z, Merlo L and Notari A 2020 *J. Cosmol. Astropart. Phys.* JCAP11(2020)025
[888] Arias P, Arza A, Jaeckel J and Vargas-Arancibia D 2021 *J. Cosmol. Astropart. Phys.* JCAP05(2021)070
[889] Aristizabal Sierra D, Branada R, Miranda O G and Sanchez Garcia G 2020 *J. High Energy Phys.* JHEP12(2020)178
[890] Athron P *et al* 2021 *J. High Energy Phys.* JHEP05(2021)159
[891] Babu K S, Jana S and Lindner M 2020 *J. High Energy Phys.* JHEP10(2020)040
[892] Babu K S, Jana S, Lindner M and V P K 2021 *J. High Energy Phys.* JHEP10(2021)240
[893] Baek S, Kim J and Ko P 2020 *Phys. Lett.* B **810** 135848
[894] Baek S 2021 *J. High Energy Phys.* JHEP10(2021)135
[895] Bally A, Jana S and Trautner A 2020 *Phys. Rev. Lett.* **125** 161802
[896] Baryakhtar M, Berlin A, Liu H and Weiner N 2020 arXiv:2006.13918
[897] Baym G and Peng J-C 2021 *Phys. Rev. Lett.* **126** 191803
[898] Benakli K, Branchina C and Lafforgue-Marmet G 2020 *Eur. Phys. J.* C **80** 1118
[899] Bhattacherjee B and Sengupta R 2021 *Phys. Lett.* B **817** 136305
[900] Bloch I M, Caputo A, Essig R, Redigolo D, Sholapurkar M and Volansky T 2021 *J. High Energy Phys.* JHEP01(2021)178
[901] Boehm C, Cerdeno D G, Fairbairn M, Machado P A N and Vincent A C 2020 *Phys. Rev.* D **102** 115013
[902] Borah D, Mahapatra S, Nanda D and Sahu N 2020 *Phys. Lett.* B **811** 135933
[903] Borah D, Mahapatra S and Sahu N 2021 *Nucl. Phys.* B **968** 115407
[904] Borah D, Dutta M, Mahapatra S and Sahu N 2021 *Phys. Lett.* B **820** 136577
[905] Bramante J and Song N 2020 *Phys. Rev. Lett.* **125** 161805
[906] Brdar V, Greljo A, Kopp J and Opferkuch T 2021 *J. Cosmol. Astropart. Phys.* JCAP01(2021)039
[907] Buch J, Buen-Abad M A, Fan J and Leung J S C 2020 *J. Cosmol. Astropart. Phys.* JCAP10(2020)051
[908] Budnik R, Kim H, Matsedonskyi O, Perez G and Soreq Y 2020 arXiv:2006.14568
[909] Buttazzo D, Panci P, Teresi D and Ziegler R 2021 *Phys. Lett.* B **817** 136310
[910] Cai R-G, Sun S, Zhang B and Zhang Y-L 2020 arXiv:2009.02315

[911] Cao Q-H, Ding R and Xiang Q-F 2021 *Chin. Phys.* C **45** 045002
[912] Cao J, Du X, Li Z, Wang F and Zhang Y 2020 arXiv:2007.09981
[913] Chakraborty S, Jung T H, Loladze V, Okui T and Tobioka K 2020 *Phys. Rev.* D **102** 095029
[914] Chala M and Titov A 2020 *J. High Energy Phys.* JHEP09(2020)188
[915] Chao W, Gao Y and Jin M j 2020 arXiv:2006.16145
[916] Chen Y, Cui M-Y, Shu J, Xue X, Yuan G-W and Yuan Q 2021 *J. High Energy Phys.* JHEP04(2021)282
[917] Chen M, Gelmini G B and Takhistov V 2021 *J. Cosmol. Astropart. Phys.* JCAP12(2021)048
[918] Chen Z, Li T and Liao J 2021 *J. High Energy Phys.* JHEP05(2021)131
[919] Chiang C-W and Lu B-Q 2020 *Phys. Rev.* D **102** 123006
[920] Chigusa S, Endo M and Kohri K 2020 *J. Cosmol. Astropart. Phys.* JCAP10(2020)035
[921] Choi G, Yanagida T T and Yokozaki N 2020 *Phys. Lett.* B **810** 135836
[922] Choi G, Suzuki M and Yanagida T T 2020 *Phys. Lett.* B **811** 135976
[923] Choi S-M, Lee H M and Zhu B 2021 *J. High Energy Phys.* JHEP04(2021)251
[924] Choudhury D, Maharana S, Sachdeva D and Sahdev V 2021 *Phys. Rev.* D **103** 015006
[925] Coloma P, Huber P and Link J M 2020 arXiv:2006.15767
[926] Croon D, McDermott S D and Sakstein J 2021 *Phys. Dark Universe* **32** 100801
[927] Davighi J, McCullough M and Tooby-Smith J 2020 *J. High Energy Phys.* JHEP11(2020)120
[928] Davoudiasl H, Denton P B and Gehrlein J 2020 *Phys. Rev.* D **102** 091701
[929] Delle Rose L, Hütsi G, Marzo C and Marzola L 2021 *J. Cosmol. Astropart. Phys.* JCAP02(2021)031
[930] DeRocco W, Graham P W and Rajendran S 2020 *Phys. Rev.* D **102** 075015
[931] Dessert C, Foster J W, Kahn Y and Safdi B R 2021 *Phys. Dark Universe* **34** 100878
[932] Dey U K, Maity T N and Ray T S 2020 *Phys. Lett.* B **811** 135900
[933] Di Luzio L, Fedele M, Giannotti M, Mescia F and Nardi E 2020 *Phys. Rev. Lett.* **125** 131804
[934] Du P, Egana-Ugrinovic D, Essig R and Sholapurkar M 2022 *Phys. Rev.* X **12** 011009
[935] Du M, Liang J, Liu Z, Tran V Q and Xue Y 2021 *Chin. Phys.* C **45** 013114
[936] Dutta K, Ghosh A, Kar A and Mukhopadhyaya B 2021 arXiv:2103.14664
[937] Dutta M, Mahapatra S, Borah D and Sahu N 2021 *Phys. Rev.* D **103** 095018
[938] Ema Y, Sala F and Sato R 2021 *Eur. Phys. J.* C **81** 129
[939] Escribano P and Vicente A 2021 *J. High Energy Phys.* JHEP03(2021)240
[940] Farzan Y and Rajaee M 2020 *Phys. Rev.* D **102** 103532
[941] Fayet P 2021 *Phys. Rev.* D **103** 035034
[942] Fonseca N and Morgante E 2021 *Phys. Rev.* D **103** 015011
[943] Foot R 2020 arXiv:2011.02590
[944] Fornal B, Sandick P, Shu J, Su M and Zhao Y 2020 *Phys. Rev. Lett.* **125** 161804
[945] Gao C, Liu J, Wang L-T, Wang X-P, Xue W and Zhong Y-M 2020 *Phys. Rev. Lett.* **125** 131806
[946] Lin Y, Gao Y and Li T 2020 arXiv:2006.16192
[947] Ge S-F, Pasquini P and Sheng J 2020 *Phys. Lett.* B **810** 135787
[948] Guo G, Tsai Y-L S, Wu M-R and Yuan Q 2020 *Phys. Rev.* D **102** 103004
[949] Han C, López-Ibáñez M L, Melis A, Vives O and Yang J M 2021 *Phys. Rev.* D **103** 035028
[950] Harigaya K, Nakai Y and Suzuki M 2020 *Phys. Lett.* B **809** 135729
[951] Harnik R, Plestid R, Pospelov M and Ramani H 2021 *Phys. Rev.* D **103** 075029
[952] Haselschwardt S J, Kostensalo J, Mougeot X and Suhonen J 2020 *Phys. Rev.* C **102** 065501
[953] Hayen L, Simonucci S and Taioli S 2020 arXiv:2009.08303
[954] He H-J, Wang Y-C and Zheng J 2021 *Phys. Rev.* D **104** 115033
[955] He H-J, Wang Y-C and Zheng J 2021 *J. Cosmol. Astropart. Phys.* JCAP01(2021)042
[956] Hoof S, Jaeckel J and Thormaehlen L J 2021 *J. Cosmol. Astropart. Phys.* JCAP09(2021)006
[957] Hryczuk A and Jodłowski K 2020 *Phys. Rev.* D **102** 043024
[958] Ibe M, Kobayashi S, Nakayama Y and Shirai S 2020 *J. High Energy Phys.* JHEP12(2020)004
[959] Ilie C and Levy C 2021 *Phys. Rev.* D **104** 083033
[960] İnan S C and Kisselev A V 2021 *Chin. Phys.* C **45** 043109
[961] Jaeckel J and Yin W 2021 *J. Cosmol. Astropart. Phys.* JCAP02(2021)044
[962] Jeong J, Kim J E and Youn S 2021 *Int. J. Mod. Phys.* A **36** 2150182
[963] Jho Y, Park J-C, Park S C and Tseng P-Y 2020 *Phys. Lett.* B **811** 135863
[964] Jia L-B and Li T 2020 arXiv:2012.07209
[965] Kahlhoefer F 2021 *Proc. Sci.* **390** 635
[966] Kannike K, Raidal M, Veermäe H, Strumia A and Teresi D 2020 *Phys. Rev.* D **102** 095002

[967] Karmakar S and Pandey S 2020 arXiv:2007.11892
[968] Karozas A, King S F, Leontaris G K and Papoulias D K 2021 *Phys. Rev.* D **103** 035019
[969] Keung W-Y, Marfatia D and Tseng P-Y 2021 *J. High Energy Astrophys.* **30** 9
[970] Khan A N 2021 *Phys. Lett.* B **819** 136415
[971] Khan S 2021 *Eur. Phys. J.* C **81** 598
[972] Khruschov V V 2020 arXiv:2008.03150
[973] Kim J, Nomura T and Okada H 2020 *Phys. Lett.* B **811** 135862
[974] Ko P and Tang Y 2021 *Phys. Lett.* B **815** 136181
[975] Lee H M 2021 *J. High Energy Phys.* JHEP01(2021)019
[976] Li T 2020 arXiv:2007.00874
[977] Lin T 2020 *APS Phys.* **13** 135
[978] Lindner M, Mambrini Y, de Melo T B and Queiroz F S 2020 *Phys. Lett.* B **811** 135972
[979] Long H N, Soa D V, Binh V H and Cárcamo Hernández A E 2020 arXiv:2007.05004
[980] McKeen D, Pospelov M and Raj N 2020 *Phys. Rev. Lett.* **125** 231803
[981] Miranda O G, Papoulias D K, Tórtola M and Valle J W F 2020 *Phys. Lett.* B **808** 135685
[982] Nakayama K and Tang Y 2020 *Phys. Lett.* B **811** 135977
[983] Okada N, Okada S, Raut D and Shafi Q 2020 *Phys. Lett.* B **810** 135785
[984] Paz G, Petrov A A, Tammaro M and Zupan J 2021 *Phys. Rev.* D **103** L051703
[985] Robinson A E 2020 arXiv:2006.13278
[986] Seymour B C and Yagi K 2020 *Phys. Rev.* D **102** 104003
[987] Shakeri S, Hajkarim F and Xue S-S 2020 *J. High Energy Phys.* JHEP12(2020)194
[988] Shoemaker I M, Tsai Y-D and Wyenberg J 2021 *Phys. Rev.* D **104** 115026
[989] Straniero O, Pallanca C, Dalessandro E, Domínguez I, Ferraro F R, Giannotti M, Mirizzi A and Piersanti L 2020 *Astron. Astrophys.* **644** A166
[990] Studenikin A 2021 *Proc. Sci.* **390** 180
[991] Su L, Wang W, Wu L, Yang J M and Zhu B 2020 *Phys. Rev.* D **102** 115028
[992] Sun J and He X-G 2020 *Phys. Lett.* B **811** 135881
[993] Szydagis M, Levy C, Blockinger G M, Kamaha A, Parveen N and Rischbieter G R C 2021 *Phys. Rev.* D **103** 012002
[994] Takahashi F, Yamada M and Yin W 2020 *Phys. Rev. Lett.* **125** 161801
[995] Takahashi F, Yamada M and Yin W 2021 *J. High Energy Phys.* JHEP01(2021)152
[996] Tan H B T, Derevianko A, Dzuba V A and Flambaum V V 2021 *Phys. Rev. Lett.* **127** 081301
[997] Vagnozzi S, Visinelli L, Brax P, Davis A-C and Sakstein J 2021 *Phys. Rev.* D **104** 063023
[998] Van Dong P, Nam C H and Van Loi D 2021 *Phys. Rev.* D **103** 095016
[999] Xu S and Zheng S 2021 *Eur. Phys. J.* C **81** 446
[1000] Ye Z, Zhang F, Xu D and Liu J 2021 *Chin. Phys. Lett.* **38** 111401
[1001] Lei Z-H, Tang J and Zhang B-L 2020 arXiv:2008.07116
[1002] Zioutas K, Cantatore G, Karuza M, Kryemadhi A, Maroudas M and Semertzidis Y K 2020 arXiv:2006.16907
[1003] Zu L, Foot R, Fan Y-Z and Feng L 2021 *J. Cosmol. Astropart. Phys.* JCAP01(2021)070
[1004] Zu L, Yuan G-W, Feng L and Fan Y-Z 2021 *Nucl. Phys.* B **965** 115369
[1005] Ipser J and Sikivie P 1983 *Phys. Rev. Lett.* **50** 925
[1006] Duffy L D and van Bibber K 2009 *New J. Phys.* **11** 105008
[1007] Krauss L, Moody J, Wilczek F and Morris D E 1985 *Phys. Rev. Lett.* **55** 1797
[1008] Hagmann C, Sikivie P, Sullivan N S and Tanner D B 1990 *Phys. Rev.* D **42** 1297
[1009] Sikivie P 2000 *Nucl. Phys.* B **87** 41
[1010] Raffelt G G 2007 *J. Phys. A: Math. Theor.* **40** 6607
[1011] Aune S *et al* (CAST) 2011 *Phys. Rev. Lett.* **107** 261302
[1012] Du N *et al* (ADMX) 2018 *Phys. Rev. Lett.* **120** 151301
[1013] Hagmann C *et al* (ADMX) 1998 *Phys. Rev. Lett.* **80** 2043
[1014] Krauss L M, Moody J E and Wilczek F 1984 *Phys. Lett.* B **144** 391
[1015] Dimopoulos S, Frieman J, Lynn B W and Starkman G D 1986 *Phys. Lett.* B **179** 223
[1016] Kim J E 1979 *Phys. Rev. Lett.* **43** 103
[1017] Shifman M A, Vainshtein A I and Zakharov V I 1980 *Nucl. Phys.* B **166** 493
[1018] Dine M, Fischler W and Srednicki M 1981 *Phys. Lett.* B **104** 199
[1019] Zhitnitsky A R 1980 *Sov. J. Nucl. Phys.* **31** 260
Zhitnitsky A R 1980 *Yad. Fiz.* **31** 497
[1020] Redondo J 2013 *J. Cosmol. Astropart. Phys.* JCAP12(2013)008

[1021] Primakoff H 1951 *Phys. Rev.* **81** 899
[1022] Moriyama S 1995 *Phys. Rev. Lett.* **75** 3222
[1023] Armengaud E *et al* (IAXO) 2019 *J. Cosmol. Astropart. Phys.* JCAP06(2019)047
[1024] Ahmed Z *et al* (CDMS) 2009 *Phys. Rev. Lett.* **103** 141802
[1025] Abe K *et al* (XMASS) 2013 *Phys. Lett.* B **724** 46
[1026] Harnik R, Kopp J and Machado P A N 2012 *J. Cosmol. Astropart. Phys.* JCAP07(2012)026
[1027] Schwemberger T and Yu T-T 2022 Detecting beyond the standard model interactions of solar neutrinos in low-threshold dark matter detectors (arXiv:2202.01254)
[1028] Chen J-W, Chi H-C, Liu C-P and Wu C-P 2017 *Phys. Lett.* B **774** 656
[1029] Agostini M *et al* (Borexino) 2017 *Phys. Rev.* D **96** 091103
[1030] Bellini G *et al* 2011 *Phys. Rev. Lett.* **107** 141302
[1031] Beda A G, Brudanin V B, Egorov V G, Medvedev D V, Shirchenko M V, Starostin A S, Shirchenko M V and Vylov T 2010 *Phys. Part. Nuclei Lett.* **7** 406
[1032] Abe K *et al* (XMASS) 2020 *Phys. Lett.* B **809** 135741
[1033] Aguilar-Arevalo A *et al* (CONNIE) 2016 *J. Phys.: Conf. Ser.* **761** 012057
[1034] Coloma P, Huber P and Link J M 2014 *J. High Energy Phys.* JHEP11(2014)042
[1035] Dirac P A M 1931 *Proc. R. Soc.* A **133** 60
[1036] Pati J C and Salam A 1973 *Phys. Rev.* D **8** 1240
[1037] Georgi H and Glashow S L 1974 *Phys. Rev. Lett.* **32** 438
[1038] Dobroliubov M I and Ignatiev A Y 1990 *Phys. Rev. Lett.* **65** 679
[1039] Prinz A A *et al* 1998 *Phys. Rev. Lett.* **81** 1175
[1040] Davidson S, Hannestad S and Raffelt G 2000 *J. High Energy Phys.* JHEP05(2000)003
[1041] Prinz A A 2001 *PhD Thesis* Stanford University http://lib.umi.com/dissertations/fullcit?p3002033
[1042] Golowich E and Robinett R W 1987 *Phys. Rev.* D **35** 391
[1043] Babu K S, Gould T M and Rothstein I Z 1994 *Phys. Lett.* B **321** 140
[1044] Gninenko S N, Krasnikov N V and Rubbia A 2007 *Phys. Rev.* D **75** 075014
[1045] Chatrchyan S *et al* (CMS) 2013 *Phys. Rev.* D **87** 092008
[1046] Agnese R *et al* (CDMS) 2015 *Phys. Rev. Lett.* **114** 111302
[1047] Haas A, Hill C S, Izaguirre E and Yavin I 2015 *Phys. Lett.* B **746** 117
[1048] Ball A *et al* 2016 arXiv:1607.04669
[1049] Alvis S I *et al* (Majorana) 2018 *Phys. Rev. Lett.* **120** 211804
[1050] Magill G, Plestid R, Pospelov M and Tsai Y-D 2019 *Phys. Rev. Lett.* **122** 071801
[1051] Kelly K J and Tsai Y-D 2019 *Phys. Rev.* D **100** 015043
[1052] Berlin A, Blinov N, Krnjaic G, Schuster P and Toro N 2019 *Phys. Rev.* D **99** 075001
[1053] Dienes K R, Kolda C and March-Russell J 1997 *Nucl. Phys.* B **492** 104
[1054] Abel S A, Goodsell M D, Jaeckel J, Khoze V V and Ringwald A 2008 *J. High Energy Phys.* JHEP07(2008)124
[1055] Dubovsky S L, Gorbunov D S and Rubtsov G I 2004 *JETP Lett.* **79** 1
[1056] Pospelov M and Ramani H 2021 *Phys. Rev.* D **103** 115031
[1057] Shiu G, Soler P and Ye F 2013 *Phys. Rev. Lett.* **110** 241304
[1058] Babu K S *et al* 2013 *Proc., 2013 Community Summer Study on the Future of U.S. Particle Physics: Snowmass on the Mississippi (CSS2013)* (Minneapolis, MN, USA 29 July–6 August 2013)
[1059] Bernabei R *et al* 2000 *Phys. Lett.* B **493** 12
[1060] Bernabei R *et al* 2006 *Eur. Phys. J.* A **27** 35
[1061] Albert J B *et al* (EXO-200) 2018 *Phys. Rev.* D **97** 072007
[1062] Mohapatra R N and Perez-Lorenzana A 2003 *Phys. Rev.* D **67** 075015
[1063] Abazajian K N 2017 *Phys. Rep.* **711–712** 1
[1064] Diaz A, Argüelles C A, Collin G H, Conrad J M and Shaevitz M H 2019 arXiv:1906.00045
[1065] Mei D and Hime A 2006 *Phys. Rev.* D **73** 053004
[1066] Kudryavtsev V A, Pandola L and Tomasello V 2008 *Eur. Phys. J.* A **36** 171
[1067] Bettini A 2014 *Phys. Dark Universe* **4** 36
[1068] Votano L 2012 *Eur. Phys. J. Plus* **127** 109
[1069] Wu J, Li J, Yao Y and Qi Z 2013 *J. Semicond.* **34** 086001
[1070] Cheng J-P *et al* 2017 *Annu. Rev. Nucl. Part. Sci.* **67** 231
[1071] Polaczek-Grelik K *et al* 2020 *Nucl. Instrum. Methods Phys. Res.* A **969** 164015
[1072] Trzaska W H *et al* 2019 *Eur. Phys. J.* C **79** 721
[1073] Morales J *et al* 2005 *Identif. Dark Matter* 447pp –52

[1074] Zhang C and Mei D-M 2014 *Phys. Rev.* D **90** 122003
[1075] Zhang Y *et al* (Super-Kamiokande) 2016 *Phys. Rev.* D **93** 012004
[1076] Tang A, Horton-Smith G, Kudryavtsev V A and Tonazzo A 2006 *Phys. Rev.* D **74** 053007
[1077] Reichhart L *et al* 2013 *Astropart. Phys.* **47** 67
[1078] Agostini M *et al* (Borexino) 2019 *J. Cosmol. Astropart. Phys.* JCAP02(2019)046
[1079] Abgrall N *et al* (MAJORANA) 2017 *Astropart. Phys.* **93** 70
[1080] Cherry M L, Deakyne M, Lande K, Lee C K, Steinberg R I, Cleveland B and Fenyves E J 1983 *Phys. Rev.* D **27** 1444
[1081] Berger C *et al* (FREJUS) 1989 *Phys. Rev.* D **40** 2163
[1082] Aharmim B *et al* (SNO) 2009 *Phys. Rev.* D **80** 012001
[1083] Guo Z-y *et al* (JNE) 2021 *Chin. Phys.* C **45** 025001
[1084] Bettini A 2007 arXiv:0712.1051
[1085] Li J, Ji X, Haxton W and Wang J S Y 2015 *Phys. Proc.* **61** 576
[1086] Heise J 2017 *15th Int. Conf. on Topics in Astroparticle and Underground Physics (TAUP 2017)* (Sudbury, Ontario, Canada 24–28 July 2017)
[1087] Paling S and Sadler S 2015 *Phys. World* **28** 23
[1088] Piquemal F 2012 *Eur. Phys. J. Plus* **127** 110
[1089] Lawson I, Smith N and Vazquez Jauregui E 2012 *Nucl. Phys. News* **23** 5
[1090] Aprile E *et al* (XENON100) 2011 *Phys. Rev.* D **83** 082001
Aprile E *et al* (XENON100) 2012 *Phys. Rev.* D **85** 029904 (erratum)
[1091] Akerib D S *et al* (LZ) 2020 *Nucl. Instrum. Methods Phys. Res.* A **953** 163047
[1092] Akerib D S *et al* (LUX) 2017 *J. Inst.* **12** P11022
[1093] Aprile E *et al* (XENON) 2017 *Eur. Phys. J.* C **77** 890
[1094] Akerib D S *et al* (LZ) 2020 *Eur. Phys. J.* C **80** 1044
[1095] Aprile E *et al* (XENON) 2021 *Eur. Phys. J.* C **81** 337
[1096] Wang Z, Bao L, Hao X and Ju Y 2014 *Rev. Sci. Instrum.* **85** 015116
[1097] Aprile E *et al* (XENON) 2017 *Eur. Phys. J.* C **77** 275
[1098] Bolozdynya A I, Brusov P P, Shutt T, Dahl C E and Kwong J 2007 *Nucl. Instrum. Methods Phys. Res.* A **579** 50
[1099] Akerib D S *et al* (LUX) 2018 *Astropart. Phys.* **97** 80
[1100] Aprile E *et al* (XENON) 2021 arXiv:2112.12231
[1101] Lindemann S and Simgen H 2014 *Eur. Phys. J.* C **74** 2746
[1102] Aprile E *et al* (XENON100) 2017 *Eur. Phys. J.* C **77** 358
[1103] Murra M, Schulte D, Huhmann C and Weinheimer C 2022 arXiv:2205.11492
[1104] Schulte D, Murra M, Schulte P, Huhmann C and Weinheimer C 2021 *J. Inst.* **16** P09011
[1105] Burenkov A A, Akimov D Y, Grishkin Y L, Kovalenko A G, Lebedenko V N, Solovov V N, Stekhanov V N, Neves F and Sumner T J 2009 *Phys. Atom. Nuclei* **72** 653
[1106] Santos E *et al* (ZEPLIN-III) 2011 *J. High Energy Phys.* JHEP12(2011)115
[1107] Angle J *et al* (XENON10) 2011 *Phys. Rev. Lett.* **107** 051301
Angle J *et al* (XENON10) 2013 *Phys. Rev. Lett.* **110** 249901 (erratum)
[1108] Edwards B *et al* 2008 *Astropart. Phys.* **30** 54
[1109] Edwards B N V *et al* 2018 *J. Inst.* **13** P01005
[1110] Xu J, Pereverzev S, Lenardo B, Kingston J, Naim D, Bernstein A, Kazkaz K and Tripathi M 2019 *Phys. Rev.* D **99** 103024
[1111] Tomás A, Araújo H M, Bailey A J, Bayer A, Chen E, López Paredes B and Sumner T J 2018 *Astropart. Phys.* **103** 49
[1112] Aprile E *et al* (XENON) 2019 *Phys. Rev.* D **99** 112009
[1113] Agostinelli S *et al* (GEANT4) 2003 *Nucl. Instrum. Methods Phys. Res.* A **506** 250
[1114] Hagiwara K *et al* 2019 *Prog. Theor. Exp. Phys.* **2019** 023D01
[1115] Tanaka T *et al* 2020 *Prog. Theor. Exp. Phys.* **2020** 043D02
[1116] Bečvář F 1998 *Nucl. Instrum. Methods Phys. Res.* A **417** 434
[1117] Akerib D S *et al* (LUX-ZEPLIN) 2021 *Astropart. Phys.* **125** 102480
[1118] Sorensen P *et al* 2011 *Proc. Sci.* **110** 017
[1119] Akerib D S *et al* (LUX) 2016 arXiv:1608.05381
[1120] Akerib D S *et al* (LUX) 2019 *Phys. Rev.* D **100** 022002
[1121] Akerib D S *et al* (LUX) 2016 *Phys. Rev.* D **93** 072009
[1122] Akerib D S *et al* (LUX) 2017 *Phys. Rev.* D **96** 112011
[1123] Akerib D S *et al* (LUX) 2017 *Phys. Rev.* D **95** 012008

[1124] Aprile E *et al* (XENON) 2018 *Phys. Rev.* D **97** 092007
[1125] Boulton E M *et al* 2017 *J. Inst.* **12** P08004
[1126] Aprile E *et al* (XENON100) 2011 *Phys. Rev.* D **84** 052003
[1127] Mock J, Barry N, Kazkaz K, Stolp D, Szydagis M, Tripathi M, Uvarov S, Woods M and Walsh N 2014 *J. Inst.* **9** T04002
[1128] Singh A G *et al* 2020 *J. Inst.* **15** P01023
[1129] Plante G, Aprile E, Budnik R, Choi B, Giboni K L, Goetzke L W, Lang R F, Lim K E and Melgarejo Fernandez A J 2011 *Phys. Rev.* C **84** 045805
[1130] Goetzke L W, Aprile E, Anthony M, Plante G and Weber M 2017 *Phys. Rev.* D **96** 103007
[1131] Baudis L, Biondi Y, Capelli C, Galloway M, Kazama S, Kish A, Pakarha P, Piastra F and Wulf J 2018 *Eur. Phys. J.* C **78** 351
[1132] Temples D J 2019 Understanding Neutrino Background Implications in LXe-TPC Dark Matter Searches Using ^{127}Xe Electron Captures (TAUP 2019) http://kam2.icrr.u-tokyo.ac.jp/indico/event/3/session/10/contribution/414/material/slides/0.pdf
[1133] Temples D J, McLaughlin J, Bargemann J, Baxter D, Cottle A, Dahl C E, Lippincott W H, Monte A and Phelan J 2021 *Phys. Rev.* D **104** 112001
[1134] Lang R F, Brown A, Brown E, Cervantes M, Macmullin S, Masson D, Schreiner J and Simgen H 2016 *J. Inst.* **11** P04004
[1135] Aprile E *et al* (XENON) 2017 *Phys. Rev.* D **95** 072008
[1136] Collar J I 2013 *Phys. Rev. Lett.* **110** 211101
[1137] Aprile E *et al* (XENON100) 2013 *Phys. Rev.* D **88** 012006
[1138] Srednicki M, Watkins R and Olive K A 1988 *Nucl. Phys.* B **310** 693
Srednicki M, Watkins R and Olive K A 1988 *Nucl. Phys.* B **310** 247
[1139] Feng J L 2010 *Annu. Rev. Astron. Astrophys.* **48** 495
[1140] Profumo S, Shepherd W and Tait T 2013 *Phys. Rev.* D **88** 056018
[1141] Evans L and Bryant P 2008 *J. Inst.* **3** S08001
[1142] Golfand Y A and Likhtman E P 1971 *JETP Lett.* **13** 323
Golfand Y A and Likhtman E P 1971 *Pisma Zh. Eksp. Teor. Fiz.* **13** 452
[1143] Clavelli L and Ramond P 1971 *Phys. Rev.* D **3** 988
[1144] Penning B 2018 *J. Phys. G: Nucl. Part. Phys.* **45** 063001
[1145] Bonilla J, Brivio I, Machado-Rodríguez J and de Trocóniz J F 2022 arXiv:2202.03450
[1146] Aaij R *et al* (LHCb) 2018 *Phys. Rev. Lett.* **120** 061801
[1147] Finkbeiner D P, Galli S, Lin T and Slatyer T R 2012 *Phys. Rev.* D **85** 043522
[1148] Galli S, Slatyer T R, Valdes M and Iocco F 2013 *Phys. Rev.* D **88** 063502
[1149] Boyarsky A, Malyshev D, Neronov A and Ruchayskiy O 2008 *Mon. Not. R. Astron. Soc.* **387** 1345
[1150] Yüksel H, Beacom J F and Watson C R 2008 *Phys. Rev. Lett.* **101** 121301
[1151] Perez K, Ng K C Y, Beacom J F, Hersh C, Horiuchi S and Krivonos R 2017 *Phys. Rev.* D **95** 123002
[1152] Gunn J E, Lee B W, Lerche I, Schramm D N and Steigman G 1978 *Astrophys. J.* **223** 1015
Gunn J E, Lee B W, Lerche I, Schramm D N and Steigman G 1978 *Astrophys. J.* **223** 190
[1153] Stecker F W 1978 *Astrophys. J.* **223** 1032
[1154] Berezinsky V, Bottino A and Mignola G 1994 *Phys. Lett.* B **325** 136
[1155] Bergström L, Ullio P and Buckley J H 1998 *Astropart. Phys.* **9** 137
[1156] Gondolo P and Silk J 1999 *Phys. Rev. Lett.* **83** 1719
[1157] Gehrels N and Michelson P 1999 *Astropart. Phys.* **11** 277
[1158] Cesarini A, Fucito F, Lionetto A, Morselli A and Ullio P 2004 *Astropart. Phys.* **21** 267
[1159] Peirani S, Mohayaee R and de Freitas Pacheco J A 2004 *Phys. Rev.* D **70** 043503
[1160] Dodelson S, Hooper D and Serpico P D 2008 *Phys. Rev.* D **77** 063512
[1161] Actis M *et al* (CTA Consortium) 2011 *Exp. Astron.* **32** 193
[1162] Cholis I, Hooper D and McDermott S D 2014 *J. Cosmol. Astropart. Phys.* JCAP02(2014)014
[1163] Ando S and Ishiwata K 2015 *J. Cosmol. Astropart. Phys.* JCAP05(2015)024
[1164] Ackermann M *et al* (Fermi-LAT) 2015 *J. Cosmol. Astropart. Phys.* JCAP09(2015)008
[1165] Di Mauro M and Donato F 2015 *Phys. Rev.* D **91** 123001
[1166] Ajello M *et al* 2015 *Astrophys. J. Lett.* **800** L27
[1167] Abdallah H *et al* (HESS) 2016 *Phys. Rev. Lett.* **117** 111301
[1168] Ahnen M *et al* (MAGIC, Fermi-LAT) 2016 *J. Cosmol. Astropart. Phys.* JCAP02(2016)039
[1169] Zitzer B (VERITAS) 2016 *Proc. Sci.* **282** 446

[1170] Blanco C, Harding J P and Hooper D 2018 *J. Cosmol. Astropart. Phys.* JCAP04(2018)060
[1171] Archambault S *et al* (VERITAS) 2017 *Phys. Rev.* D **95** 082001
[1172] Lisanti M, Mishra-Sharma S, Rodd N L and Safdi B R 2018 *Phys. Rev. Lett.* **120** 101101
[1173] Ahnen M *et al* (MAGIC) 2018 *J. Cosmol. Astropart. Phys.* JCAP03(2018)009
[1174] Abeysekara A *et al* (HAWC) 2018 *J. Cosmol. Astropart. Phys.* JCAP02(2018)049
[1175] Blanco C and Hooper D 2019 *J. Cosmol. Astropart. Phys.* JCAP03(2019)019
[1176] Abdalla H *et al* (HESS) 2018 *J. Cosmol. Astropart. Phys.* JCAP11(2018)037
[1177] Abdallah H *et al* (HESS) 2018 *Phys. Rev. Lett.* **120** 201101
[1178] Blanco C, Delos M S, Erickcek A L and Hooper D 2019 *Phys. Rev.* D **100** 103010
[1179] Aguilar M *et al* (AMS) 2016 *Phys. Rev. Lett.* **117** 091103
[1180] Cuoco A, Krämer M and Korsmeier M 2017 *Phys. Rev. Lett.* **118** 191102
[1181] Cui M-Y, Yuan Q, Tsai Y-L S and Fan Y-Z 2017 *Phys. Rev. Lett.* **118** 191101
[1182] Cuoco A, Heisig J, Korsmeier M and Krämer M 2017 *J. Cosmol. Astropart. Phys.* JCAP10(2017)053
[1183] Cuoco A, Heisig J, Korsmeier M and Krämer M 2018 *J. Cosmol. Astropart. Phys.* JCAP04(2018)004
[1184] Cui M-Y, Pan X, Yuan Q, Fan Y-Z and Zong H-S 2018 *J. Cosmol. Astropart. Phys.* JCAP06(2018)024
[1185] Cholis I, Goodenough L, Hooper D, Simet M and Weiner N 2009 *Phys. Rev.* D **80** 123511
[1186] Bergström L, Bringmann T and Edsjö J 2008 *Phys. Rev.* D **78** 103520
[1187] Harnik R and Kribs G D 2009 *Phys. Rev.* D **79** 095007
[1188] Cirelli M and Strumia A 2008 *Proc. Sci.* **064** 089
[1189] Hooper D, Blasi P and Serpico P D 2009 *J. Cosmol. Astropart. Phys.* JCAP01(2009)025
[1190] Silk J, Olive K and Srednicki M 1985 *Phys. Rev. Lett.* **55** 257
[1191] Hagelin J S, Ng K W and Olive K A 1986 *Phys. Lett.* B **180** 375
[1192] Freese K 1986 *Phys. Lett.* B **167** 295
[1193] Krauss L M, Srednicki M and Wilczek F 1986 *Phys. Rev.* D **33** 2079
[1194] Gaisser T K, Steigman G and Tilav S 1986 *Phys. Rev.* D **34** 2206
[1195] Desai S *et al* (Super-Kamiokande) 2004 *Phys. Rev.* D **70** 083523
Desai S *et al* (Super-Kamiokande) 2004 *Phys. Rev.* D **70** 109901 (erratum)
[1196] Palomares-Ruiz S 2008 *Phys. Lett.* B **665** 50
[1197] Murase K and Beacom J F 2012 *J. Cosmol. Astropart. Phys.* JCAP10(2012)043
[1198] Aartsen M G *et al* (IceCube) 2017 *Eur. Phys. J.* C **77** 146
Aartsen M G *et al* (IceCube) 2019 *Eur. Phys. J.* C **79** 214 (erratum)
[1199] Aartsen M G *et al* (IceCube) 2017 *Eur. Phys. J.* C **77** 82
[1200] Aartsen M G *et al* (IceCube) 2016 *Eur. Phys. J.* C **76** 531
[1201] Aartsen M G *et al* (IceCube) 2017 *Eur. Phys. J.* C **77** 627
[1202] Ellis J, Flores R A, Freese K, Ritz S, Seckel D and Silk J 1988 *Phys. Lett.* B **214** 403
[1203] Donato F, Fornengo N and Salati P 2000 *Phys. Rev.* D **62** 043003
[1204] Fuke H *et al* 2005 *Phys. Rev. Lett.* **95** 081101
[1205] Donato F, Fornengo N and Maurin D 2008 *Phys. Rev.* D **78** 043506
[1206] Ibarra A and Wild S 2013 *Phys. Rev.* D **88** 023014
[1207] Hryczuk A, Cholis I, Iengo R, Tavakoli M and Ullio P 2014 *J. Cosmol. Astropart. Phys.* JCAP07(2014)031
[1208] Carlson E, Coogan A, Linden T, Profumo S, Ibarra A and Wild S 2014 *Phys. Rev.* D **89** 076005
[1209] Aramaki T *et al* (GAPS) 2016 *Astropart. Phys.* **74** 6
[1210] Korsmeier M, Donato F and Fornengo N 2018 *Phys. Rev.* D **97** 103011
[1211] Reinert A and Winkler M W 2018 *J. Cosmol. Astropart. Phys.* JCAP01(2018)055
[1212] Argüelles C A, Diaz A, Kheirandish A, Olivares-Del-Campo A, Safa I and Vincent A C 2021 *Rev. Mod. Phys.* **93** 035007
[1213] Hisano J, Matsumoto S, Nojiri M M and Saito O 2005 *Phys. Rev.* D **71** 063528
[1214] Gelmini G, Gondolo P, Soldatenko A and Yaguna C E 2006 *Phys. Rev.* D **74** 083514
[1215] Gelmini G B and Gondolo P 2006 *Phys. Rev.* D **74** 023510
[1216] Merle A, Niro V and Schmidt D 2014 *J. Cosmol. Astropart. Phys.* JCAP03(2014)028
[1217] König J, Merle A and Totzauer M 2016 *J. Cosmol. Astropart. Phys.* JCAP11(2016)038
[1218] Graesser M L, Shoemaker I M and Vecchi L 2011 *J. High Energy Phys.* JHEP10(2011)110
[1219] Lin T, Yu H-B and Zurek K M 2012 *Phys. Rev.* D **85** 063503
[1220] Iminniyaz H, Drees M and Chen X 2011 *J. Cosmol. Astropart. Phys.* JCAP07(2011)003

[1221] Griest K and Seckel D 1991 *Phys. Rev.* D **43** 3191
[1222] Edsjö J and Gondolo P 1997 *Phys. Rev.* D **56** 1879
[1223] Ellis J, Falk T and Olive K A 1998 *Phys. Lett.* B **444** 367
[1224] Fornengo N, Riotto A and Scopel S 2003 *Phys. Rev.* D **67** 023514
[1225] Boeckel T and Schaffner-Bielich J 2010 *Phys. Rev. Lett.* **105** 041301
Boeckel T and Schaffner-Bielich J 2011 *Phys. Rev. Lett.* **106** 069901 (erratum)
[1226] Boeckel T and Schaffner-Bielich J 2012 *Phys. Rev.* D **85** 103506
[1227] Kane G, Sinha K and Watson S 2015 *Int. J. Mod. Phys.* D **24** 1530022
[1228] Davoudiasl H, Hooper D and McDermott S D 2016 *Phys. Rev. Lett.* **116** 031303
[1229] Berlin A, Hooper D and Krnjaic G 2016 *Phys. Rev.* D **94** 095019
[1230] Berlin A, Hooper D and Krnjaic G 2016 *Phys. Lett.* B **760** 106
[1231] Abdalla H *et al* (HESS) 2016 *Phys. Rev. Lett.* **117** 151302
[1232] Chiappo A, Cohen-Tanugi J, Conrad J and Strigari L E 2019 *Mon. Not. R. Astron. Soc.* **488** 2616
[1233] Navarro J F, Frenk C S and White S D M 1997 *Astrophys. J.* **490** 493
[1234] Navarro J F, Eke V R and Frenk C S 1996 *Mon. Not. R. Astron. Soc.* **283** L72
[1235] Donato F, Gentile G, Salucci P, Frigerio Martins C, Wilkinson M I, Gilmore G, Grebel E K, Koch A and Wyse R 2009 *Mon. Not. R. Astron. Soc.* **397** 1169
[1236] Gentile G, Salucci P, Klein U, Vergani D and Kalberla P 2004 *Mon. Not. R. Astron. Soc.* **351** 903
[1237] Oh S-H, de Blok W J G, Brinks E, Walter F and Kennicutt R C Jr 2011 *Astron.* J **141** 193
[1238] Salucci P, Wilkinson M I, Walker M G, Gilmore G F, Grebel E K, Koch A, Frigerio Martins C and Wyse R F G 2012 *Mon. Not. R. Astron. Soc.* **420** 2034
[1239] de Martino I, Chakrabarty S S, Cesare V, Gallo A, Ostorero L and Diaferio A 2020 *Universe* **6** 107
[1240] Seidel K, Simon F, Tesař M and Poss S 2013 *Eur. Phys. J.* C **73** 2530
[1241] Horiguchi T, Ishikawa A, Suehara T, Fujii K, Sumino Y, Kiyo Y and Yamamoto H 2013 arXiv:1310.0563
[1242] Kiyo Y, Mishima G and Sumino Y 2015 *J. High Energy Phys.* JHEP11(2015)084
[1243] Beneke M, Kiyo Y, Marquard P, Penin A, Piclum J and Steinhauser M 2015 *Phys. Rev. Lett.* **115** 192001
[1244] Bicer M *et al* (TLEP Design Study Working Group) 2014 *J. High Energy Phys.* JHEP01(2014)164
[1245] Lepage G P, Mackenzie P B and Peskin M E 2014 arXiv:1404.0319
[1246] Dunsky D, Hall L J and Harigaya K 2019 *J. High Energy Phys.* JHEP07(2019)016
[1247] Dunsky D, Hall L J and Harigaya K 2021 *J. High Energy Phys.* JHEP04(2021)052
[1248] Bernstein A *et al* 2020 *J. Phys.: Conf. Ser.* **1468** 012035
[1249] Dell'Oro S, Marcocci S, Viel M and Vissani F 2016 *Adv. High Energy Phys.* **2016** 2162659
[1250] Agostini M *et al* (GERDA) 2019 *Science* **365** 1445
[1251] Adams D Q *et al* (CUORE) 2020 *Phys. Rev. Lett.* **124** 122501
[1252] Gando Y (KamLAND-Zen) 2020 *J. Phys.: Conf. Ser.* **1468** 012142
[1253] Abgrall N *et al* (LEGEND) 2017 *AIP Conf. Proc.* **1894** 020027
[1254] Adams C *et al* (NEXT) 2021 *J. High Energy Phys.* JHEP08(2021)164
[1255] Armstrong W *et al* (CUPID) 2019 arXiv:1907.09376
[1256] Nakamura R, Sambonsugi H, Shiraishi K and Wada Y 2020 *J. Phys.: Conf. Ser.* **1468** 012256
[1257] Andringa S *et al* (SNO+) 2016 *Adv. High Energy Phys.* **2016** 6194250
[1258] Akimov D *et al* (COHERENT) 2018 arXiv:1803.09183
[1259] de la Vega L M G, Flores L J, Nath N and Peinado E 2021 arXiv:2107.04037
[1260] Ciuffoli E, Evslin J, Fu Q and Tang J 2018 *Phys. Rev.* D **97** 113003
[1261] Coloma P, Denton P B, Gonzalez-Garcia M C, Maltoni M and Schwetz T 2017 *J. High Energy Phys.* JHEP04(2017)116
[1262] Coloma P, Gonzalez-Garcia M C, Maltoni M and Schwetz T 2017 *Phys. Rev.* D **96** 115007
[1263] Liao J and Marfatia D 2017 *Phys. Lett.* B **775** 54
[1264] Akimov D *et al* (COHERENT) 2021 *Phys. Rev. Lett.* **126** 012002
[1265] Akimov D Y *et al* (RED) 2013 *J. Inst.* **8** P10023
[1266] Soma A K *et al* (TEXONO) 2016 *Nucl. Instrum. Methods Phys. Res.* A **836** 67
[1267] Agnolet G *et al* (MINER) 2017 *Nucl. Instrum. Methods Phys. Res.* A **853** 53
[1268] Akimov D Y *et al* 2017 *J. Inst.* **12** C06018
[1269] Strauss R *et al* 2017 *Eur. Phys. J.* C **77** 506
[1270] Leder A *et al* 2018 *J. Inst.* **13** P02004

[1271] Akimov D Y *et al* (RED-100) 2020 *J. Inst.* **15** P02020
[1272] Ni K, Qi J, Shockley E and Wei Y 2021 *Universe* **7** 54
[1273] Arpesella C *et al* (Borexino) 2008 *Phys. Lett.* B **658** 101
[1274] Zaklad H, Derenzo S E, Muller R A and Smits R G 1973 *IEEE Trans. Nucl. Sci.* **20** 429
[1275] Lavoie L 1976 *Med. Phys.* **3** 283
[1276] Egorov V V, Miroshnichenko V P, Rodionov B U, Bolozdinja A I, Kalashnikov S D and Krivoshein V L 1983 *Nucl. Instrum. Methods Phys. Res.* **205** 373
[1277] Bolozdynya A I, Egorov V V, Koutchenkov A V, Safronov G A, Smirnov G N, Medved S A and Morgunov V L 1997 *IEEE Trans. Nucl. Sci.* **44** 2408
[1278] Bolozdynya A, Ordonez C and Chang W 1997 *IEEE 1997 Nuclear Science Symp. Medical Imaging Conf.* vol 2 p 1047
[1279] Rogers W L, Clinthorne N H and Bolozdynya A 2004 *Emission Tomography: The Fundamentals of PET and SPECT* ed M Wernick and J Aarsvold (San Diego: Academic Press) pp 383–419
[1280] Chepel V Y 1993 *Nucl. Tracks Radiat. Meas.* **21** 47
[1281] Chepel V, Solovov V, Van Der Marel J, Lopes M I, Crespo P, Janeiro L, Santos D, Marques R F and Policarpo A J P L 1999 *IEEE Trans. Nucl. Sci.* **46** 1038
[1282] Chepel V, Lopes M I, Solovov V, Ferreira Marques R and Policarpo A J P L 2002 *Technique and Application of Xenon Detectors. Proc., Int. Workshop* (Kashiwa, Japan, 3–4 December 2001) pp pp 28–40
[1283] Gallego Manzano L *et al* 2015 *Nucl. Instrum. Methods Phys. Res.* A **787** 89
[1284] Ferrario P 2018 *J. Inst.* **13** C01044
[1285] Zhu Y *et al* 2019 *IEEE Int. Conf. on Dielectric Liquids*
[1286] Giovagnoli D *et al* 2021 *IEEE Trans. Radiat. Plasma Med. Sci.* **5** 826
[1287] Kevles B H 1998 *Naked to the Bone; Medical Imaging in the Twentieth Century* (New Brunswick: Rutgers University Press)
[1288] Renner J *et al* 2021 arXiv:2109.12899
[1289] Lynch C III, Baum J, Tenbrinck R and Weiskopf R B 2000 *Anesthesiology* **92** 865
[1290] Law L S-C, Lo E A-G and Gan T J 2016 *Anesth. Analg.* **122** 678
[1291] Campos-Pires R *et al* 2015 *Crit Care Med.* **43** 149–58
[1292] Dobrovolsky A, Bogin V and Meloni E 2018 *Ann. Psychiatry Ment. Health* **6** 1133 https://jscimedcentral.com/Psychiatry/psychiatry-6-1133.pdf
[1293] Nikkel J A, Gozani T, Brown C, Kwong J, McKinsey D N, Shin Y, Kane S, Gary C and Firestone M 2012 *J. Inst.* **7** C03007
[1294] Boireau G *et al* (NUCIFER) 2016 *Phys. Rev.* D **93** 112006
[1295] Khosa C K, Mars L, Richards J and Sanz V 2020 *J. Phys. G: Nucl. Part. Phys.* **47** 095201
[1296] Barrand G *et al* 2001 *Comput. Phys. Commun.* **140** 45
[1297] Jayatilaka B, Levshina T, Sehgal C, Gardner R, Rynge M and Würthwein F 2017 *J. Phys.: Conf. Ser.* **898** 082048
[1298] Albrecht J *et al* (HEP Software Foundation) 2019 *Comput. Softw. Big Sci.* **3** 7
[1299] van den Berg A *et al* 2011 *Astroparticle Physics—The European Roadmap*
[1300] Cushman P *et al* 2013 Snowmass CF1 summary: WIMP dark matter direct detection (arXiv:1310.8327)
[1301] APPEC 2017 European astroparticle physics strategy 2017–2026 http://appec.org/wp-content/uploads/2017/08/APPEC-Strategy-Book-Proof-23-Nov-2.pdf
[1302] Department of Particles and Fields 2018 APS division of particles and fields response to European strategy group call for white papers: community planning and science drivers https://aps.org/units/dpf/upload/DPF-strategy.pdf
[1303] Department of Particles and Fields 2018 APS division of particles and fields response to European strategy group call for white papers: tools for particle physics https://aps.org/units/dpf/upload/DPF-tools.pdf
[1304] Cao J *et al* 2022 *Non-accelerator particle physics in china: A strategic Plan* in Chinese (in preparation)
[1305] Billard J *et al* 2021 arXiv:2104.07634
[1306] Group E S 2020 *The European Strategy for Particle Physics Update 2020*
[1307] Ritz S *et al* 2014 *Building for Discovery: Strategic Plan for U.S. Particle Physics in the Global Context* https://science.energy.gov/~/media/hep/hepap/pdf/May-2014/FINAL_P5_Report_Interactive_060214.pdf

[1308] Zeitnitz C 2018 Particle physics strategy in Germany https://indico.desy.de/indico/event/20166/contribution/6/material/slides/0.pdf
[1309] Wallny R *et al* 2021 *Swiss Academies Reports* vol 16 p 6 https://api.swiss-academies.ch/site/assets/files/24379/chipp_roadmap_2021.pdf
[1310] van den Berg A *et al* 2014 *Strategic Plan for Astroparticle Physicsin the Netherlands 2014–2024*
[1311] Geesaman D *et al* 2015 *Reaching for the Horizon: The 2015 Long Range Plan for Nuclear Science* https://science.energy.gov/~/media/np/nsac/pdf/2015LRP/2015_LRPNS_091815.pdf
[1312] Giuliani A, Gomez Cadenas J J, Pascoli S, Previtali E, Saakyan R, Schäffner K and Schönert S (APPEC Committee) 2019 arXiv:1910.04688
[1313] Panesor T 2015 *A Review of UK Astroparticle Physics Research*
[1314] Tyurin N 2012 *Particle Physics in Russia*
[1315] Nakada T *et al* 2013 *The European Strategy for Particle Physics Update 2013*
[1316] Bai C *et al* 2020 *Neutrinoless Double Beta Decay: A Study of Strategic Development by Chinese Academy of Sciences* in Chinese
[1317] Faulkner P J W *et al* (GridPP) 2006 *J. Phys. G: Nucl. Part. Phys.* **32** N1
[1318] Britton D *et al* 2009 *Phil. Trans. R. Soc.* A **367** 2447